1-1-1987

Studies of polymer solidification using the technique of impulse viscoelasticity/

Menas Spyros Vratsanos
University of Massachusetts Amherst

STUDIES OF POLYMER SOLIDIFICATION USING THE TECHNIQUE OF IMPULSE VISCOELASTICITY

A Dissertation Presented

By

MENAS SPYROS VRATSANOS

Submitted to the Graduate School of the
University of Massachusetts in partial fulfillment
of the requirements for the degree of

DOCTOR OF PHILOSOPHY

September 1987

Polymer Science and Engineering

STUDIES OF POLYMER SOLIDIFICATION

USING THE TECHNIQUE OF IMPULSE VISCOELASTICITY

A Dissertation Presented

By

Menas Spyros Vratsanos

Approved as to style and content by:

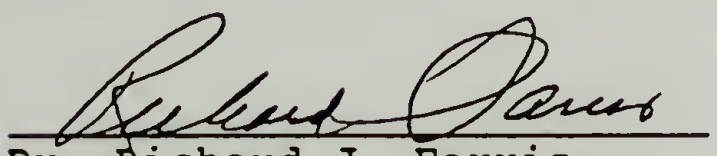

Dr. Richard J. Farris
Committee chairman

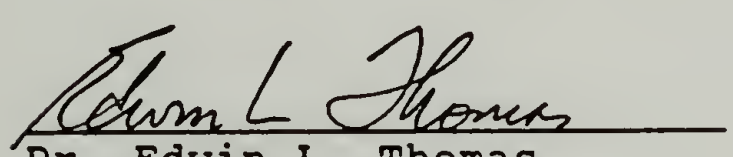

Dr. Edwin L. Thomas
Committee member

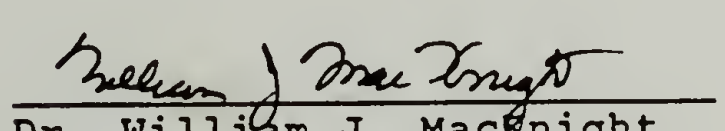

Dr. William J. MacKnight
Committee member

Dr. James A. Donovan
Committee member

Dr. Edwin L. Thomas
Department Head
Polymer Science and Engineering
Department

To my father, mother and brother for
their encouragement to pursue my best.

Knowledge is not a loose-leaf notebook of facts.

- Jacob Bronowski,
  The Ascent of Man

ACKNOWLEDGEMENT

In such a small space, it is difficult to individually thank each person who contributed to this dissertation. I thank my committee members, Drs. Farris, Thomas, MacKnight and Donovan for their advice and useful discussions during my five year stay. I know I have benefited from their experiences. I extend a special appreciation and respect to Dr. Farris for helping transform me into a scientist. Moreover, I thank him for teaching me to approach research from a fundamental perspective; this is the purpose of any Ph.D. experience.

Many of my classmates helped make graduate school more enjoyable. Among them are Steve DeTeresa, Gary Jaycox, Carmen Gabriel, Chris Costello, Dave Kinning, Steve Arnold and many others. Without their friendship it would have been much more difficult to endure the long hours and dedication required to complete this dissertation. I hope our friendships will last thrcugh the years.

I thank Lori Anderson for her love and support over the past two years. Her friendship has been the most pleasant surprise during my stay in Amherst.

Finally, I acknowledge the financial support of CUMIRP, as well as the support of the technical staff and secretaries. Without it, this research could not have been accomplished.

ABSTRACT

Studies of Polymer Solidification Using the
Technique of Impulse Viscoelasticity

(September 1987)

Menas Spyros Vratsanos, B.S., Columbia University
M.S., Ph.D., University of Massachusetts
Directed by: Professor Richard J. Farris

An *in situ* study of the solidification process in polymers using the technique of Impulse Viscoelasticity is presented. The Impulse Viscoelastic technique examines the mechanical response of a material to an arbitrary deformation. By periodically deforming the material throughout its solidification history, it is possible to follow the development of many of its mechanical and rheological properties.

The Impulse Viscoelastic technique was applied to several thermosetting systems in an effort to relate the network mechanical properties to the reactant stoichiometry. Measurements were made in a uniaxial mode using a novel sample geometry which consisted of a soft rubber membrane as a sample support. Experimental emphasis was placed on the determination of the stresses and volumetric changes due to cure, equilibrium tensile modulus, steady state elongational viscosity, mean relaxation time, thermal expansion coefficient, glass transition temperature and dynamic

mechanical properties during cure. From these measurements it was possible to qualitatively and quantitatively determine the processes involved during network formation.

Two thermosetting systems were studied in detail. First, the curing of an epoxy resin using well characterized tetra- and hexafunctional amines of various molecular weights was examined. Using three amine/epoxy ratios, a wide range of network structures were formed. All of the epoxy networks investigated cured elastically. Many of the measured mechanical properties, e.g., the molecular weight between crosslinks, correlated well with the predictions of rubber elasticity theory. Second, the copolymerization of an epoxy resin with a ring opening monomer was investigated. It is suggested that during copolymerization two possibly interpenetrating networks form. For relatively low ring opening monomer contents, network formation was accompanied by vitrification. It was found that the addition of ring opening monomer decreases the volumetric shrinkage without significantly altering the magnitude of the one-dimensional cure stress. In general, the one-dimensional stresses due to cure were found to be small in comparison to load bearing or thermal stresses.

TABLE OF CONTENTS

LIST OF TABLES

LIST OF FIGURES

CHAPTER 1

INTRODUCTION

1.1 Polymer Solidification

The phenomenon of polymer solidification has been the subject of great interest to both the scientific and industrial communities. Solidification is the transformation of a liquid to a solid. Part of this interest results from the variety of fields that are affected by the solidification process. These include polymer morphology, rheology, transport and mechanics. In each case, large changes in polymer behavior are observed as a result of the liquid to solid transition. In contrast to the behavior of low molecular materials, polymer solidification is not a distinct process. Instead, it occurs over a broad range in temperature or time. This results partially from the unique properties which typify polymer materials, such as molecular weight distributions, branches, etc.

Commercially, polymer solidification is a vital part of many forming operations. Among the products that rely upon polymer solidification are: moldings, extrusions, coatings, adhesives, composites and a variety of others. For these articles, however, it is difficult to determine the relationship between the observed mechanical properties,

especially the aging characteristics, and the processing variables used during solidification. Part of this difficulty can be attributed to the variety of industrial processing conditions which are used during solidification. In order to understand the mechanical property-processing relationship in such complex operations, it is necessary to study the solidification process under simpler and more controlled circumstances.

Polymers can solidify in one of six ways. The first is via crystallization, whereby a polymer melt is transformed into a semi-crystalline ordered solid. Such polymers are characterized by the presence of a melting point and a crystalline diffraction pattern. The second method involves the solidification of an amorphous polymer liquid above its entanglement molecular weight as a result of entanglements, physical crosslinks and frictional contributions. This solidification process is usually accompanied by vitrification. Vitrification is the term used to describe the presence of long term relaxations typical of glassy materials. The resulting solid is amorphous in structure. Mechanical evidence for this type of solid is the presence of a glass transition temperature, T_g. The removal of solvent from a polymer solution is the third method of solidification. The mechanics of the solidification process are similar to those observed for both crystalline and amorphous thermoplastics. This method is encountered in the

casting of films, coatings, etc. The fourth and fifth methods by which solidification can occur are through the polymerization of monomer. The resulting polymers can be thermoplastic or thermosetting. In the case of thermoplastic polymers, solidification is evidenced by vitrification, physical crosslinks and entanglements. Thermosetting or crosslinking polymers become solid as a result of the formation of a three dimensional structure or network. This process is commonly referred to as gelation. The sixth method of solidification involves the gelation of polymer solutions. The mechanism by which this occurs is via molecular aggregation. In contrast to thermosetting materials, these gels form reversibly in that they can be transformed back to isotropic liquids. These methods by which solidification can occur are discussed in more detail in Chapter II, section 2.6. In the discussion which follows, the problems associated with the characterization of the solidification process of thermosetting materials are presented.

In the fields of mechanics and rheology, many investigations have been performed on polymers in their liquid state or their solid state. While information of this kind is important, there is a distinct lack of knowledge about the mechanical property changes that occur during the solidification process. It seems clear that in order to understand the mechanical properties that one

observes for a solid polymer, it is important to characterize the mechanical properties while these changes are occurring. In this regard, relatively few studies have been performed which investigate the solidification process from the liquid state to the solid state. One possible explanation for this lack of knowledge is the fact that the transition from the liquid to the solid state is accompanied by large changes in mechanical properties. These changes in properties can range over many orders of magnitude. Thus, in order to characterize this transition, a technique or apparatus must be of sufficient mechanical sensitivity so that it is capable of measuring both the properties of the liquid and those of the solid.

With regard to the liquid-solid transition as a result of network formation, various calorimetric [1-5], dielectric [6-14], acoustic [15,16], spectroscopic [17-19], dynamic mechanical [20-29] and torsional braid [30-34] methods have been developed for the *in situ* monitoring of the cure process. The latter two mechanical techniques, however, suffer from either of the following problems. First, the mechanical contribution of the sample support can dominate the mechanical response during cure and limit the applicability of the technique to the incipient stages of polymerization. Second, the inability to apply small deformations or measure large loads limits characterization to the pre-glassy state. In addition to these mechanical

limitations, these techniques offer limited information regarding the cure process. While dynamic mechanical methods over a limited frequency range are useful in the analysis of solids under conditions of vibrational loading, they are generally unable to differentiate liquid from solid behavior. This inability is a fundamental limitation when studying the transition from the liquid to the solid state. While no technique can monitor the entire cure process, an Impulse Viscoelastic method for monitoring solidification was recently developed by Farris [35]. Impulse Viscoelasticity examines the mechanical response of an aging linear viscoelastic material subject to deformation. In this context, aging refers to changes in material behavior as a function of time. Aging phenomena may be recognized as polymerization, crystallization, swelling, densification or degradation. With the Impulse Viscoelastic technique it is possible to measure or calculate many of the engineering properties as a function of cure. These include gelation time, gelation temperature (for non-isothermal cures), equilibrium modulus, cure stress, cure shrinkage, steady state elongational viscosity, relaxation spectrum, thermal expansion coefficient, glass transition temperature and dynamic mechanical properties. It should be noted that except for the glass transition temperature, dynamic mechanical properties and the relaxation spectrum, none of

the other properties can be obtained by dynamic mechanical methods.

Of particular experimental interest is the mechanical characterization of the curing process and its relationship to network structure. In this regard, great amounts of mechanical data have been obtained for cured thermosets [20-34,36-47]. Excellent reviews of the state of network analysis were recently prepared by Dusek and others [48,49]. Many of these studies, however, offer little information regarding the stresses and volumetric changes which accompany solidification. For network structures, properties such as the gel point, equilibrium modulus, molecular weight between crosslinks, stress due to cure, volumetric changes during cure and T_g are some of the important aspects greatly affected by the cure conditions. These properties are readily obtained from Impulse Viscoelastic measurements on thermosetting systems. From such information it should be possible to choose the proper curing conditions for a particular application and eliminate the need of complicated cure schedules. This ability to determine optimum cure conditions should be especially helpful for those interested in the curing of high performance resins and composites where the established cure schedules are time and energy intensive.

Since the introduction of the technique of Impulse Viscoelasticity in 1984 two efforts have been made in the

area of polymer solidification using the technique. Farris and Lee first used the Impulse Viscoelastic technique to characterize the isothermal curing of Narmco 5208 epoxy resin using a shear mode of deformation [50]. They measured the equilibrium shear modulus at two different cure temperatures and related their findings to the dynamic shear properties. These studies were limited to the very early stages of cure and did not not discuss the development of the network structure.

The second effort using the Impulse Viscoelastic technique was aimed at the solidification of thermoplastics. Isothermal shear deformations were used to characterize the mechanical properties of polycarbonate and polystyrene as functions of time, temperature and molecular weight [51]. It was found that an apparent equilibrium shear modulus existed above the glass transition temperature for polystyrene while the polycarbonate samples had an equilibrium shear modulus of zero above T_g. These preliminary studies, however, were limited to the early stages of solidification because of sample slippage in the test machine.

1.2 Dissertation Overview

One of the goals of this research is to establish the technique of Impulse Viscoelasticity as a method for obtaining useful information over a large portion of the

solidification process for polymers. A second goal is to investigate and develop an understanding of the solidification process as a result of cure. In particular, the technique will be systematically applied to the curing of two thermosetting materials. It is expected that from these studies an understanding of the transition from liquid to solid behavior can be elucidated from a mechanical perspective. In contrast to the previous studies using the technique of Impulse Viscoelasticity which used shear deformations, these studies employ uniaxial deformations to characterize the curing process. The use of uniaxial deformation makes it possible to measure mechanical properties unattainable through shear deformation modes. Essential to the attainment of these goals was the development of an experimental apparatus of sufficient mechanical sensitivity so that the large property changes which result from solidification could be monitored.

Chapter II presents the theoretical and experimental aspects of the Impulse Viscoelastic method. Starting from a linear viscoelastic constitutive equation, the equations necessary to calculate the mechanical and rheological properties of a material are derived. Though the method requires no particular deformation mode, the discussion is limited to uniaxial deformation, as opposed to shear, because of its sensitivity to dimensional changes which occur during solidification. An important subset of the

Impulse Viscoelastic analysis is the calculation of the dynamic mechanical properties of a material from an arbitrary deformation. As an integral part of the Impulse Viscoelastic technique, the theory of incremental linear elasticity is also presented. Using the incremental linear elastic approach it is possible to calculate the stresses and volumetric changes which occur during polymerization.

Chapter II also elaborates on the experimental methodology used with the Impulse Viscoelastic approach. Two examples of the application of the Impulse Viscoelastic method are presented. These include the results of the thermally reversible gelation of a polypeptide solution, poly(γ-benzyl-L-glutamate) in benzyl alcohol, and a comparison of the Fourier transform method with the traditional dynamic mechanical method for determining dynamic mechanical properties. Applications of the Impulse Viscoelastic method to other modes of solidification are also discussed. An Impulse Dielectric method for monitoring cure is proposed.

Chapter III presents the Impulse Viscoelastic results on the curing of Epon 828, a diglycidyl ether of bisphenol-A epoxy, with several multi-functional amines. In order to correlate the network mechanical properties with reactant stoichiometry, relatively well characterized amines were obtained. Emphasis was placed on the determination of the molecular weight between crosslinks and correlations of the

network properties with results obtained from rubber elasticity theory. Three amine/epoxy molar ratios were examined and both di- and triamines of various molecular weights were studied. The mechanical property variation, as a result of the systematic variation of the amine/epoxy molar ratio, was used to provide insight into the network structure.

In Chapter IV results of the Impulse Viscoelastic characterization of the curing behavior of epoxy copolymerized with a ring opening monomer are presented. These ring opening materials recently developed by Bailey and others expand volumetrically upon polymerization [52-55]. When these ring opening monomers are copolymerized with epoxy resins, it has been suggested that there is a decrease in volumetric shrinkage and an increase in adhesion when compared to the neat epoxy resin [56]. As a result these monomers have been used in epoxy resins in an effort to reduce the volumetric shrinkage typical of thermosetting materials [36]. Particular emphasis was placed on volumetric changes and the residual cure stress behavior of these copolymers.

Some of the limitations of the Impulse Viscoelastic method are discussed in Chapter V. Both an experimental and theoretical approach were taken. For the experimental approach, a fully cured epoxy was subjected to a variety of deformation conditions. Among the variables of interest

were the pulse shape, duration, amplitude and deformation temperature. The theoretical approach consisted of modeling the responses of a standard linear solid and Maxwell element to a given pulse deformation. The approach uses dimensionless variables for two of the key experimental parameters; pulse duration and integration time. A comparison of the experimental and the theoretical results is included.

Chapter VI summarizes the major findings of this dissertation and presents suggestions for future work.

C H A P T E R 2

THE IMPULSE VISCOELASTIC METHOD

2.1 Introduction

The liquid to solid transition represents a fundamental material change. While this transition may be easy to identify for most non-polymeric materials, it remains relatively elusive for polymers. Its determination is important not only to the fields of mechanics but to the areas of rheology, diffusion and morphology. For thermosetting systems, the onset of gelation and the formation of a three-dimensional structure defines the liquid-solid transition. In rheology, gelation has been regarded as the transition from a liquid of infinite viscosity to a network solid of finite modulus. Tung and Dynes [26] and others [27] have used the equivalence of the dynamic storage modulus G' with the dynamic loss modulus G" as a criterion for determining the point of gelation. While this criterion may be simple to apply experimentally, it has no theoretical basis and yields gelation times which are dependent upon the frequency of measurement [26]. This results from the fact that single frequency dynamic mechanical methods are unable to differentiate liquid from solid behavior except in the limit of zero frequency.

Since gelation is the transition from liquid to solid behavior, it seems clear that one should use the definition of a liquid and solid to determine that transition. A solid can be differentiated from a liquid by the existence of a non-zero equilibrium shear or tensile modulus [57]. Using this approach to gelation, Farris [35] has developed the theory of Impulse Viscoelasticity for determining the gel point and following the mechanical changes associated with the solidification process.

The Impulse Viscoelastic approach to solidification is based upon examining the stress response of a material to a deformation of general shape. For materials whose properties are changing with time as a result of cure, the duration of the deformation must be short in comparison to the polymerization time. In this way the mechanical properties can be considered constant over the duration of deformation. By periodically applying arbitrary deformations throughout the solidification event, it is possible to obtain useful mechanical and phenomenological information regarding the processes involved during solidification. The use of periodic deformations to measure the mechanical properties of a material whose properties are changing with time can be traced to Tobolsky's work in the 1940's on elastic, vulcanized rubbers [58]. In those studies, continuous and "intermittent" stress relaxation measurements were made on rubbers in order to separately

determine the effects of chain scission and crosslinking. In contrast to Tobolsky's work on elastic materials, the Impulse Viscoelastic approach analyzes the stress response to deformation for linear viscoelastic materials. Thus the Impulse Viscoelastic technique can be viewed as the viscoelastic generalization of Tobolsky's methodology. The name Impulse Viscoelasticity is derived from physics where the term impulse is used to describe the moment or integral of a force-time curve. Viscoelasticity refers to the general stress response to deformation.

Though the Impulse Viscoelastic method can be used to characterize previously solidified materials, this chapter will address the mathematics of Impulse Viscoelasticity as applied to the curing process. The analyses used are time-weighted moments and Laplace and Fourier transforms of both the stress and deformation histories. Among the properties which can be measured or calculated using Impulse Viscoelasticity for a polymerizing system are: gelation time and temperature, equilibrium modulus, steady state viscosity, relaxation spectrum and dynamic mechanical properties.

An important aspect of Impulse Viscoelasticity is that it is independent of a particular piece of equipment or mode of deformation. Thus, the theory developed in this dissertation could find application in fields other than in the area of mechanics. Such applications will be discussed.

Sections 2.2.1 and 2.3 discuss the calculation of the dynamic mechanical properties and the theory of incremental linear elasticity, respectively. When combined with the theory of Impulse Viscoelasticity, incremental linear elasticity enables one to determine other quantities during solidification, such as the stresses generated in dimensionally constrained systems.

2.2 Theory of Impulse Viscoelasticity

The transition from the liquid to the rubbery state for thermosetting resins is accompanied by large changes in material properties. One approach to characterizing these changes is to regard them as the result of an aging process due to polymerization. As mentioned, Impulse Viscoelasticity examines the response of an aging linear viscoelastic material subjected to deformation. A typical deformation pulse and stress response for a viscoelastic epoxy sample are shown in Figure 2.1. Contained in the stress and strain responses depicted in Figure 2.1 is all of the information necessary to calculate the mechanical properties of interest. One of the more important advantages of this technique is the fact that the path of deformation is arbitrary. As will be demonstrated later, in order to simplify the mathematics, the deformation path of the sample must return to its initial value at the end of the deformation. By virtue of the assumption of linear

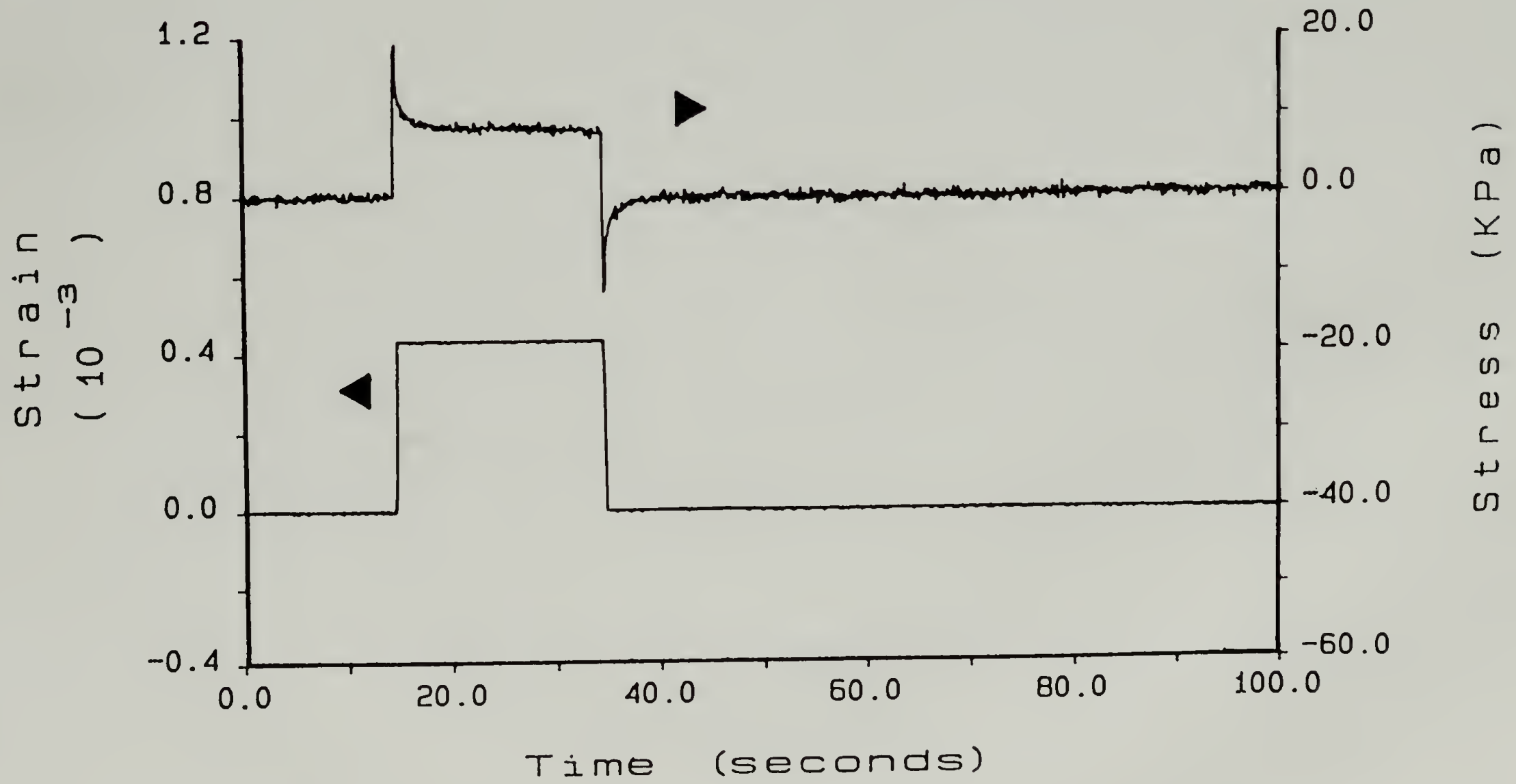

Figure 2.1. Typical uniaxial pulse-strain deformation for an epoxy sample exhibiting a viscoelastic stress response. The equilibrium tensile modulus (Eeq) of this sample is listed at the top of the figure.

viscoelasticity and assuming an equilibrium starting condition, the stress must also return to its initial value after such a deformation. There are no restrictions on the path of the deformation as long as the stress and strain obey that criterion.

In the discussion which follows only deformations which return to their initial level will be considered. Basically there are two types of deformation experiments that can be performed. The first involves the application of a deformation which starts and returns to a zero displacement level. For this case, the stress in the sample is monitored until it reaches its pre-deformation value. These types of deformations are commonly referred to as displacement control experiments. The second type of experiment involves the application of a stress which starts and returns to zero. These load control experiments, however, are more difficult experimentally in the incipient stages of polymerization when the material is still liquid. Once the material solidifies, the sample strain is monitored until it reaches its pre-deformation value.

For the mathematics which follow we consider the response of a material to a short duration uniaxial deformation which returns to its initial level at the end of deformation. As mentioned, the shape of the deformation is arbitrary. The choice of uniaxial deformation, as opposed to shear, is based upon the fact that it is sensitive to the

volumetric changes which can occur during polymerization. This fact will be demonstrated in section 2.3 on the theory of incremental linear elasticity. The experimental details involved in obtaining such data, including the technique for constraining liquid samples in a uniaxial geometry are discussed in section 2.4 of this chapter. In addition, deformations that induce large stress relaxation in materials are best for use with the Impulse Viscoelastic method because they yield higher order information more readily than those of a smoother path.

Equation (2.1) is the one-dimensional, non-aging, linear viscoelastic constitutive equation written in a form such that the time-independent elastic contributions are separate from the time-dependent viscoelastic contributions [59]:

$$\sigma(t) = Eeq\varepsilon(t) + \int_o^t Er(t - t') \frac{\partial \varepsilon}{\partial t'} dt' , \qquad (2.1)$$

where $\sigma(t)$ = stress response

$\varepsilon(t)$ = strain history

Eeq = equilibrium tensile modulus

$Er(t)$ = time-dependent portion of the tensile relaxation modulus, where $Er(t = \infty) = 0$

t = time

t' = time parameter.

Since Equation (2.1) applies to a non-aging material, it is valid only for deformations of short duration when polymerization is occurring. This requirement is equivalent

to assuming that the aging process is slow in comparison to the duration of the deformation. In this way, both the time-dependent and time-independent properties can be considered constant over the duration of the deformation. Clearly, for some processes, such as reaction injection molding (RIM) or photo-initiated polymerizations, this requirement may be limiting. Polymerization is studied by analyzing the mechanical response to several short duration deformations. Although the mechanical properties are changing as a result of aging, they will be considered non-aging, but at new values for each pulse. Equation (2.1), using these new values for $\sigma(t)$, $\varepsilon(t)$, Eeq and Er(t), can then be reapplied to calculate the mechanical properties. Thus, by periodically deforming a material as it polymerizes, it is possible to measure the changes in mechanical properties as a result of polymerization. Except for the difference in time scale, this approach to monitoring polymerization is analogous to the photographer who uses a motor drive attachment on his camera to capture events which are changing with time. In both cases, the polymerization or event can be reconstructed by sequentially combining the static or "frozen" frames.

Taking the Laplace transform of Equation (2.1) and assuming that $\varepsilon(t = 0) = 0$ yields:

$$\bar{\sigma} = Eeq\ \bar{\varepsilon} + s\ \bar{Er}\ \bar{\varepsilon}\ , \qquad (2.2)$$

where the Laplace transform $\bar{f}(s)$ of a function F(t) is given by Equation (2.3).

$$\bar{f}(s) = \int_o^\infty F(t)\exp(-st)dt \qquad (2.3)$$

At this point it is useful to recall three theorems from the theory of Laplace transforms [60]. These theorems are given by Equations (2.4-6).

$$\lim_{s \to 0} \bar{f}(s) = \int_o^\infty F(t)dt \qquad (2.4)$$

$$\lim_{s \to 0} s\,\bar{f}(s) = \lim_{t \to \infty} F(t) = F(\infty) \qquad (2.5)$$

$$-(1)^n \lim_{s \to 0} \frac{d^n\,\bar{f}(s)}{ds^n} = \int_o^\infty t^n F(t)dt \qquad (2.6)$$

The proper application of Equations (2.4) and (2.5) to Equation (2.2) yields:

$$\int_o^\infty \sigma(t)dt = Eeq \int_o^\infty \varepsilon(t)dt + \varepsilon(t = \infty) \int_o^\infty Er(t)dt\ . \qquad (2.7)$$

Since these uniaxial deformations are strain pulses which start and return to zero, $\varepsilon(t = \infty) = 0$. This experimental requirement simplifies Equation (2.7) to Equation (2.8):

$$\int_o^\infty \sigma(t)dt = Eeq \int_o^\infty \varepsilon(t)dt\ . \qquad (2.8)$$

Rearrangement of Equation (2.8) yields Equation (2.9):

$$Eeq = \frac{\int_0^\infty \sigma(t)dt}{\int_0^\infty \varepsilon(t)dt} . \qquad (2.9)$$

Thus the equilibrium tensile modulus (Eeq) can be calculated by evaluating the ratio of the stress-time integral to the strain-time integral. For a positive or negative definite uniaxial pulse-strain, the denominator of Equation (2.9) is always non-zero. Recall that by definition a liquid has an Eeq = 0, whereas a solid has a non-zero Eeq. This implies that in order for a liquid to have an Eeq = 0, the numerator of Equation (2.9) must be zero. Hence, the transition from liquid to solid in a material (gelation) can be determined by the onset of a non-zero stress-time integral. While any deformation is viable, those which have a total strain impulse of zero, e.g., one cycle of a full sine wave deformation, must have a total stress impulse of zero independent of the linear viscoelastic character of the material. Thus, from zero total strain impulse waveforms it is more difficult to differentiate materials based upon their mechanical response without resorting to higher moments of the stress and strain integrals. In addition to the gel time, the temperature at gelation can be determined for non-isothermal cures.

The equations needed to calculate the steady state elongational viscosity (η) and mean relaxation time (τ) as

functions of the polymerization history are derived in Equations (2.10-16). Differentiating Equation (2.2) with respect to the Laplace parameter s results in Equation (2.10).

$$d\bar{\sigma}/ds = Eeq(d\bar{\varepsilon}/ds) + \bar{\varepsilon}\,\bar{Er} + s\,(d\bar{\varepsilon}/ds)\bar{Er} + s\,\bar{\varepsilon}(d\bar{Er}/ds) \tag{2.10}$$

Taking the limit of Equation (2.10) as s approaches zero by applying Equations (2.4-6) and recalling that $Er(t = \infty) = 0$, yields Equation (2.11).

$$\int_o^\infty t\sigma(t)dt = Eeq \int_o^\infty t\varepsilon(t)dt - \int_o^\infty Er(t)dt \int_o^\infty \varepsilon(t)dt \tag{2.11}$$

The steady state elongational viscosity (η) has been derived from viscoelastic theory to be [59]:

$$\eta = \int_o^\infty Er(t)dt \ . \tag{2.12}$$

It should be mentioned that in this manner it is possible to measure the viscosity even of solid materials. Realizing that Equation (2.12) is part of Equation (2.11), it is possible to determine η, since all of the other terms in Equation (2.11) can be calculated from the pulse data. One can proceed in a similar fashion for determining the mean relaxation time τ. Taking the second derivative of Equation (2.2) with respect to s results in Equation (2.13).

$$d^2\bar{\sigma}/ds^2 = Eeq(d^2\bar{\varepsilon}/ds^2) + 2\,\bar{Er}(d\bar{\varepsilon}/ds) + 2\,\bar{\varepsilon}(d\bar{Er}/ds) + s\,\bar{\varepsilon}(d^2\bar{Er}/ds^2) + s\,\bar{Er}(d^2\bar{\varepsilon}/ds^2) + 2\,s\,(d\bar{Er}/ds)(d\bar{\varepsilon}/ds) \tag{2.13}$$

Again taking the limit as the Laplace parameter goes to zero and applying Equation (2.6) to Equation (2.13) yields:

$$\int_o^\infty t^2\sigma(t)dt = Eeq\int_o^\infty t^2\varepsilon(t)dt - 2\,\eta\int_o^\infty t\varepsilon(t)dt - 2\int_o^\infty \varepsilon(t)dt\int_o^\infty tEr(t)dt\ . \tag{2.14}$$

The mean relaxation time τ is defined by Equation (2.15):

$$\tau = \frac{\int_o^\infty tEr(t)dt}{\int_o^\infty Er(t)dt}\ . \tag{2.15}$$

Thus it is possible to calculate the mean relaxation time from Equation (2.14) since all of the other terms are known. By taking higher order derivatives (with respect to the Laplace parameter) of Equation (2.2) it is possible to obtain moments of the relaxation spectrum of the curing material. The equation for the (n + 1)th moment ($n \geq 2$) of the relaxation modulus is given by Equation (2.16):

$$\int_o^\infty t^n\sigma(t)dt = Eeq\int_o^\infty t^n\varepsilon(t)dt - \sum_{m=0}^{n-1}\binom{n-1}{m}n\int_o^\infty t^{n-m-1}Er(t)dt\int_o^\infty t^m\varepsilon(t)dt\ , \tag{2.17}$$

where the expression $\binom{n-1}{m}$ are the binomial coefficients. These coefficients can be found in a mathematics reference book [60]. For example, consider the fourth (n = 3) moment:

$$\int_o^\infty t^3 \sigma(t)dt = Eeq \int_o^\infty t^3 \varepsilon(t)dt - 3 \int_o^\infty tEr(t)dt \int_o^\infty \varepsilon(t)dt$$

$$- 6 \int_o^\infty tEr(t)dt \int_o^\infty t\varepsilon(t)dt - 3 \int_o^\infty Er(t)dt \int_o^\infty t^2 \varepsilon(t)dt \ .$$

This procedure of obtaining moments of the relaxation modulus is exactly analogous to constructing the molecular weight distribution of a linear polymer knowing the number, weight and viscosity-average molecular weights.

A method of directly determining the distribution of relaxation times is also described. It involves the application of a series of uniaxial pulse-strain deformations of duration δ and whose strain magnitudes are given by the binomial coefficients. Figure 2.2 illustrates the first two deformations in this family of deformations. By combining the time-independent and time-dependent terms, Equation (2.1) can be equivalently written as Equation (2.18):

$$\sigma(t) = \int_o^t E(t - t') \frac{\partial \varepsilon}{\partial t'} dt' \ , \qquad (2.18)$$

where E(t) = tensile relaxation modulus, where $E(t = \infty)$ = Eeq.

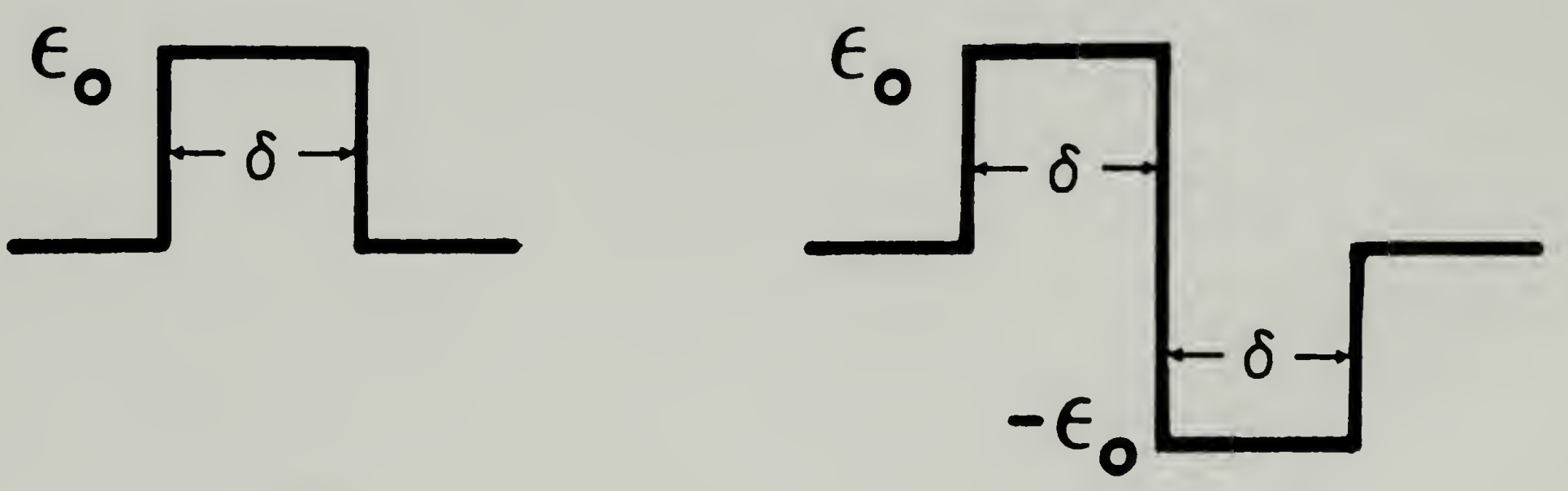

Figure 2.2. The first two of a family of deformation histories that can be used to calculate the relaxation spectrum.

Using Equation (2.18) it is possible to write the stress responses for the two deformations histories given in Figure 2.2. These equations are given in Equations (2.19) and (2.20), respectively.

$$\sigma(t) = [E(t) - E(t - \delta)]\varepsilon_o \qquad \text{for } t > \delta \qquad (2.19)$$

$$\sigma(t) = [E(t) - 2E(t - \delta) + E(t - 2\delta)]\varepsilon_o \quad \text{for } t > 2\delta \qquad (2.20)$$

Rearranging these two equations results in Equations (2.21) and (2.22).

$$\sigma(t)/\varepsilon_o\delta = [E(t) - E(t - \delta)]/\delta \qquad (2.21)$$

$$\sigma(t)/\varepsilon_o\delta^2 = [E(t) - 2E(t - \delta) + E(t - 2\delta)]/\delta^2 \qquad (2.22)$$

In the limit of short duration deformations, the right hand sides of Equation (2.21) and (2.22) are the numerical approximations to $\partial E/\partial t$ and $\partial^2 E/\partial t^2$, respectively. These partial derivatives can be obtained simply by measuring the stress response to such deformations. While the expressions given above are only for the first two derivatives of E(t), it should be clear that higher order derivatives can by obtained by using deformations whose magnitudes are given by the binomial coefficients. These experiments can easily be performed using modern servo hydraulic test equipment.

The time derivatives of the relaxation modulus can now be related to the relaxation spectrum $H(\tau)$. This relationship is given Equation (2.23) [59]:

$$E(t) = \int_{-\infty}^{\infty} H(\tau)\exp(-t/\tau)d\ln\tau \ . \qquad (2.23)$$

In order to simplify the mathematics, it will be assumed that $\exp(-t/\tau)$ can be described by a unit step function whose values are 1 for $\tau > t$ and 0 for $\tau < t$. Incorporating this simplification results in Equation (2.24).

$$E(t) \approx \int_{\ln t}^{\infty} H(\tau) d\ln\tau \qquad (2.24)$$

Differentiating Equation (2.24) with respect to the lower limit $\ln t$ and rearranging yields Equation (2.25).

$$\partial E/\partial t \approx - H(\tau)/\tau \qquad (2.25)$$

Since we can obtain expressions for the derivatives of the relaxation modulus (Equations (2.21) and (2.22)), it is possible to approximate the relaxation spectrum $H(\tau)$. Higher order approximations of $H(\tau)$ require higher order derivatives [59].

2.2.1 Dynamic Mechanical Properties

Dynamic mechanical methods have been widely used to characterize the properties of polymers. The determination of the storage modulus (E'), loss modulus (E") or equivalently, the complex modulus (E*) and tan δ can provide information on the glass transition temperature (T_g) and other molecular relaxations. Traditional dynamic mechanical methods involve determining the steady state response of a material to a "clean" and continuous sinusoidal stress or strain disturbance. The term clean implies that there are no sine waves of other frequencies. The properties are

generally determined by measuring the ratio of the amplitudes and phase lag of the input and output sinusoidal signals. While these measurements are valuable, it would be convenient if one could generate these data from arbitrary strain disturbances. Before proceeding with the methodology for determining dynamic mechanical properties using Fourier transforms, it is useful to include the derivation of some established results.

The dynamic mechanical properties can be calculated from the mechanical response of a material to sinusoidal deformation as follows. Substituting the harmonic strain input given in Equation (2.26) into Equation (2.18) yields Equations (2.27) or (2.28):

$$\varepsilon(\phi) = \varepsilon_o \sin(w\phi) \tag{2.26}$$

$$\sigma(t) = \varepsilon_o w \int_o^t E(t - \phi)\cos(w\phi)d\phi \tag{2.27}$$

$$\sigma(t) = \varepsilon_o w \int_o^t E(\phi)\cos(wt - w\phi)d\phi \ , \tag{2.28}$$

where w is the angular frequency which is related to the linear frequency f by the relation $w = 2\pi f$. Using the fact that $\cos(wt - w\phi) = \cos(wt)\cos(w\phi) + \sin(wt)\sin(w\phi)$, it is possible to simplify Equation (2.28) to Equation (2.29).

$$\sigma(t)/\varepsilon_o = \sin(wt)\ w \int_o^t E(\phi)\sin(w\phi)d\phi + \cos(wt)\ w \int_o^t E(\phi)\cos(w\phi)d\phi \tag{2.29}$$

At conditions of steady state, i.e., $t = \infty$, the integrals converge and Equation (2.29) becomes:

$$\sigma(t)/\varepsilon_o = E'(w)\sin(wt) + E''(w)\cos(wt) \quad , \tag{2.30}$$

$$\text{where } E'(w) = w \int_o^\infty E(\phi)\sin(w\phi)d\phi \tag{2.31}$$

$$E''(w) = w \int_o^\infty E(\phi)\cos(w\phi)d\phi \quad . \tag{2.32}$$

Note how the determination of the dynamic mechanical properties assumes a single-frequency harmonic input and conditions of steady state. In the discussion on the general methodology which follows, these limitations are not required.

The dynamic mechanical properties of a material may also be calculated by taking the Fourier transform of Equation (2.18), where it is assumed that the material starts from rest [61]:

$$\tilde{\sigma} = i\, w\, \tilde{E}\, \tilde{\varepsilon} \tag{2.33}$$

where the Fourier transform $\tilde{f}(w)$ of a function F(t) can be defined as [60]:

$$\tilde{f}(w) = \int_o^\infty F(t)\exp(-iwt)dt \tag{2.34}$$

Using Euler's formula, Equation (2.33) can be separated into its real and imaginary components as follows:

$$\tilde{\sigma}/\tilde{\varepsilon} = i\ w \int_0^\infty E(t)\exp(-iwt)dt = \tag{2.35}$$

$$w \int_0^\infty E(t)\sin(wt)dt + i\ w \int_0^\infty E(t)\cos(wt)dt\ . \tag{2.36}$$

Substituting Equations (2.31) and (2.32) into Equation (2.36) yields the desired result:

$$\tilde{\sigma}/\tilde{\varepsilon} = i\ w\ \tilde{E} = E'(w) + i\ E''(w) = E^*(w)\ , \tag{2.37}$$

$$\text{where } \tilde{\sigma}(w) = \int_0^\infty \sigma(t)\exp(-iwt)dt \tag{2.38}$$

and

$$\tilde{\varepsilon}(w) = \int_0^\infty \varepsilon(t)\exp(-iwt)dt\ . \tag{2.39}$$

Equations (2.38) and (2.39) represent the Fourier transforms of the stress and strain-time curves. Applying Euler's formula to Equations (2.38) and (2.39) yield Equations (2.40) and (2.41), respectively:

$$\tilde{\sigma}(w) = \tilde{\sigma}_s(w) - i\ \tilde{\sigma}_c(w) \tag{2.40}$$

$$\tilde{\varepsilon}(w) = \tilde{\varepsilon}_c(w) - i\ \tilde{\varepsilon}_s(w)\ , \tag{2.41}$$

$$\text{where } \tilde{\sigma}_s(w) = \int_0^\infty \sigma(t)\sin(wt)dt \tag{2.42}$$

$$\tilde{\sigma}_c(w) = \int_0^\infty \sigma(t)\cos(wt)dt \tag{2.43}$$

$$\tilde{\varepsilon}_s(w) = \int_0^\infty \varepsilon(t)\sin(wt)dt \tag{2.44}$$

$$\tilde{\varepsilon}_c(w) = \int_0^\infty \varepsilon(t)\cos(wt)dt\ . \tag{2.45}$$

In order to calculate $E'(w)$, $E''(w)$, $|E^*(w)|$ and tan δ, Equations (2.42-45) are combined to yield Equations (2.46-49):

$$E'(w) = \frac{\tilde{\sigma}_c(w)\tilde{\varepsilon}_c(w) + \tilde{\sigma}_s(w)\tilde{\varepsilon}_s(w)}{\tilde{\varepsilon}_c^2(w) + \tilde{\varepsilon}_s^2(w)} \qquad (2.46)$$

$$E''(w) = \frac{\tilde{\sigma}_s(w)\varepsilon_c(w) - \tilde{\sigma}_c(w)\tilde{\varepsilon}_s(w)}{\tilde{\varepsilon}_c^2(w) + \tilde{\varepsilon}_s^2(w)} \qquad (2.47)$$

$$|E^*(w)| = [E'(w)^2 + E''(w)^2]^{1/2} \qquad (2.48)$$

$$\tan \delta = E''(w)/E'(w) \qquad (2.49)$$

In this way E', E", $|E^*|$ and tan δ can be determined for any desired angular frequency w.

There are, however, several subtleties which should be noted in order to avoid erroneous results. Accordingly, care should be taken when choosing the frequencies at which the dynamic properties are to be calculated. First, the data collection rate of the stress and strain responses must be considered. In order to adequately calculate the dynamic mechanical properties at a given frequency, a sufficient number of data points should be collected so that a sine wave of that particular frequency can be adequately described. Clearly, higher collection rates will result in more accurate properties. Conversely, for a given data collection rate, the properties calculated at the lowest frequency will be the most accurate. As a general rule, the collection frequency should be ten times larger than the highest frequency to be calculated. Should high frequency

dynamic properties be desired and high data collection rates are not feasible, interpolation of the collected data is recommended.

The second subtlety concerns the numerical methods used to calculate the mechanical properties. Consider Equations (2.44) and (2.45) and a rapidly applied uniaxial pulse-strain deformation of magnitude ε_o. Mathematically this is equivalent to multiplying $\cos(wt)$ and $\sin(wt)$ by the constant ε_o. For pulse durations which are integer multiples of the frequency for which the properties are being calculated, the values for $\widetilde{\varepsilon}_c(w)$ and $\widetilde{\varepsilon}_s(w)$ will be equal to zero as will $\widetilde{\sigma}_c(w)$ and $\widetilde{\sigma}_s(w)$. For such deformations, the use of Equations (2.46-49) will result in the calculation of erroneous dynamic properties. These properties can be calculated, however, by resorting to higher moments of the stress and strain responses, as described below. In order to maximize the values of $\varepsilon_c(w)$ and $\varepsilon_s(w)$, the desired frequency or pulse duration should be chosen so as to result in an non-integer number of sine or cosine waves. Equation (2.50) states the criterion that should be employed when using uniaxial pulse-strain deformations. In order to obtain the highest degree of accuracy, one should choose parameters such that r = 0.5. While the choice of r = 0.5 is not fixed, the accuracy that one obtains decreases as r decreases.

$$p\, f_c = n + r \qquad (2.50)$$

where p = pulse duration, [sec]

f_c = desired frequency of calculated properties, [Hz]

n = integer

r = fractional part of a sine wave, $(0 < r < 1)$

In general, for a deformation of arbitrary shape, the integral of the product of $\varepsilon(t)$ and $\sin(wt)$ or $\cos(wt)$ will not be zero and Equation (2.50) can probably be disregarded. For the experiments described in section 2.4 below, which use uniaxial pulse-strain deformations, these considerations have been taken into account. The choice of the frequencies at which the dynamic properties are to be calculated and the pulse duration result in r = 0.4.

For deformations which result in $\tilde{\varepsilon}_c(w)$ and $\tilde{\varepsilon}_s(w)$ equal to zero, the dynamic mechanical properties of a material can still be recovered. The method involves the ratio of time-weighted moments of the stress and strain histories as described below. Differentiation of Equation (2.34) with respect to w yields:

$$d\tilde{\sigma}/dw = i\,\tilde{E}\,\tilde{\varepsilon} + i\,w\,\tilde{\varepsilon}(d\tilde{E}/dw) + i\,w\,\tilde{E}(d\tilde{\varepsilon}/dw)\ . \qquad (2.51)$$

Since $\tilde{\varepsilon} = 0$, the first and second terms of the right hand side of Equation (2.51) equal zero and simplifies Equation (2.51) to Equation (2.52).

$$d\tilde{\sigma}/dw = i\,w\,\tilde{E}(d\tilde{\varepsilon}/dw) \qquad (2.52)$$

It can be shown that expressions for $d\tilde{\sigma}/dw$ and $d\tilde{\varepsilon}/dw$ are given by Equations (2.53) and (2.54):

$$d\tilde{\sigma}/dw = - i \int_o^\infty t\sigma(t)\exp(-iwt)dt \qquad (2.53)$$

$$d\tilde{\varepsilon}/dw = - i \int_o^\infty t\varepsilon(t)\exp(-iwt)dt \ . \qquad (2.54)$$

Substitution of Equations (2.53) and (2.54) into Equation (2.52) yields the desired result:

$$E^*(w) = (d\tilde{\sigma}/dw)/(d\tilde{\varepsilon}/dw) = \frac{\int_o^\infty t\sigma(t)\exp(-iwt)dt}{\int_o^\infty t\varepsilon(t)\exp(-iwt)dt} \ . \qquad (2.55)$$

Hence, the dynamic mechanical properties can be calculated by evaluating the ratio of the time-weighted moments of the stress and strain transforms. For those deformation histories whose first time-weighted moment of strain equals zero, this method can be further generalized to yield the desired results. Repeated differentiation of Equation (2.33) with respect to w results in successively higher moments of stress and strain. This differentiation is continued until a non-zero time-weighted moment of $\tilde{\varepsilon}(w)$ is obtained. The generalized form for determining the dynamic mechanical properties is given by Equation (2.56).

$$(d^n\tilde{\sigma}/dw^n)/d^n\tilde{\varepsilon}/dw^n) = i\ w\ \tilde{E} = \frac{\int_o^\infty t^n\sigma(t)\exp(-iwt)dt}{\int_o^\infty t^n\varepsilon(t)\exp(-iwt)dt} \qquad (2.56)$$

It should be noted, however, that since these calculations utilize higher order moments of stress and strain, the resulting properties calculated from such information are subject to more inaccuracy.

Finally with regard to the path of deformation, a displacement which returns to its pre-deformation level must be used. Under these conditions, the assumption of linear viscoelasticity requires the stress to return to zero, and ensures that the integrals used in the above calculations are defined. Similarly, it should be noted that by virtue of the assumption of linear viscoelasticity, if $\tilde{\varepsilon}$ equals zero then $\tilde{\sigma}$ must also equal zero. For nonlinear viscoelastic materials this is not generally true. Thus, this technique can also be used as test for the linearity of a material. An identical approach can be used in the derivatives of Eeq, η, etc., when inputs having a total strain integral equal to zero are used.

2.3 Theory of Incremental Linear Elasticity

As mentioned, *in situ* mechanical studies of the solidification process have been limited to curing studies using dynamic mechanical methods. The data generated from these studies has been limited, especially with regard to the determination of engineering properties. In part, a more complete mechanical characterization requires knowledge of the stresses due to polymerization, temperature

fluctuations or solvent removal together with the corresponding volumetric changes associated with each of these processes. In this section the mathematics necessary to calculate the mechanical properties associated with the method of incremental elasticity are presented.

In the previous section it was shown that the technique of Impulse Viscoelasticity can be used to calculate the gelation time and temperature, equilibrium tensile modulus, steady state elongational viscosity, relaxation spectrum and dynamic mechanical properties of a curing resin. In order to further characterize the curing process it is desired to calculate properties such as the stress due to cure, shrinkage due to cure, stress due to temperature changes, thermal expansion coefficient and the glass transition temperature T_g. While these properties are changing as a result of polymerization, they will be assumed to have no viscoelastic character. This assumption is justified on the basis that the relaxation times associated with these properties are generally much less than the times associated with polymerization.

The equations of isotropic linear thermoelasticity [57], appropriately modified to include the volumetric changes associated with polymerization, can be written as:

$$Eeq \{ \varepsilon_{ij} - \delta_{ij} [\alpha(T_f - T_i) + \dot{\gamma}(t_f - t_i)] \} = (1 + \nu)\sigma_{ij} - \delta_{ij} \nu \sigma_{kk} \qquad (2.57)$$

where σ_{ij} = stress tensor

ε_{ij} = strain tensor

Eeq = equilibrium tensile modulus

v = Poisson's ratio

α = linear thermal expansion coefficient

$\dot{\gamma}$ = linear rate of polymerization shrinkage

T_i = initial temperature

T_f = final temperature

t_i = initial time

t_f = final time

δ_{ij} = Kronecker delta

Such an equation is valid only if all of the physical properties were constant. If these properties, i.e., Eeq, v, α and $\dot{\gamma}$ depend upon time, and linearity still applies, then Equation (2.57) should be written in incremental form. The equation for an aging, linear thermoelastic material written in differential form, is then given by Equation (2.62):

$$Eeq\ [\ d\varepsilon_{ij} - \delta_{ij}(\alpha dT - \dot{\gamma} dt)] = (1 + v)d\sigma_{ij} - \delta_{ij}\ v\ d\sigma_{kk} \qquad (2.58)$$

where Eeq, v, α and $\dot{\gamma}$ are dependent upon the particular polymerization history. The d preceding the ε, T, t and σ signifies the incremental or differential operator. The author has found that this linear incremental equation is an excellent approximation to the polymerization process.

Implicit in Equation (2.58) are the assumptions of a) incrementally linear elastic behavior, b) material isotropy,

c) history dependent elastic coefficients, d) no viscoelastic behavior such as creep or relaxation and e) volume changes induced by pressure, temperature and polymerization. Since Equation (2.58) is written for the most general deformation, it can be simplified for several special cases. For the case of simple shear (i = 1, j = 2) Equation (2.58) reduces to Equation (2.59):

$$d\sigma_{12} = Eeq\ d\varepsilon_{12} / (1 + \nu) = 2\ Geq\ d\varepsilon_{12}\ , \qquad (2.59)$$

where Geq is the equilibrium shear modulus. In a similar fashion, Equation (2.60) describes the uniaxial stress case (i = j = 1):

$$d\sigma_{11} = Eeq\ (d\varepsilon_{11} - \alpha dT + \dot{\gamma} dt)\ . \qquad (2.60)$$

For the equi-biaxial stress case (i = j = 1, 2) Equation (2.58) reduces to Equations (2.61) and (2.62):

$$d\sigma_{11} = Eeq\ (d\varepsilon_{11} - \alpha dT + \dot{\gamma} dt) / (1 - \nu) \qquad (2.61)$$

$$d\sigma_{22} = Eeq\ (d\varepsilon_{22} - \alpha dT + \dot{\gamma} dt) / (1 - \nu)\ . \qquad (2.62)$$

For the case of applied hydrostatic pressure P, Equation (2.58) reduces to Equation (2.63).

$$d\sigma_{kk} = -3dP = Eeq(d\varepsilon_{kk} - 3\alpha dT + 3\dot{\gamma} dt) / (1 - 2\nu) \qquad (2.63)$$

An experiment involving uniaxial deformation with superimposed pressure can provide information on cure shrinkage, thermal stress and Poisson's ratio as a function of the polymerization. Equation (2.64) describes the relationship between the cure parameters for such a deformation:

$$Eeq(d\varepsilon_{11} - \alpha dT + \dot{\gamma}dt) = d(\sigma_{11} - P) - (1 - 2\nu)dP \ , \quad (2.64)$$

where P is the superimposed pressure.

From these simplifications, it is clear that shear experiments yield the least information regarding the details of polymerization. In order to obtain information regarding the dimensional changes during polymerization, it is necessary to use deformations other than shear. Considering the difficulty in applying both hydrostatic pressure and uniaxial deformation, only the case of uniaxial deformation will be examined.

2.3.1 Cure Stresses

If Equation (2.60) is rewritten for conditions of constant strain and temperature, it is possible to calculate the one-dimensional stress due to cure using Equation (2.65):

$$\sigma_{11}(t_f) - \sigma_{11}(t_i) = \int_{t_i}^{t_f} Eeq(t')\dot{\gamma}(t')dt' \ . \quad (2.65)$$

The stress due to cure can be obtained experimentally by measuring the load of an isothermally curing sample held at constant strain. Similarly, one can calculate the linear post gelation shrinkage $\gamma(t)$ due to cure using Equation (2.66):

$$\gamma(t_f) - \gamma(t_i) = \int_{t_i}^{t_f} \frac{d\sigma(t')}{Eeq(t')} \ . \quad (2.66)$$

2.3.2 Thermal Stresses

For completely polymerized samples held at constant strain, the stress associated with temperature change may be calculated by simplifying Equation (2.60) to yield Equation (2.67).

$$\sigma_{1\,1}(T_f) - \sigma_{1\,1}(T_i) = - \int_{T_i}^{T_f} Eeq(T)\alpha(T)dT \qquad (2.67)$$

Knowing the equilibrium tensile modulus and the change in stress due to temperature, the linear thermal expansion coefficient of the sample can also be calculated by properly reducing Equation (2.60) to Equation (2.68).

$$\alpha(T) = \frac{-1}{Eeq(T)} (d\sigma_{1\,1}/dT) \qquad (2.68)$$

Assuming that the coefficient $Eeq(T)\alpha(T)$ changes magnitude as the material goes from the the rubbery to the glassy state, it is possible to determine the glass transition temperature T_g, as well.

2.4 Experimental

This section describes the apparatus and basic collection information used in conjunction with the Impulse Viscoelastic method. The experimental techniques used to follow the curing process of the thermosetting systems presented in this dissertation are highlighted.

In order to characterize a large extent of the cure process it was necessary to find a sample substrate which did not dominate the measured loads. For this purpose, Vratsanos and Farris developed a simple and novel method for obtaining the uniaxial mechanical properties during solidification [62]. A rubber membrane sample assembly was used to physically constrain a monomer in a uniaxial geometry. This geometry was chosen because it is sensitive to the dimensional changes of a material during cure. In order to prepare a sample the closed end of a soft rubber cylindrical balloon (Imperial Toy Corp., Los Angeles, CA) was cut off so as to form a uniform rubber tube. The ends of the tube were stretched over two aluminum tabs and held in place with hose clamps. The lower tab was solid aluminum while the upper tab had a 1/4" hole drilled through its center. The sample assembly was filled with monomer through this hole. Figure 2.3 is a photograph of the components involved in specimen preparation, including an assembled sample. The cured samples were typically 25 mm in length and 6 mm in diameter. A photograph of the cured samples is shown in Figure 2.4. These sample dimensions were chosen so that deformations could be applied in the glassy state without exceeding the 10 kg load cell capacity of the Dynastat mechanical spectrometer (Imass, Inc., Hingham, MA) used for testing. It was found in other studies that the contribution of the rubber tube sample support to the

Figure 2.3. Photograph of the components involved in specimen preparation, including an assembled sample.

Figure 2.4. Photograph of the cured samples.

overall mechanical response was quickly dominated by the sample after gelation for curing systems [62].

Once the rubber membrane sample assembly was filled it was placed within the environmental chamber of the Dynastat. This environmental chamber has a temperature range of -150 to 280° C and offers a wide range of programming capabilities suitable for the study of most polymers. The Dynastat can perform deformations in load control or displacement control mode. Both a low range (5×10^{-5} m/V) and a high range (5×10^{-4} m/V) displacement transducer are available on the Dynastat. All of the experiments discussed in this dissertation were performed in displacement control using the low range displacement transducer. After fixing the sample within the chamber, the weight of the sample was balanced to zero. The sample was then stretched so as to form a uniform, slender cylindrical, dumbbell-shaped specimen. In most cases, the load required to stretch the rubber sample assembly was balanced off to zero prior to the collection of data. Using the Dynastat's displacement control mode, uniaxial step-strain deformations were applied to the sample in order to characterize the solidification process. This choice of deformation is based upon the fact that such "abrupt" changes in strain yield higher order information more accurately than smooth deformations. At this time, it is useful to examine the response of four basic material classes to a uniaxial pulse strain

deformation. The predicted responses of a newtonian liquid, viscoelastic liquid, viscoelastic solid, and elastic solid are very different and are shown in Figure 2.5a-d. It is possible to surmise something about the nature of a material by merely examining its stress response to this deformation. These four material responses demonstrate the range of responses which may be observed during the curing of a single sample. A timer located on the Dynastat allowed the operator to periodically apply deformations. Although the Dynastat can apply sinusoidal or step-strain deformations in a tensile mode, it has the capability to apply other deformation waveforms using an external function generator as an input. By applying these deformations periodically it was possible to monitor the solidification history. Between 50 and 200 pulse deformations were used to characterize the solidification experiments presented in this dissertation.

For each pulse, analog signals of the sample displacement, load and temperature were collected at an operator selected rate and duration. For most materials, a data collection frequency of 10 Hz was found to be adequate. For the experiments described in this dissertation, pulse durations of 10-100 seconds were used and pulse data were collected for periods of 40-600 seconds. The analog data were digitized by a 16 bit Digital Equipment Corporation (DEC) (Maynard, MA) Analog Data module and stored on the

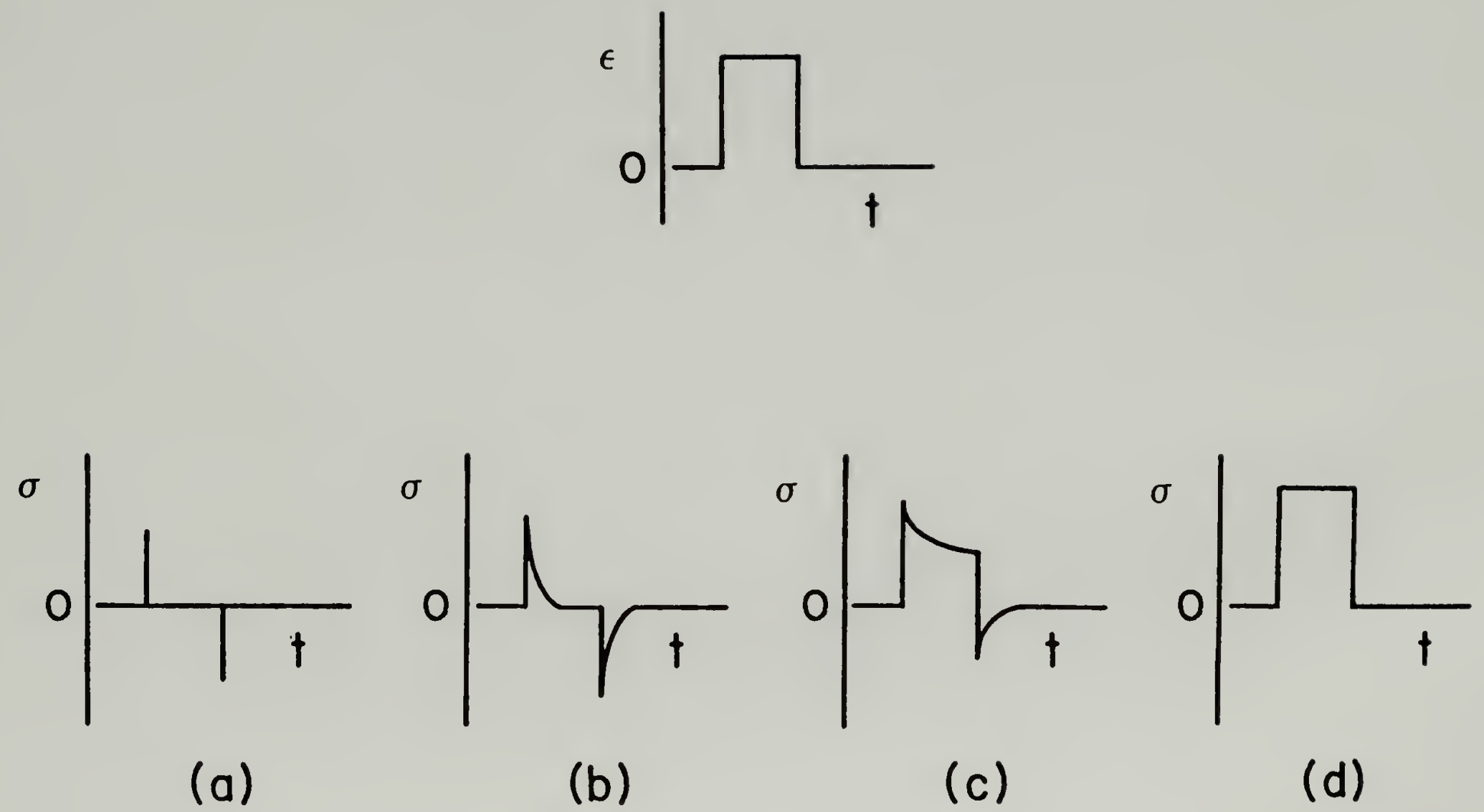

Figure 2.5. Stress response to a uniaxial pulse-strain deformation for a) a newtonian liquid, b) a viscoelastic liquid, c) a viscoelastic solid and d) an elastic solid.

hard disk of a DEC PRO 380 computer. A block diagram of the experimental apparatus is given in Figure 2.6.

Having collected a series of pulse deformations it is possible to calculate the Impulse Viscoelastic properties of interest. Baselines for the load (or stress) and displacement (or strain) signals were determined for each pulse by fitting a straight line through ten points just before the deformation and at the end of the data collection period. The two sets of points which were used to determine the baselines are shown in Figure 2.7 by the open circles. This method of determining baselines requires that the operator collect data for a period of time sufficient for the stress to return to its pre-deformation level. As a result, intuition on the part of the operator to judge the viscoelastic character of a material at a given time is required.

Having determined the load and displacement baselines, it is necessary to define the end of the pulse experiment. Since displacement-controlled deformations were used, the end of the pulse was determined by the return of the load (or stress) signal to its pre-deformation level. The software developed for the determination of the pulse end compares the load signal (in volts) with that of the baseline level (in volts) for each increment in time over the entire data collection period. When the difference between these two voltages is equivalent to the noise level

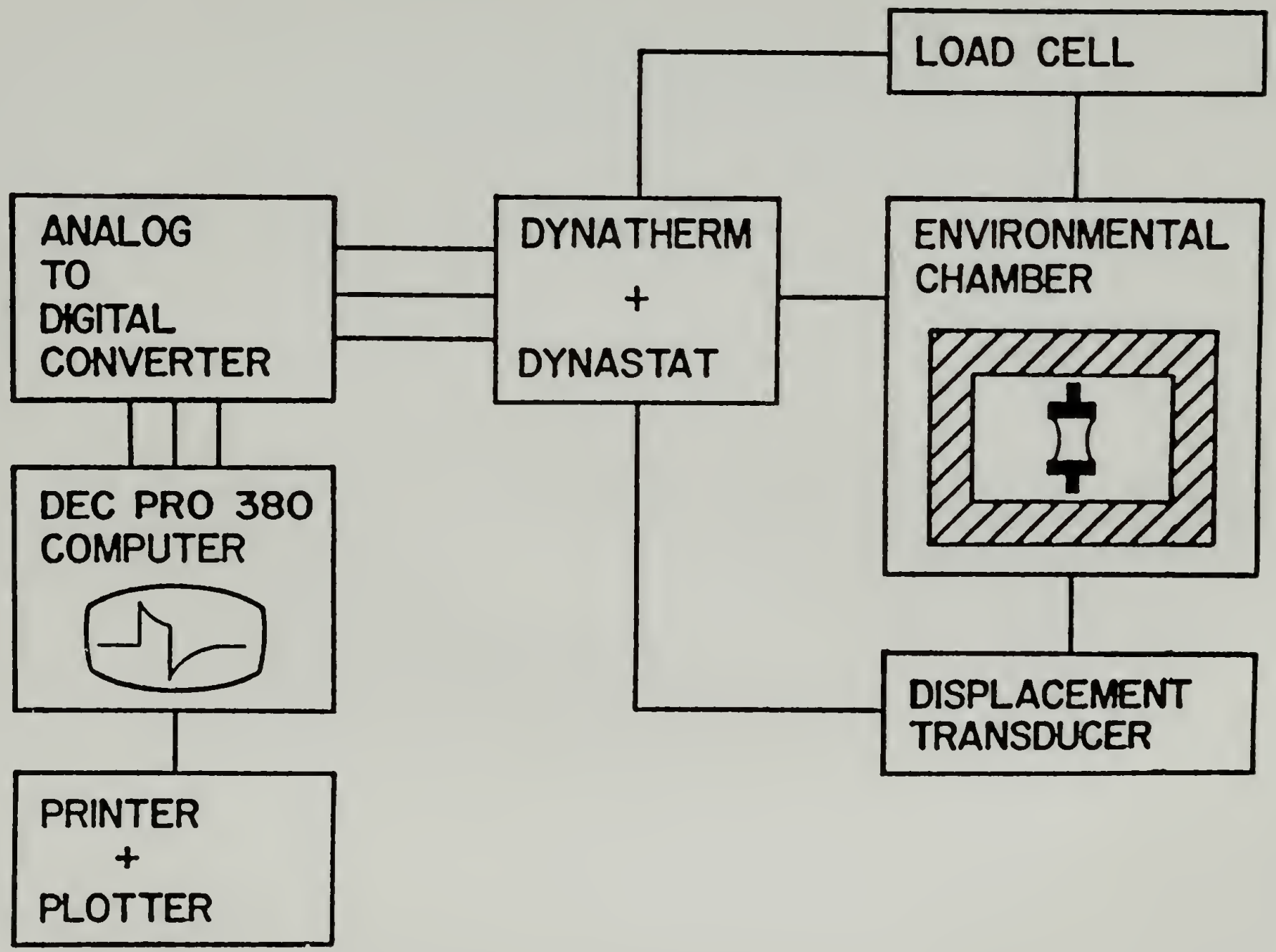

Figure 2.6. Experimental block diagram of the apparatus used with the Impulse Viscoelastic method.

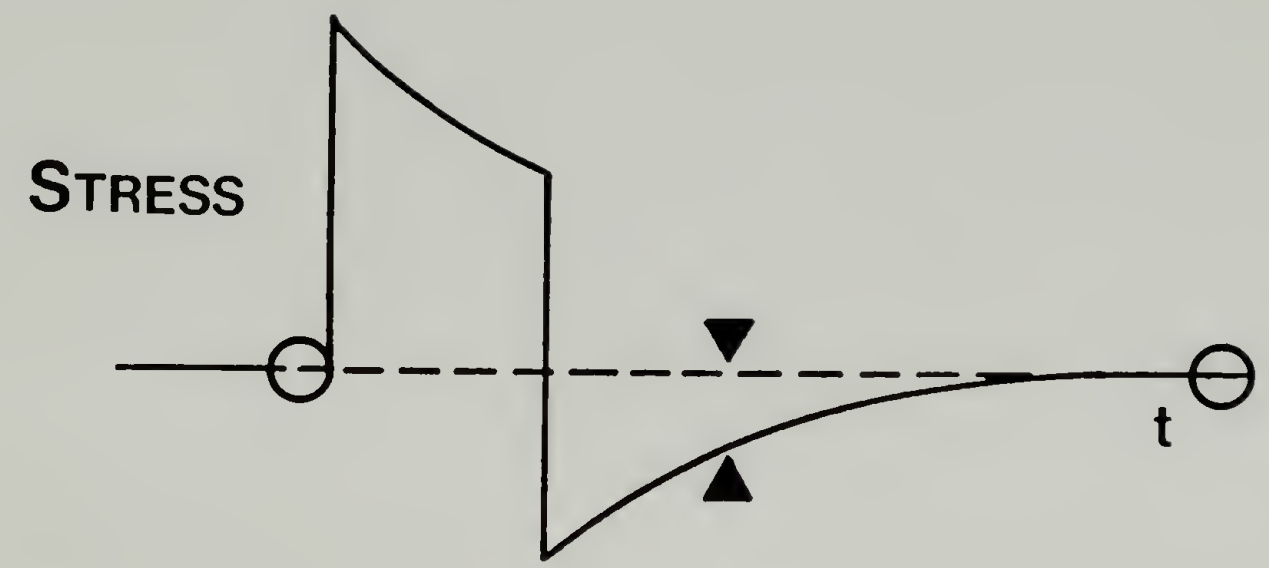

Figure 2.7. Schematic of the method used to determine the pulse baselines (dashed line between the points inside the open circles) and the time defined as the end of the pulse experiment (when the distance between the solid arrows is smaller than the voltage tolerance).

of the instrumentation (typically 3-5 mV), then the end of the pulse has been found. This difference in voltages is shown graphically on Figure 2.7 as the distance between the solid arrows. Since the noise level can depend upon the experimental conditions, the operator must specify a voltage which reflects the noise level. This voltage is referred to in the software as the voltage tolerance. After determining the pulse start and end times the equations presented earlier in this chapter were used to calculate the various mechanical properties. By sequentially combining the information generated from each pulse, it was possible to construct composite plots of the above-mentioned properties. All of the software regarding the Impulse Viscoelastic technique was written in-house, making it possible for it to be modified as needed. A summary of the software used to collect, analyze and display the data appears in Appendix I.

2.5 Results

Having presented some of the experimental aspects of the Impulse Viscoelastic method, two examples of its application are discussed. First is the temperature-induced gelation of a poly(γ-benzyl-L-glutamate) solution. Second is a comparison of dynamic mechanical method with the Fourier transform method for calculating dynamic mechanical properties of a fully cured epoxy.

2.5.1 Gelation of Poly(-benzyl-L-glutamate)

In order to demonstrate an application of the Impulse Viscoelastic method to the solidification process, data on the gelation of a 10 weight % solution of poly(γ-benzyl-L-glutamate) (PBLG) in benzyl alcohol are presented. This polypeptide is known to gel thermoreversibly [63,64]. A rubber membrane sample assembly was prepared as described in section 2.4 and placed within the environmental chamber of the Dynastat where the sample was heated to 70° C. At this temperature the PBLG solution is a fluid of low viscosity. The sample was held at constant strain and cooled at a programmed rate of 1° C/min until reaching 40° C where it was held for 30 minutes and then cooled to room temperature. Starting at 70° C, pulse data were collected for 40 seconds at a rate of 10 Hz. Uniaxial pulse deformations of 10 seconds duration were applied to the sample every 140 seconds. A voltage tolerance of 0.003 V was used to reduce the collected data. Initially a strain amplitude of 1.8% was applied and decreased during solidification in order to maintain linear viscoelastic conditions. Figure 2.8 is a series of four pulse deformations taken from various portions of the PBLG solidification experiment. Specifically, Figure 2.8a is a pulse taken 10 minutes into the experiment, prior to gelation, and illustrates the contribution of the rubber membrane used to support the

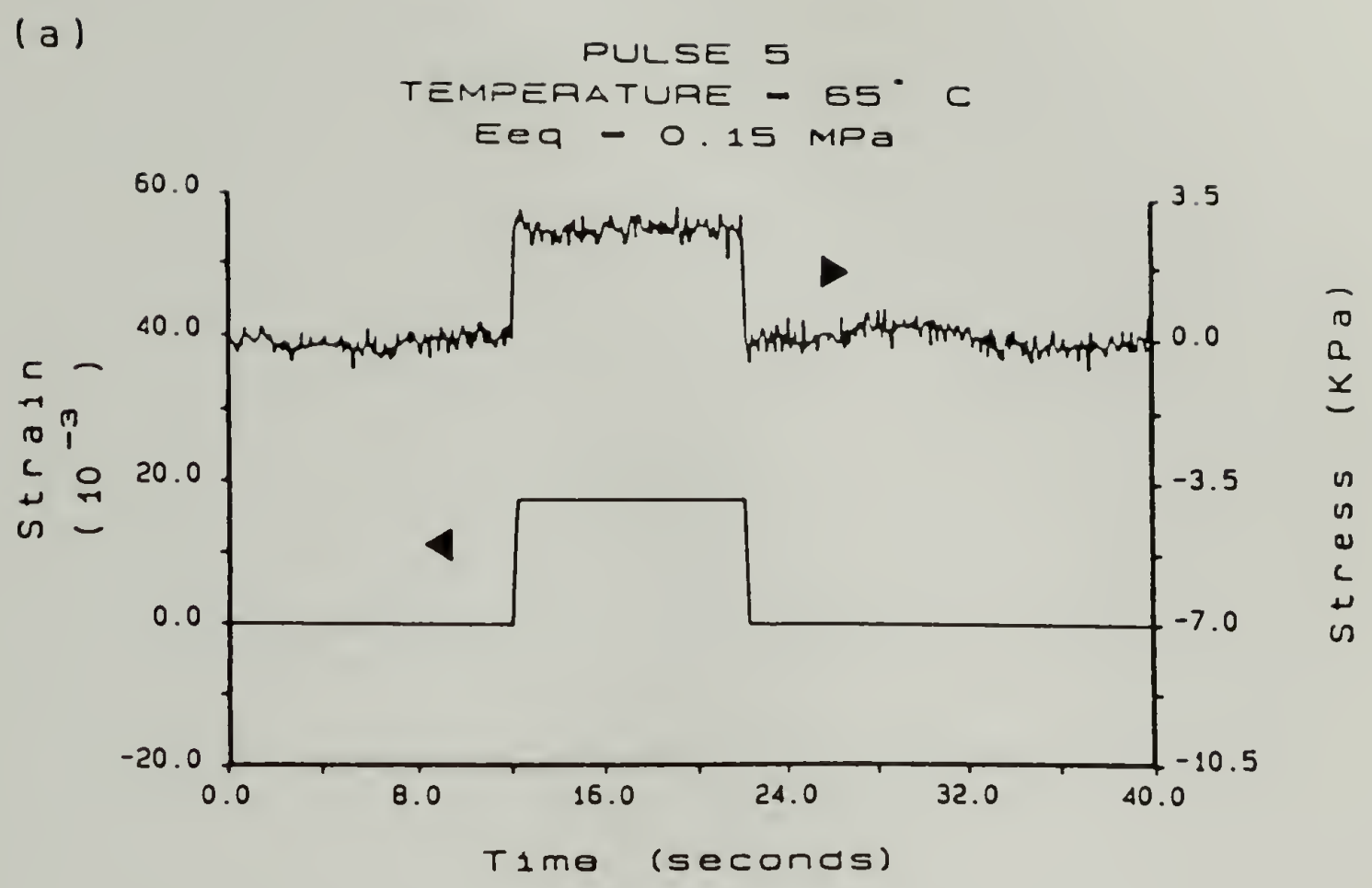

Figure 2.8. Stress response to a uniaxial pulse-strain deformation for a 10 wt % solution of PBLG in benzyl alcohol during solidification at a) 10 minutes (prior to gelation), b) 56 minutes (just after gelation) (continued on next page)

(c)

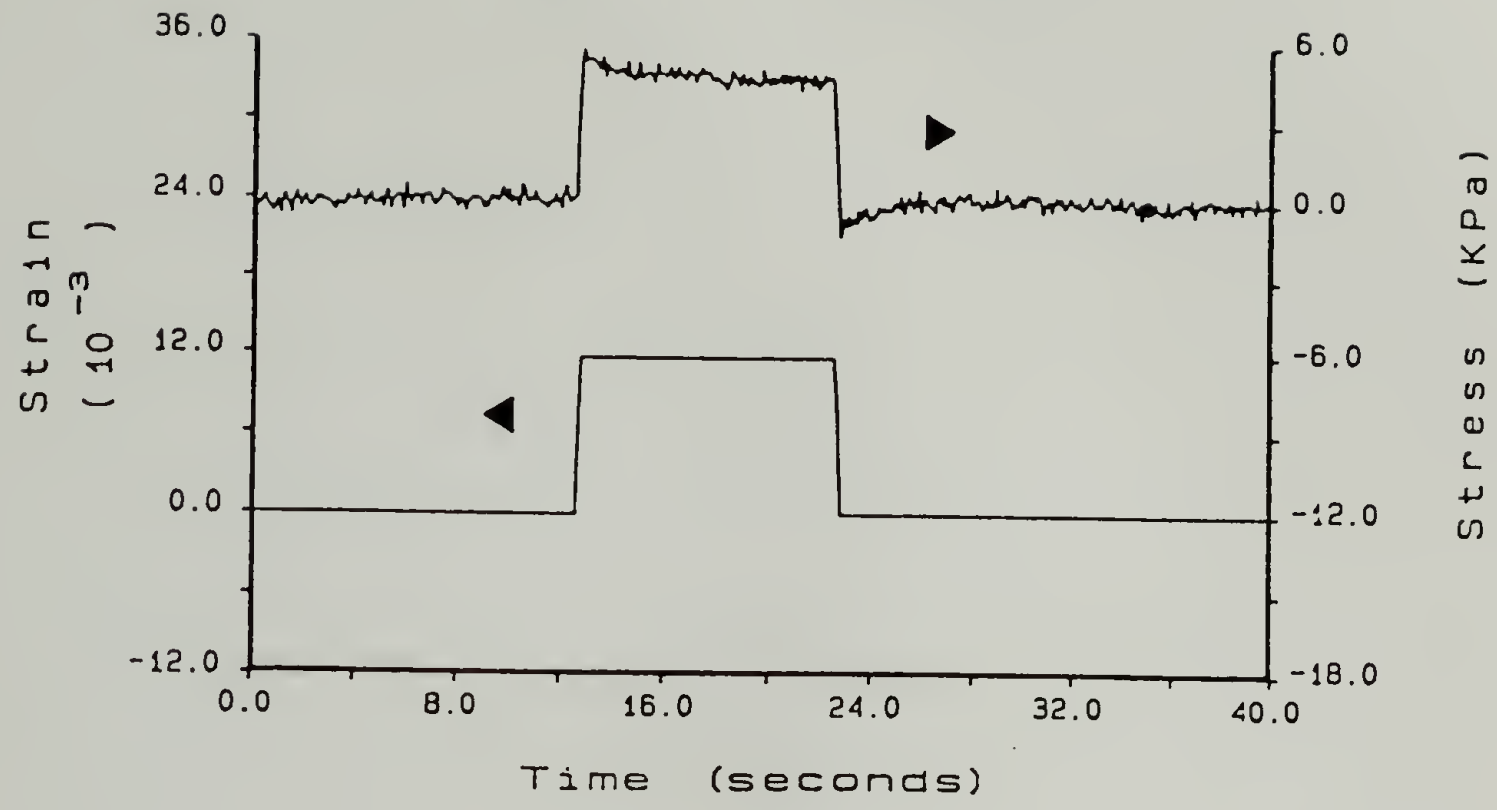

(d)

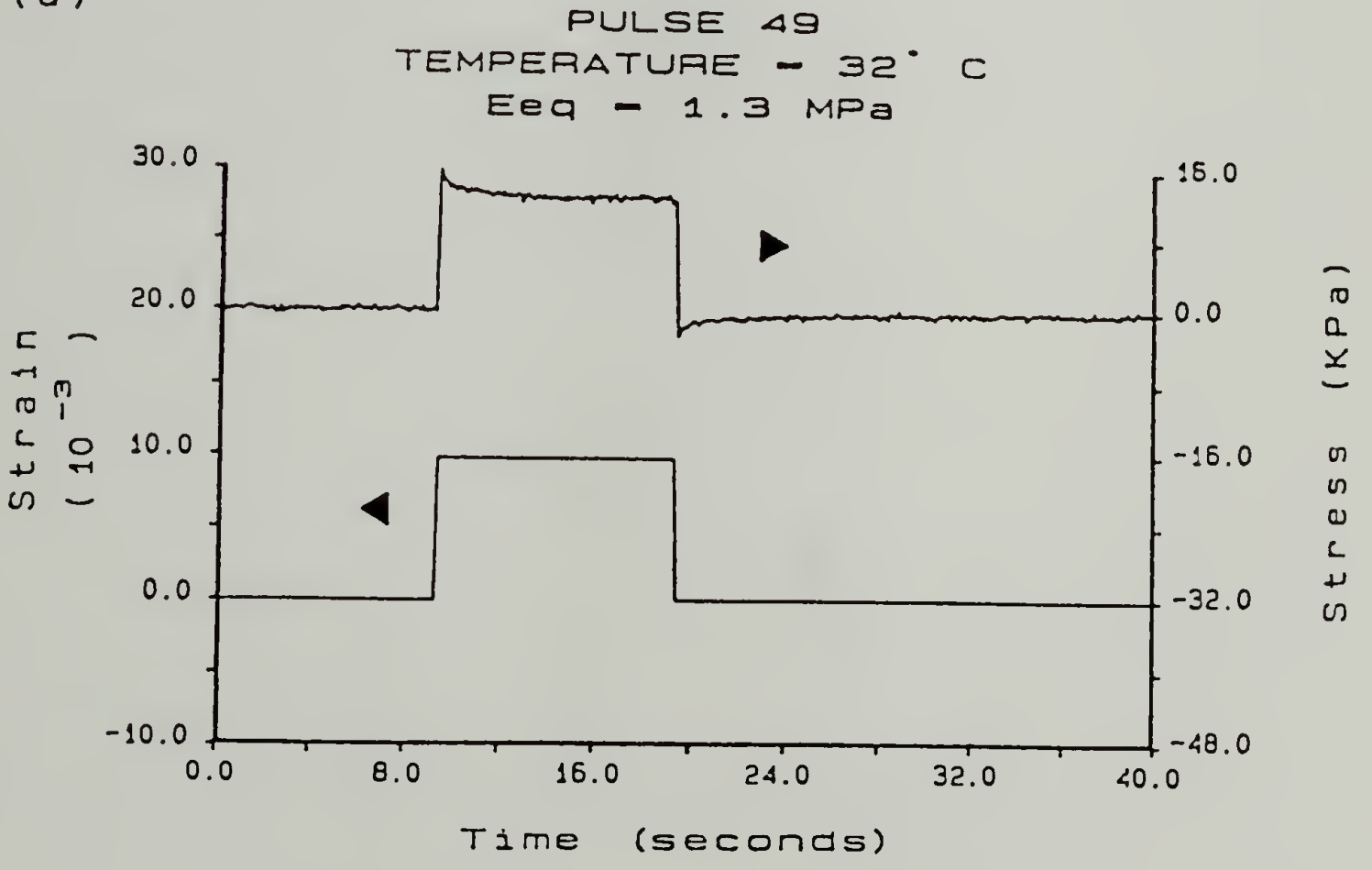

Figure 2.8 (cont). Stress response to a uniaxial pulse-strain deformation for a 10 wt % solution of PBLG in benzyl alcohol during solidification at c) 75 minutes and d) 112 minutes.

sample in a uniaxial geometry. The noise level in the stress signal is due to the greatly expanded scale. Figure 2.8b is a pulse 56 minutes into the experiment, shortly after gelation, and indicates nearly elastic mechanical behavior. Figures 2.8c and d are pulse deformations applied at 75 and 112 minutes, respectively, into the solidification and indicate increasingly viscoelastic behavior. It should be noted that the degree of viscoelastic behavior for this sample, as indicated by the magnitude of stress relaxation after the imposition of deformation, was much smaller than that observed for many other materials. On each plot the pulse number, temperature and equilibrium tensile modulus (Eeq) are included. Figure 2.9 combines the Eeq data obtained from each pulse in sequential fashion making it possible to view the behavior of Eeq as a function of time and temperature.

2.5.2 Comparison of Dynamic Mechanical and Fourier Transform Methods

In order to further investigate the validity of the Impulse Viscoelasticity Fourier transform approach to the calculation of dynamic mechanical properties, a cured epoxy was chosen as a sample for the purposes of comparing the traditional dynamic mechanical approach with the Fourier transform approach. Specifically, Epon 828, a diglycidyl ether of bisphenol-A (DGEBA) epoxy resin was cured for one

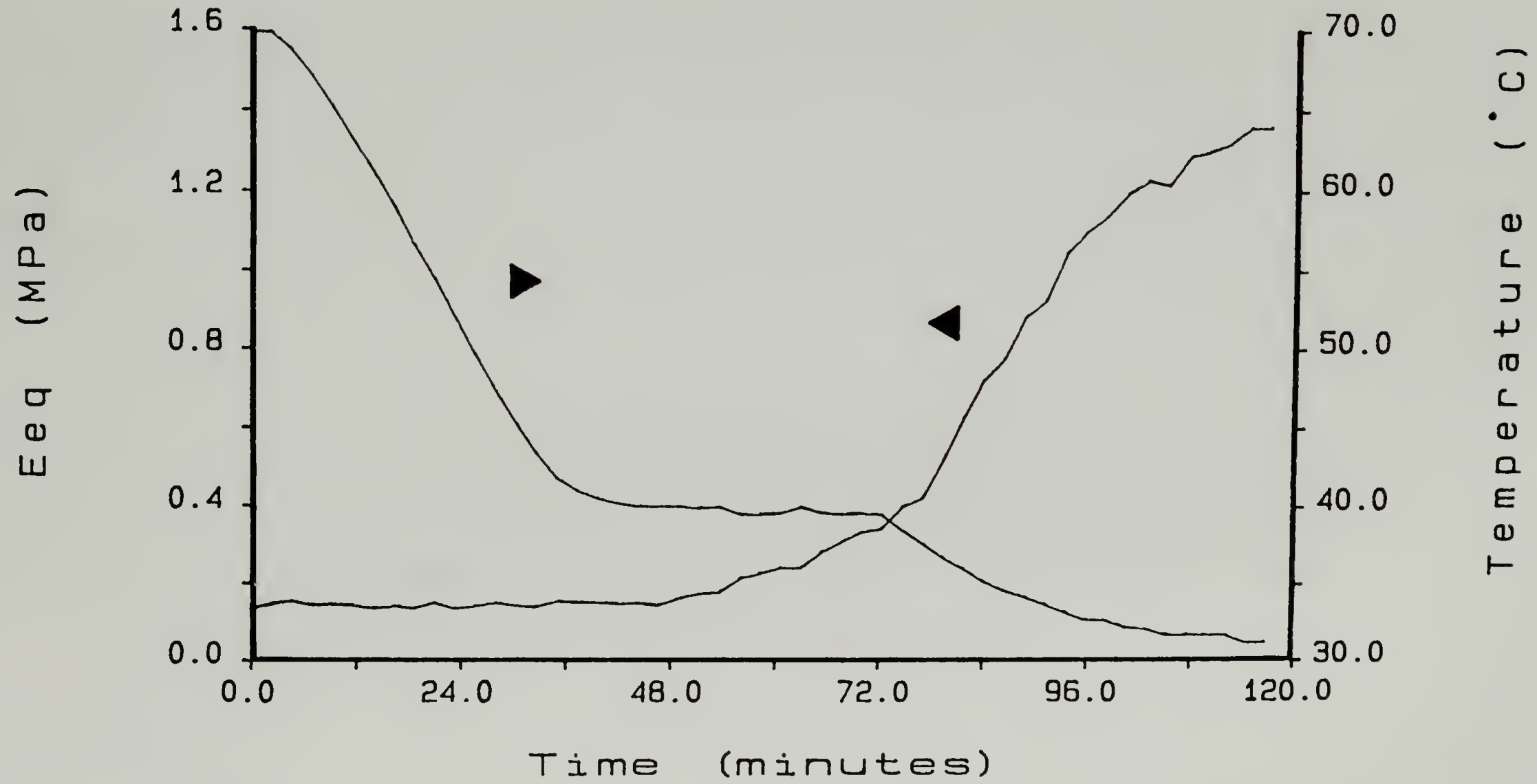

Figure 2.9. Equilibrium tensile modulus (Eeq) for a 10 wt % solution of PBLG in benzyl alcohol as a function of temperature and solidification time.

hour at 115° C with a stoichiometric amount of polyamide polyamine V-40. The chemical structure of V-40 is primarily a flexible methylene backbone containing both primary and secondary amine functionalities [65-67]. Both the Epon 828 and V-40 materials were obtained from the Shell Chemical Co. (Houston, TX). Based upon Impulse Viscoelastic curing studies on this sample, these conditions resulted in a fully cured sample [68]. In this way, measurements could be made without the complication of continued polymerization.

Sinusoidal deformations in a uniaxial mode were conducted at frequencies of 0.12, 0.52 and 0.92 Hz on the Dynastat. Measurements were made in the displacement control mode using the low range displacement transducer. $|E^*|$, E', E" and tan δ based upon dynamic deformations were calculated by the Dynastat's microprocessor using standard methods.

Approximately one minute after the dynamic testing was complete, a uniaxial pulse-strain deformation of twenty seconds duration was applied to the sample. Analog signals of the stress and strain were collected and digitized at a rate of 10 Hz. At this data collection frequency, this corresponds to 83, 19 and 11 points per sine wave for the 0.12, 0.52 and 0.92 Hz frequencies, respectively. Data collection began ten seconds prior to the uniaxial deformation and continued for 100 seconds. Because of fast sample relaxation at the higher temperatures, the data

collection period was reduced to 50 seconds. The numerical calculations indicated in the previous section (Equations (2.46-53)) were then used to determine $|E^*|$, E', E" and tan δ at 0.12, 0.52 and 0.92 Hz using simple quadrature integration routines to approximate the Fourier integrals, e.g., Simpson's rule, and a voltage tolerance of 0.005 V. As mentioned, these frequencies were specifically chosen to avoid the numerical complications associated with uniaxial pulse-strain deformations.

For both modes of deformation, sample strain was kept small (< .05%) in order to help assure conditions of linear viscoelasticity. Two measurements were made at 30, 40, 50, 60, 70, 75, 80, 90, 100, 110 and 115° C. Temperature was controlled to ± 0.1° C. Prior to deformation the samples were allowed to reach thermal equilibrium.

Figure 2.10 plots the storage modulus E' at 0.12 Hz as calculated by the Dynastat as a function of temperature for the cured epoxy sample. From such data, a T_g of 85-90° C can be estimated. This value is approximately 10° C higher than that obtained by Impulse Viscoelastic measurements studying the polymerization and subsequent cooling of similar specimens [68]. Those data are based on Eeq which is the limit of E'(*w*) as *w* approaches 0. This increase in T_g is attributed to the frequency dependence of T_g.

Figures 2.11a-e plot the stress response to uniaxial deformation for the epoxy sample at temperatures of 30, 50,

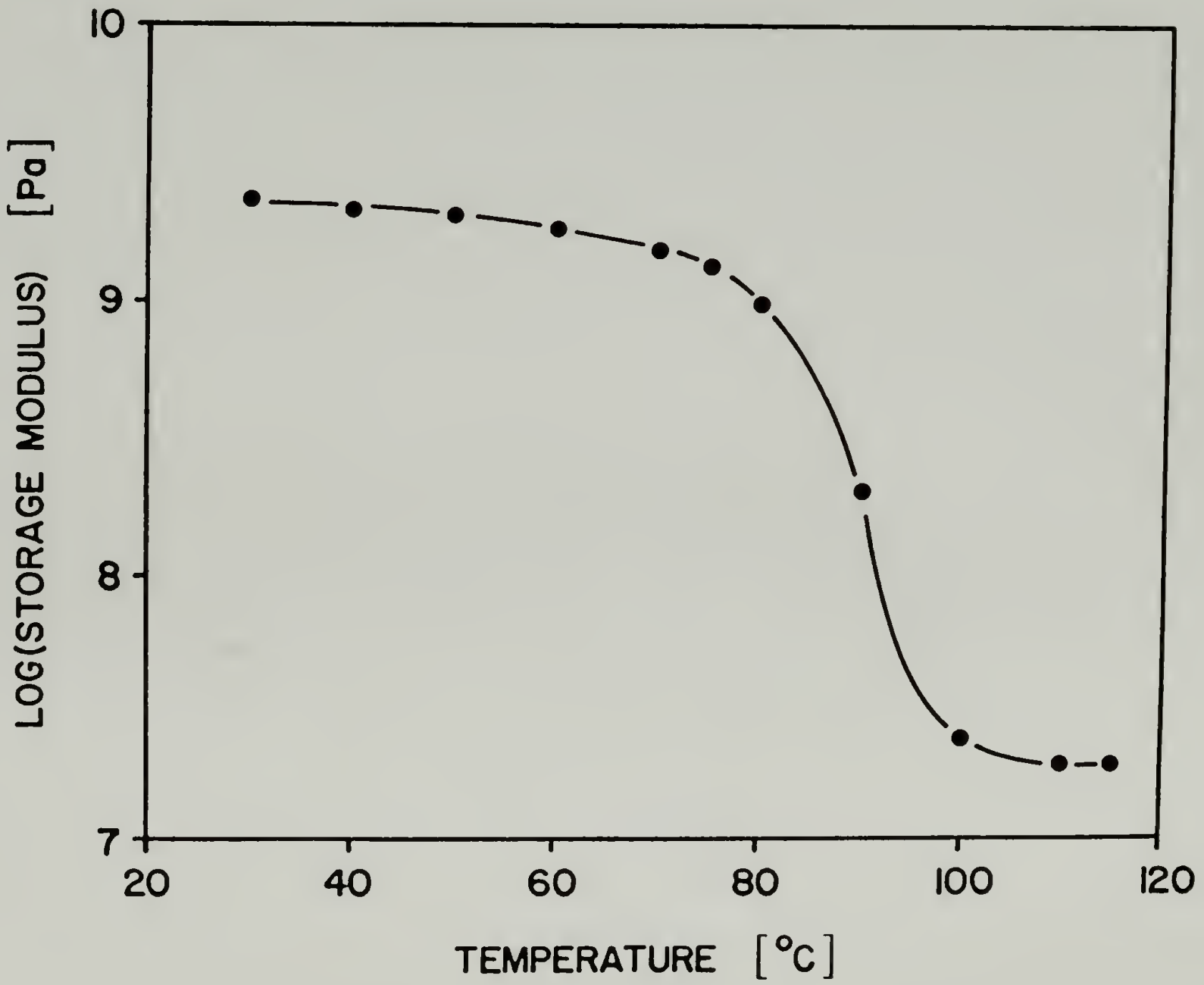

Figure 2.10. Log(storage modulus E') at 0.12 Hz as a function of temperature for a cured V-40/Epon 828 epoxy. The figure was generated from data based upon dynamic deformations.

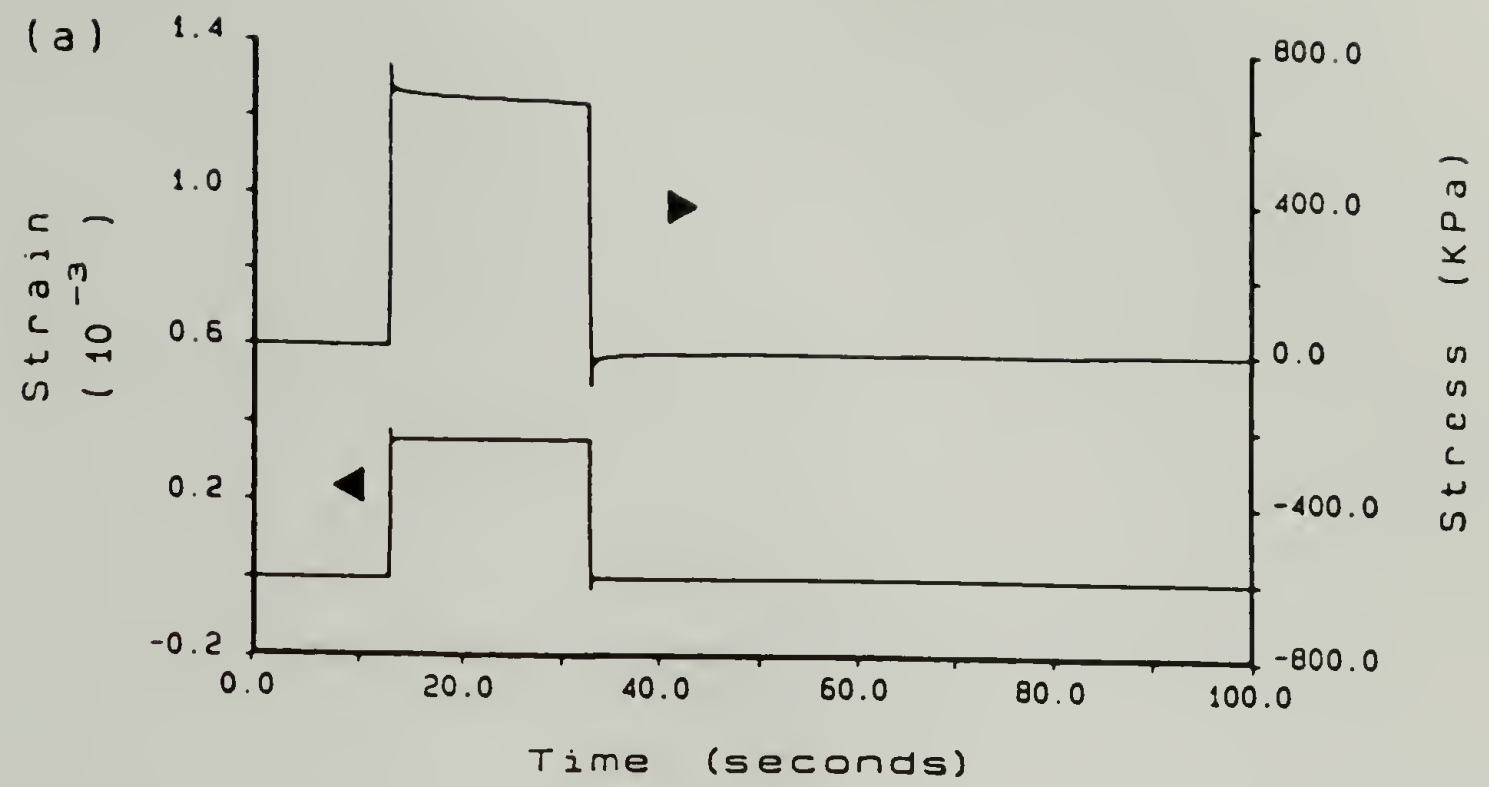

Figure 2.11. Stress response to a uniaxial pulse-strain deformation for a cured V-40/Epon 828 epoxy sample at a temperature of a) 30, b) 50° C **(continued on next page)**

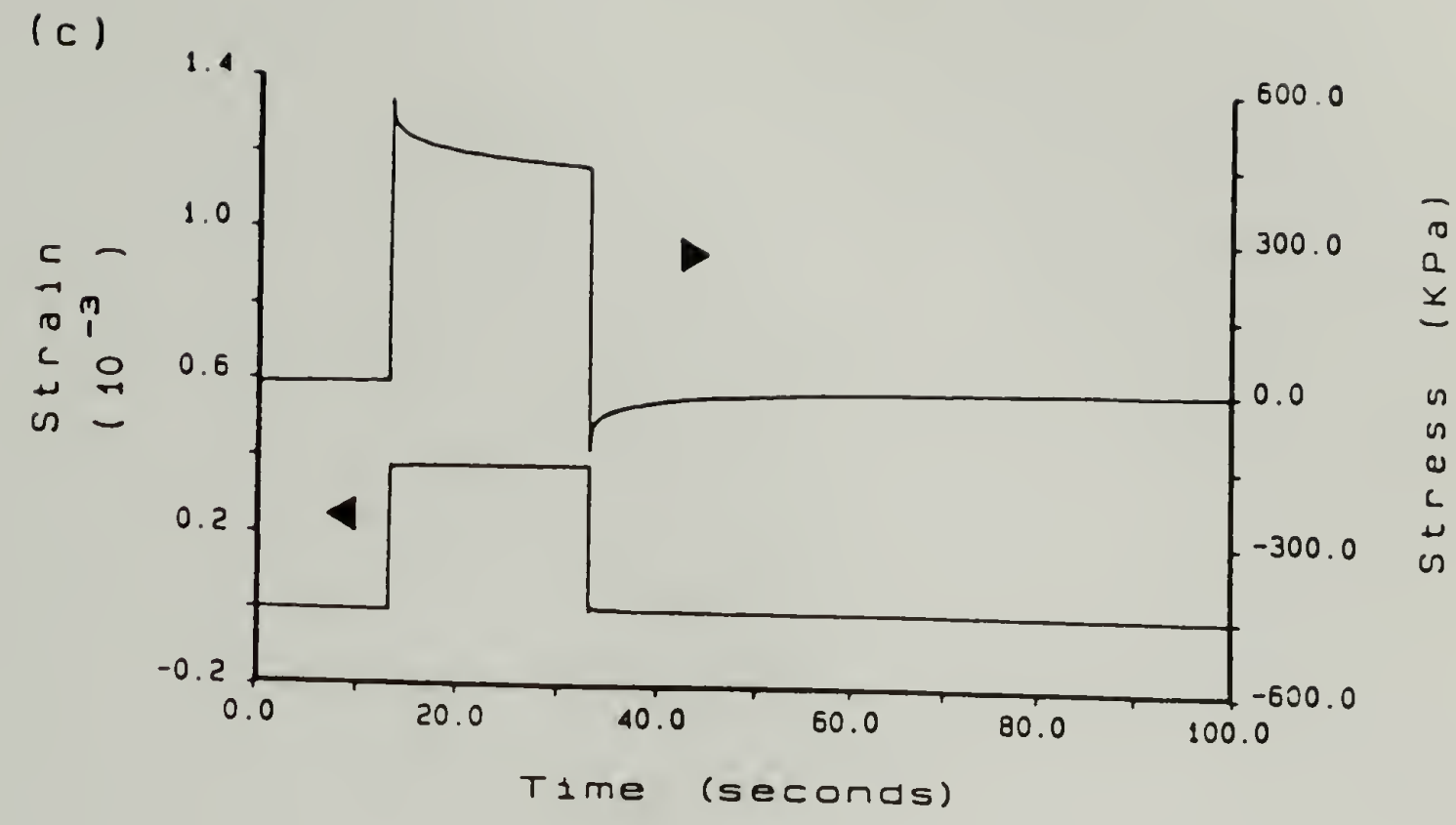

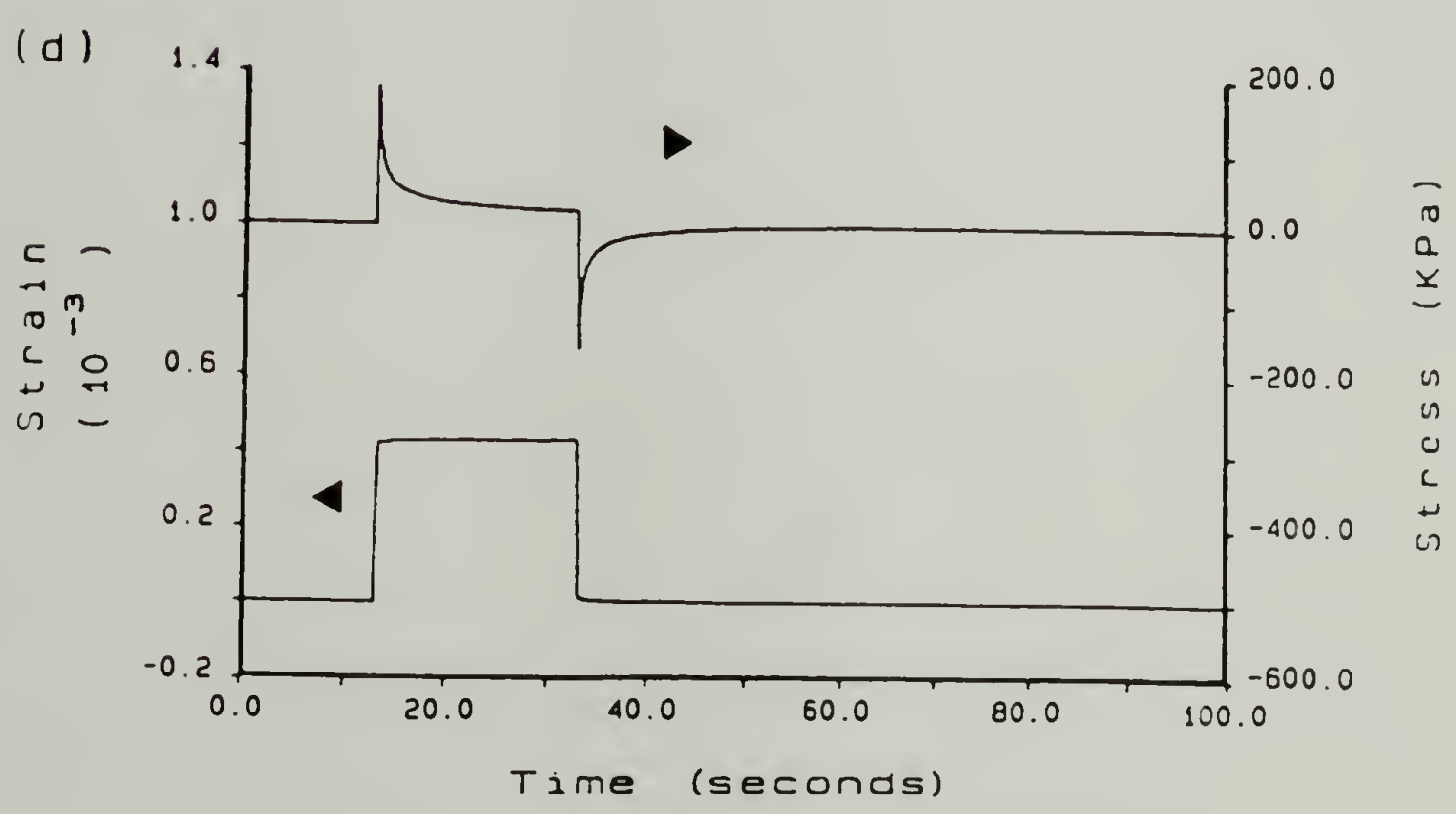

Figure 2.11 (cont). Stress response to a uniaxial pulse-strain deformation for a cured V-40/Epon 828 epoxy sample at a temperature of c) 70, d) 90° C (continued on next page)

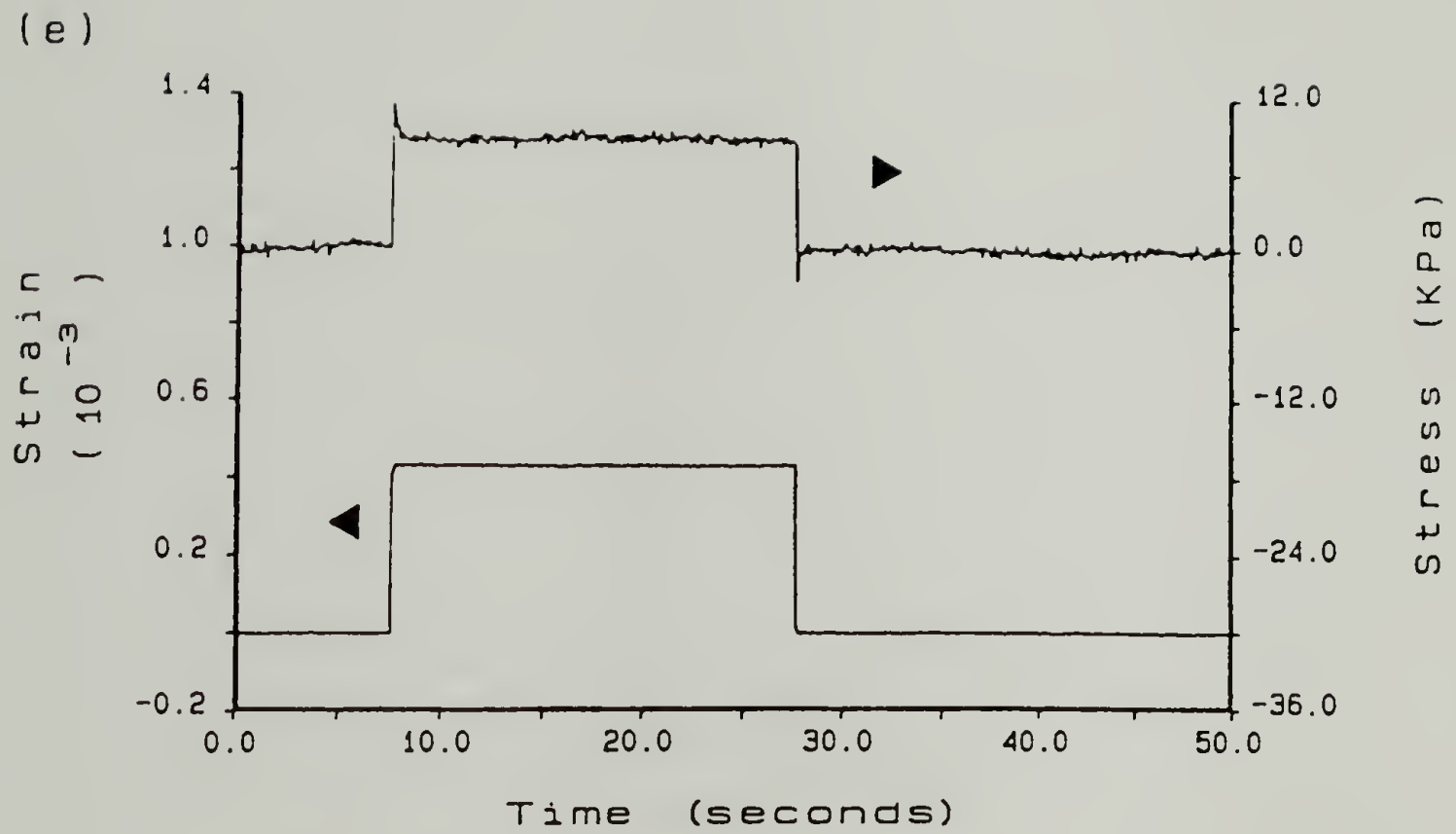

Figure 2.11 (cont). Stress response to a uniaxial pulse-strain deformation for a cured V-40/Epon 828 epoxy sample at a temperature of e) 110° C.

70, 90 and 110° C, respectively. In each of these figures the stress relaxation during the deformation pulse is indicative of the viscoelastic nature of the material. The slow relaxations in stress shown in Figures 2.11a and b are evidence for the relatively long relaxation times associated with the glassy state. As T_g is approached there is a trend towards increasingly viscoelastic behavior. This increase in viscoelastic behavior can be seen on Figures 2.11c and d. About 20° C above T_g the sample behaved almost elastically, as evidenced by Figure 2.11e.

Table 2.1 compares the dynamic data generated by both methods at all three frequencies for all temperatures. The agreement between the two methods appears to be excellent over the entire range in mechanical behavior. A comparison of both methods for $|E^*|$ and E' indicates differences of less than 6% over the entire temperature range. Because of the good agreement it was deemed that the differences in mechanical properties would not appear clearly on a figure. It should be noted that the results presented in Table 2.1 are the average of two measurements at each condition. It should be noted that the accuracy of the data presented in Table 2.1 is unrealistic. It is included for the purposes of data comparison only. In general, the sample to sample variations for the data obtained via dynamic methods were smaller than those obtained by the Fourier transform method.

Table 2.1

Comparison of Dynamic Mechanical Data Using Dynamic Mechanical and Fourier Transform Methods

Temp [°C]	Prop.	Dynamic Mechanical Method 0.12 Hz	0.52 Hz	0.92 Hz	Fourier Transform Method 0.12 Hz	0.52 Hz	0.92 Hz
30	|E*|	2376	2433	2452	2405	2460	2471
	E'	2375	2432	2451	2404	2459	2469
	E"	65	58	56	60	71	82
	Tan δ	0.027	0.024	0.023	0.025	0.029	0.033
40	|E*|	2201	2262	2289	2227	2280	2295
	E'	2200	2261	2288	2226	2278	2294
	E"	70	64	62	62	70	55
	Tan δ	0.032	0.028	0.027	0.028	0.031	0.024
50	|E*|	2033	2094	2126	2058	2125	2143
	E'	2032	2093	2125	2057	2124	2142
	E"	74	71	67	62	67	56
	Tan δ	0.036	0.034	0.031	0.030	0.032	0.026
60	|E*|	1842	1912	1946	1860	1931	1955
	E'	1840	1911	1944	1858	1929	1953
	E"	88	79	76	80	72	70
	Tan δ	0.048	0.041	0.039	0.043	0.037	0.036
70	|E*|	1558	1654	1687	1575	1632	1671
	E'	1554	1651	1684	1572	1629	1669
	E"	112	99	93	102	89	75
	Tan δ	0.072	0.060	0.055	0.065	0.055	0.045
75	|E*|	1325	1444	1485	1357	1439	1543
	E'	1317	1438	1481	1350	1433	1538
	E"	141	125	116	135	130	128
	Tan δ	0.11	0.087	0.078	0.10	0.091	0.083
80	|E*|	985	1138	1190	993	1131	1162
	E'	969	1126	1181	978	1123	1152
	E"	176	160	152	174	135	150
	Tan δ	0.18	0.14	0.13	0.18	0.12	0.13
90	|E*|	199	329	388	197	319	360
	E'	166	292	351	166	283	321
	E"	108	153	165	106	146	161
	Tan δ	0.65	0.52	0.47	0.64	0.52	0.50

Table 2.1 (cont.)

Comparison of Dynamic Mechanical Data Using Dynamic Mechanical and Fourier Transform Methods

Temp [°C]	Prop.	Dynamic Mechanical Method 0.12 Hz	0.52 Hz	0.92 Hz	Fourier Transform Method 0.12 Hz	0.52 Hz	0.92 Hz
100	|E*|	25.0	39.0	48.4	25.1	34.0	38.3
	E'	24.3	33.5	40.1	23.6	30.3	33.2
	E"	7.6	20.0	27.2	8.6	14.5	18.7
	Tan δ	0.31	0.60	0.68	0.36	0.48	0.56
110	|E*|	19.5	20.3	21.1	19.3	20.7	19.7
	E'	19.5	20.2	20.9	19.3	20.6	19.7
	E"	0.49	2.4	3.3	0.59	*	1.5
	Tan δ	0.025	0.12	0.16	0.031	*	0.075
115	|E*|	19.6	19.8	20.1	18.5	18.4	21.2
	E'	19.6	19.8	20.1	18.5	18.4	21.2
	E"	0.13	0.88	1.2	0.43	*	*
	Tan δ	0.0066	0.044	0.061	0.023	*	*

The values for |E*|, E' and E" are in units of MPa.
The asterisks (*) represent negative numbers.

The differences between the dynamic data and the Fourier transform data in the glassy state could be reduced by using longer pulse durations. In this way it would be possible to help recover some of the long term relaxations present in the glassy state. For this study it was assumed that a twenty second pulse was sufficient. The negative loss moduli and tan δ data at 110 and 115° C can be attributed to the fact that it is very difficult to calculate the loss properties of a nearly elastic material without resorting to extremely high data collection frequencies. Negative values have also been observed when deforming other elastic materials using standard dynamic methods.

As a measure of the viscoelastic character of a material, one can use the dependence of the dynamic mechanical properties upon frequency. Though the range of frequency investigated is less than a decade, near T_g there is a factor of two difference between the low and high frequency E' and $|E^*|$ data. The Fourier transform-based properties indicate excellent qualitative and quantitative agreement. In addition, this trend in viscoelastic character is qualitatively supported by Figures 2.11a-e.

An additional feature of the Fourier transform method is that it is also possible to calculate the very low frequency or nearly equilibrium properties. From such data, one can calculate the ratio of the equilibrium tensile modulus to

the storage modulus. This quantity is another measure of the viscoelastic character of a material.

2.6 Applications

Having derived the Impulse Viscoelastic equations for the case of uniaxial deformation, it is clear that one can measure or calculate many of the relevant engineering properties associated with the solidification process. Examples of the use of the Impulse Viscoelastic technique were presented in the previous section. While most of the discussion in sections 2.2 and 2.3 has been concerned with the polymerization of thermosetting materials, one can apply many of these concepts to other methods of solidification, namely the crystallization of thermoplastics and solvent removal from a solution. Some of these other applications are discussed below.

2.6.1 Thermoplastics

Since thermoplastics are linear polymers, they can not form a gel in the classical sense of a three-dimensional network typical of thermosetting materials. It might be expected, however, that thermoplastics at the melt temperature and below would exhibit a non-zero equilibrium tensile modulus. The existence of an equilibrium tensile modulus could be attributed to entangled polymer chains which act as physical crosslinks on the time scale of the

pulse experiment [69-73]. As in the case of thermoplastics, these chain entanglements might also contribute to the equilibrium modulus of thermosetting polymers as well [69]. While Impulse Viscoelasticity theoretically allows for all relaxation processes to occur, in reality some of the long term molecular relaxations are "frozen in" during the actual pulse experiment. This limitation can partially be overcome with more precise equipment or by using pulse durations that are a significant fraction of the longest relaxation time. Some of these ideas are discussed further in Chapter V.

Finally, with regard to entanglements, one should be able to determine the entanglement molecular weight of a thermoplastic polymer. Below the entanglement molecular weight it would be expected that chain relaxations would occur rapidly enough to be detected by the Impulse Viscoelastic method. By lengthening the pulse duration, it would be possible to recover some of the long term relaxations at the higher molecular weights.

It is well known that semi-crystalline thermoplastics undergo large volumetric changes during solidification [74-76]. The stress associated with crystallization should be very dependent upon the crystallization environment. For instance, at low undercoolings the crystal nucleation density is low and crystals may form "islands" within the melt. The surrounding molten polymer phase would probably be compliant enough to absorb the volumetric changes and

prevent the onset of stress. However, at large undercoolings the nucleation density would be high and the crystals might form a network incapable of accommodating all of the associated volumetric changes. This would result in the development of shrinkage stresses. Impulse Viscoelasticity, in combination with the theory of incremental linear elasticity, could lend insight into the kinetics of crystallization and the stresses associated with the process.

2.6.2 Solvent Removal

The removal of solvent from polymer solutions also results in a solidification. It is expected that at a critical solvent concentration there is a transition from liquid to solid behavior. The further removal of solvent for systems subjected to dimensional constraint results in residual stress. These concepts find application in the area of coatings. The mechanics of these processes can be understood using Impulse Viscoelastic methods.

2.6.3 Determination of Residual Stresses

There has been concern regarding the evolution of stresses as a result of dimensional constraints during the solidification of polymers. These residual cure and thermal stresses have found importance in polymer composites, coatings, moldings and extrusions. Specifically, there have

been questions regarding the role of residual stresses in the mechanical performance of cured materials, especially in adhesive bonds [77-86]. Many techniques have been developed for the determination of these stresses. These include photoelastic [87-94], beam bending [95-97], bimetallic [98], strain gauge [38] and layer removal [99,100] techniques. While many methods have been developed for determining these stresses, most of them are indirect, i.e. most of these techniques measure a strain and convert it to a stress by multiplying by a modulus. In addition to these techniques for measuring residual stress, a simple and direct determination of the one-dimensional shrinkage stress can be made using the sample configuration employed in the Impulse Viscoelastic experiments. One of the more significant aspects of the Impulse Viscoelastic technique is the ability to simply and directly measure the residual stresses associated with solidification, i.e., a load is measured and converted to a stress. In addition, it is possible to differentiate these stresses as to their origin, e.g., polymerization, temperature or solvent removal.

While the emphasis in this chapter has been on uniaxially constrained systems, Equation (2.62) can easily be solved for the stresses induced in biaxially or volumetrically constrained systems. For isotropic systems the effect of these additional dimensional constraints is to increase the residual stress levels by factors of

approximately $1/(1 - \nu)$ and $1/(1 - 2\nu)$, respectively, where ν is Poisson's ratio. This generalization has particular significance in the area of coatings and composites. For example, in prepreg materials the fibers are closely packed and the relative amount of matrix is small. It is easy to imagine regions in the composite which would be subject to conditions of nearly volumetric constraint. Such sites would have large residual stresses and could be initiation sites for fracture [84-86]. Additionally, these stresses which may act across the fiber surface can have a pronounced effect on the adhesive properties [77,82].

2.6.4 Impulse Dielectric Method

Another area where the principles of Impulse Viscoelasticity could be applied is in monitoring cure using dielectric methods. Traditional dielectric approaches to cure are exactly analogous to the dynamic mechanical approach where the in-phase and out-of-phase permittivities ε' and ε'' correspond to the in-phase and out-of-phase viscoelastic compliances J' and J" [61,101]. Dynamic dielectric methods suffer from many of the same limitations encountered with dynamic mechanical methods. An Impulse Dielectric method would be expected to yield analogous information to the Impulse Viscoelastic method. One possible difference between Impulse Viscoelastic and Impulse Dielectric methods would be in the scale of observation.

While Impulse Viscoelasticity examines the mechanical response of polymer chains, Impulse Dielectric methods examine the electrical response of monomeric units of the chains. Thus, for gelation studies using Impulse Dielectric methods one might be required to assume that there is a transition in the dipolar relaxation behavior at the gel point. In this regard, Senturia and Sheppard have suggested that no abrupt dielectric transition occurs at the gel point [7].

2.7 Summary and Conclusions

The mathematics of Impulse Viscoelasticity and incremental linear elasticity have been presented for characterizing the mechanical and rheological properties of a material. The method involves the analysis of the stress response of a material to an arbitrary deformation. Despite this, the discussion was limited to the use of uniaxial deformations since they are sensitive to the dimensional changes which occur during solidification. Emphasis was placed on the application of the Impulse Viscoelastic technique to curing systems. In this regard, many of the relevant engineering properties such as gelation time and temperature, equilibrium modulus, cure stress, cure shrinkage, thermal stress, thermal expansion coefficient, glass transition temperature, steady state elongational viscosity, relaxation spectrum and dynamic mechanical

properties can be measured or calculated. While the methodology developed can be applied to liquids and solids, it is most useful in the study of the *in situ* characterization of the solidification process. In Chapters III and IV the Impulse Viscoelastic technique is systematically applied to the curing behavior of two thermosetting systems.

In addition to the study of thermosetting systems, studies of the crystallization behavior and contribution of entanglements in thermoplastics and the solidification of polymer solutions as a result of solvent removal are also possible using Impulse Viscoelasticity.

As an alternative but analogous technique, an Impulse Dielectric method is proposed. This approach uses mathematics similar to Impulse Viscoelasticity as applied to dielectric methods for monitoring cure.

C H A P T E R 3

NETWORK MECHANICAL PROPERTIES OF AMINE-CURED EPOXIES

3.1 Introduction

In Chapters I and II the Impulse Viscoelastic approach for determining the mechanical properties of aging materials was presented. Before proceeding with the analysis of complicated networks using the technique of Impulse Viscoelasticity, it is necessary to demonstrate its viability as a characterization method on comparatively simple systems. Such systems are typified by "clean" chemistry and cures without the complication of vitrification. The requirement of a simple cure chemistry was achieved experimentally by using relatively well characterized starting materials. As a result of these experimental conditions, a good correlation between the network mechanical properties and reactant stoichiometry should exist.

This chapter focuses on the use of the Impulse Viscoelastic technique to study network formation in amine-cured epoxies. Though many efforts have been made in this area, most of them have employed dynamic mechanical methods. With the Impulse Viscoelastic approach it should be possible to overcome many of the limitations of these studies already mentioned and enrich our understanding of networks.

3.2 Materials

The amines chosen for this study were kindly provided by the Texaco Chemical Company (Bellaire, TX) and are marketed under the Jeffamine® tradename. These amines have the desired feature of being relatively well characterized with regard to chemical structure and offer a wide range in functionality and molecular weight. Though these materials are not generally used as epoxy curing agents, they are suitable for tailoring the network properties of widely varying crosslink densities. Both diamines and triamines of various molecular weights were investigated. For the triamines, three amine-terminated polyether arms emanate from a central initiator molecule and it was assumed that each of the arms are identical in molecular weight.

The chemical structure of these amines is predominantly a polyether backbone terminated by primary amines. The polyether backbone is either poly(ethylene oxide) (PEO) or poly(propylene oxide) (PPO). Because of their similar backbones and relatively high molecular weights, the reactivity of these amines towards epoxides should be comparable [102]. In this way direct comparisons of the resulting networks can be made without concern over unequal amine reactivities. This complication might occur in epoxides that are cured with shorter chain amines, such as diethylene triamine or triethylene tetramine, where the

reaction of neighboring amines may affect the reactivity of other amine functionalities.

The amine equivalent weight for each Jeffamine^{R} was determined by performing an elemental analysis for nitrogen together with the chemical structure provided by Texaco [103]. The results represent the average of two measurements done for each material. The densities of the liquid Jeffamines^{R} (D-2000, T-403, T-3000 and T-5000) were determined volumetrically. With regard to the identification of these amines, the D- or ED- designation refers to diamine (tetrafunctional) and T- refers to triamine (hexafunctional). The number listed after the D-, ED- or T- designation indicates the approximate molecular weight of the amine. Some of the physical properties of the amines used in this study are listed in Table 3.1.

3.3 Experimental

Each amine was mixed at room temperature with Epon 828 epoxy resin and placed in a forced air Blue M oven at 40-60° C for 15-20 minutes in order to promote mixing. An epoxy equivalent weight of 190 g/mole was used for Epon 828. Amine/epoxy (A/E) molar ratios of 0.7, 1.0 and 1.3 were investigated. The rubber membrane sample assembly discussed in Chapter II was filled and placed into the environmental chamber of the Dynastat which was preheated to about 10° C below the isothermal cure temperature. The preheating of

Table 3.1

Physical Properties of the Jeffamine^{R} Amines

Amine	Primary Amines	Backbone Structure	Density [g/cm^3]	Molecular Weight [g/mole]	Equivalent Weight [g/mole]
D-2000	2	PPO	1.08	2100	525
ED-900	2	PEO	1.06	1000	250
ED-2001	2	PEO	1.08	2200	550
T-403	3	PPO	0.98	470	78
T-3000	3	PPO	1.00	3400	570
T-5000	3	PPO	1.00	6100	1020

the environmental chamber was done in order to minimize the time required for the sample to reach the cure temperature. After the weight of the sample assembly was balanced off, the assembly was stretched so as to form a uniform uniaxial specimen. The load required to stretch the sample was also balanced to zero volts at the start of data collection.

Data collection began approximately 0.2° C below the cure temperature. Uniaxial step strain pulses of 10 seconds duration were used to characterize cure. Pulse data were collected at a frequency of 10 Hz for 40 seconds. In most cases, pulse deformations were applied to the samples every 90 seconds. The samples were allow to gel under isothermal conditions. In order to accomplish this with amines of different reactivities, initial cure temperatures of 85, 110 and 125° C were used depending upon the amine. Soon after the samples gelled, the temperature was ramped to 140° C at a programmed rate of 2° C/min. In this way the reactions could be driven to higher extents of reaction more quickly and a comparison of the network properties of the epoxies could be made at the same temperature. Because of the different cure rates for each amine/epoxy reaction the cure schedules varied slightly. Table 3.2 indicates the schedule used for each sample. Polymerization was considered complete when the equilibrium tensile modulus became constant. The samples were then cooled at constant strain at a rate of 1° C/min. At the end of each experiment the

Table 3.2

Cure Schedules used for the Jeffamine^{R}/Epon 828 Epoxies

Amine	Amine/Epoxy Ratio	Time @ 85° C [min]	Time @ 110° C [min]	Time @ 125° C [min]	Time @ 140° C [min]
D-2000	0.7	0	0	100	100
	1.0	0	0	100	255
	1.3	0	0	*	
ED-900	0.7	0	60	0	60
	1.0	0	60	0	260
	1.3	0	60	0	100
ED-2001	0.7	0	150	0	125
	1.0	0	350	60	115
	1.3	0	160	0	185
T-403	0.7	30	0	0	65
	1.0	30	0	0	145
	1.3	30	0	0	50
T-3000	0.7	0	0	60	165
	1.0	0	0	60	165
	1.3	0	0	65	250
T-5000	0.7	0	0	150	135
	1.0	0	0	440	60
	1.3	0	0	*	

* Did not gel after 2½ hr.

collected data were corrected using precise values for the gage length and cross sectional area of the samples. The cured samples were then sectioned for density measurements.

Since many of the cures took several hours, the collected pulse data were condensed by 1/2 or 2/3 in order to reduce the volume of data. This was accomplished by saving every second or third pulse.

3.4 Results

The results of the Impulse Viscoelastic studies conducted on the polymerization of Epon 828 cured with Jeffamine^{R} amines are summarized in this section. Specifically the properties of interest are the gel time, equilibrium tensile modulus, shrinkage stress, molecular weight between crosslinks, glass transition temperature, thermal expansion coefficient and volumetric changes due to cure.

3.4.1 Density Measurements

The densities of the amine-cured epoxies were determined using Archimedes' principle of hydrostatic weighing. Air and n-hexane were used as the fluid media. All of the cured densities were measured at room temperature. Four measurements were made for each cured sample. Typically a cured sample was cut into sections measuring ≈ 0.1 cm^3 in volume. The initial densities were calculated assuming

ideal solutions were formed. Table 3.3 summarizes the volumetric data for each of the epoxy samples.

The volumetric data for the amines based upon a poly(ethylene oxide) backbone (ED-900 and ED-2001) indicate reduced shrinkage at the 0.7 equivalence ratio relative to the other two stoichiometries. In contrast to this behavior, the trends in volumetric shrinkage for the poly(propylene oxide) amines indicate increased or equivalent shrinkage at the 0.7 stoichiometry relative to the 1.0 and 1.3 ratios. This trend for the PPO-based amines is surprising considering that more reaction should take place at the 1.0 amine/epoxy ratio than at the 0.7 or 1.3 equivalences. The presence of side reactions may explain the differences in the volumetric trends for the PEO and PPO-based amines. It is suggested that because of their molecular structure, the triamines (T-403, T-3000, T-5000) can not pack well when incorporated into the network. Therefore, since more reaction (or amine incorporation) occurs at the 1.0 equivalence, less perfect amine packing and a lower cured density are expected. The cure schedule data in Table 3.2 support the observation that the times required for complete cure for the non-stoichiometric samples were much shorter.

Table 3.3

Volumetric Data for the Jeffamine^{R}/Epon 828 Epoxies

Amine	Amine/Epoxy Ratio	Initial Density [g/cm^3]	Cured Density [g/cm^3]	Volumetric Shrinkage [%]
D-2000	0.7	1.05	1.08	2.9
	1.0	1.04	1.06	1.9
ED-900	0.7	1.11	1.16	4.5
	1.0	1.10	1.16	5.4
	1.3	1.09	1.15	5.5
ED-2001	0.7	1.11	1.15	3.6
	1.0	1.10	1.15	4.5
	1.3	1.10	1.15	4.5
T-403	0.7	1.11	1.17	5.4
	1.0	1.10	1.15	4.5
	1.3	1.09	1.15	5.5
T-3000	0.7	1.05	1.08	2.9
	1.0	1.04	1.07	2.9
	1.3	1.03	1.06	2.9
T-5000	0.7	1.03	1.06	2.9
	1.0	1.02	1.04	2.0

3.4.2 Molecular Weight Between Crosslinks

The molecular weight between crosslinks (Mc) for each network was determined using theory which has been developed in the field of rubber elasticity [104-108]. Equation 3.1 which has been derived describes the relationship between the equilibrium tensile modulus and the molecular weight between crosslinks for a non-ideal network:

$$Eeq = \frac{3\ \phi\ d\ R\ T}{Mc}\ [1 - 2Mc/M]\ , \qquad (3.1)$$

where Eeq = equilibrium tensile modulus, [MPa]

ϕ = front factor

d = density, [g/cm^3]

R = gas constant = 8.314 MPa/gmolK

T = absolute temperature, [K]

M = molecular weight of network, [g/mole]

Mc = molecular weight between crosslinks, [g/mole]

The front factor ϕ is the ratio of the end-to-end distance squared of a chain in the network relative to the same chain in an isolated state. Simplifying Equation (3.1) by assuming the front factor to be equal to one and neglecting the effect of dangling ends yields Equation (3.2):

$$Eeq = 3\ d\ R\ T\ /\ Mc\ . \qquad (3.2)$$

The average Mc for each network was calculated using Equation (3.2) together with the Eeq value obtained from Impulse Viscoelastic measurements performed at 140° C.

These Mc data are reported below in Table 3.6 along with other mechanical property data.

Equation (3.2), which applies to ideal networks, predicts that the equilibrium modulus at absolute zero is zero. The ideality of these networks from an entropic perspective was investigated over a limited temperature range by deforming the epoxy networks periodically as they cooled and plotting Eeq versus absolute temperature. A plot of Eeq and the thermal stress (as indicated by the baseline or shrinkage stress level) during cooling is given for Epon 828 cured with Jeffamine^R T-3000 (A/E = 0.7) in Figure 3.1. From a plot such as that shown in Figure 3.1, ten equally spaced Eeq and thermal stress data points were chosen over the entire temperature range for regression analysis for each Jeffamine^R/Epon 828 epoxy. An exception to this was made for the Epon 828 epoxy samples cured with T-403, where care was taken not to chose Eeq data in the range of the glass transition temperature. For these particular samples, the effect of vitrification would cause the equilibrium tensile modulus to appear greater than that predicted by ideal network theory and would skew the regression results. It should be pointed out that these thermal stress data in Figure 3.1 have not been corrected for the contribution of the metal hardware within the environmental chamber of the Dynastat. This hardware correction is small (≈ 3%) and is only significant when a material is glassy. The results of

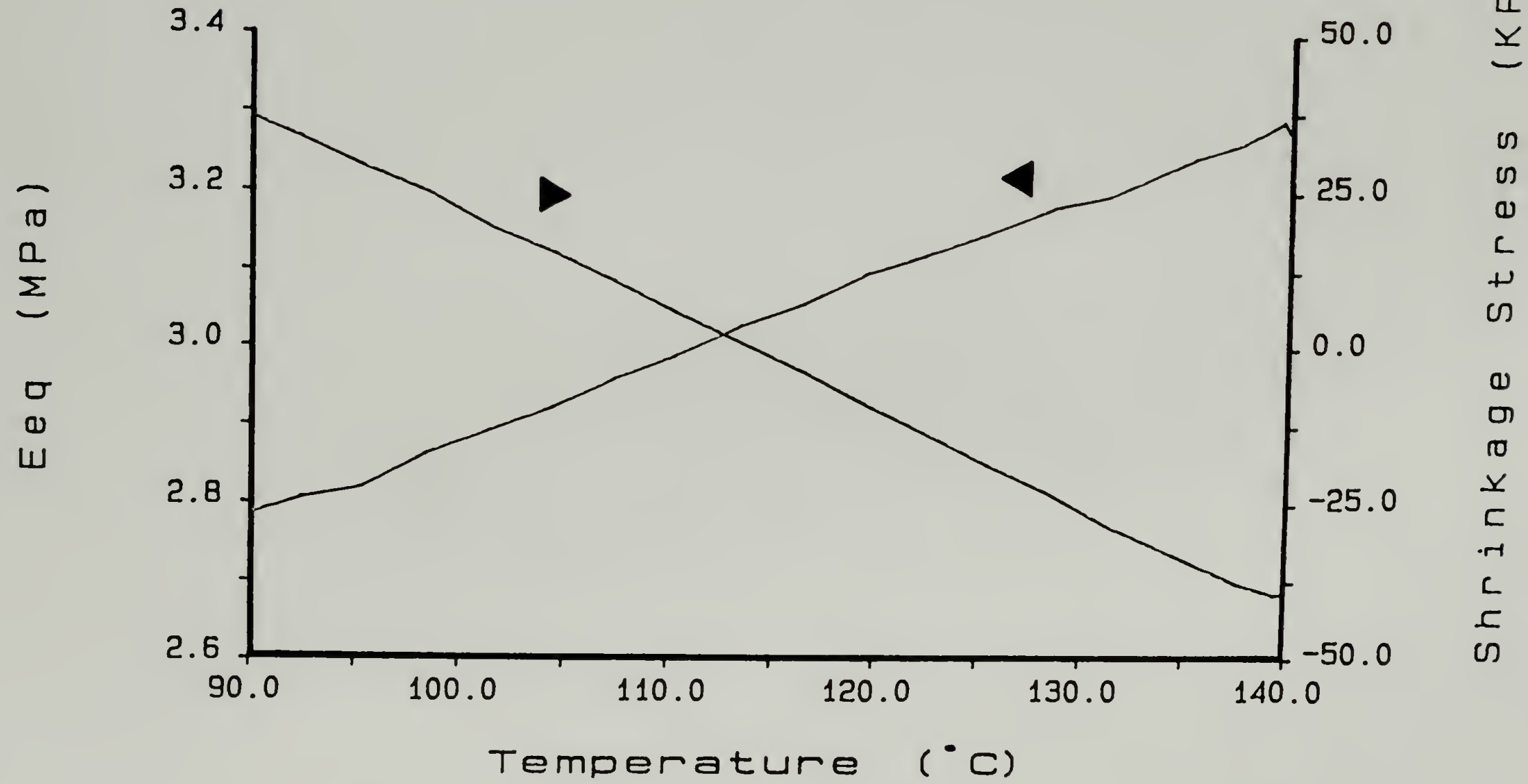

Figure 3.1. Equilibrium tensile modulus (Eeq) and shrinkage (thermal) stress as a function of temperature during cooling of Jeffamine® T-3000/Epon 828 (A/E = 0.7) sample.

the linear regression analyses of the equilibrium tensile modulus and thermal stress versus absolute temperature are displayed in Tables 3.4 and 3.5, respectively. The intercept of the Eeq regression analysis yields the Eeq of the network at absolute zero and the slope can be related to 3dR/Mc.

The magnitudes of the intercept data presented in Table 3.4 can be qualitatively related to the relative contribution of the energetic (rather than entropic) behavior of these networks. An example of a deformation which contributes to the energetic portion of the force required to deform the network is carbon-carbon bond bending or stretching. Such deformation conditions can occur at large strains, as the ultimate extensibility of the chain segments between crosslink junctions is approached. In this regard, tightly crosslinked materials are more apt to be non-ideal than those networks loosely crosslinked. It should also be noted that the Eeq intercept determined from the above regression analysis is insensitive to the topographical perfection of the network since network imperfections such as residual oligomeric species or dangling chains do not contribute to the elastic modulus. This analysis serves to highlight some of the differences between topographically and entropically ideal elastomers.

Table 3.4

Linear Regression Data for Equilibrium Tensile Modulus versus Absolute Temperature

Amine	A/E Ratio	Slope [MPa/K]	Intercept [MPa]	Correlation Coefficient
D-2000	0.7	0.00300	-0.201	.953
	1.0	0.0113	-0.837	.998
ED-900	0.7	0.00571	-0.349	.987
	1.0	0.0329	-3.89	.998
	1.3	0.0154	-1.51	.999
ED-2001	0.7	0.00500	-0.477	.996
	1.0	0.0123	-0.370	.829
	1.3	0.0114	-0.943	.998
T-403	0.7	0.0197	-1.61	.991
	1.0	0.0811	-8.83	.996
	1.3	0.0812	-10.31	.996
T-3000	0.7	0.0105	-1.02	.998
	1.0	0.0155	-0.988	.999
	1.3	0.0142	-1.25	.999
T-5000	0.7	0.00188	0.1873	.842
	1.0	0.00491	-0.263	.990

Table 3.5

Linear Regression Data for Thermal Stress versus Absolute Temperature

Amine	A/E Ratio	Slope [KPa/K]	Intercept [KPa]	Correlation Coefficient
D-2000	0.7	-0.449	159	.996
	1.0	-1.61	632	.999
ED-900	0.7	-0.706	263	.997
	1.0	-5.37	2120	1.000
	1.3	-2.70	1060	.998
ED-2001	0.7	-0.622	218	.994
	1.0	-2.47	950	.999
	1.3	-1.49	559	.983
T-403	0.7	-3.01	1130	.999
	1.0	-8.48	3330	.999
	1.3	-10.13	3847	.998
T-3000	0.7	-1.58	610	1.000
	1.0	-1.95	778	.996
	1.3	-1.79	691	.999
T-5000	0.7	-0.515	177	.997
	1.0	-0.798	380	.999

3.4.3 Coefficient of Thermal Expansion

Data were also obtained on the linear coefficient of thermal expansion (CTE) for each Jeffamine®/Epon 828 epoxy network. In order to determine the CTE it is necessary to know the change of Eeq and the uniaxial thermal stress with temperature. By combining these data with those obtained from the regression results presented in Tables 3.4 and 3.5, the coefficient of thermal expansion was calculated using the equations presented in Chapter II. In this analysis it was assumed that the thermal stress and Eeq during cooling can both be described by equations of the form $y = a + bT$, where a and b are constants and T is the absolute temperature. From the correlation coefficient data in Tables 3.4 and 3.5 the linear equation is an excellent approximation. As a result of the linear fits for the thermal stress and Eeq, the thermal expansion coefficient that is obtained is a slight function of temperature. Similar results were obtained by Lyon and Farris [109]. In order to compare the CTE data at equivalent conditions, a temperature of 120° C was chosen. This temperature is well above the glass transition temperature of any of the networks. The CTE data calculated at 120° C for each network are summarized in Table 3.6. The CTE values obtained are in good agreement with those of typical elastomers.

Table 3.6

Network Mechanical Properties of the Jeffamine® /Epon 828 Epoxies

Amine	A/E Ratio	Gel Temp [°C]	Gel Time [min]	Eeq [MPa]	Mc [g/mole]	T_g [°C]	CTE (10^{-4}) [K^{-1}]
D-2000	0.7	125	60	1.1	10100		4.6
	1.0	125	75	3.8	2900	<-40	4.4
	1.3	125	>150				
ED-900	0.7	110	30	2.0	6000		3.7
	1.0	110	25	9.7	1200	-35	5.9
	1.3	110	35	4.8	2500		5.9
ED-2001	0.7	110	115	1.6	7400		4.2
	1.0	110	85	4.8	2500	<-40	5.5
	1.3	110	130	3.8	3100		4.2
T-403	0.7	85	15	6.7	1800		4.9
	1.0	85	10	24.5	480	80	3.7
	1.3	85	15	23.0	510	65	4.7
T-3000	0.7	125	30	3.3	3400		5.1
	1.0	125	35	5.4	2000	-45	3.8
	1.3	125	50	4.6	2400		4.1
T-5000	0.7	125	120	1.0	11000		5.6
	1.0	125	140	1.7	6300	<-50	4.8
	1.3	125	>150				

3.5 Discussion

The gelation time of each network was determined by the onset of an equilibrium tensile modulus (Eeq) greater than that of the rubber membrane used to support the sample. This approach to gelation uses the fact that a liquid has an equilibrium tensile modulus of zero, whereas a solid has some finite, non-zero Eeq value. Because of the imprecision associated with the polymerization times, the gel times are ± 5 minutes.

The network mechanical properties of the Jeffamine^{R}/ Epon 828 epoxies are summarized in Table 3.6. These include the gelation time and temperature, equilibrium tensile modulus (Eeq), molecular weight between crosslinks (Mc), glass transition temperature (T_g) and the linear coefficient of thermal expansion (CTE). The T_g of several of the networks were calculated by determining the point of intersection of the rubbery and glassy thermal stress curves during cooling. An example of this is shown in Figure 3.2 where the shrinkage stress during cooling is plotted for the Jeffamine^{R} T-403/Epon 828 (A/E = 1.3) sample. From Figure 3.2 a T_g of 65° C can be estimated for this material.

3.5.1 Cure Stresses

Absent from Table 3.6 are the cure stress data for these networks. The stress due to cure (indicated by the baseline

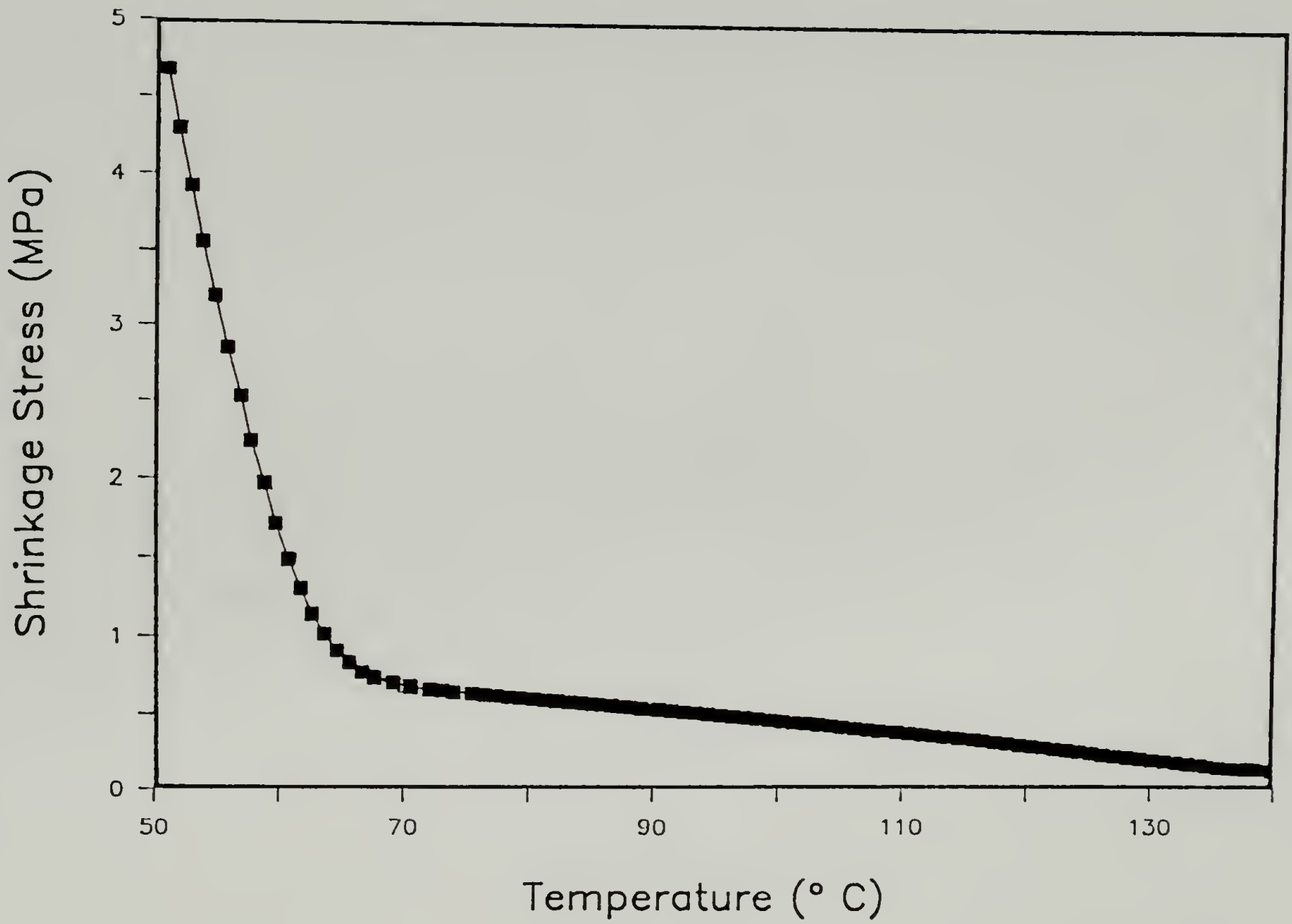

Figure 3.2. Shrinkage (thermal) stress as a function of temperature during cooling of Jeffamine^{R} T-403/Epon 828 (A/E = 1.3) sample.

stress level for an isothermally curing material) was difficult to measure for these samples since the cures were not isothermal and there was thermal degradation of the rubber membrane. As the rubber membrane sample assembly degraded, it was unable to fully maintain the load that was used to stretch it prior to curing. This degradation changes the shrinkage stress level during polymerization. In most cases the load required to stretch the rubber sample assembly was completely eliminated. This degradation also led to a decrease in Eeq during the early portions of the experiment, prior to the gelation of the epoxy. These effects can be observed on Figure 3.3 where the Eeq and shrinkage stress are plotted for Epon 828 cured with T-5000 at an amine/epoxy ratio of 0.7. Such effects were not noted at the lower cure temperatures. Since these materials, however, cured to a relatively low modulus the stresses associated with cure are necessarily small. In order to circumvent the problems associated with the thermal stability of the rubber membranes employed in these polymerization studies, other support materials can be used. Such materials include silicone membranes or, more generally, materials which are soft mechanically in comparison to the sample.

The cure stress measurements were also influenced by the fact that these networks were partially formed under conditions of tensile deformation. The behavior of networks

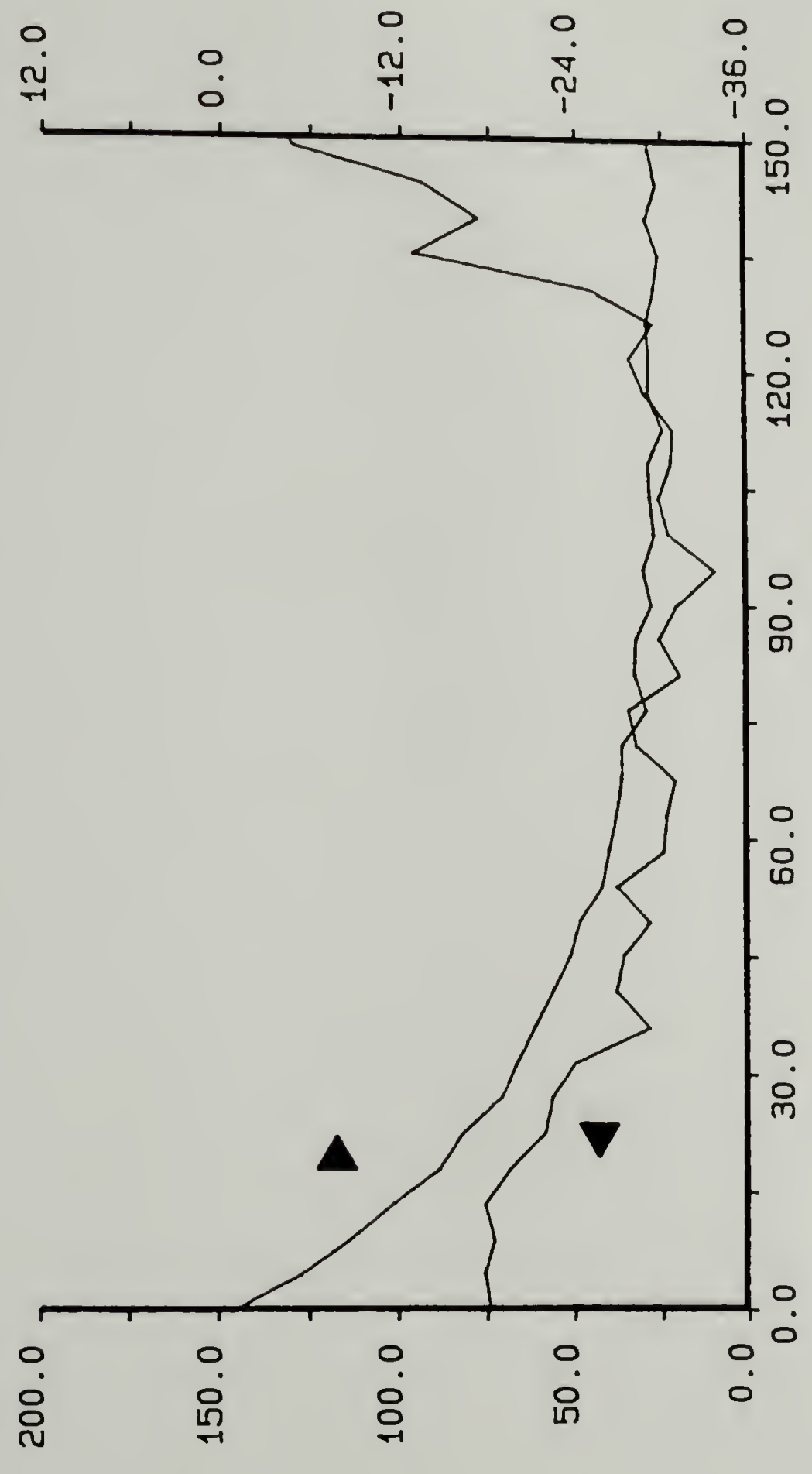

Figure 3.3. Equilibrium tensile modulus (Eeq) and shrinkage stress during the early portion of the isothermal (T = 125° C) cure of Epon 828 with Jeffamine® T-5000 (A/E = 0.7).

formed under tension has been extensively studied [110-112]. If it is assumed that the network bonds form stress-free, then there is a compressive stress associated with returning the strained network to its pre-deformation level. This additional compressive stress can be observed for the Jeffamine® T-3000/Epon 828 sample (A/E = 0.7) by comparing Figure 3.4a with Figure 3.4b. Figure 3.4a plots Eeq during polymerization together with the temperature profile. Figure 3.4b displays the shrinkage stress level during cure for the same sample. Note how the shrinkage stress decreases after the sample has reached 140° C. This small compressive contribution to the shrinkage stress is not attributed to further degradation of the rubber membrane or expansion of the network due to polymerization or thermal stress associated with non-isothermal conditions.

In order to verify the fact that the observed cure stresses are relatively independent of the deformations applied to the sample during cure, three isothermal cure experiments (T = 85° C) were conducted on Epon 828 polymerized with Jeffamine® T-403 (A/E = 1.3). The first sample was undeformed throughout the cure. A second sample was subjected to a tensile strain of 0.85% for 10 seconds every 60 seconds. In the third experiment, a compressive strain of 0.85% was applied to the sample for 10 seconds every 60 seconds. For these cure stress measurements, the strain magnitude was not was not reduced during cure. The

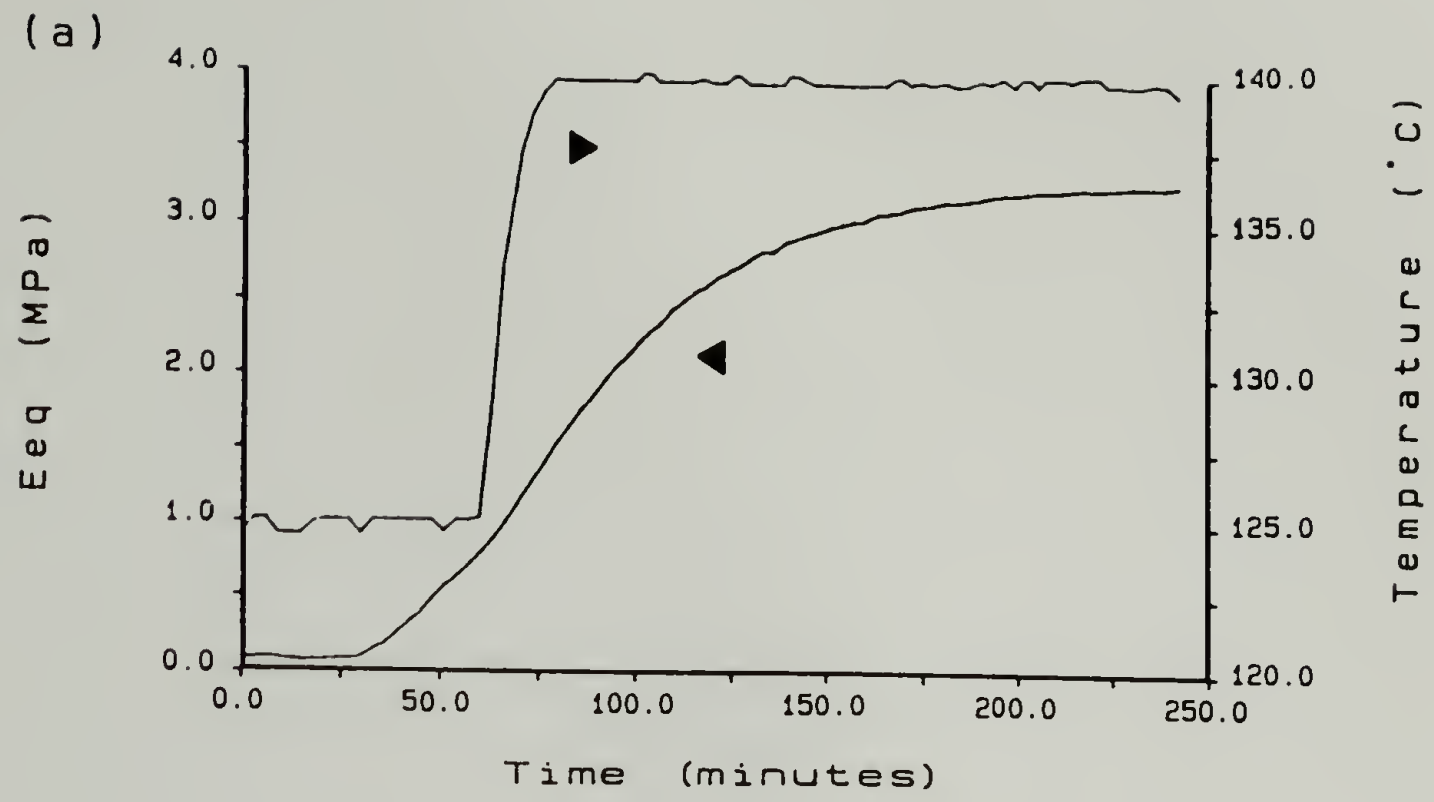

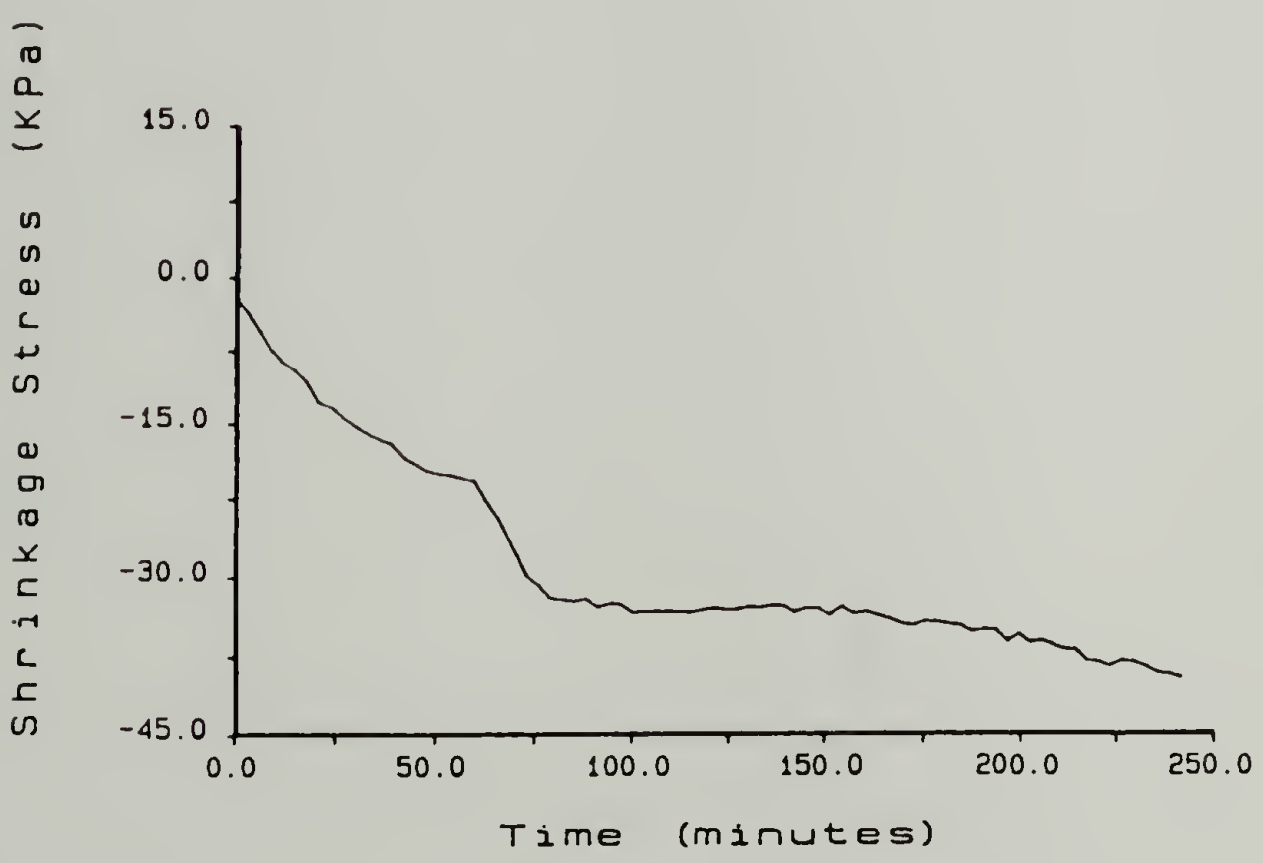

Figure 3.4. a) Equilibrium tensile modulus (Eeq) and temperature profile used during polymerization of Jeffamine® T-3000/Epon 828 (A/E = 0.7) and b) shrinkage stress during polymerization for the same sample.

undeformed sample yielded a one-dimensional cure stress of 0.095 MPa. The sample subjected to tensile deformation resulted in a cure stress of 0.07 MPa, whereas the compressively deformed sample yielded a 0.11 MPa cure stress level. These results indicate that the cure stress is relatively independent of the direction of deformation. Furthermore, under the usual experimental conditions, the magnitude of deformation is reduced during polymerization so as to maintain linear viscoelastic conditions. This reduction in strain magnitude would reduce the differences in the one-dimensional cure stress magnitudes.

Each of the amine-epoxide formulations cured elastically. Evidence for this is illustrated in Figure 3.5 by a series of pulse deformations taken from the polymerization of Epon 828 cured with Jeffamine® T-403 at an amine/epoxy ratio of 1.3. Specifically, Figure 3.5a is a pulse applied prior to gelation and indicates the contribution of the rubber membrane. Figure 3.5b is a pulse after 18 minutes of polymerization, just after gelation has occurred. Note the lack of any viscoelastic behavior in the response of the stress to deformation. Figures 3.5c and d were taken 48 and 81 minutes into the cure and further demonstrate the elastic nature of the curing network. Finally, Figures 3.5e and f are pulses taken during the cooling portion of the experiment and demonstrate the decrease in Eeq with decreasing temperature due to entropic

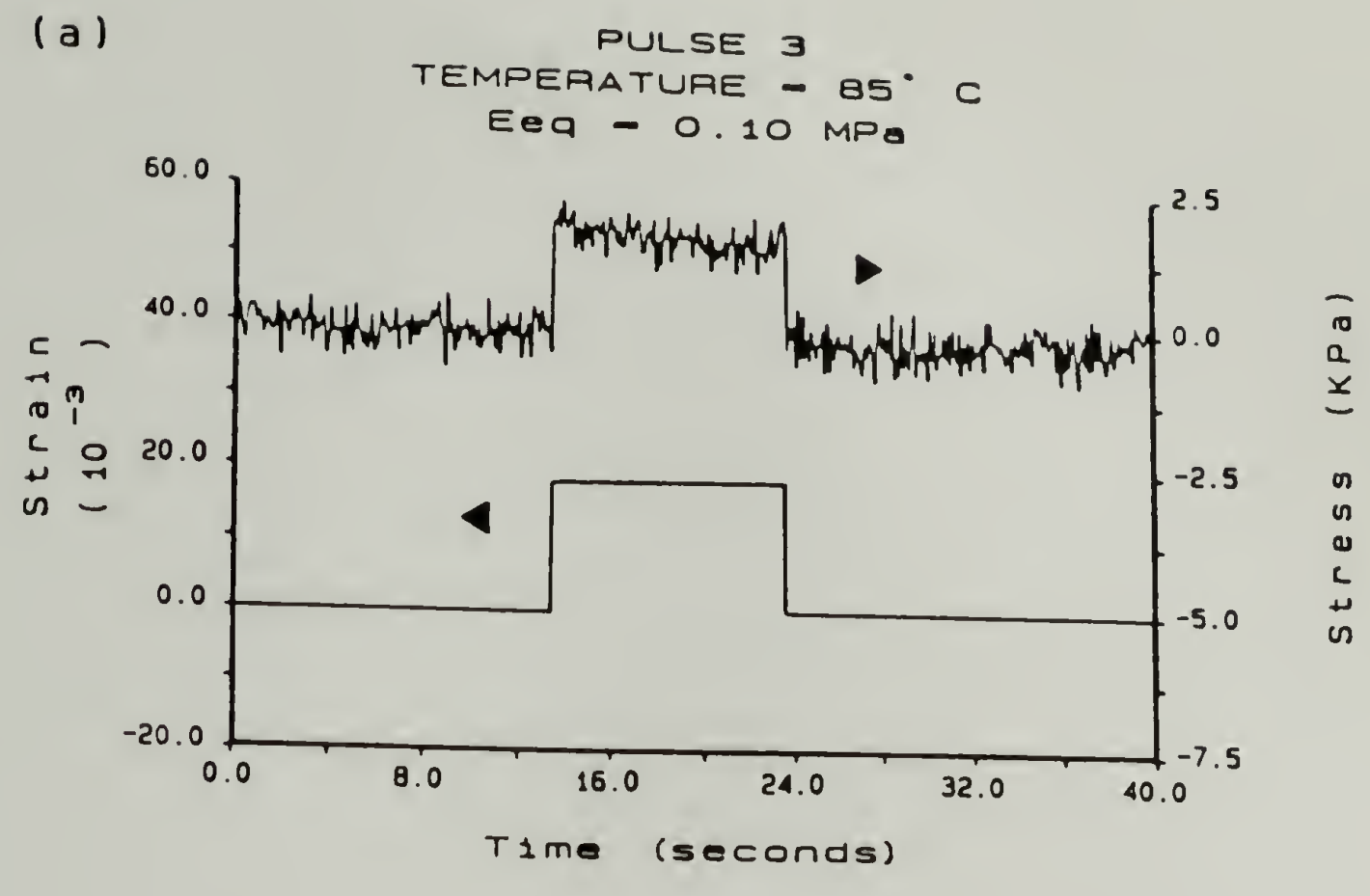

Figure 3.5. Stress response to uniaxial pulse deformations taken from the polymerization of Jeffamine® T-403/Epon 828 (A/E = 1.3) at a) 6 minutes (prior to gelation), b) 18 minutes (just after gelation)**(continued on next page)**

(c)

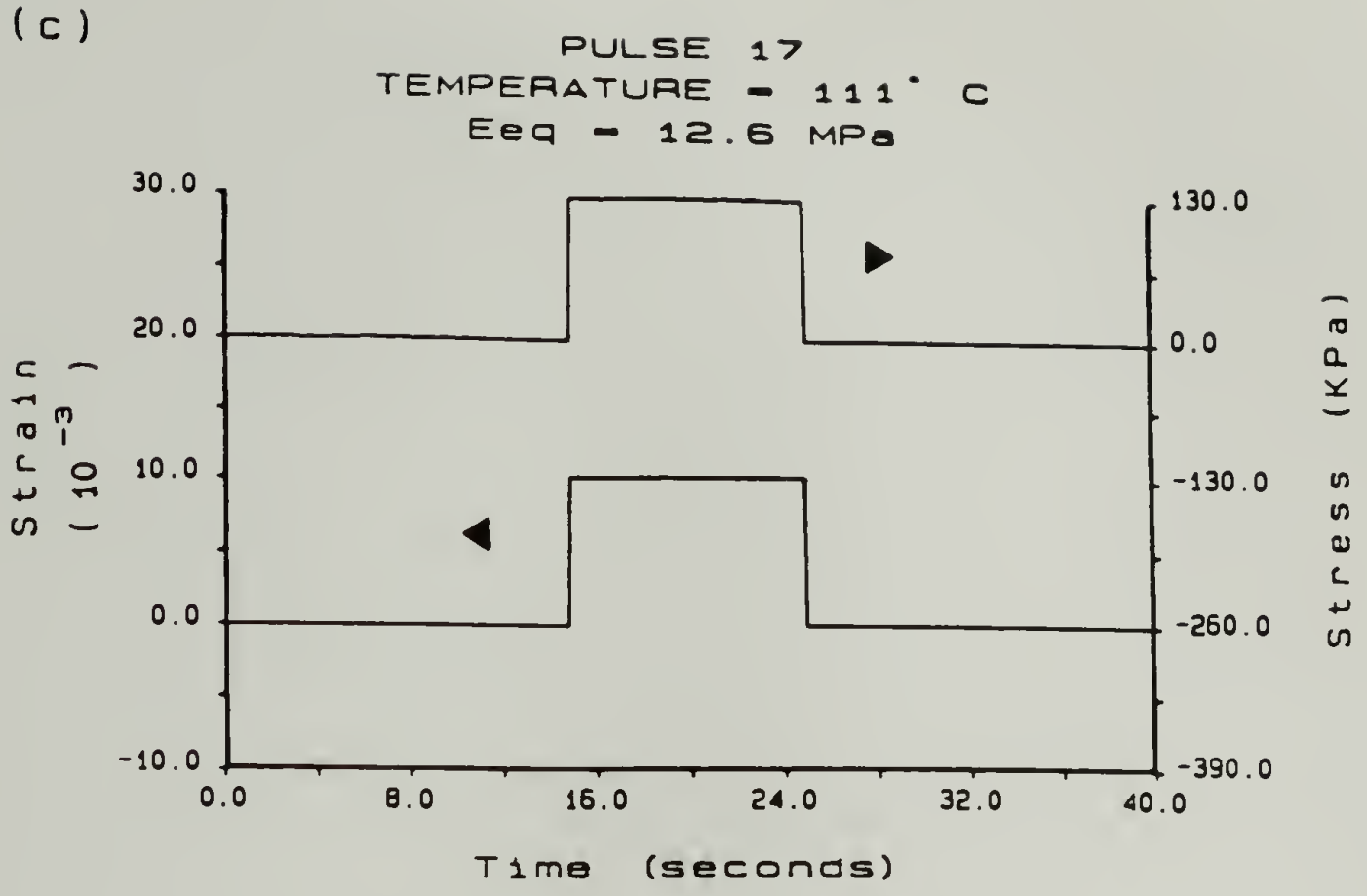

(d)

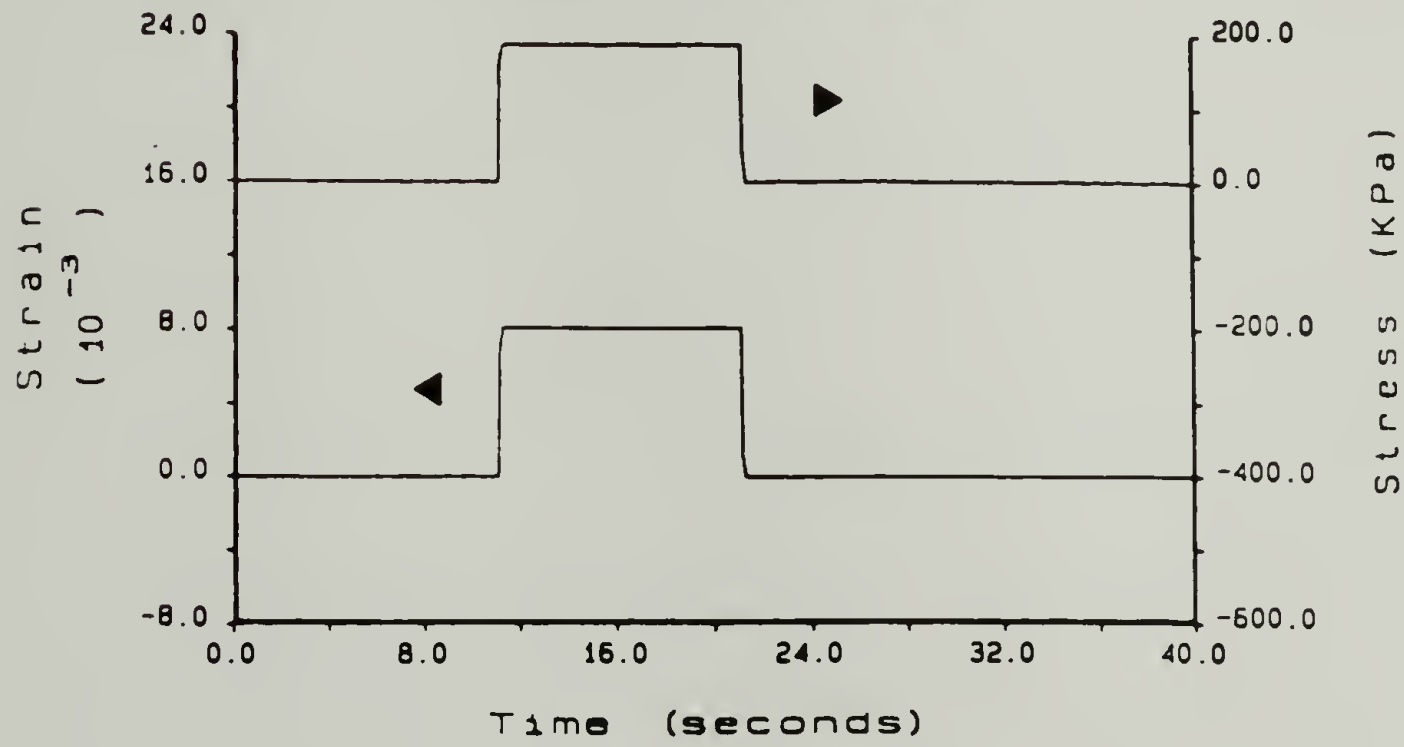

Figure 3.5 (cont). Stress response to uniaxial pulse deformations taken from the polymerization of Jeffamine® T-403/Epon 828 (A/E = 1.3) at c) 48 minutes, d) 81 minutes

(continued on next page)

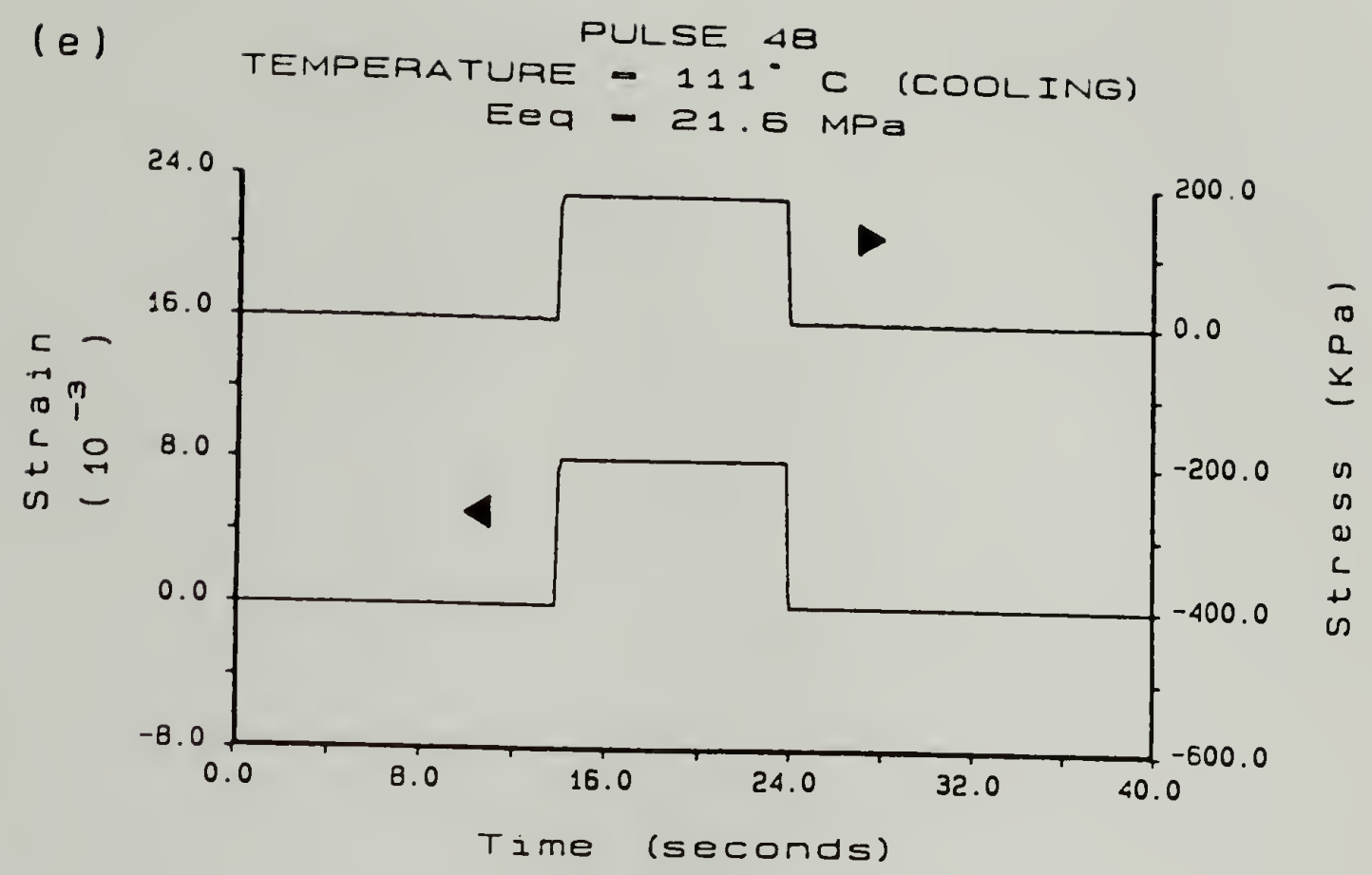

Figure 3.5 (cont). Stress response to uniaxial pulse deformations taken from the polymerization of Jeffamine^{R} T-403/Epon 828 (A/E = 1.3) at e) 144 minutes (during cooling) and f) 182 minutes (during cooling).

considerations [104]. Because these formulations cured elastically it was difficult to obtain higher order information such as the steady state elongational viscosity or mean relaxation time. Viscoelastic behavior was observed on some samples (Epon 828 cured with Jeffamine^R T-403) which approached their T_g during the cooling portion of the experiment.

3.5.2 Network Structure

In Table 3.6 the molecular weight between crosslinks for each network were presented. These Mc values were calculated using the measured Eeq and Equation (3.2). A second measure of Mc can be calculated from considerations of the reactant chemistry. Using the mole fractions and molecular weights of the amine and epoxy for the networks formed at an amine/epoxy ratio = 1.0, it is possible to calculate Mc from a chemical perspective. This Mc represents the lower bound on Mc and assumes that the network is topographically perfect. A third measure of Mc can be determined using a simple qualitative picture of the topographically perfect network. For this analysis, consider that the molecular weight of the Epon 828 (380 g/mole) is small relative to the amine molecular weights, excluding Jeffamine^R T-403. Assuming that complete reaction occurs, two Epon 828 molecules will be attached to each amine end. For such a situation, the Epon 828 can be

considered as a cluster or macro-junction point within the network. The Mc for this macro-junction approach represents an upper bound on Mc. It is calculated by summing the amine contribution (the amine molecular weight for diamines and 2/3 of the amine molecular weight for triamines) with the molecular weight of one of the Epon 828 clusters (760 g/mole). Table 3.7 summarizes the Mc's determined by the chemical and macro-junction approaches along with the T_g for each network formed at conditions of balanced stoichiometry. Comparing the Mc data presented in Table 3.6 (calculated from rubber elasticity theory) with the Mc data in Table 3.7, one finds that the Mc's fall within the lower and upper bounds of Mc for each network, except the one formed with Jeffamine^R T-5000.

The experimentally determined Mc's were close to the macro-junction Mc, except for the Jeffamine^R T-403/Epon 828 network. This exception is not surprising since the molecular weights of amine T-403 and Epon 828 are similar. The agreement between the Mc's reported in Table 3.6 and the macro-junction Mc's improved as the molecular weight of the amine increased. This behavior is expected since the assumptions involved in the macro-junction theory become more accurate at higher amine molecular weights. For all of the networks, the Mc determined from reactant chemistry underestimates the value of Mc. Incomplete reaction and the presence of network defects such as chain ends and loops

Table 3.7

Chemical and Macro-junction Approaches to the Molecular Weight Between Crosslinks for Jeffamine^{R}/Epon 828 Epoxies

Amine	A/E Ratio	Mc Chemical Approach [g/mole]	Mc Macro-junction Approach [g/mole]
D-2000	1.0	950	2900
ED-900	1.0	590	1800
ED-2001	1.0	990	3000
T-403	1.0	350	920
T-3000	1.0	760	1900
T-5000	1.0	1200	2800

contribute to higher values of Mc. This two effects can be used to explain the Mc discrepancies for the network formed with Jeffamine^R T-5000. Since the molecular weight of the T-5000 amine is relatively high, it is expected that the degree of incomplete reaction is greatest for this network. As a result, the Mc for this network is most sensitive to the network topography.

The trend in T_g of each network also correlates with the reciprocal in the experimentally determined molecular weight between crosslinks, or equivalently, the crosslink density. It is difficult to further correlate the T_g data with the Mc data since the backbone structures of the amines were not identical.

3.5.3 Effect of Stoichiometry

The gelation time for each series of amine was shortest at conditions 0.7 and 1.0 stoichiometry. At the 1.3 ratio, however, the times required to gel greatly increase. Part of this increase is due to the fact that relatively few reactions occur per amine molecule at this stoichiometry.

In order to illustrate the effect of stoichiometry, Figure 3.6 plots the equilibrium tensile modulus during the polymerization of Epon 828 with Jeffamine^R ED-900 for each equivalence ratio. The Eeq of these samples during cooling are displayed in Figure 3.7. The Eeq data in Table 3.6 indicate that at either side of stoichiometry there is a

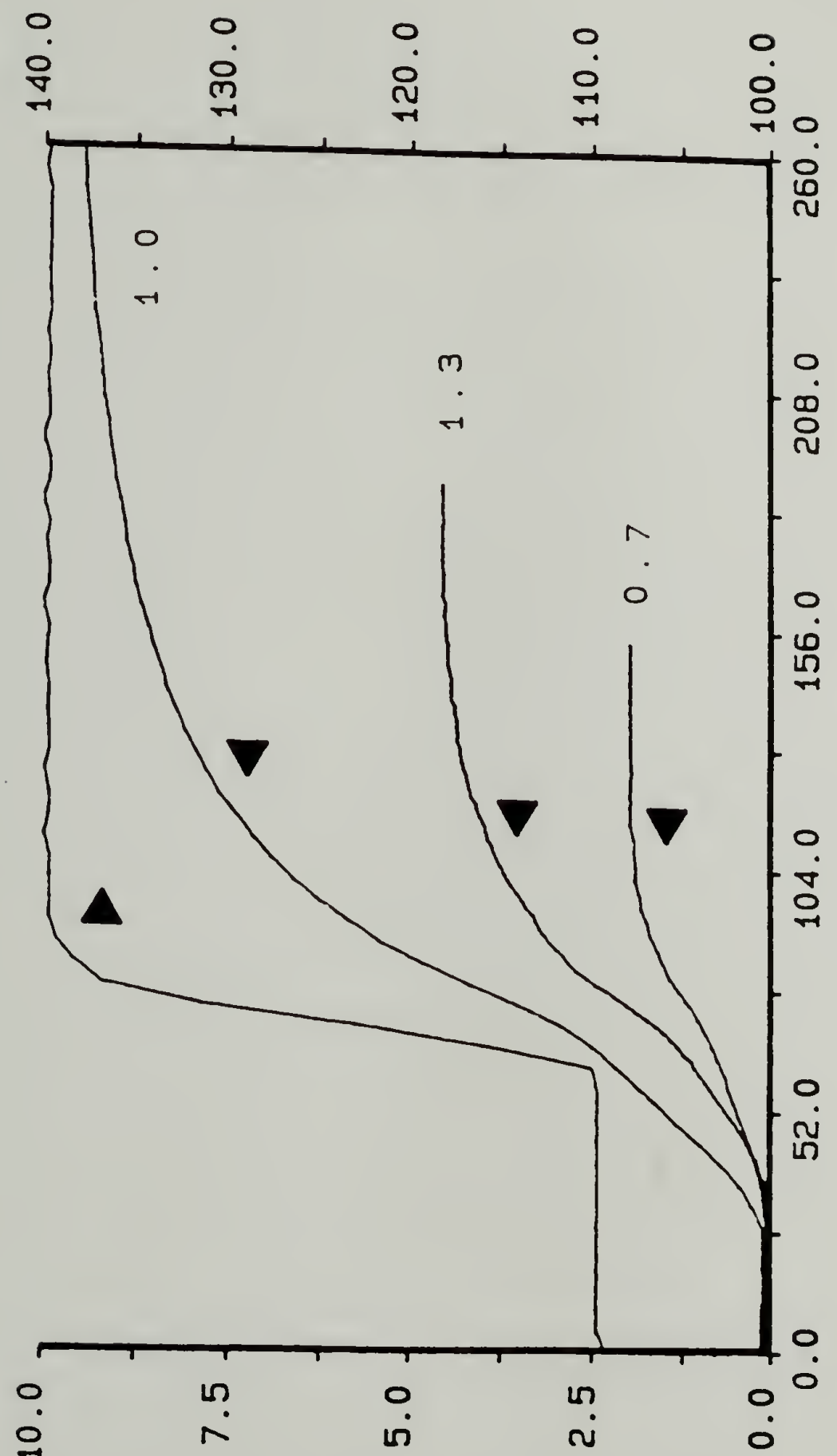

Figure 3.6. Equilibrium tensile modulus (Eeq) and temperature profile as a function of polymerization time for Epon 828 cured with Jeffamine® ED-900 at the 0.7, 1.0 and 1.3 amine/epoxy ratios.

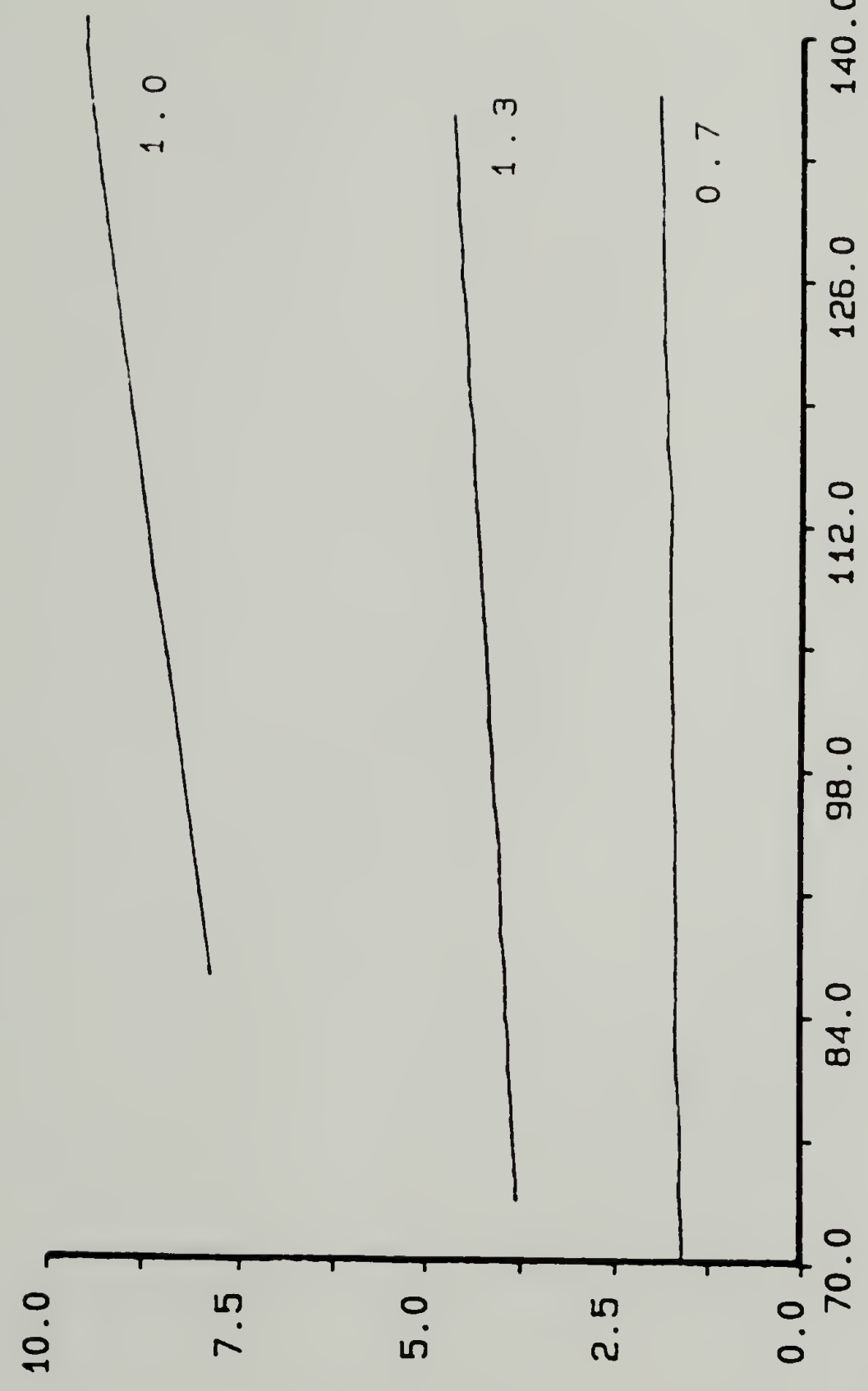

Figure 3.7. Equilibrium tensile modulus (Eeq) as a function of temperature during cooling of Jeffamine® ED-900/Epon 828 samples for the 0.7, 1.0 and 1.3 amine/epoxy equivalences.

decrease in Eeq, where the Eeq obtained at the 1.3 amine/epoxy ratio is greater than that obtained at the 0.7 ratio. Similar trends have been obtained by Morgan et al. for the curing of Jeffamine^{R} T-403 with DGEBA epoxy [47].

At the 0.7 amine/epoxy ratio there is an excess of epoxide groups and suggests the possibility of epoxy homopolymerization. In order to investigate this, a sample of Epon 828 was heated to 130° C for about 3 hr. After this time, no observable change in viscosity was noted. These data indicate that negligible epoxy etherification occurs in the absence of amine. It is unlikely that significant homopolymerization occurs in the presence of amine either. Epoxide-epoxide reactions are known to be catalyzed by tertiary amines [36]. In order for this to occur, it is necessary to form a tertiary amine from a primary amine since no tertiary amines are present at the start of cure. If this were to occur, it is believed that the geometric restrictions imposed by the incorporation of the tertiary amine into the network precludes the possibility of catalyzing any epoxide-epoxide reaction. At the 1.3 equivalence an excess of amine exists. This excess of amine suggests that fewer reactions per amine molecule occur and increases the average molecular weight between crosslinks. It should be mentioned that at this amine/epoxy ratio it is unlikely that free, unreacted amine exists because of the relatively high functionality of the amine.

As noted, at the 0.7 equivalence there is an excess of Epon 828 present within the network. While the possibility of unreacted Epon 828 exists at each equivalence, it is most prevalent at the 0.7 equivalence. If it is assumed that a significant fraction of unreacted Epon 828 does exist at the 0.7 equivalence then two effects can be attributed to its presence. The first effect is its ability to plasticize the network. This effectively lowers the network modulus. Second, the free or unreacted Epon 828 acts as a network diluent. Flory and others have noted that for such cases it is necessary to modify Equation (3.2) by including a term which accounts for the volumetric swelling of the network in comparison to the unswollen network [105,113]. Since elastically ineffective chains, such as pendant chains, act in a similar fashion to that of a diluent, this term also includes these contributions. However, without having data on the volume fraction of extractables present at the end of reaction or the fraction of pendant chains within the network, it is difficult to estimate this contribution. It can be stated, though, that the contribution of diluent and pendant chains would lower the calculated Mc for each of the networks. As a result, the calculated Mc's based upon the Impulse Viscoelastic measurements would be in closer agreement with the Mc's predicted from considerations of the reactant chemistry. As mentioned above, at the 1.3 amine/epoxy ratio it is unlikely that free, unreacted amine

is present. As a result, the effect of amine swelling due to can be neglected.

It is interesting to compare the trends in Eeq observed for the Jeffamine® series of amines at the different stoichiometric ratios with those measured for a V-40 cured Epon 828 epoxy system [68]. In those studies it was seen that the Eeq monotonically decreased with increasing amine/epoxy ratio for 0.8, 1.0 and 1.2 amine/epoxy equivalences. The difference in the trend of Eeq as a function of stoichiometry can be attributed to differences in chemical structure, particularly the amine functionality of the V-40 when compared to the Jeffamines®.

3.5.4 Effect of Amine Molecular Weight

The range in amine molecular weight investigated was 470 - 6100 g/mole. It was observed that at the higher molecular weights the times required to cure were much longer. This trend in cure time can be understood considering that the concentration of reactive groups is smaller at the higher molecular weights. As a result, the effective concentration of functional groups is smaller and the rate of reaction is therefore lower and a higher percentage of conversion would be required for gelation.

As expected, increasing the amine molecular weight increases the Mc of the network. Comparing the data in Tables 3.4 and 3.5 indicates that the most ideal entropic

networks were formed at the highest Mc, independent of the stoichiometric ratio used. Recall that Equation (3.2) postulates that the network has chain segments between crosslinks that are in a gaussian configuration. As a result, the chain segments are relatively mobile and unhindered by the presence of the crosslink junction [104,106]. The assumption of gaussian behavior becomes more accurate for loosely crosslinked systems, i.e., systems with many repeat chemical units between crosslinks, and should be contrasted to those networks formed by reacting Epon 828 with short chain aromatic amines. In order to check the validity of this network theory postulate, Figure 3.8 plots the Eeq predicted at 0 K (determined by the linear regression analysis presented in Table 3.4, section 3.4.2) against the Eeq measured at 140° C for each network. A linear regression analysis of the Eeq data in Figure 3.8 yields the following parameters: intercept = 0.661 MPa, slope = -0.425 and correlation coefficient = 0.967. This results of the linear regression are also plotted on Figure 3.8. The data in Figure 3.8 indicate excellent agreement with the network theory predictions for both relatively soft and stiff Jeffamine^{R}/Epon 828 networks. The fact that the regression intercept of 0.661 MPa is relatively close to zero is also encouraging, especially when one considers that a broad range of network structures (di- and triamines and three amine/epoxy stoichiometries) were examined. These

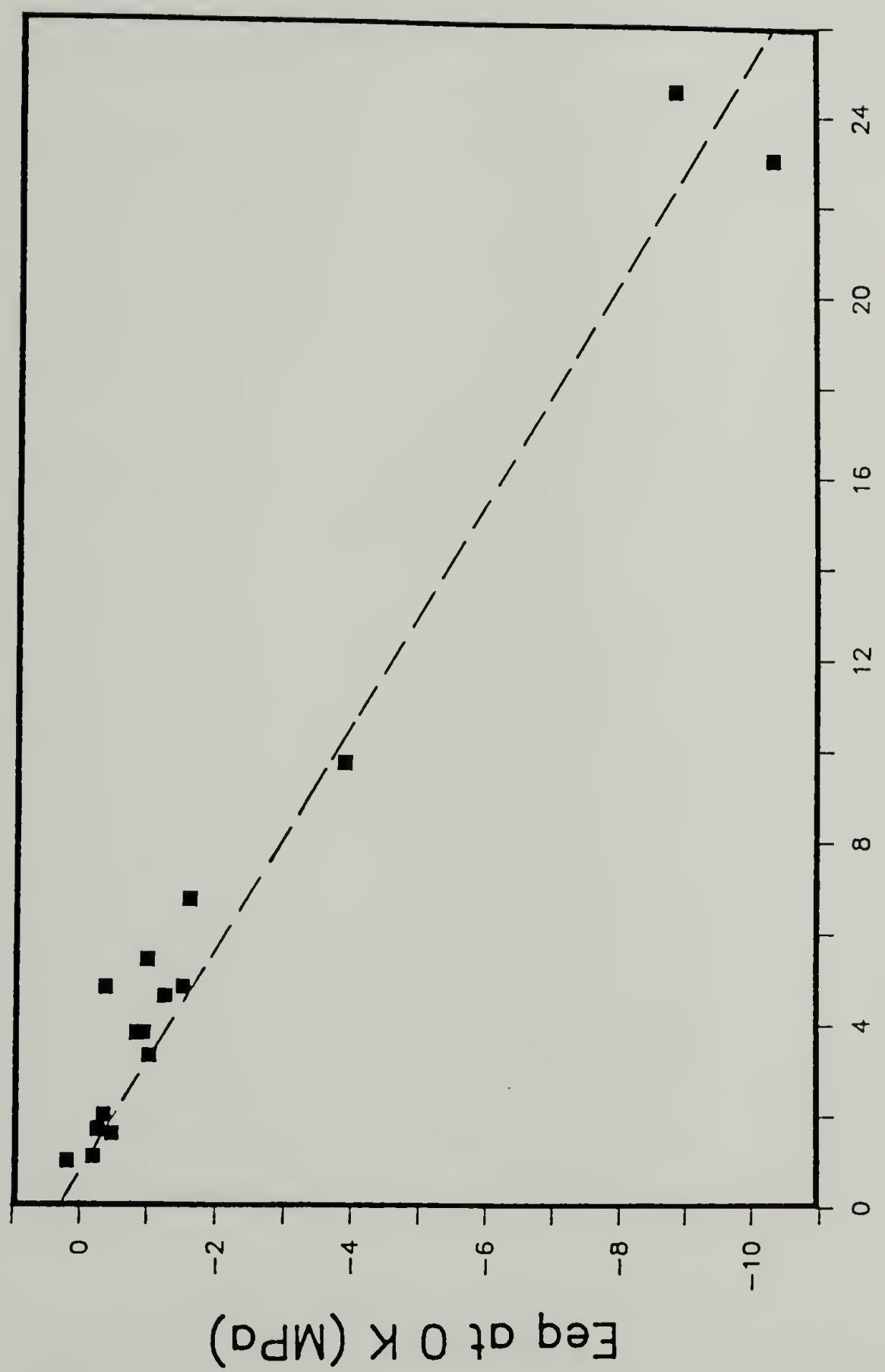

Figure 3.8. Equilibrium tensile modulus (Eeq) predicted at 0 K versus the Eeq measured at 140° C. Dashed line indicates the results of a linear regression analysis.

data suggest that for these materials it is possible to judge the ideality of a network from an entropic perspective based upon its equilibrium tensile modulus at 140° C.

3.6 Summary and Conclusions

The network mechanical properties of Epon 828 epoxy cured with several polyether amines were studied using the technique of Impulse Viscoelasticity. Several amine functionalities and molecular weights were examined. The resulting networks were useful to study since the starting materials were relatively well characterized and the network mechanical properties could be correlated to the reactant chemistry. In contrast to many thermosetting materials these Jeffamine^{R}/Epon 828 networks cured elastically and could accurately be described using rubber elasticity theory. The networks prepared at the 1.0 equivalence produced materials with the highest equilibrium tensile modulus and required the longest time to completely cure. In general the networks prepared at the 0.7 amine/epoxy ratio underwent more shrinkage and behaved more like ideal entropic networks than the networks formed at the 1.0 ratio.

It is believed that the goal of demonstrating the viability of the Impulse Viscoelastic technique as a useful characterization method was achieved. In Chapter IV the

results of a more complicated reacting system, Epon 828 copolymerized with ring opening monomer, are presented.

C H A P T E R 4

CURING BEHAVIOR OF EPOXY COPOLYMERIZED WITH RING OPENING MONOMER

4.1 Introduction

Recently much attention has focused on the importance of residual cure and thermal stresses on the mechanical performance of cured materials [77-86]. Cure stresses arise in materials which normally exhibit volume changes (due to cure chemistry) but are prevented from doing so by dimensional constraints. In a similar fashion, thermal stresses also arise from conditions of dimensional constraints, such as mismatches in the filler and matrix thermal expansion coefficients. With regard to the volumetric changes due to polymerization, it is known that thermosetting materials undergo approximately 5% shrinkage during cure [36]. In order to minimize the stresses associated with this process it might be advantageous to use materials which expand upon polymerization. In this regard, Bailey et al. recently synthesized monomers which dilate when polymerized [52-54]. When copolymerized with epoxy resins, these ring opening monomers have been suggested to improve the strength, toughness and adhesion of epoxies while reducing the volumetric shrinkage due to cure [56,114,115]. In particular, it is important to understand

how the copolymerization affects the residual cure and thermal stresses. Previous researchers have examined the mechanical properties of cured copolymers of epoxy and ring opening monomers [116]. *In situ* mechanical studies during cure, however, have yet to be conducted.

This chapter presents results on the *in situ* curing behavior of an epoxy resin copolymerized with ring-opening monomer using the technique of Impulse Viscoelasticity coupled with incremental linear elasticity. Experimental emphasis was placed on the determination of the equilibrium tensile modulus, cure stress, volumetric changes and glass transition temperature of these copolymers during cure.

4.2 Materials

Epon 828, a DGEBA (diglycidyl ether of bisphenol-A) epoxy was chosen as the matrix resin. For these studies, Armstrong World Industries, Inc. (Lancaster, PA) generously provided us with a spiro orthocarbonate (SPOC) ring-opening monomer for evaluation as an additive in epoxy resins. The equivalent weights for these materials are 190 and 288 g/mole, respectively. Nadic methyl anhydride (NMA) and benzyl dimethylamine (BDMA) were used as curing agent and accelerator, respectively. The chemical structures of Epon 828, SPOC, NMA and BDMA are shown in Figure 4.1. This choice of materials was based upon suggestions in the

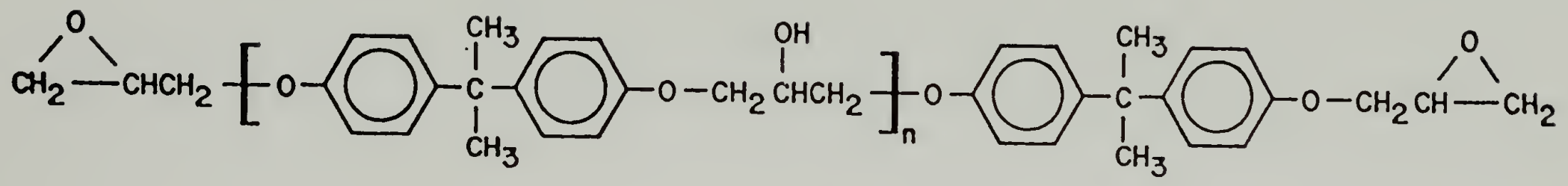

EPON 828

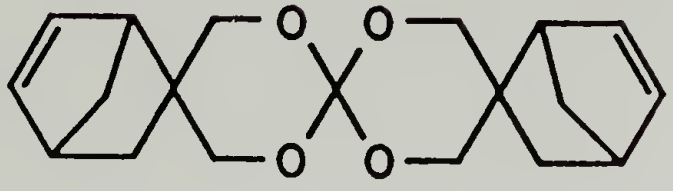

SPOC

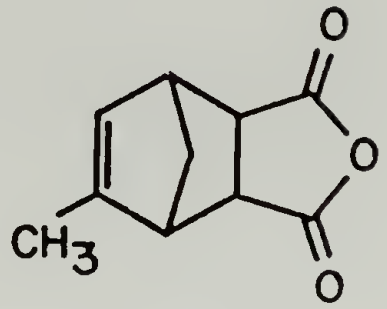

NMA

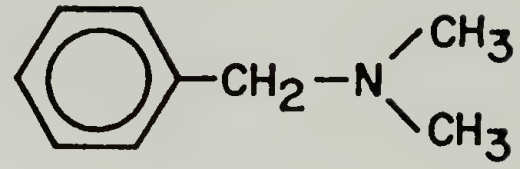

BDMA

Figure 4.1. Chemical structures for Epon 828 (85% n = 0, 15% n = 1), spiro orthocarbonate (SPOC), nadic methyl anhydride (NMA) and benzyl dimethylamine (BDMA).

available technical literature [56]. All materials were used as received.

4.3 Experimental

In order to better understand the relationship between network mechanical properties and cure chemistry, two sets of samples were formulated. In the first set, referred to as the EPON- series, the amounts of SPOC, NMA and BDMA added were based upon the amount of Epon 828 used. Specifically, the base or neat formulation consisted of 94 parts by weight NMA and 2.5 parts by weight BDMA added to 100 parts Epon 828 epoxy resin. Note that this formulation contains a stoichiometric amount of NMA relative to Epon 828. To this neat formulation 10, 30, 50, 70, 90 and 110 parts by weight SPOC were added. Thus a sample designated as EPON-100/70 refers to the sample based upon 100 parts Epon 828 modified by 70 parts SPOC.

In the second set of samples, designated the SPOC- series, the amounts of NMA and BDMA added were based upon the total weight of Epon 828 and SPOC used. Specifically, 94 parts by weight NMA and 2.5 parts by weight BDMA added to 100 total parts of Epon 828 and SPOC. Epon 828/SPOC weight ratios of 70/30, 50/50 and 30/70 were formulated. Thus, a sample designated as SPOC-70/30 refers to the sample based upon 70 parts Epon 828 modified by 30 parts SPOC. Note that

sample EPON-100/0 can also be referred to as SPOC-100/0. A summary of the formulations is given in Table 4.1.

Each formulation was weighed and partially mixed at room temperature. The mixture was heated to 50° C in order to promote dissolution of the SPOC powder in the anhydride-epoxy mixture. Upon subsequent cooling to room temperature no macroscopic phase separation was observed. It should be noted that at the higher levels of SPOC complete dissolution did not occur.

In order to study the uniaxial mechanical properties the already discussed rubber membrane-aluminum tab sample assembly was used as a sample substrate. This method constrains the initially liquid samples in a uniaxial geometry. After filling the rubber membrane assembly with the resin mixture, the samples were placed inside the environmental chamber of the Dynastat for curing. A cure temperature of 125° C was selected. In order to minimize the heating time and help assure isothermal polymerization conditions, the chamber was preheated to 110° C. After the samples were secured within the chamber the temperature was ramped to 125° C as quickly as possible. It was, however, difficult to control the time required to accomplish this for each sample. As a result, the cure time at 125° C for each sample varied slightly. A 70 ± 5 min polymerization was used after which the samples were cooled at fixed strain

Table 4.1

Formulations used in the Copolymerization of Epon 828 and SPOC

Sample	Epon 828	SPOC	NMA	BDMA
EPON-100/0	100	0	94	2.5
EPON-100/10	100	10	94	2.5
EPON-100/30	100	30	94	2.5
EPON-100/50	100	50	94	2.5
EPON-100/70	100	70	94	2.5
EPON-100/90	100	90	94	2.5
EPON-100/110	100	110	94	2.5
SPOC-70/30	70	30	94	2.5
SPOC-50/50	50	50	94	2.5
SPOC-30/70	30	70	94	2.5

Data are in units of parts by weight.

at a rate of 1° C/min in order to obtain the glass transition temperature, T_g.

Uniaxial step-strain deformations were used to characterize the curing process. The advantage of this type of deformation was discussed in Chapter II. The magnitude of the deformations was initially 3% and decreased during the experiment in order to maintain linear viscoelastic conditions. Each pulse deformation was 10 seconds in duration and was applied to the sample every 70 to 100 seconds depending upon the relaxation time of the sample. For each pulse, the sample load, displacement and temperature were collected at a rate of 10 Hz. The equations presented in Chapter II were used to calculate the Impulse Viscoelastic properties using a voltage tolerance of 0.003 V. In order to obtain pre-gel information, pulse deformation data collection began at a temperature between 120 and 125° C. Typically, a total of 40-120 pulses were taken during the polymerization and cooling portions of each experiment. At the end of each experiment, the cured samples (typically 6 mm in diameter and 25 mm in length) were sectioned into small volumes for density measurements using hydrostatic weighing techniques.

4.4 Results

The results of the curing studies using the Impulse Viscoelastic technique are presented in this section together with the volumetric data obtained by density measurements.

4.4.1 Density Measurements

The initial densities were calculated using a weighted average of the individual constituent densities (d_{828} = 1.16 g/cm^3, d_{SPOC} = 1.29 g/cm^3, d_{NMA} = 1.23 g/cm^3, and d_{BDMA} = 0.89 g/cm^3) and assuming ideal solution behavior. The final densities were calculated using Archimedes' principle of hydrostatic weighing. Air and methanol were used as the fluid media. Each cured sample was sectioned into pieces measuring 0.1-0.2 cm^3 in volume. Two density measurements were made for each sample at room temperature. Table 4.2 summarizes the volumetric data for each composition.

4.4.2 Impulse Viscoelastic Measurements

Figures 4.2a-e are a set of pulse deformations taken from the cure of sample SPOC-70/30. Specifically, Figure 4.2a is a pulse 3 minutes into the polymerization and illustrates the small contribution of the rubber membrane used to support the sample. At this time in the polymerization, the material has not yet gelled. Figure

Table 4.2

Volumetric Data for SPOC/Epon 828 Copolymers

Sample	Initial Density [g/cm³]	Final Density [g/cm³]	Volumetric Expansion [%]
EPON-100/0	1.19	1.225	-2.9
EPON-100/10	1.20	1.228	-2.3
EPON-100/30	1.21	1.234	-2.0
EPON-100/50	1.21	1.233	-1.9
EPON-100/70	1.22	1.207	+1.1
EPON-100/90	1.23	1.200	+2.4
EPON-100/110	1.23	1.167	+5.1
SPOC-70/30	1.21	1.234	-2.0
SPOC-50/50	1.23	1.235	-0.4
SPOC-30/70	1.24	1.228	+1.0

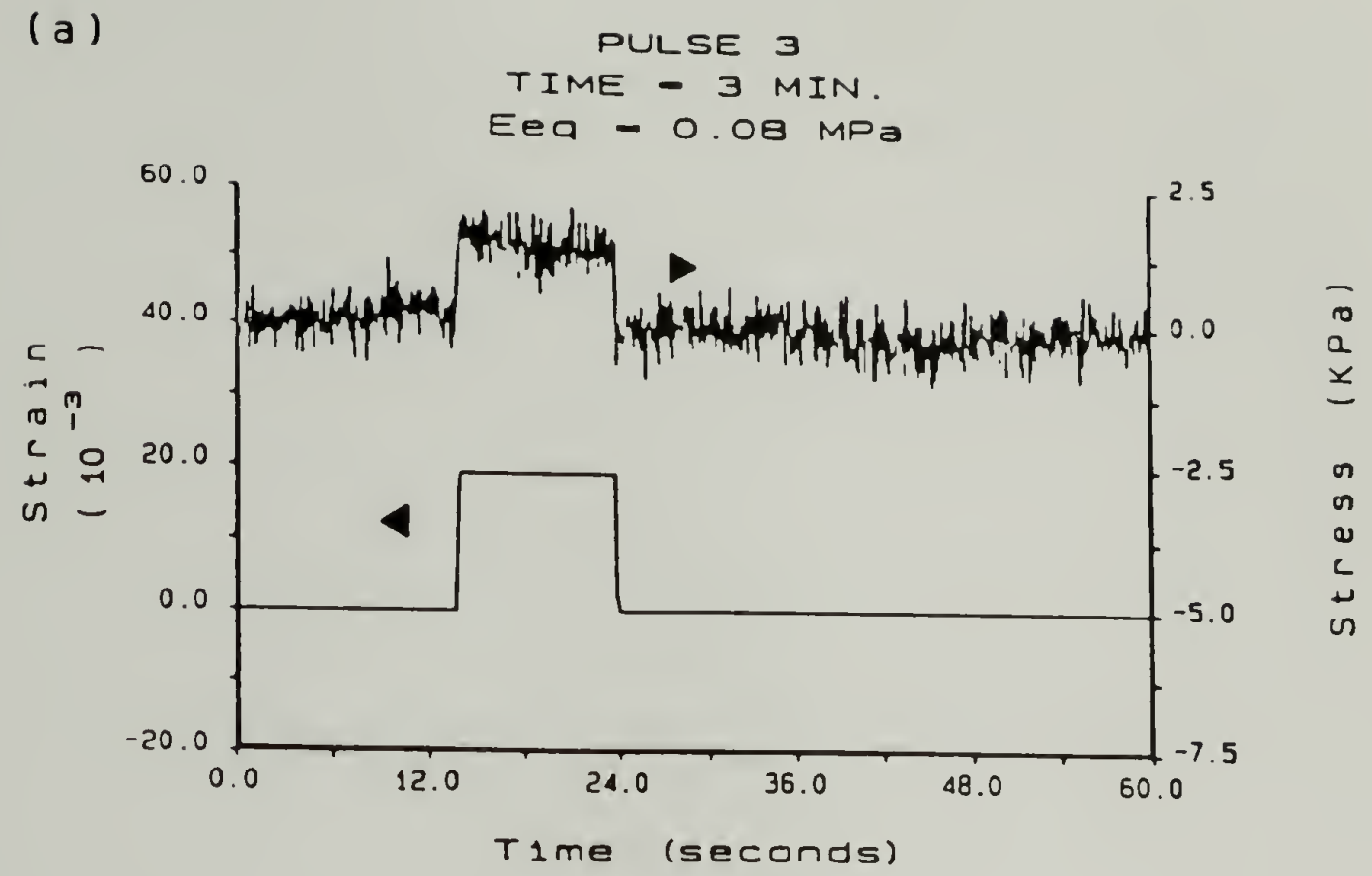

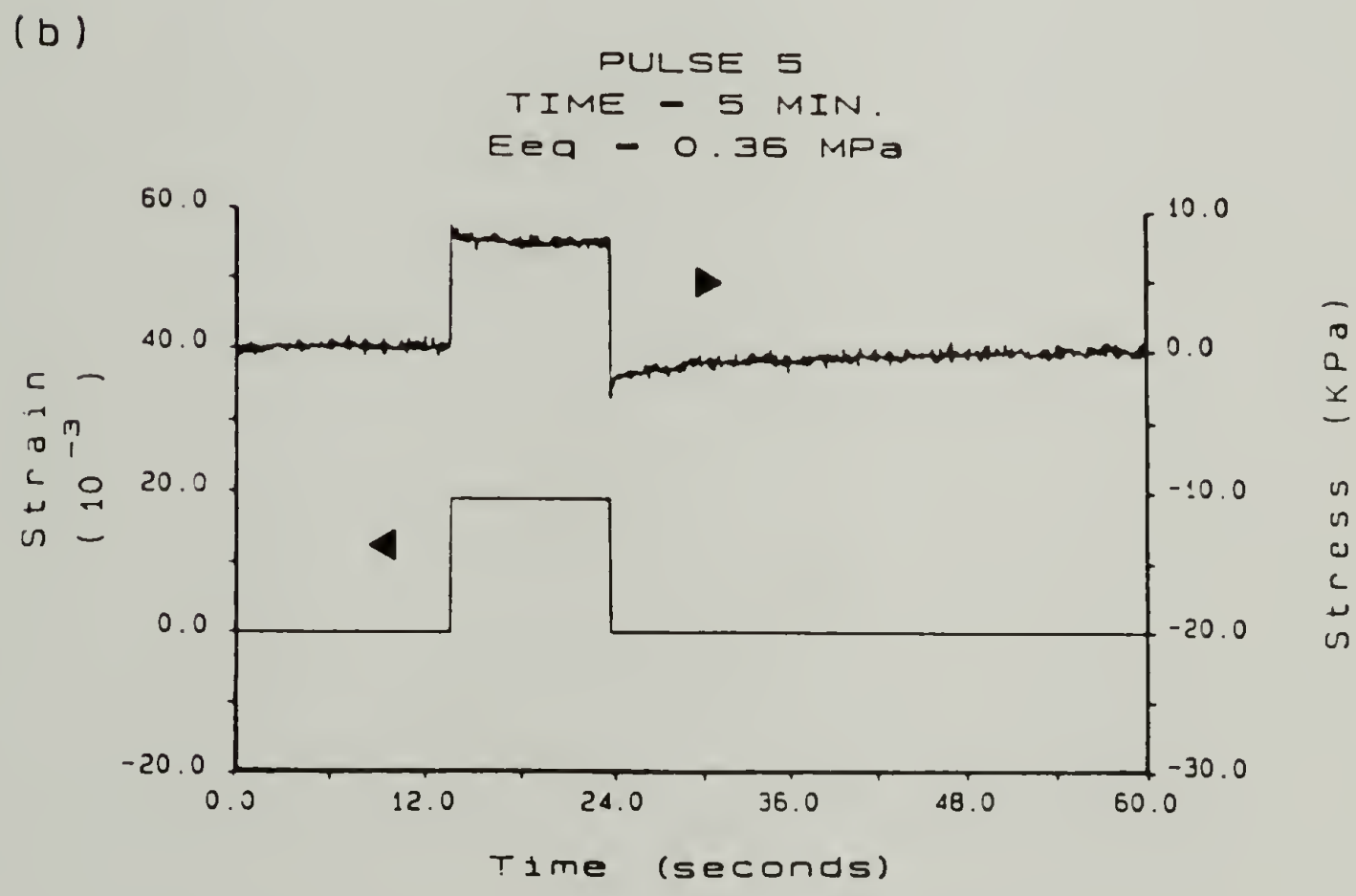

Figure 4.2. Pulse deformations and the resulting stress responses for sample SPOC-70/30 at the following stages of cure: a) 3 minutes (prior to gelation), b) 5 minutes (just after gelation) **(continued on next page)**

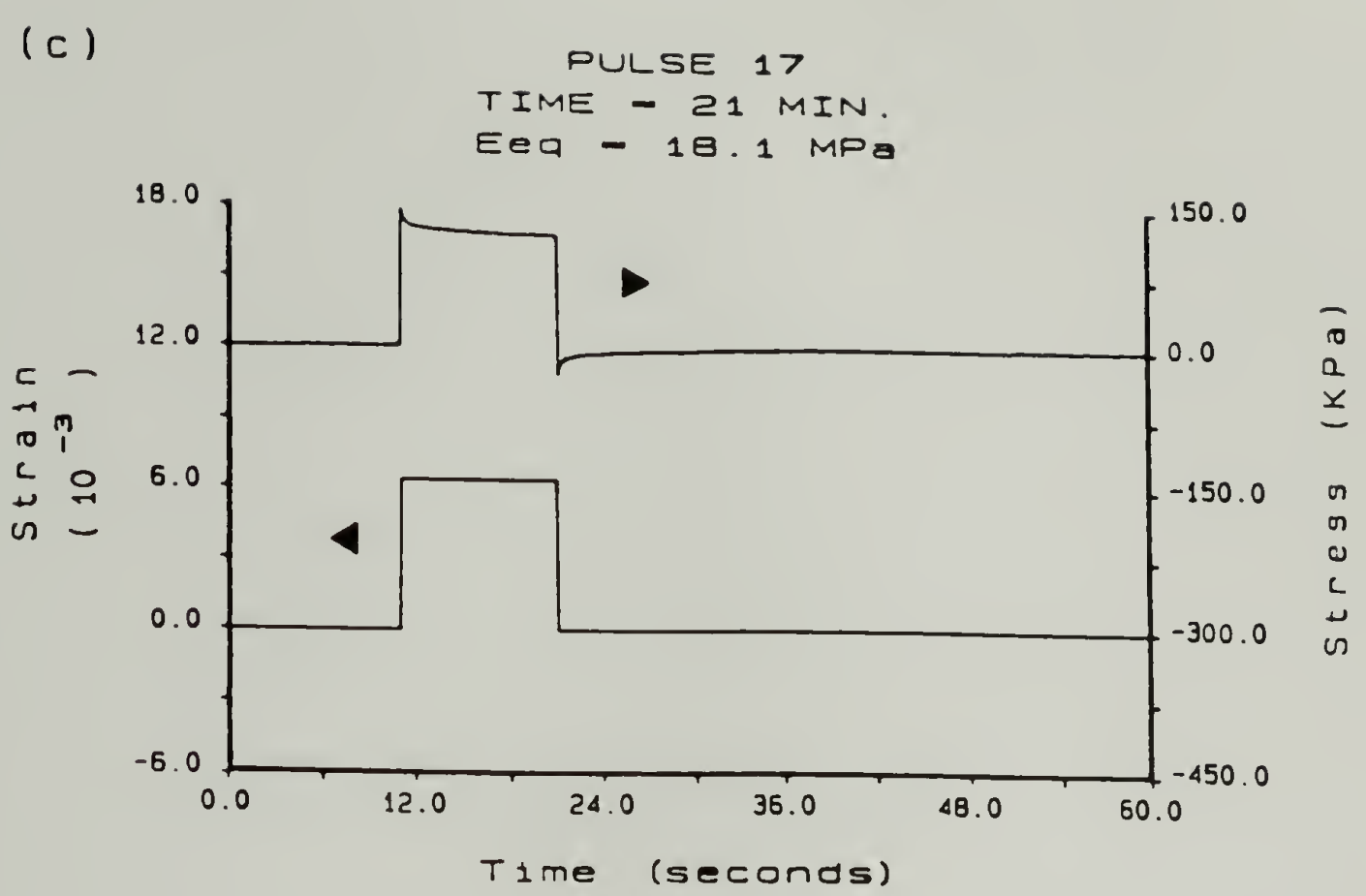

Figure 4.2 (cont). Pulse deformations and the resulting stress responses for sample SPOC-70/30 at the following stages of cure: c)21 minutes, d) 33 minutes **(continued on next page)**

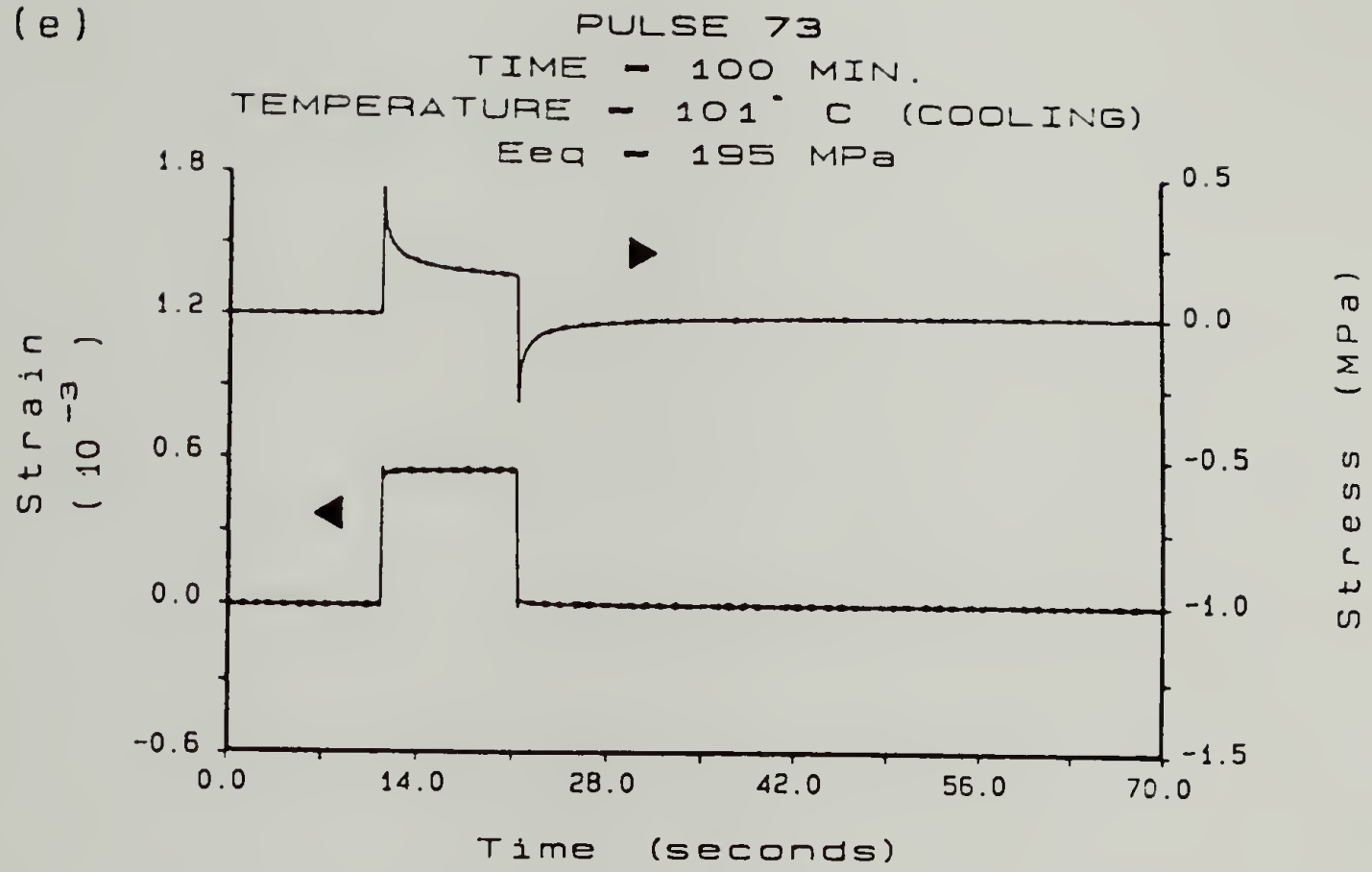

Figure 4.2 (cont). Pulse deformations and the resulting stress responses for sample SPOC-70/30 at the following stages of cure: e) 100 minutes (during cooling).

4.2b is a pulse taken just after gelation and indicates that the material possesses long relaxation times. Figures 4.2c and d are pulse deformations applied at 21 and 33 minutes, respectively, into the polymerization and indicate increasing degrees of time dependency in the stress response of the sample to deformation. Figure 4.2e was taken from the cooling portion of the experiment. At the top of each figure the pulse number, time into the polymerization and equilibrium tensile modulus (Eeq) are listed. From each pulse, the mechanical properties of the material were calculated using time-weighted moments and Laplace and Fourier analyses of the load and displacement signals as discussed in Chapter II.

The data that have been included in this section are representative of the behavior of the ring opening materials. Figure 4.3 plots the equilibrium tensile modulus (Eeq) and the shrinkage stress as functions of time during the isothermal polymerization (T = 125° C) of sample EPON-100/0. The bulk of the rise in Eeq after 40 minutes of cure is attributed to vitrification. The shrinkage stress plotted on Figure 4.3 is exactly the one-dimensional cure stress since for a sample held at constant strain which is polymerizing isothermally. Similarly, for a polymerized sample held at constant strain, the shrinkage stress is exactly the one-dimensional thermal stress. For the uniaxial geometry a tensile (+) stress is indicative of

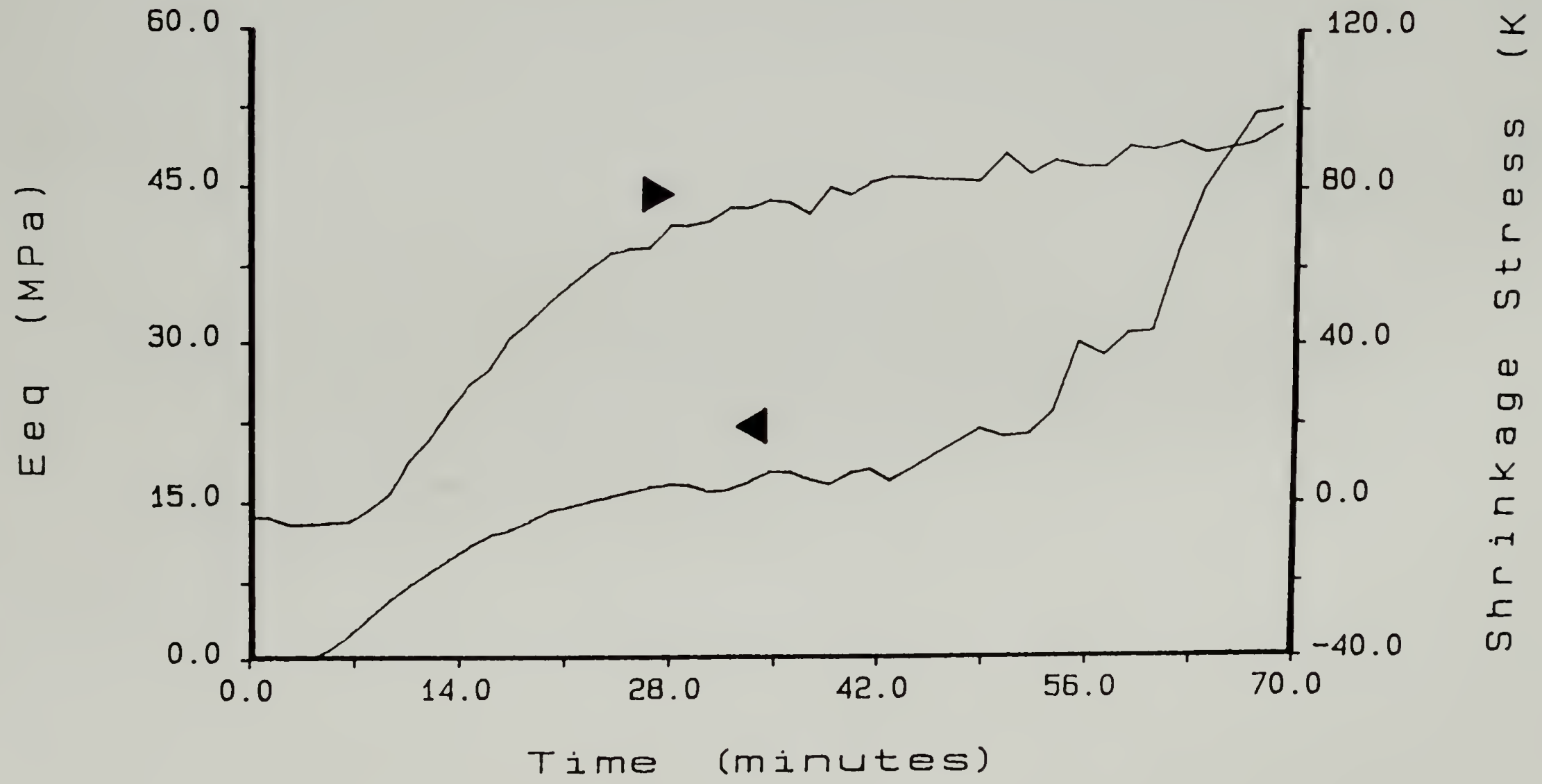

Figure 4.3. Equilibrium tensile modulus (Eeq) and shrinkage (cure) stress obtained during the isothermal polymerization (T = 125° C) of sample EPON-100/0.

contraction, while a compressive (-) stress is indicative of expansion. Knowing this stress, in combination with the equations of elasticity and Poisson's ratio, the stresses in multi-dimensionally constrained systems can be estimated. These ideas will be developed more fully below. In addition, Figure 4.4 plots the steady state elongational viscosity (SSEV) and mean relaxation time (MRT) during isothermal polymerization. The quantities Eeq/E' at 0.15 Hz and tan δ at 0.15 Hz are shown on Figure 4.5 as functions of polymerization time for sample EPON-100/0. Note that Eeq/E' is equal to unity and tan δ is approximately zero at the beginning of polymerization. Both of these values are consequences of the elastic rubber membrane. The properties displayed in Figures 4.6 and 4.7 were measured for sample EPON-100/0 during the cooling portion of the experiment. These data obtained during cooling indicate that it is possible to measure mechanical properties of glassy materials. As a result of instrumentation noise and the numerical integration techniques, fluctuations in the calculated data are to be expected, especially for the viscosity and relaxation data which involve higher moments of the stress and strain responses.

In order to examine the effect of SPOC content on the mechanical properties, Figure 4.8 plots the equilibrium tensile modulus (Eeq) during isothermal cure for samples EPON-100/30, EPON-100/70 and EPON-100/110. The shrinkage

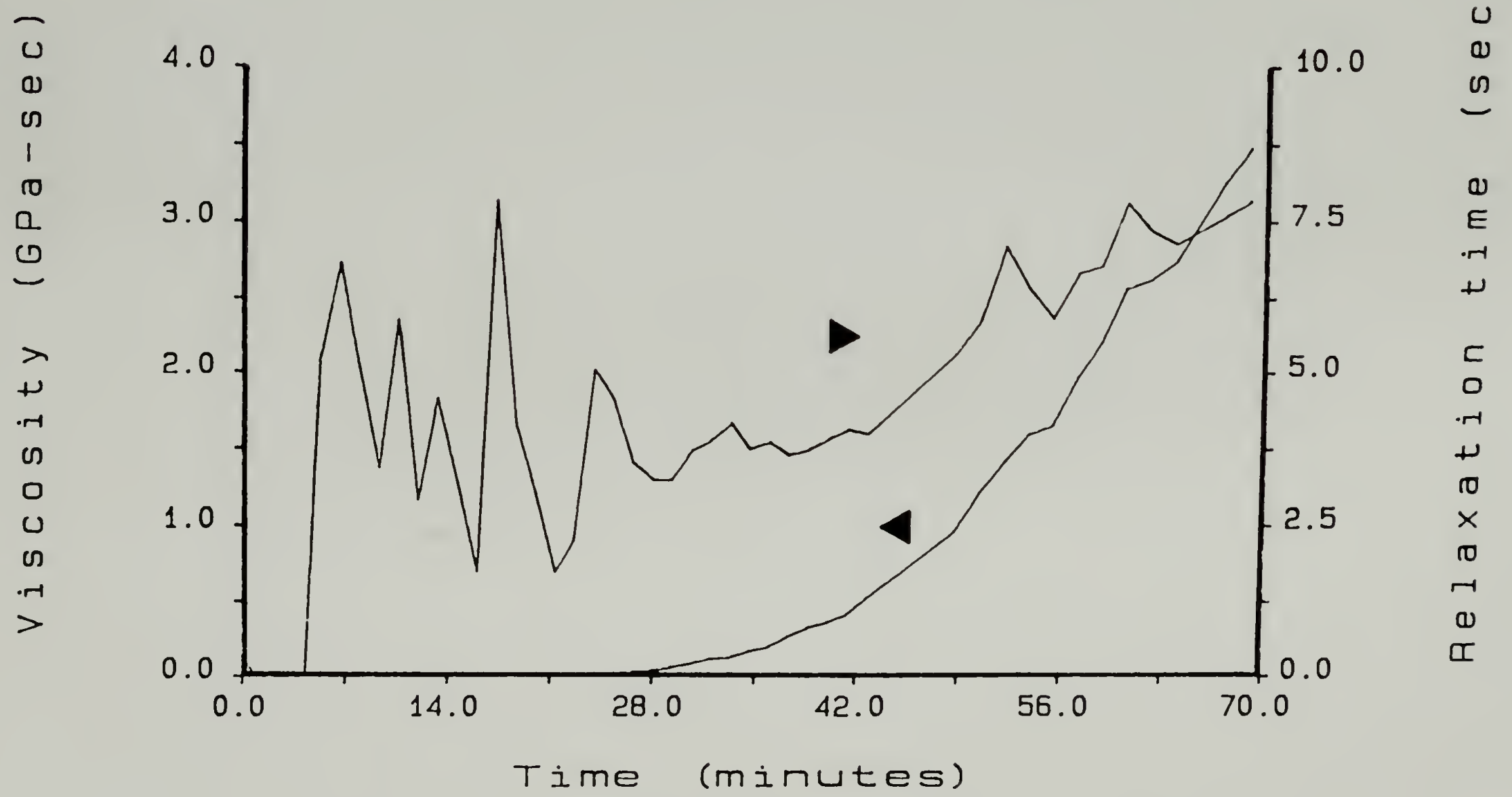

Figure 4.4. Steady state elongational viscosity and mean relaxation time obtained during the isothermal polymerization (T = 125° C) of sample EPON-100/0.

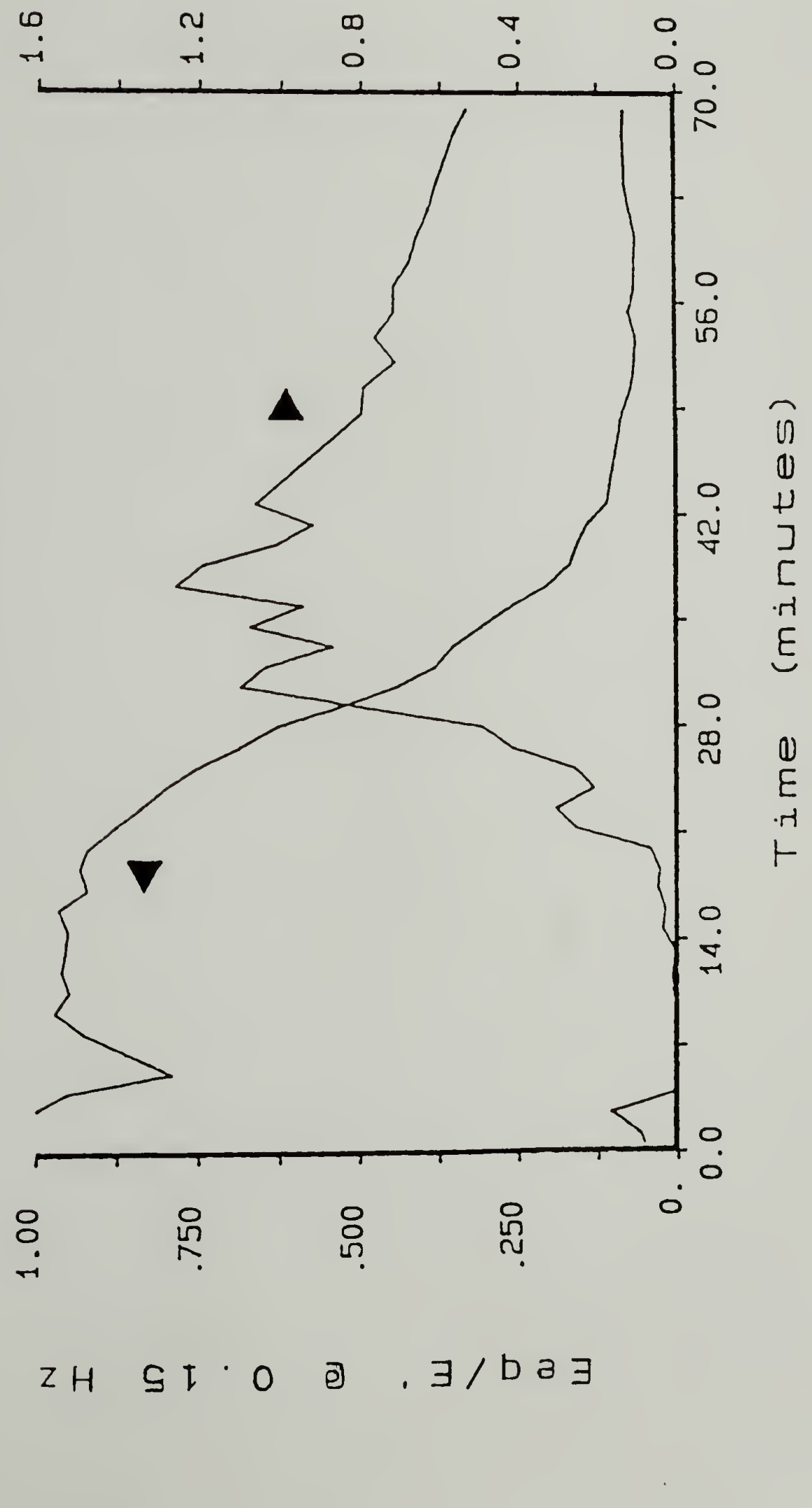

Figure 4.5. Eeq/E' @ 0.15 Hz and tan δ @ 0.15 Hz obtained during the isothermal polymerization (T = 125° C) of sample EPON-100/0.

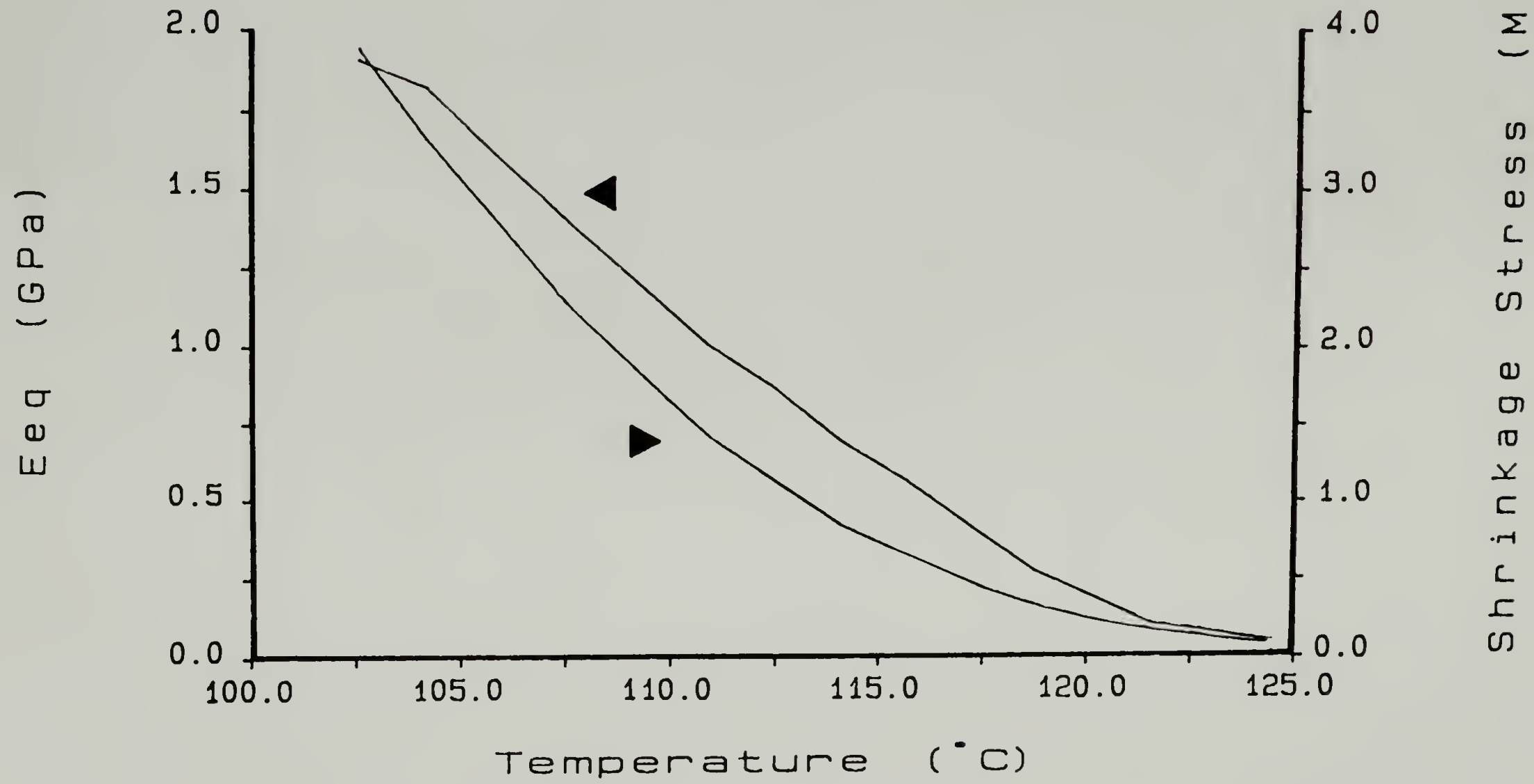

Figure 4.6. Equilibrium tensile modulus (Eeq) and shrinkage (thermal) stress obtained for sample EPON-100/0 during cooling.

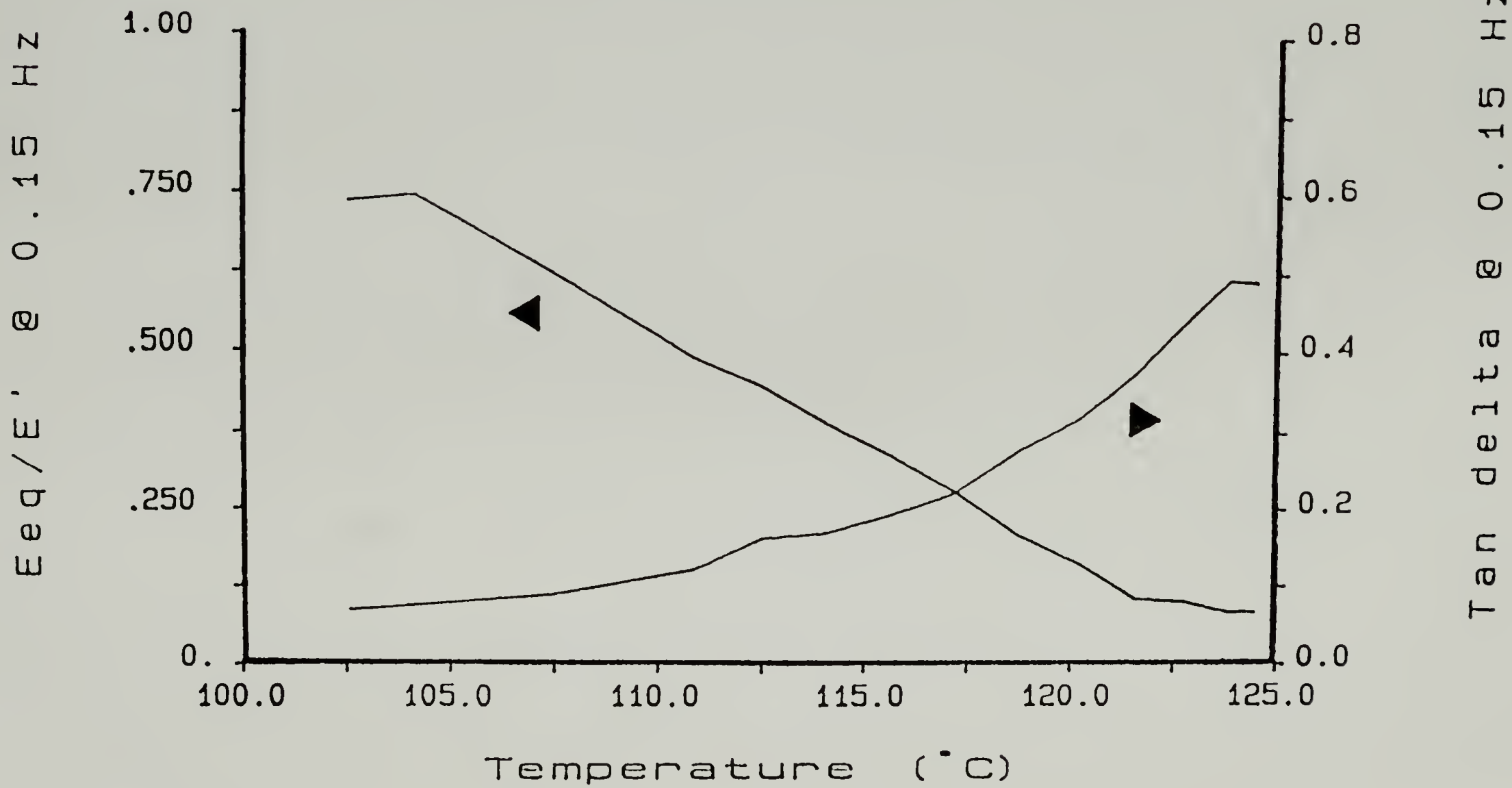

Figure 4.7. Eeq/E' @ 0.15 Hz and tan δ @ 0.15 Hz obtained for sample EPON-100/0 during cooling.

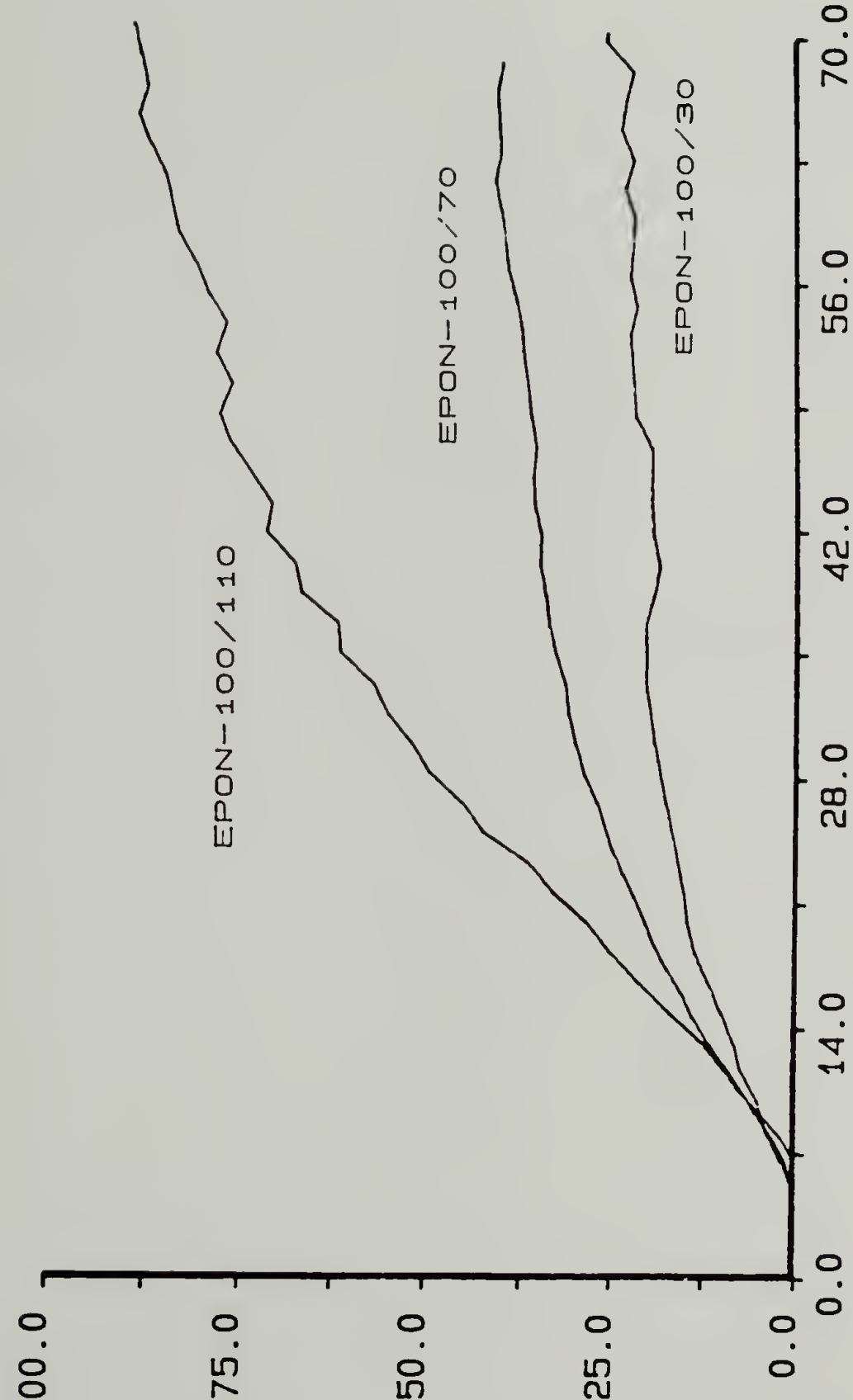

Figure 4.8. Equilibrium tensile modulus (Eeq) for samples EPON-100/30, EPON-100/70 and EPON-100/110 during isothermal polymerization (T = 125° C).

or cure stress for these EPON- samples during polymerization are shown on Figure 4.9. In order to contrast the EPON- from the SPOC- series of samples, Figure 4.10 presents the equilibrium tensile modulus during cure for the SPOC-30/70, SPOC-50/50 and SPOC-70/30 samples. The corresponding shrinkage stress behavior for these SPOC- samples is given on Figure 4.11. In order to more clearly view the development of Eeq and shrinkage stress during cure, Figure 4.12 plots the equilibrium tensile modulus and the shrinkage stress of sample SPOC-30/70 during isothermal polymerization.

Impulse Viscoelastic data obtained during cooling are displayed in Figure 4.13, where Eeq is shown as a function of temperature for samples EPON-100/30, EPON-100/70 and EPON-100/110. For these same samples, the shrinkage or thermal stress during the cooling portion of the experiment are displayed on Figure 4.14. The Eeq behavior of samples SPOC-30/70, SPOC-50/50 and SPOC-70/30 are plotted as a function of temperature during cooling on Figure 4.15. The corresponding thermal stress behavior (during cooling) for each of the SPOC- samples is illustrated in Figure 4.16.

Table 4.3 summarizes the Eeq, steady state elongational viscosity (SSEV), mean relaxation time (MRT), ratio of Eeq/E' at 0.15 Hz, one-dimensional cure stress and glass transition temperature (T_g) measured at the end of

Figure 4.9. Shrinkage (cure) stress for samples EPON-100/110 during isothermal polymerization (T = 125° C).

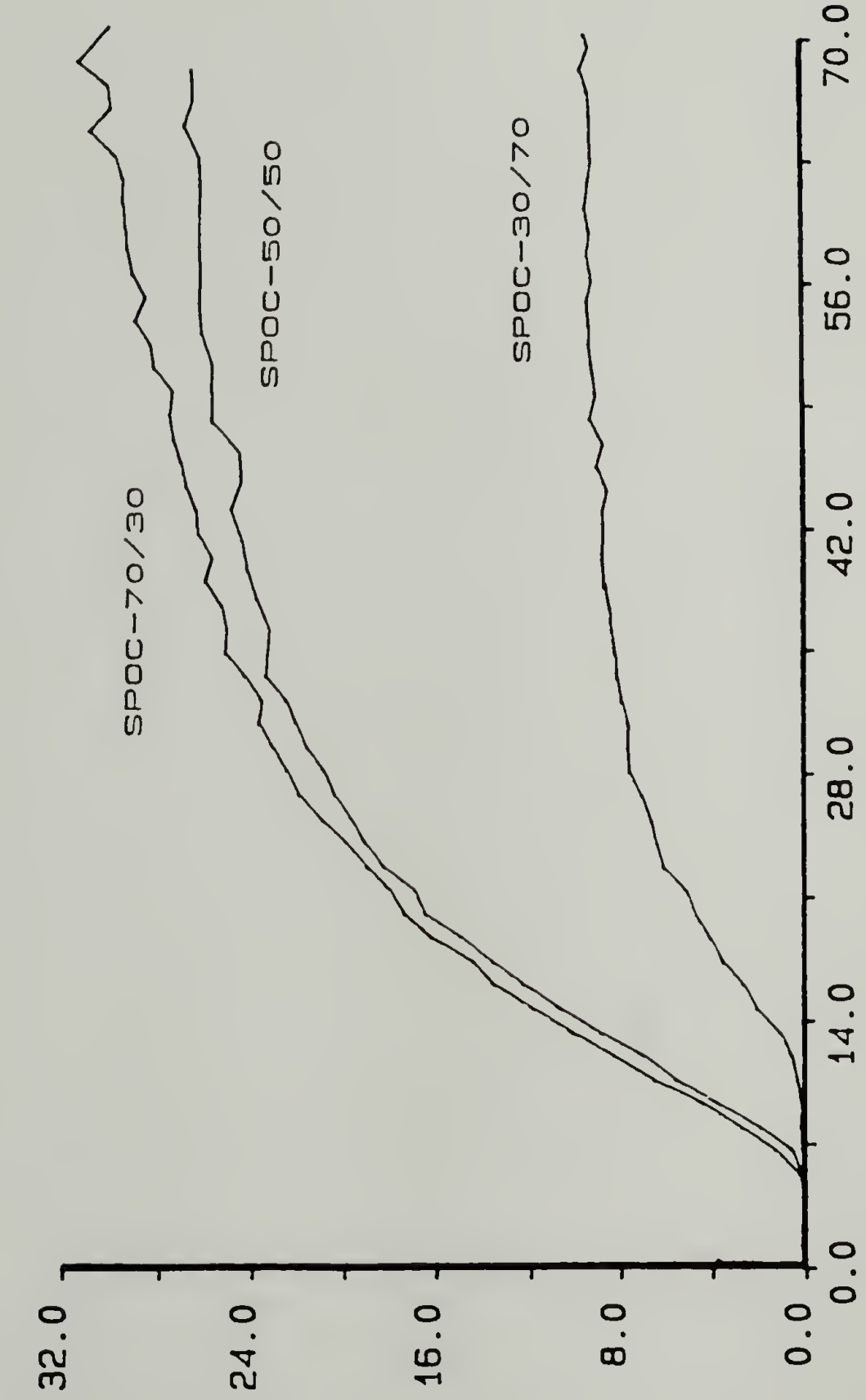

Figure 4.10. Equilibrium tensile modulus (Eeq) for samples SPOC-70/30, SPOC-50/50 and SPOC-30/70 during isothermal polymerization (T = 125° C).

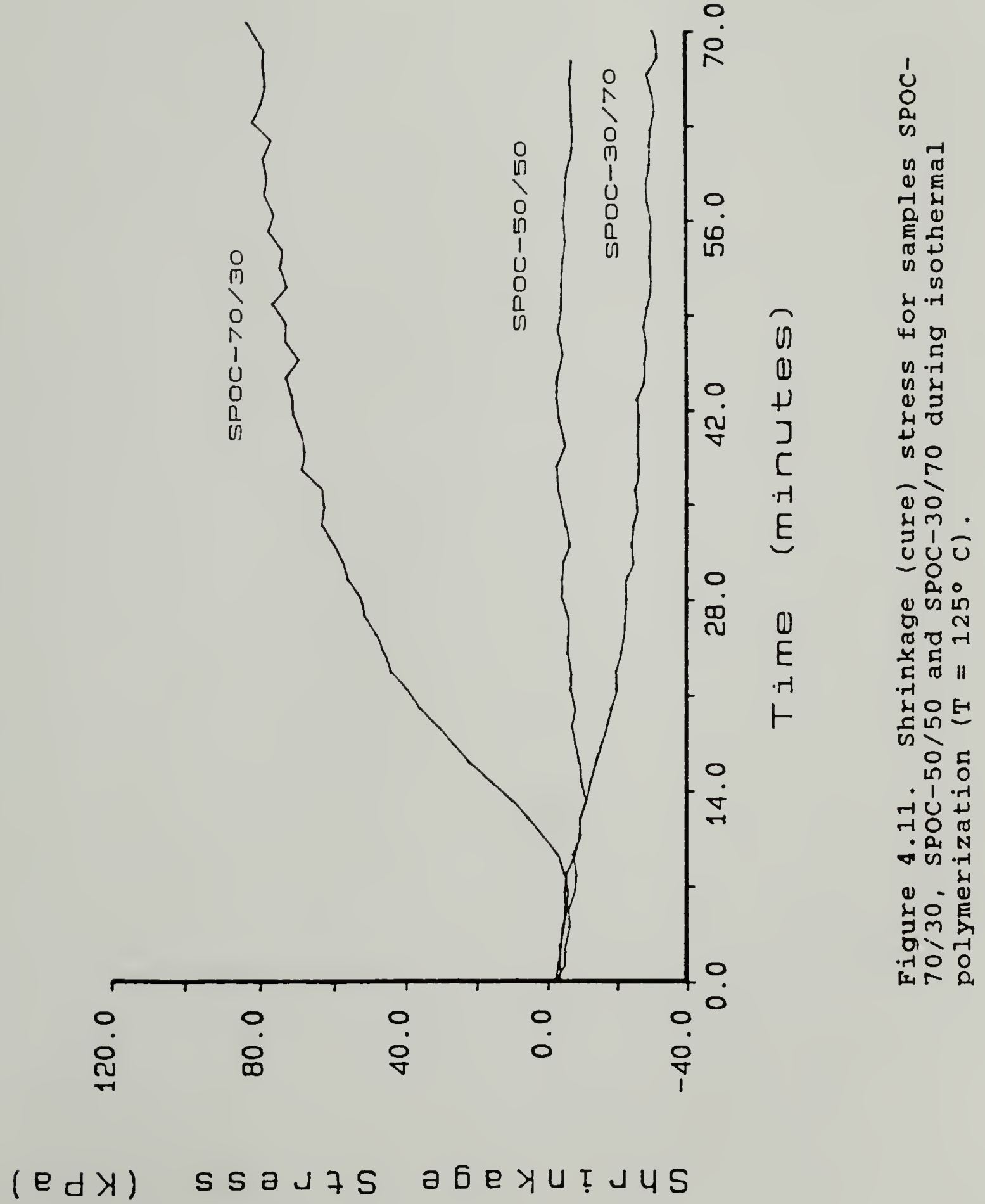

Figure 4.11. Shrinkage (cure) stress for samples SPOC-70/30, SPOC-50/50 and SPOC-30/70 during isothermal polymerization (T = 125° C).

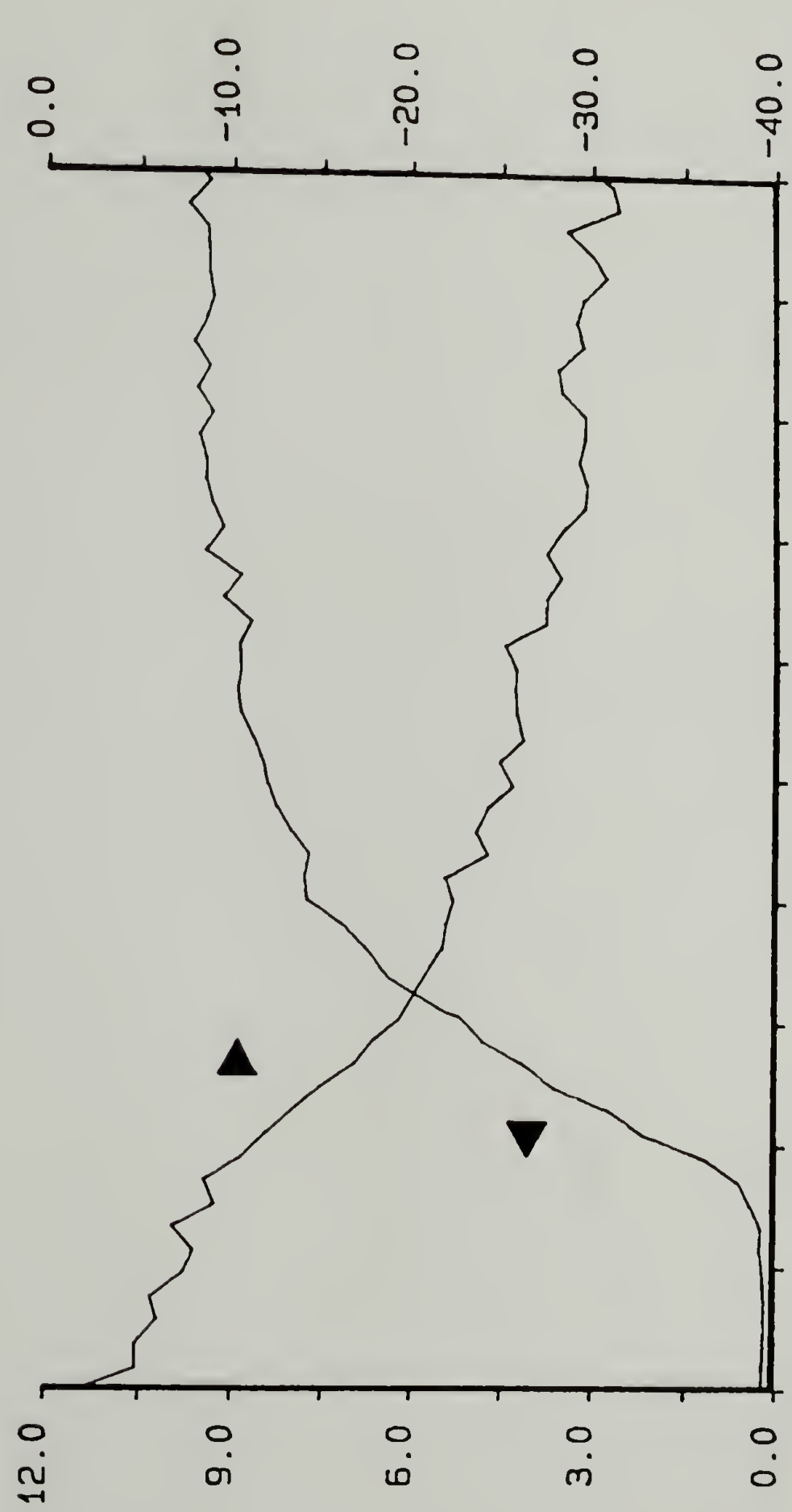

Figure 4.12. Equilibrium tensile modulus (Eeq) and shrinkage (cure) stress during isothermal polymerization (T = 125° C) of sample SPOC-30/70.

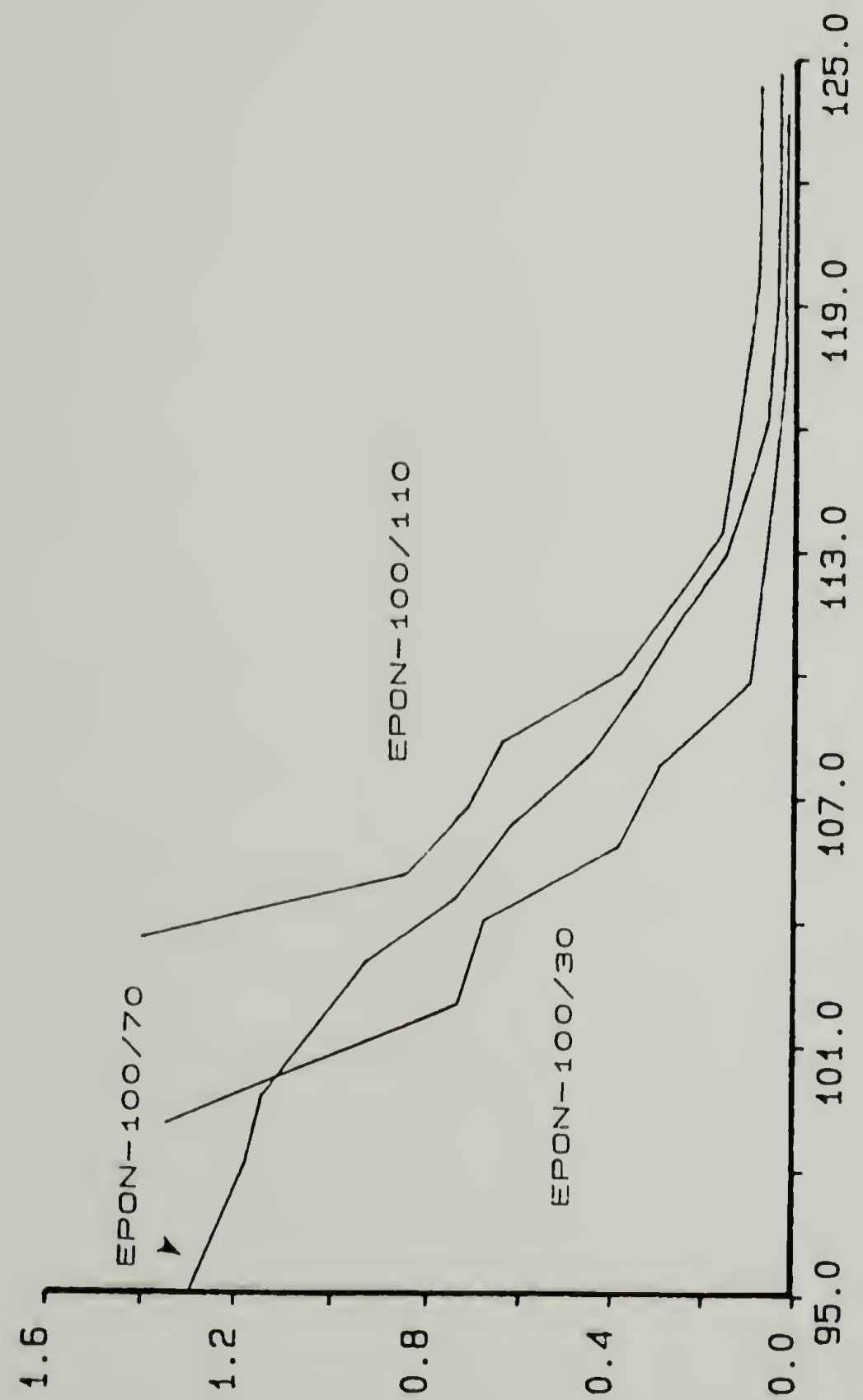

Figure 4.13. Equilibrium tensile modulus (Eeq) for samples EPON-100/30, EPON-100/70 and EPON-100/110 during cooling.

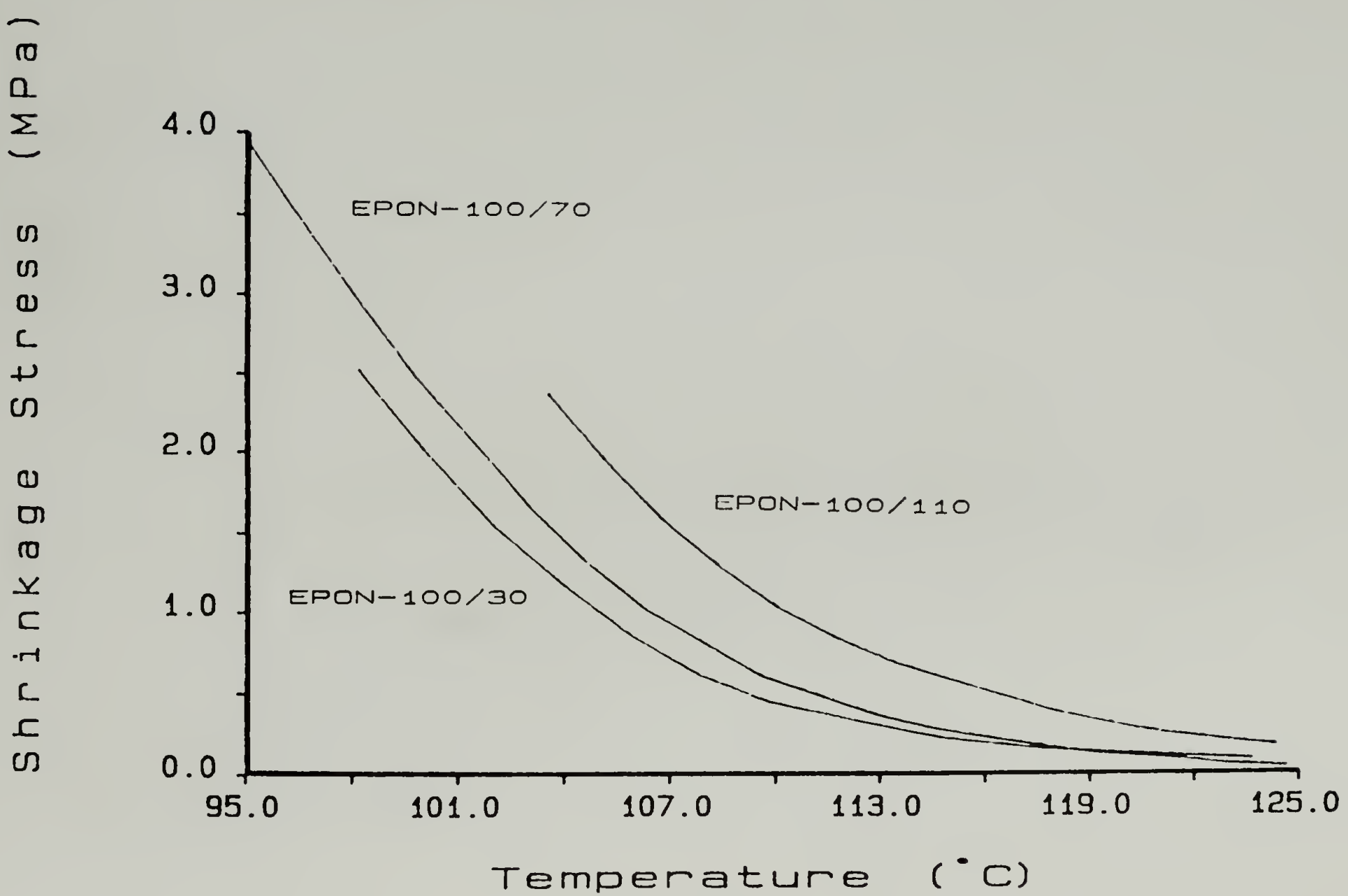

Figure 4.14. Shrinkage (thermal) stress for samples EPON-100/30, EPON-100/70 and EPON-100/110 during cooling.

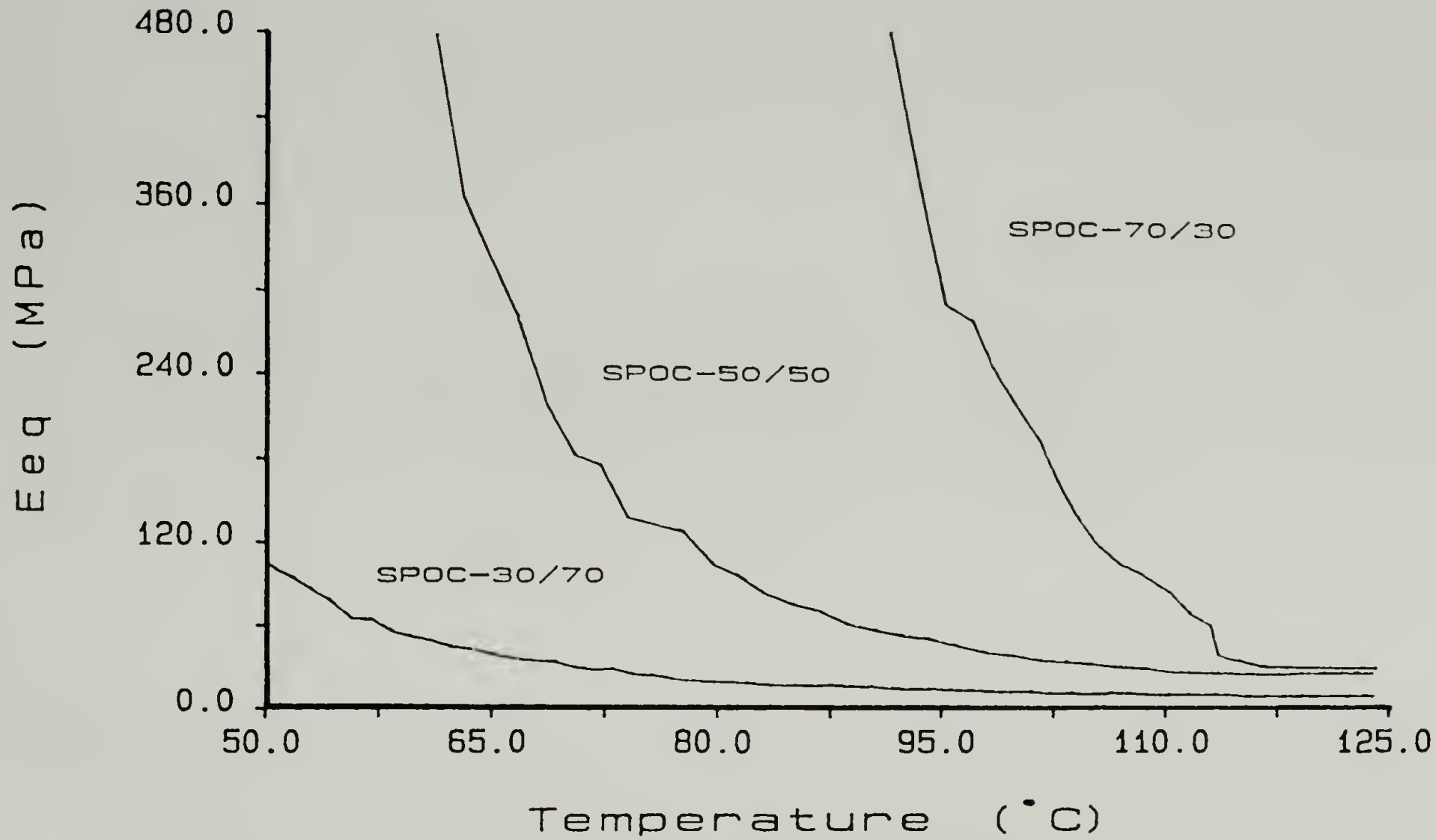

Figure 4.15. Equilibrium tensile modulus (Eeq) for samples SPOC-70/30, SPOC-50/50 and SPOC-30/70 during cooling.

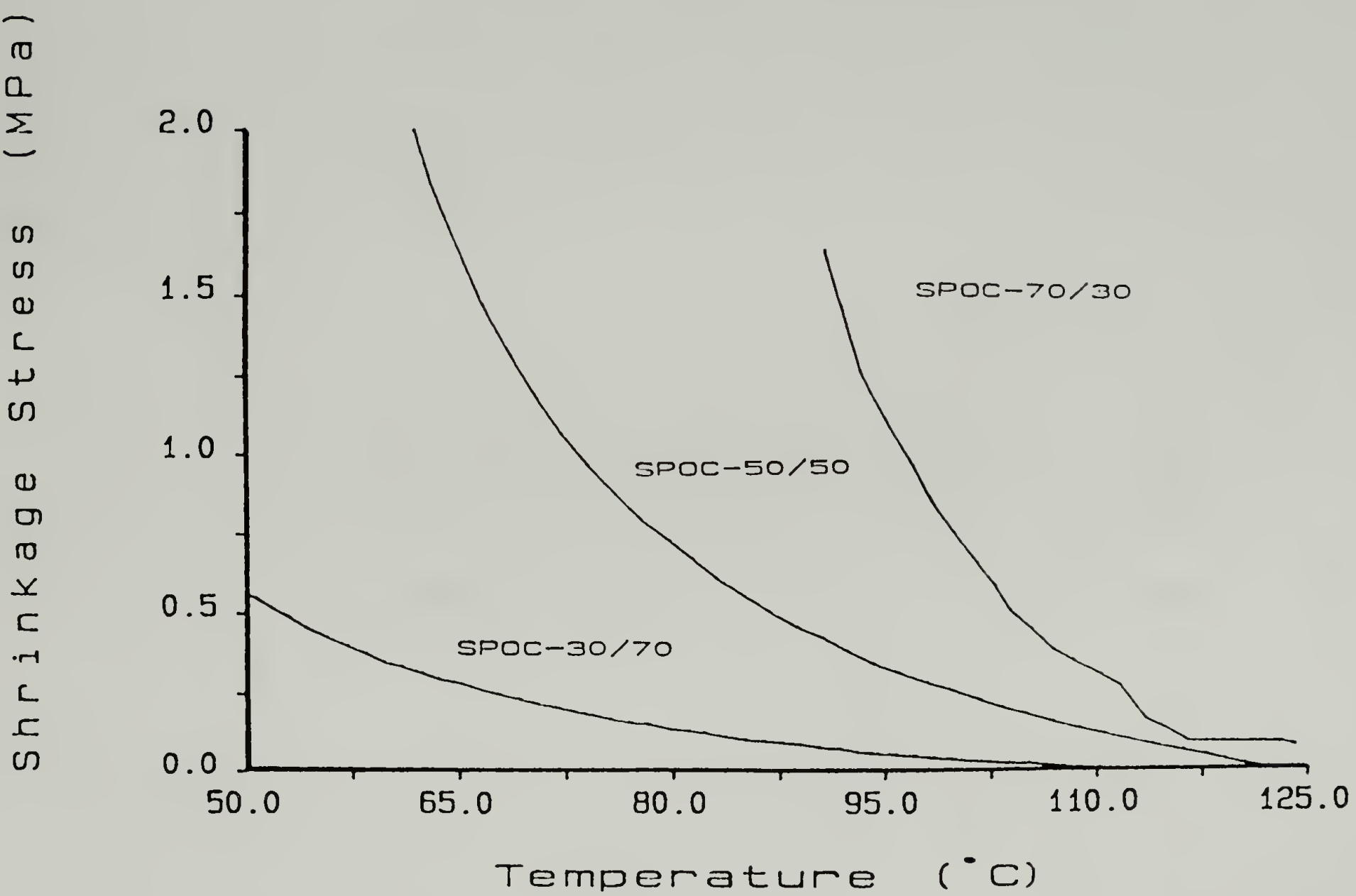

Figure 4.16. Shrinkage (thermal) stress for samples SPOC-70/30, SPOC-50/50 and SPOC-30/70 during cooling.

Table 4.3

Impulse Viscoelastic Properties
for Cured SPOC/Epon 828 Copolymers

Sample	Eeq [MPa]	SSEV [MPa-sec]	MRT [sec]	Eeq/E' @ 0.15 Hz	Cure Stress [MPa]	T_g [°C]
EPON-100/0	55	3700	8	0.10	0.095	115
EPON-100/10	29	1000	4	0.10	0.11	111
EPON-100/30	24	300	4	0.25	0.10	107
EPON-100/50	30	350	3	0.25	0.10	107
EPON-100/70	41	400	6	0.30	0.060	108
EPON-100/90	73	600	5	0.35	0.115	109
EPON-100/110	90	700	5	0.35	0.18	111
SPOC-70/30	30	150	6	0.50	0.08	100
SPOC-50/50	27	60	10	0.80	-0.01	70
SPOC-30/70	10	10	4	0.80	-0.03	<70[1]

[1] Sample did not get glassy.

polymerization. The T_g of each material was obtained by extrapolating the thermal stress responses in the rubbery and glassy states (see for example Figures 4.6, 4.14 and 4.16) and determining their point of intersection. The ratio of Eeq/E' is an indication of the viscoelastic character of the material. The limits of this ratio are zero for a liquid and unity for an elastic solid.

The T_g for each material was determined from the cooling portion of the experiment by extrapolating the rubbery and glassy thermal stress curves and determining the point of intersection. It should be mentioned that the data for Eeq presented in the previous figures have not been corrected for the contribution of the rubber membrane (≈ 0.1 MPa). Similarly, the shrinkage stress data presented in the previous figures have not been corrected for the thermal contraction of the metal hardware used to constrain the sample inside the environmental chamber of the Dynastat.

4.5 Discussion

The discussion is broadly divided into one general and four specific sections: equilibrium tensile modulus behavior and other mechanical property data, cure stress behavior, suggestions on the network structure and the application of these ring opening materials as adhesives.

It should be noted that the range of SPOC concentration that was investigated exceeds the practical limits of these

materials as additives in epoxy systems [56]. Such a range was chosen in order to amplify the effect of the SPOC material.

All of the samples gelled within ten minutes of reaching 125° C. The criterion used for gelation was the measurement of an equilibrium tensile modulus greater than that of the rubber membrane support. Gelation is graphically evidenced on Figures 4.3, 4.8, 4.10 and 4.12 by observing the rise of Eeq with time. This approach to gelation uses the fact that a liquid has zero Eeq and a solid has a finite, non-zero Eeq.

For each sample, a large increase in the mean relaxation time (MRT) was noted at the gel point. Specifically for sample EPON-100/0, this effect can be observed on Figure 4.4. Despite the scatter in the data, it can be seen that the MRT decreases slightly after gelation and increases during the latter stages of cure. The Eeq/E' and tan δ data, as evidenced by Figure 4.5, suggest that EPON-100/0 is nearly elastic after gelation and becomes progressively more viscoelastic with cure. The dip in Eeq/E' at the gel point is indicative of a viscoelastic material with long relaxation times. Figure 4.2b and the tan δ data near the gel point support this claim. Collectively these data suggest that cure of the unmodified epoxy is accompanied by extremely viscoelastic behavior and vitrification. Such

effects were not noted for the polymerization of the amine-cured epoxies presented in Chapter III.

The lack of a true rubber to glass transition in the Eeq and thermal stress data of sample EPON-100/0 obtained during cooling (Figure 4.6), indicates that at the end of polymerization T_g is close to the cure temperature. The Eeq/E' and tan δ data in Figure 4.7 suggest that the sample behaves increasingly elastic below the cure temperature.

4.5.1 Equilibrium Tensile Modulus Behavior

Examination of the EPON- series of data in Table 4.3 indicates that the apparent Eeq measured at the end of the 125° C polymerization goes through a minimum at a SPOC content of 30 parts by weight. Shimbo et al. concluded that the presence of ring opening material monotonically reduced the dynamic storage moduli of the cured epoxy copolymers [116]. It would then be expected that if SPOC was weaker mechanically than Epon 828 and was incorporated into a network, that Eeq should decrease monotonically or reach some plateau level. However, considering the chemistry of these polymerizations it is unlikely that a homogeneous network of Epon 828, NMA and SPOC form. Rather the observed trend in Eeq can be explained using the following chemical and structural model. With regard to these reacting systems it is important to realize that for both the EPON- and SPOC-series of samples it is likely that Epon 828 consumes most

of the NMA. Recall also that SPOC polymerizes cationically and that polymerization occurs without the incorporation of NMA into the structure. As a result two independent structures are expected.

For the EPON- series of samples, the drop in Eeq at low SPOC contents can be explained by low degrees of SPOC polymerization. As a result, the low molecular weight SPOC can plasticize the Epon 828 network and results in a slight drop in T_g. As a consequence of the sample being further above its T_g, there is also a decrease in the SSEV and MRT. As the concentration of SPOC increases, further polymerization occurs so that the resulting SPOC polymer is of high enough molecular weight to significantly contribute to the measured mechanical response. In addition, its ability to plasticize the Epon 828 network decreases. At the higher SPOC contents vitrification (as indicated by high SSEV values) is also occurring which artificially raises Eeq. Vitrification makes it difficult to accurately assess the mechanical and structural state of these materials in contrast to materials of a less vitreous nature.

For the SPOC- series of samples the situation is simpler. The primary reason for this is the fact that Eeq behavior is not complicated by the effects of vitrification. The effect of SPOC content upon Eeq during polymerization and cooling can be seen on Figures 4.10 and 4.15. In both cases Eeq decreases with increasing SPOC content. The

deficiency in epoxide functionality (relative to the amount of anhydride present) results in an excess of NMA at the end of cure. Recall that for the EPON- series, the epoxide to anhydride molar ratio is one, whereas for the SPOC- series it decreases to a minimum value of about one third. Clearly this excess increases as the Epon 828 content decreases. Since the homopolymerization of SPOC results in linear polymer, the resultant network mechanical properties are relatively poor. It is also suggested that residual NMA plasticizes the cured materials. Note how small the SSEV values for this series of samples are in comparison to those of the EPON- series. This is further evidence that these materials are well above their Tg. Additional discussion of the network structure is included below.

It should be mentioned that the Eeq values reported in Table 4.3 for samples with relatively large SSEV values (EPON-100/0, EPON-100/90, EPON-100/110) are only apparent equilibrium values. The Eeq values for these samples are higher than their truly equilibrium values. This relative increase in Eeq can be attributed to network vitrification. As the T_g of these samples approaches the cure temperature, the contribution of vitrification becomes significant and is evidenced by extremely long relaxation times. As part of the Impulse Viscoelastic method it is required that all of the stress relaxation after a pulse deformation be collected and the pulse duration be of the order of the longest

relaxation time. However, in order to conduct experiments which do not violate the assumption that the mechanical properties can be considered constant during deformation, it is necessary to use relatively short duration experiments. Experimentally the effect of using short duration deformations can be observed on Figures 4.3 and 4.4 where Eeq and the SSEV of the unmodified Epon 828 increase sharply 40 minutes into the polymerization. While part of the increase can be attributed to additional polymerization, it is believed that the bulk of the increase in Eeq is due to vitrification.

In order to obtain mechanical properties which are more indicative of equilibrium conditions, longer pulse deformations and collection times are required. In this way more of the long time relaxations can be obtained. Some of the effects of vitrification and data collection time upon the mechanical properties are discussed in Chapter V. Thus the reported Eeq values serve as an upper bound on the true Eeq. It is suggested that an increase in temperature would cause the values of Eeq, SSEV and MRT to drop, assuming no additional polymerization were to occur. Based on the SSEV and Eeq/E' data in Table 4.3 it is suggested that the unmodified Epon 828 epoxy cured the most viscoelastically.

The viscosity data in Table 4.3 correlate well with the observed trend in T_g. As expected for vitrifying systems, e.g., sample EPON-100/0, the cure temperature is slightly

above T_g, and the SSEV is relatively high. Similarly, for copolymers with a relatively low T_g, e.g., the SPOC- series of samples, the SSEV is low. This behavior is expected for materials further above their T_g where there is sufficient energy for chain mobility. As mentioned, a more accurate measure of Eeq can be obtained for materials which are not vitrifying. As mentioned, some of the limitations of the Impulse Viscoelastic method associated with vitrifying materials are discussed in Chapter V.

4.5.2 Cure Stress Behavior

From Figure 4.3 it can be determined that the stress associated with the anhydride crosslinking of Epon 828 (EPON-100/0) is about 0.095 MPa. A comparison of the cure stress data in Table 4.3 with the volumetric data in Table 4.2 does not yield the intuitive result of reduced stress with reduced shrinkage. In fact, almost no apparent correlation exists. Note how the sign of the cure stress does not depend upon the net volumetric change during cure. In Chapter II, Equation (2.65), it was shown that the cure stress at any time is the product of the equilibrium tensile modulus with a shrinkage rate summed over the entire cure history. Previous researchers have erroneously assumed that zero net shrinkage implies zero stress [115].

It appears that most of the volumetric expansion occurs early in the polymerization when the copolymer is soft and

the stress associated with expansion is small. After the SPOC reacts, the Epon 828 polymerization appears to take place. Evidence for this is given by the compressive dip in shrinkage stress level (Figures 4.9 and 4.11) followed by the tensile cure stress typical of the neat NMA/Epon 828 epoxy (Figure 4.3). From Figure 4.12, which is data taken from the polymerization of sample SPOC-30/70, it can be seen that when a large amount of SPOC is used relative to the amount of Epon 828, the tensile cure stress of Epon 828 is not observed. From these data it appears that the SPOC material dilates prior to the reaction of Epon 828. It might be expected that the molecular structure of such a network would be similar to that of an A-B-A block, where the A block would be Epon 828 and the B block the SPOC material. However, considering the chemistry of these materials this is highly unlikely.

The seemingly anomalous cure stress data can be explained as follows. As the SPOC material is added, the volumetric expansion associated with its ring opening does occur. From Table 4.2 this is evidenced by the increase in volumetric expansion with increasing SPOC contents for both the EPON- and SPOC- series of samples. Despite this, however, it is observed that for the lower content SPOC-modified materials in the EPON- series (EPON-100/10, EPON-100/30, EPON-100/50), the cure stress remains relatively unchanged. Note also that for these samples that as SPOC is

added there is a decrease in Eeq. As a result, the stresses associated with shrinkage or expansion are diminished. Thus two competing effects result in the observed behavior: the increase in dilation and the drop in Eeq with the addition of SPOC. For the EPON- series of samples a minimum cure stress level is reached at about 0.060 MPa for sample EPON-100/70. At the higher SPOC contents (EPON-100/90, EPON-100/110) the cure stress rises to a level above that of the neat Epon 828. Since the modulus of these materials is higher than that of the neat Epon 828, the shrinkage (cure) stress is proportionately higher. This is equivalent to supposing that for these samples the SPOC polymerization produces a higher modulus material so that the subsequent polymerization of Epon 828 effectively occurs later in the cure.

For the SPOC- series of samples the trends in cure stress and volumetric behavior are similar to those of the EPON- series. For these samples, however, the deficiency in epoxide functionality reduces the total amount of shrinkage possible. As a result, it is possible to produce materials with a net compressive cure stress (SPOC-50/50, SPOC-30/70). This is graphically illustrated on Figures 4.11 and 4.12. Since these materials have a relatively low Eeq (Figure 4.10) these stresses must be small. These results demonstrate the importance of the fact that the cure stress that one measures is the product of the equilibrium tensile

modulus and a volumetric change summed over the entire cure history. More importantly, the sign of the cure stress is independent of the sign of the overall volumetric change.

It might be possible to alter the observed cure stresses by means of chemistry. For example, by reducing the reactivity of the SPOC monomer (by changing cure temperature or initiator) or by increasing the reactivity of Epon 828 relative to SPOC (by changing the cure conditions) more of the dilation could occur later in the polymerization. In this way Eeq would be larger and the contribution of the dilation to offsetting the tensile cure stress of Epon 828 would be greater. It should be mentioned that in order to assure tensile cure stresses, the density of the polymerizing resin must monotonically increase as a function of time. Conversely, in order to assure compressive cure stresses the density of the curing resin must monotonically decrease as a function of time. Most importantly, the cure stress that one observes is dependent upon the path of polymerization, e.g., the fact that two materials have identical initial and final densities and moduli does not imply that they will have identical cure stresses.

The magnitudes of the measured one-dimensional cure stresses for these epoxies copolymerized with ring opening monomer are small in comparison to thermal stresses or design stresses. The stresses and associated volumetric changes during cure were compared with those observed with

other thermosetting materials [117]. These included a polycarbonate (CR-39^R monomer, PPG Industries, Barberton, OH), a general purpose polyester, a polyamide-cured epoxy and an amine-cured epoxy. These results, including some of the ring opening materials, are summarized in Table 4.4. Each of these thermosetting materials presented in Table 4.4 were cured under isothermal conditions. In each instance, the one-dimensional cure stresses are small despite relatively large volumetric changes. It can be shown that for conditions of biaxial constraint the stresses are approximately double those measured for the one-dimensional case, while the stresses can be very high for conditions of volumetric constraint.

4.5.3 Network Structure

The relationship between the reactant stoichiometry and the resulting mechanical properties is difficult to determine because of the complex chemical reactions which are possible in these systems. It is believed that NMA and BDMA predominantly polymerize Epon 828 anionically. However, it is known that these ring opening materials polymerize under cationic conditions [52-54,102]. As a result, a homogeneous network is not expected. Cationic reaction conditions can be probably be attributed to the hydrolysis of the NMA to its diacid form. Note that cationic conditions can also polymerize Epon 828. Because

Table 4.4

Volumetric and Cure Stress Data for Several Thermosetting Materials

Material	Cure Conditions	Volumetric Shrinkage [%]	Cure Stress [MPa]
Polycarbonate	120 min @ 80° C	10.4	0.04
	120 min @ 90° C	11.3	0.13
Polyester	90 min @ 30° C	12.3	0.14
Polyamide-Cured Epoxy	160 min @ 55° C	1	0.01
	130 min @ 85° C	1.5	0.05
Amine-Cured Epoxy	270 min @ 85° C	5	0.10
EPON-100/0	70 min @ 125° C	2.9	0.095
EPON-100/110	70 min @ 125° C	- 5.1	0.18
SPOC-30/70	70 min @ 125° C	- 1.0	- .03

of this difference in polymerization mechanisms, it is expected that true monomer copolymerization to form a single block copolymer does not occur. As a result, two distinct and possibly interpenetrating structures result. One of these structures should be a network comprised only of anionically polymerized Epon 828 and NMA. The second structure is more difficult to assess. It should be comprised of cationically polymerized SPOC (which produces linear SPOC polymer) and might also incorporate some cationically polymerized Epon 828. The cationic copolymerization of Epon 828 would change this structure from a linear one to a network type. The extent to which this happens depends greatly upon the sample homogeneity and chemical compatibility of Epon 828 and SPOC. Similarly, the interpenetrating character of these two structures also depends upon the reactants' solubilities and compatibilities. In this regard, it was observed that at the higher SPOC contents, regions of undissolved SPOC were present prior to cure, suggesting that the limits of the solubility of SPOC powder in Epon 828 and NMA were exceeded.

For the SPOC series of samples the deficiency in the amount of NMA needed to completely react with the Epon 828 results in an excess of NMA (since NMA, in its diacid form, probably acts to catalytically polymerize SPOC suggests that there is NMA present at the end of reaction that can plasticize the copolymer structure. In addition, the

decrease in Epon 828 content lowers the equilibrium tensile modulus measured since SPOC homopolymerizes into a relatively soft material. In contrast to the SPOC- series, the EPON- series of samples has a relatively large amount of Epon 828 needed to incorporate the NMA into a network and suggests an explanation for the increase in Eeq for the EPON- series of samples relative to the SPOC- series. Note how sensitive the mechanical properties are to the epoxide to anhydride molar ratio.

The copolymers made at the higher SPOC contents were shown qualitatively to have poor solvent resistance to methylene chloride, a solvent for SPOC. This suggests that the networks are not tightly bound and allow for extensive swelling. This is not surprising since there is a decrease in the total amount of curing agent available for cure as the SPOC content increases.

4.5.4 Application to Adhesives

Since these ring opening monomers have been developed in part as additives to epoxy resins for adhesive applications, it is useful to discuss the usefulness of these materials as adhesives.

Clearly one of the effects of the SPOC material is to volumetrically expand the curing material without significantly altering the uniaxial cure stress level. This has important implications in the area of adhesives where it

is beneficial to completely fill cracks with adhesive. This eliminates sites for water absorption or possible crack initiation. With regard to adhesives, there are two constraints that must be considered prior to choosing a material formulation. The first concerns the minimization of residual stresses and the second, the minimization of volumetric shrinkage. For applications which require no volumetric change on curing, the SPOC materials appear to be quite suitable. The residual stress question is more complicated. For all of the SPOC-modified Epon 828 epoxies the cure stresses are small. Recall also that the stresses that are reported are for the case of uniaxially constrained materials. Using a linear elastic approach it can be shown that conditions of biaxial constraint, such as in coatings, approximately increase the cure and thermal stress levels by a factor of $1/(1 - \nu)$, where ν is Poisson's ratio. In addition, conditions of triaxial or volumetric constraint increase the stress levels by a factor of $1/(1 - 2\nu)$. Depending upon the value of ν, volumetric constraint can lead to large stresses. This is especially problematic for adhesives where conditions of volumetric constraint are common. It is also observed that SPOC can significantly reduce T_g and thereby reduce the amount of residual thermal stress. Such findings have also been reported for similar materials by Shimbo et al. [116] who concluded that there was almost no reduction in cure stress at the cure

temperature with the addition of ring opening material. They attributed the decrease in the room temperature residual stress level to the lowering of T_g by the presence of ring opening materials [116]. It should be noted that their calculated residual stresses differed significantly from those they determined experimentally. Since thermal stresses are much greater than cure stresses, modification of the cure stresses becomes of secondary importance. Assuming that residual stresses are negligible above T_g, the important parameters are T_g and the adhesive properties of such copolymers. However, without having data on Poisson's ratio it is difficult to accurately estimate the magnitude of the residual stresses at the use temperature when these materials are used under conditions of volumetric constraint.

4.6 Summary and Conclusions

The curing behavior of Epon 828 epoxy copolymerized with a ring opening monomer (SPOC) was investigated using the technique of Impulse Viscoelasticity in combination with incremental linear elasticity. Many of the properties associated with cure were measured. Among these were gelation time, equilibrium tensile modulus, steady state elongational viscosity, mean relaxation time, cure stress and shrinkage, glass transition temperature and dynamic mechanical properties. The network mechanical properties

were found to be sensitive to the reactant stoichiometry, especially the epoxide to anhydride molar ratio. Because of different reaction mechanisms true monomer copolymerization into a single block copolymer does not occur. Instead, two independent and possibly interpenetrating networks form. It was found that while the addition of SPOC causes volumetric expansion, the stresses associated with cure are relatively unchanged when compared to those of the neat epoxy. In addition, SPOC reduces the T_g of the epoxy copolymers.

C H A P T E R 5

LIMITATIONS OF THE IMPULSE VISCOELASTIC METHOD

5.1 Introduction

Thus far, results have been presented on the curing of thermosetting materials. For some systems, it was pointed out that several of the properties, such as the equilibrium tensile modulus (Eeq), steady state elongational viscosity (SSEV) and mean relaxation time (MRT), were not exact indications of the state of the material. These inaccuracies arise, in part, from an inability to recover all of the relaxations in a material. In this regard, some of these limitations have been pointed out by Buckley [118]. Two approaches were used to qualitatively and quantitatively characterize the effect of such factors as the pulse duration, amplitude and shape and the time defined as the end of the pulse deformation on the calculated mechanical properties. The first approach is experimental and examines the effects of pulse duration, amplitude and shape on the calculated mechanical properties for a cured epoxy sample at several temperatures. These results are presented in section 5.2. The second approach is theoretical and applies the mathematics of the Impulse Viscoelastic method to a model whose properties can be easily calculated analytically. The model chosen was a standard linear solid.

Section 5.3 of this chapter presents the results of these modeling efforts.

5.2 Experimental

In Chapters II, III and IV the Impulse Viscoelastic technique was used to characterize the solidification process of thermosetting materials using uniaxial pulse-strain deformations. These deformation shapes have the advantage that they readily yield higher order information, such as relaxation data, when compared to less abrupt deformations. In Chapter II it was stated that the path of deformation method is arbitrary as long as the deformation disturbance returns to its original level. In order to investigate the limits of the Impulse Viscoelastic technique, a systematic series of pulse deformations were applied to a fully cured material. In this way, measurements could be made without the complication of changing mechanical properties. The sample chosen was Epon 828 cured with Jeffamine^{R} T-403 using an amine/epoxy ratio of 1.3. The curing behavior of this epoxy sample is discussed in Chapter III.

5.2.1 Effect of Pulse Duration

For this portion of the study, uniaxial pulse-strain deformations were used to characterize the network mechanical properties. Measurements were made in the

vicinity of the glass transition temperature of this material. Specifically, isothermal deformation measurements were made at 65, 70, 75 and 80° C. Pulse durations of 10, 20 and 100 seconds were investigated. Temperatures below 65° C were not investigated in order to avoid the problems of stress baseline shifts induced by temperature fluctuations. These shifts can cause changes in the mechanical properties calculated. For the purposes of this study, this effect was not desirable. At temperatures above 80° C the sample was nearly elastic and the effect of pulse duration on mechanical properties was unimportant. In order to eliminate any effect of pulse amplitude on the mechanical properties, the deformation strain level was maintained at 0.88% for each temperature. A 10 Hz data collection frequency was used for all of the measurements, except for those made at 65° C for the 100 second pulses which were collected at 5 Hz. The collection time for each pulse deformation was chosen so that sufficient time was allowed for the stress to return to its pre-deformation level. Since the fluctuations in the stress baseline (due to thermal excursions) were not equal at the four temperatures, different voltage tolerances for convergence were used to determine the Impulse Viscoelastic parameters. These were 0.010, 0.005, 0.004 and 0.003 V for the 65, 70, 75 and 80° C test temperatures, respectively. While these tolerances are not sufficient to eliminate the effect of the thermal stress

drifts, it is a first attempt at minimizing its effects. Four measurements were made at each condition. Figure 5.1 illustrates the series of stress responses for the 20 second pulse deformations for each of the four temperatures. At the top of each figure is the average Eeq measured for the four deformations. Table 5.1 summarizes the mean values and standard deviations of the Impulse Viscoelastic properties for this cured epoxy at each of the deformation conditions.

For the 10 and 20 second duration pulses, the Eeq values are somewhat higher than the values obtained at 100 second pulse duration, especially at the 65° C test condition. Some scatter, as evidenced by the magnitude of the standard deviation, is expected in the mechanical properties because of numerical integration techniques and baseline variations induced by thermal fluctuations. The trends in the steady state elongational viscosity (SSEV) and mean relaxation time (MRT) indicate higher values for longer pulse durations. This behavior is to be expected since more of the relaxations are allowed to take place at the longer duration deformations.

The Eeq versus temperature regression data presented in Chapter III, Table 3.4, for the Jeffamine^{R} T-403/Epon 828 epoxy, predict that at 65, 70, 75 and 80° C Eeq should be about 17.1, 17.6, 18.0 and 18.4 MPa, respectively. From Table 5.1 it can be seen that even a pulse deformation of 100 seconds duration can not recover the true equilibrium

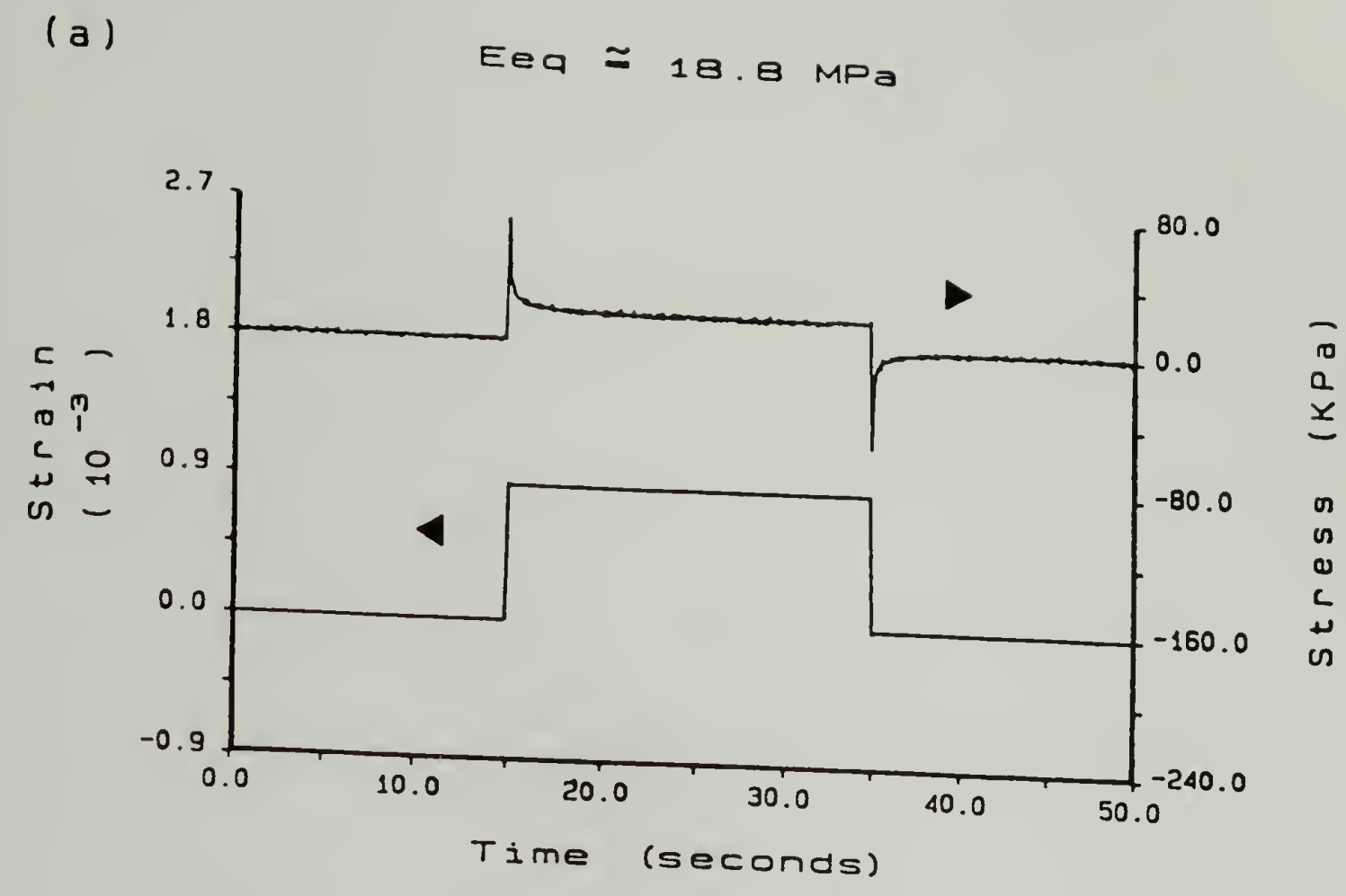

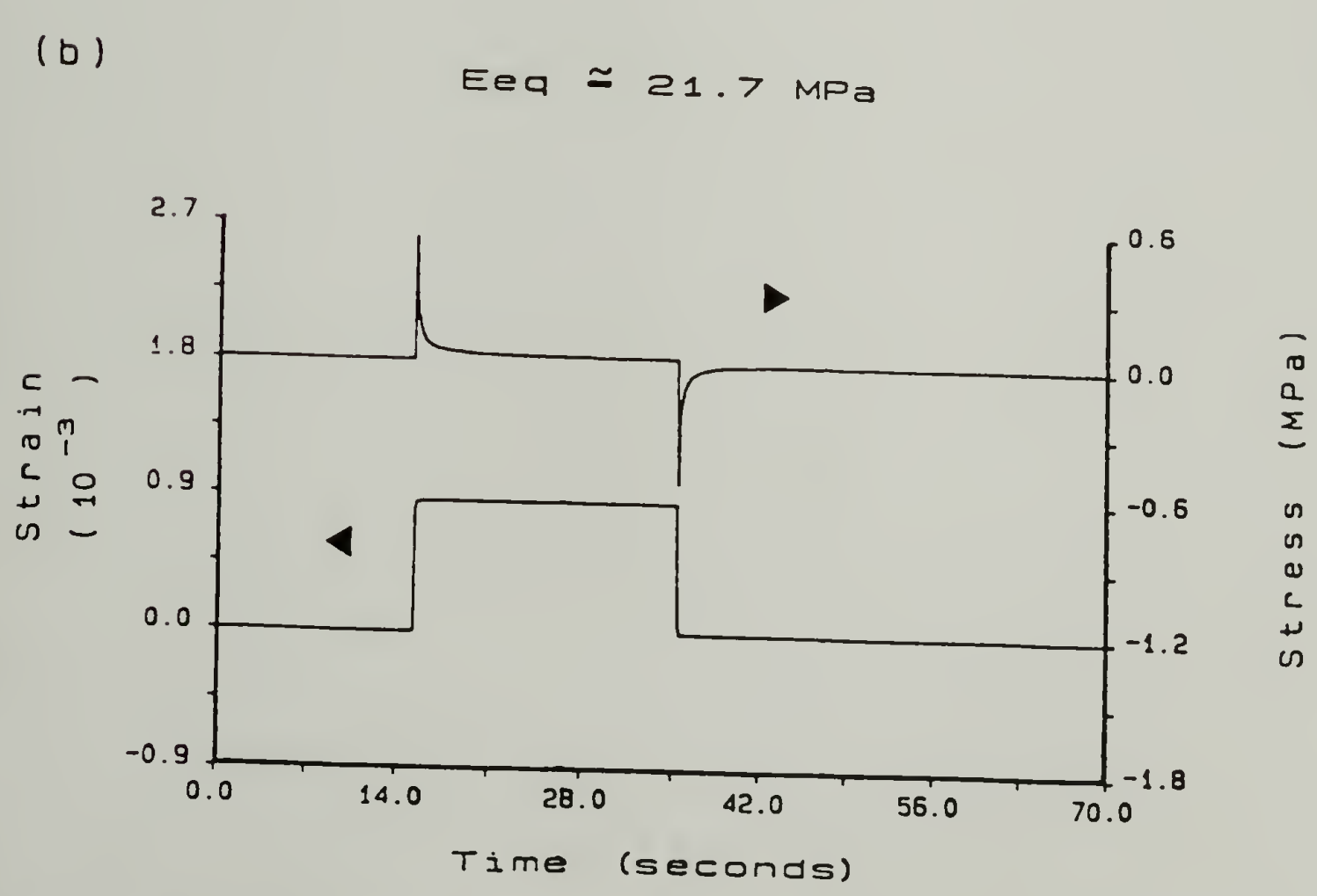

Figure 5.1 Stress response to a 20 second uniaxial pulse deformation for a cured Jeffamine® T-403/Epon 828 epoxy (A/E = 1.3) at a temperature of a) 80, b) 75 °C (continued on next page)

(c)

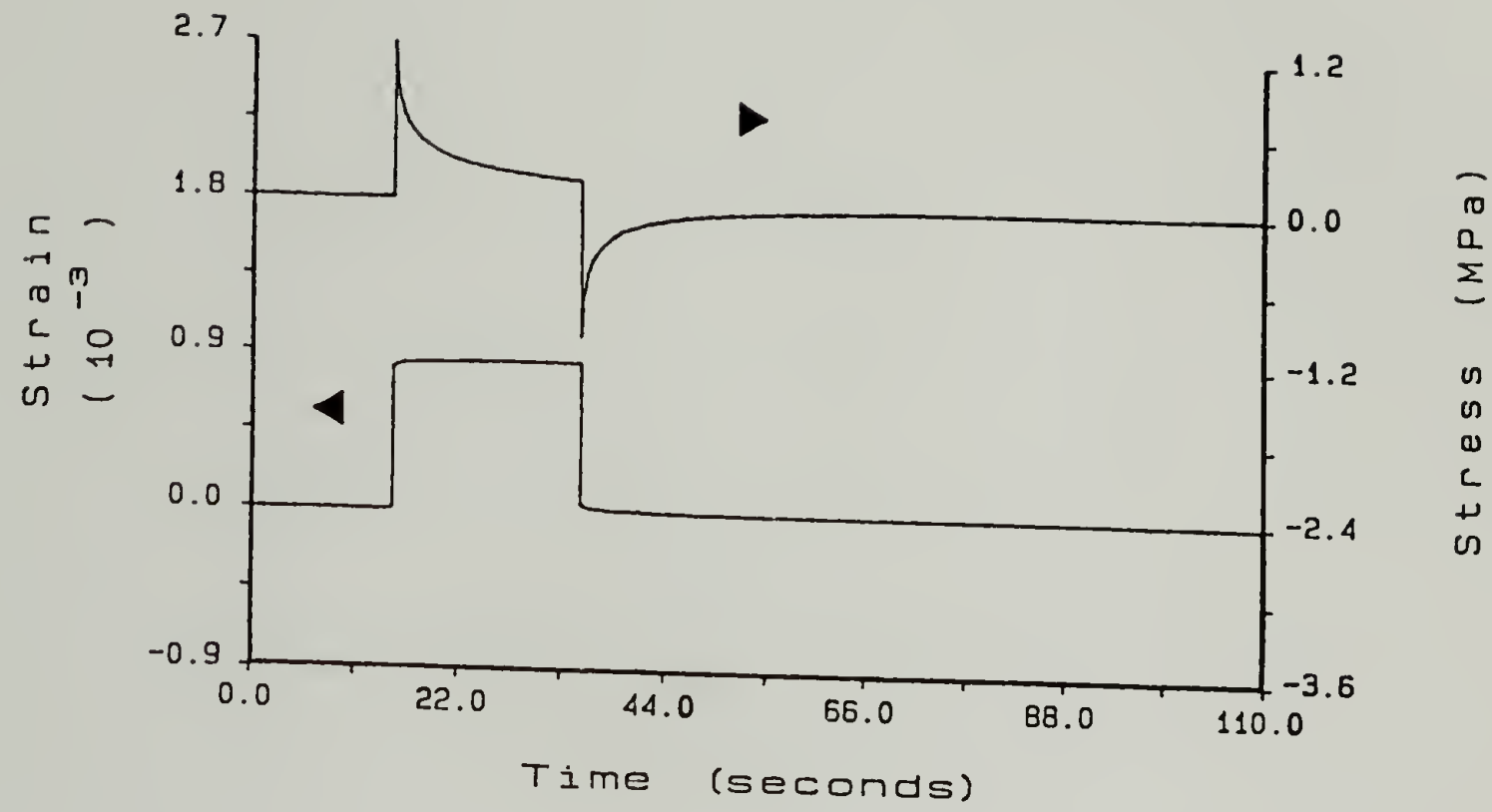

(d)

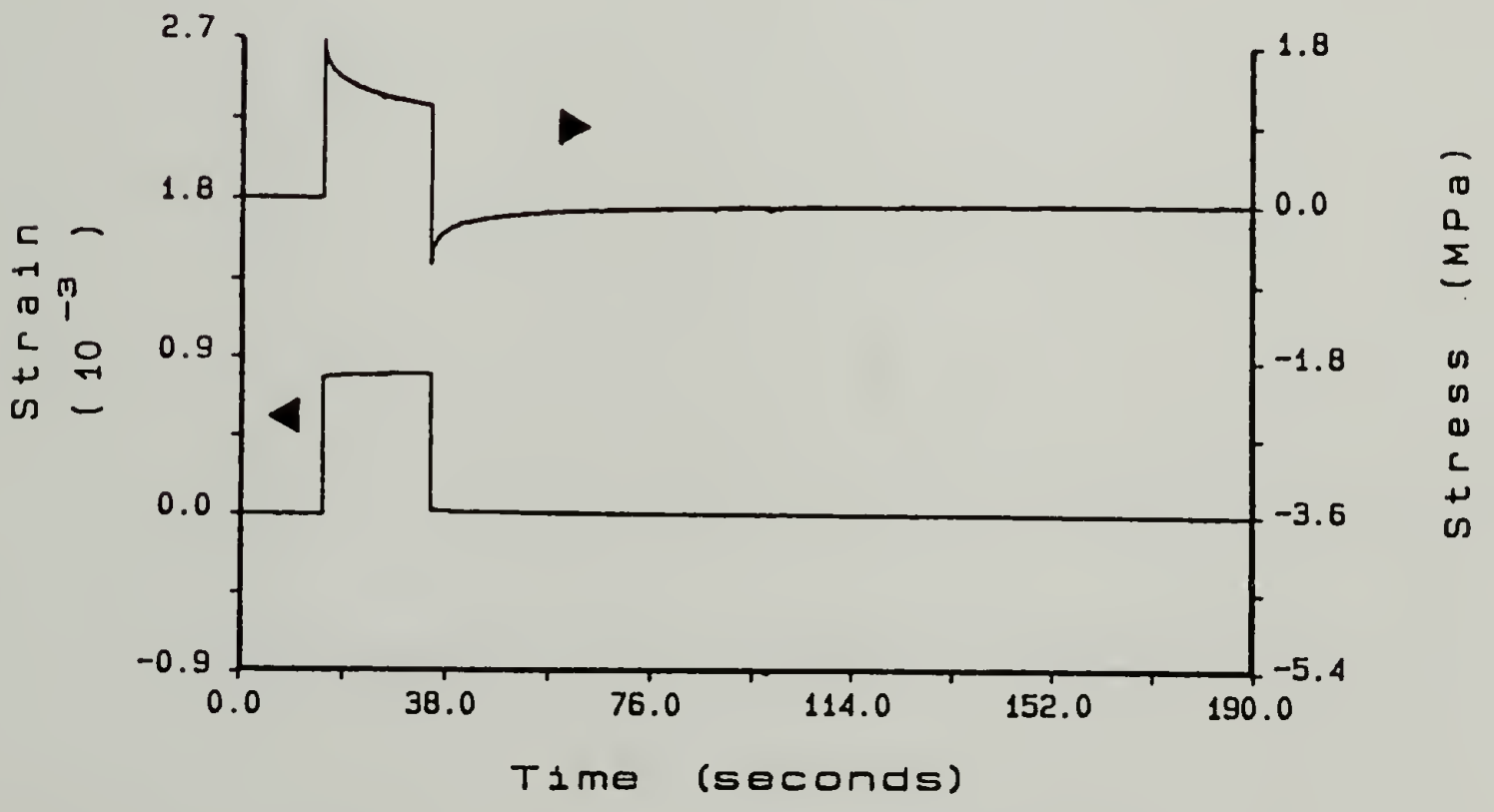

Figure 5.1 (cont). Stress response to a 20 second uniaxial pulse deformation for a cured Jeffamine^{R} T-403/Epon 828 epoxy (A/E = 1.3) at a temperature of c) 70 and d) 65° C.

Table 5.1

Impulse Viscoelastic Properties for a Cured Jeffamine® T-403/Epon 828 Epoxy as a Function of Temperature and Pulse Duration

Temp. [°C]	Pulse Duration [sec]	Eeq [MPa]	SSEV [MPa-sec]	MRT [sec]
65	10	860 ± 30	25000 ± 800	22 ± 0.8
	20	890 ± 70	31000 ± 3000	28 ± 0.8
	100	590 ± 30	92000 ± 5800	83 ± 7
70	10	87.5 ± 6.9	6100 ± 210	10 ± 0.6
	20	86.8 ± 3.0	6600 ± 170	11 ± 0.2
	100	64.4 ± 1.3	9000 ± 150	19 ± 0.4
75	10	21.7 ± 0.7	290 ± 8.3	1.9 ± 0.2
	20	21.7 ± 0.7	300 ± 14	2.5 ± 0.3
	100	22.4 ± 0.4	320 ± 13	2.7 ± 0.4
80	10	18.9 ± 0.4	19.7 ± 5.3	0.7 ± 0.1
	20	18.8 ± 0.4	22.1 ± 0.5	0.7 ± 0.3
	100	18.6 ± 0.1	25.2 ± 5.5	*

* denotes a negative value

tensile modulus of this material at 65 or 70° C. This inability to recover the true Eeq is a reflection of the fact that all of the relaxations were not collected. The inability to measure the true Eeq was caused by deformation pulses that were too short in duration. Experimental evidence of a relatively short deformation pulse can be observed on Figure 5.2 where the stress response to deformation is plotted for the 100 second pulse applied at 65° C. Note how the stress continues to slowly relax at the end of the 100 second deformation period. In contrast to the 65 and 70° C deformations, the results at the 75 and 80° C test conditions indicate that the measured Eeq is very close to that predicted by the Eeq regression results.

The results presented in Table 5.1 generally indicate that longer pulse durations are required in order to obtain more accurate measures of the mechanical and rheological properties of a material. Clearly, the proper pulse duration and data collection period are strong functions of the relaxation time of a material. Recall that the equilibrium tensile modulus (Eeq) is a time-independent material property and describes the state of a material after all relaxations have taken place. Thus it is in theory possible to recover the Eeq for a glassy materials where molecular relaxations occur slowly. The data in Table 5.1 suggest that in order to recover Eeq for glasses may

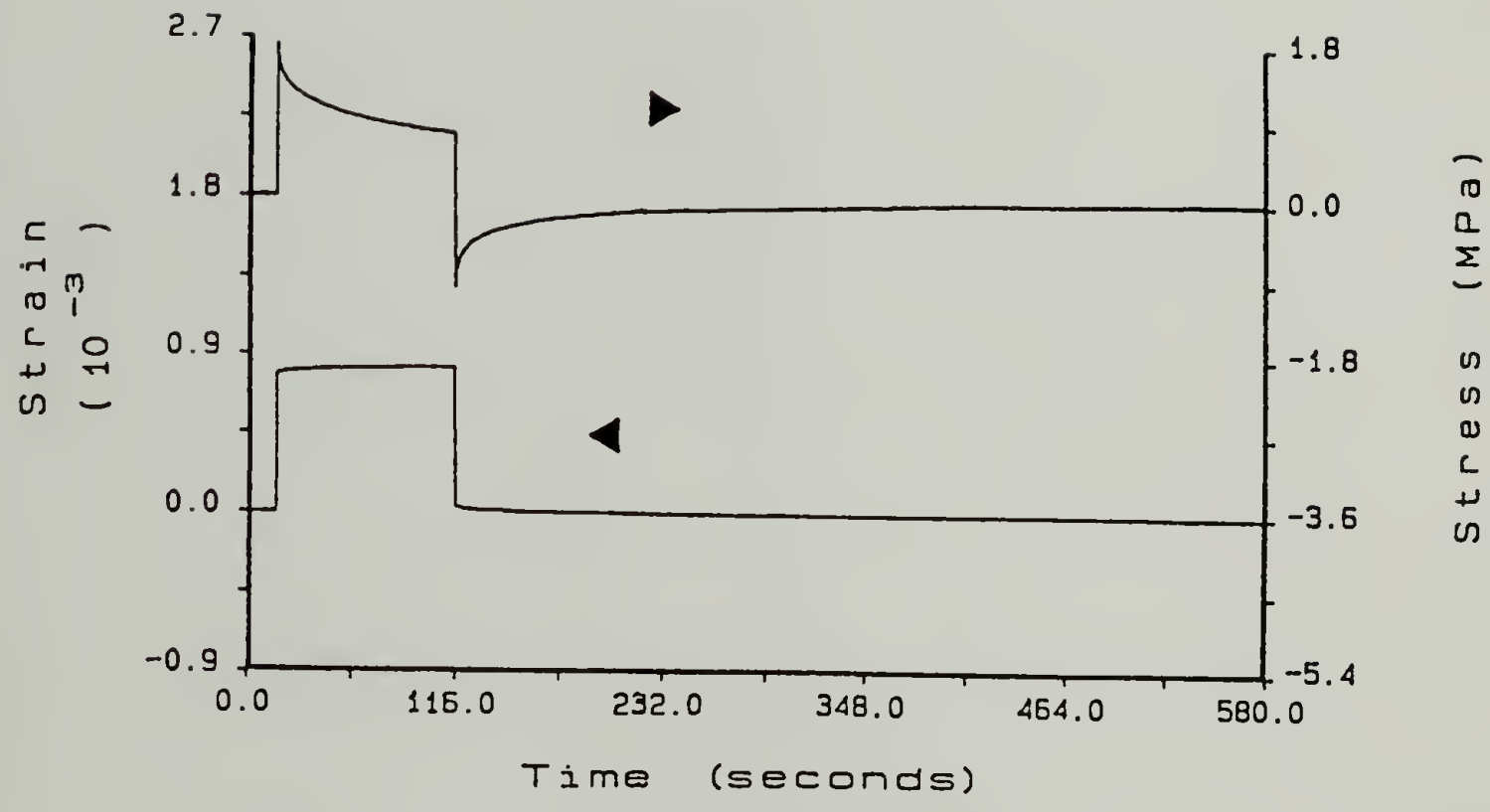

Figure 5.2. Stress response to a 100 second uniaxial pulse deformation for a cured Jeffamine^{R} T-403/Epon 828 epoxy (A/E = 1.3) at a temperature of 65° C.

require a pulse deformation lasting hours, days or possibly longer.

It should be mentioned that the Impulse Viscoelastic approach to the determination of mechanical properties much more closely approximates the true equilibrium behavior of a material than commonly used dynamic mechanical methods. In order to use dynamic methods to approximate equilibrium properties, deformation frequencies on the order of 10^{-3} Hz or less would have to be used. Evidence for this is presented in Table 5.2 where the ratio of Eeq/E' is calculated for five frequencies. As discussed in Chapter II, this ratio is a measure of the viscoelastic character of a material, with limits of unity for an elastic solid and zero for a liquid. The dynamic data were calculated using the methods outlined in Chapter II, section 2.2.1. In that section it was also shown that these methods yield results which are in excellent agreement with those obtained using conventional dynamic mechanical methods. For a given test temperature and pulse duration the data in Table 5.2 indicate that the Eeq/E' ratio rapidly decreases as the frequency for which E' is calculated increases. This trend in Eeq/E' is to expected since viscoelastic materials show an increase in E' with increasing frequency. For a given Eeq/E' ratio and a given temperature, Eeq/E' decreases as the pulse duration increases. This is due to the fact that at the longer pulse durations more of the material

Table 5.2

Eeq/E' as a Function of Temperature and Pulse Duration for a Cured Jeffamine® T-403/Epon 828 Epoxy

Temp. [°C]	Pulse Duration [sec]	Eeq/E' @ .003 Hz	Eeq/E' @ .035 Hz	Eeq/E' @ .135 Hz	Eeq/E' @ .535 Hz	Eeq/E' @ .935 Hz
65	10	.82	.45	.40	.36	.35
	20	.77	.47	.41	.38	.37
	100	.44	.30	.27	.27	.24
70	10	.81	.16	.10	.07	.06
	20	.77	.16	.10	.07	.06
	100	.53	.12	.07	.05	.05
75	10	1.00	.50	.23	.10	.07
	20	.98	.47	.21	.09	.06
	100	.97	.49	.23	.10	.07
80	10	1.00	.95	.81	.56	.46
	20	1.00	.96	.72	.47	.36
	100	.99	.93	.77	.50	.42

relaxations are collected. This is in contrast to the Eeq/E' behavior at the 10 second pulse durations where the relaxations are "frozen", i.e., not recovered by the Impulse Viscoelastic method. These frozen relaxations contribute to the elastic, time-independent component of the mechanical properties and hence cause Eeq/E' to tend towards unity. Note how at even the 0.003 Hz frequency, the Eeq/E' ratio is substantially less than unity at the 65 and 70° C test conditions.

5.2.2 Effect of Pulse Amplitude

Using the Jeffamine® T-403/Epon 828 epoxy sample described in the previous section, uniaxial pulse deformations of eight different magnitudes were applied to the sample which was held isothermally at a temperature of 75° C. This temperature was chosen based on the fact that it had a relatively stable baseline stress level and displayed a significant amount of viscoelastic character. Deformation magnitudes of 0.22, 0.44, 0.66 and 0.88% strain were applied in both the positive and negative directions. For these experiments the pulse duration was kept constant at 20 seconds. Data were collected at a rate of 10 Hz. Four measurements were made at each condition and the averages of the calculated Impulse Viscoelastic parameters for this sample are summarized in Table 5.3. Figure 5.3 plots the pulse stress response to deformation for the 0.44

Table 5.3

Impulse Viscoelastic Properties for a Cured Jeffamine® T-403/Epon 828 Epoxy as a Function of Pulse Amplitude

Temp. [°C]	Strain Amplitude [%]	Eeq [MPa]	SSEV [MPa-sec]	MRT [sec]
75	-0.22	25.5 ± 1.2	190 ± 10	1.0 ± 0.1
	-0.44	20.6 ± 2.0	230 ± 10	2.0 ± 0.5
	-0.66	21.9 ± 0.6	220 ± 20	2.0 ± 0.1
	-0.88	21.7 ± 0.9	240 ± 10	2.0 ± 0.2
	0.22	23.1 ± 1.3	200 ± 30	1.3 ± 0.5
	0.44	21.6 ± 0.7	230 ± 20	1.5 ± 0.2
	0.66	22.0 ± 0.7	220 ± 10	2.0 ± 0.2
	0.88	20.9 ± 1.5	230 ± 30	2.4 ± 0.3

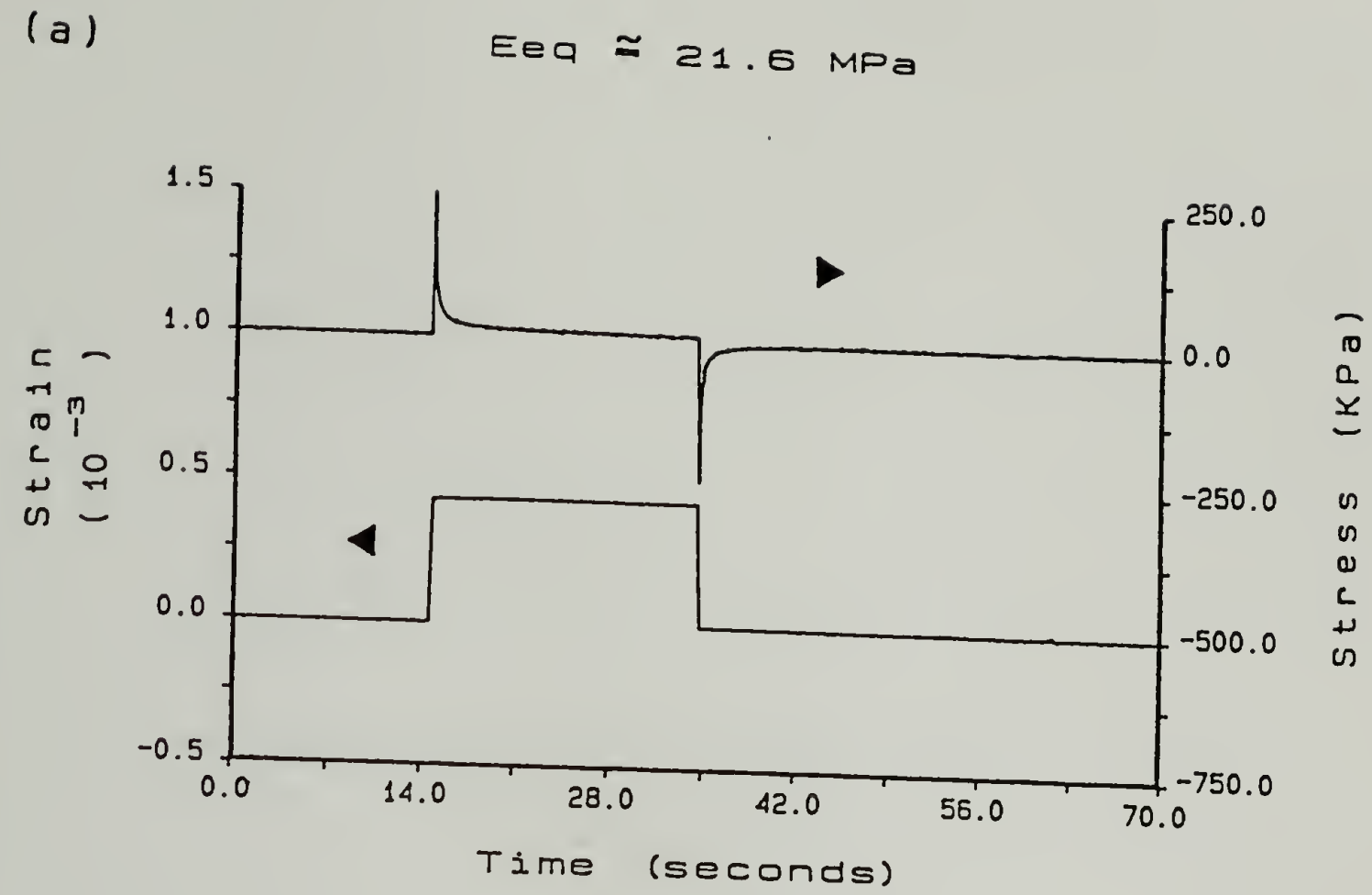

Figure 5.3. Stress response to a uniaxial deformation for a cured Jeffamine® T-403/Epon 828 epoxy (A/E = 1.3) at a temperature of 75° C using pulses of a) 0.44 and b) -0.44% strain amplitude.

and -0.44% strain amplitudes. Table 5.4 compares the Eeq/E' ratios at frequencies of 0.003, 0.035, 0.135, 0.535 and 0.935 Hz for each of the deformation conditions. The data presented in Tables 5.3 and 5.4 indicate excellent agreement for all of the Impulse Viscoelastic properties measured. This is encouraging since the Impulse Viscoelastic method predicts that there should not be any effect of pulse amplitude or direction on mechanical properties. It should be remembered that it is assumed that a linear viscoelastic behavior describes the mechanical response of the sample. In this regard, no evidence for nonlinear or plastic deformation was observed. Clearly, if the material were nonlinear viscoelastic in character, the mechanical properties that would be obtained would be dependent upon the deformation conditions.

5.2.3 Effect of Pulse Shape

As a further check of the Impulse Viscoelastic method, several different uniaxial deformation waveforms were used to characterize the cured Jeffamine^{R} T-403/Epon 828 epoxy. In order to perform these types of experiments a function generator was used as input to the Dynastat. Triangular, double step (both positive and negative amplitudes), single ramp and some randomly-shaped waveforms were investigated. Care was taken so as not to choose waveforms whose strain-time integral was close to zero. From Chapter II, Equation

Table 5.4

Eeq/E' as a Function of Pulse Amplitude
for a Cured Jeffamine^{R} T-403/Epon 828 Epoxy

Temp. [°C]	Strain Amplitude [%]	Eeq/E' @ .003 Hz	Eeq/E' @ .035 Hz	Eeq/E' @ .135 Hz	Eeq/E' @ .535 Hz	Eeq/E' @ .935 Hz
75	-0.22	1.00	.71	.27	.11	.08
	-0.44	.99	.51	.24	.10	.08
	-0.66	.99	.55	.26	.11	.08
	-0.88	.99	.52	.24	.10	.07
	0.22	1.00	.62	.28	.11	.08
	0.44	1.00	.55	.25	.10	.07
	0.66	1.00	.54	.26	.11	.08
	0.88	.99	.51	.25	.10	.08

(2.9), it can be seen that this would cause large errors in the calculation of the mechanical properties. Four isothermal deformation measurements were conducted at 75° C for each waveform. The mean values and standard deviations of the Impulse Viscoelastic properties are summarized in Table 5.5. Examples of the deformation waveforms and the resulting stress responses for each deformation are given in Figures 5.4a-d. The average equilibrium tensile modulus for each set of waveforms is listed at the top of each figure. The stress responses to two randomly-shaped deformation waveforms are shown in Figure 5.5. Table 5.6 presents the Eeq/E' data for frequencies of 0.003, 0.035, 0.135, 0.535 and 0.935 Hz.

The values obtained for the equilibrium tensile modulus (Eeq) and the dynamic data, as represented by Eeq/E', were in excellent agreement over the range of deformation waveforms investigated. For the triangular and ramp deformations, however, the elongational viscosity (SSEV) and mean relaxation time (MRT) data that were calculated were low in comparison to the data obtained using double step strain deformations. In this regard, it has been stated several times throughout this dissertation that uniaxial step strain deformations are useful for obtaining relaxation data. It can be shown from the equations presented in Chapter II that the calculation of the SSEV and MRT are sensitive to the amount of stress relaxation present in a

Table 5.5

Impulse Viscoelastic Properties for a Cured Jeffamine® T-403/Epon 828 Epoxy as a Function of Pulse Shape

Waveform	Sign	Pulse Duration [sec]	Eeq [MPa]	SSEV [MPa-sec]	MRT [sec]
Triangular	(+)	10	21.2 ± 3.1	220 ± 20	1.8 ± 0.6
Double Step	(+)	20	19.5 ± 1.6	280 ± 30	7.6 ± 1.0
Double Step	(-)	20	19.1 ± 2.9	280 ± 50	7.6 ± 1.3
Ramp	(+)	20	21.8 ± 0.8	210 ± 10	1.7 ± 0.2

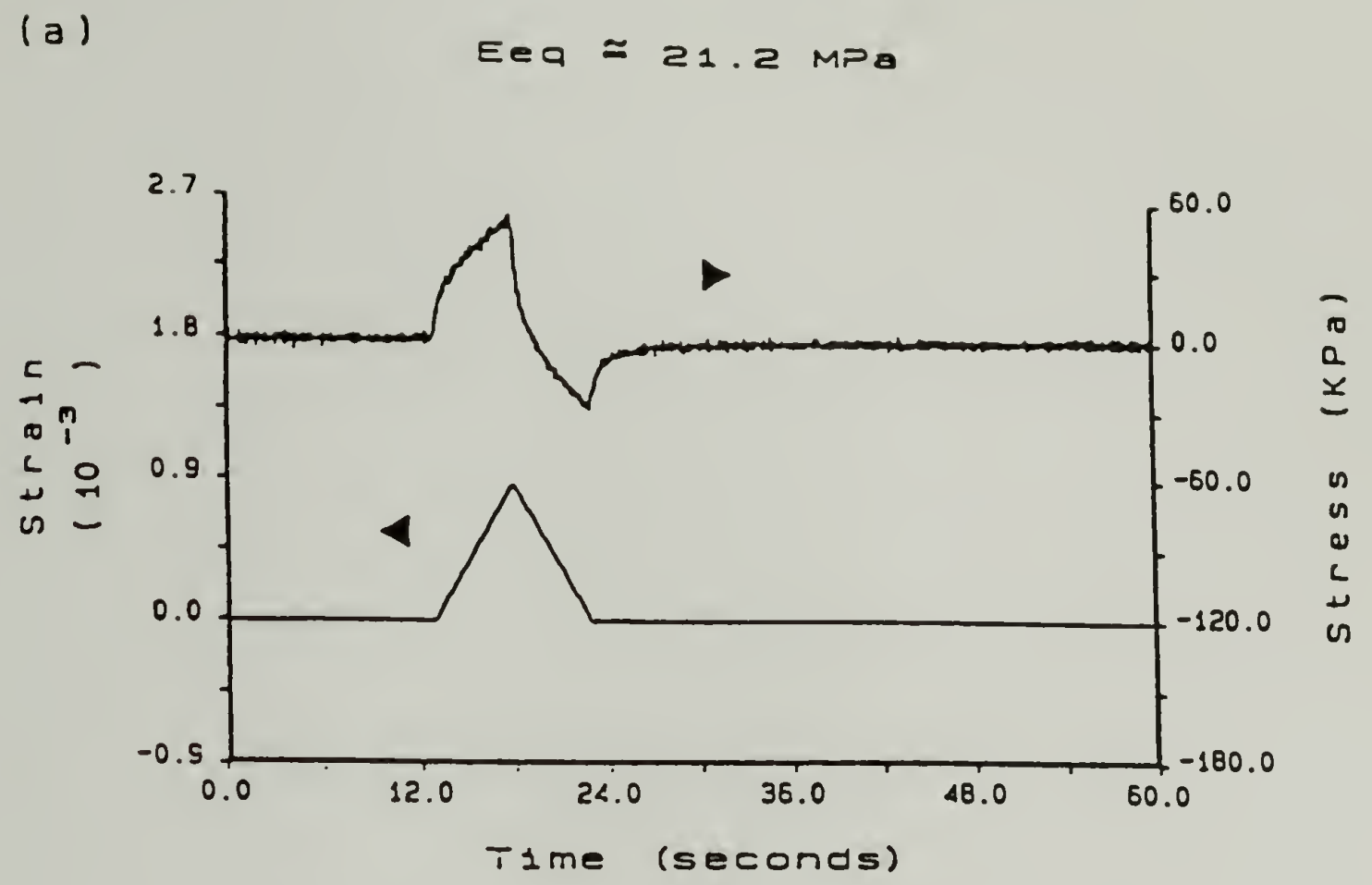

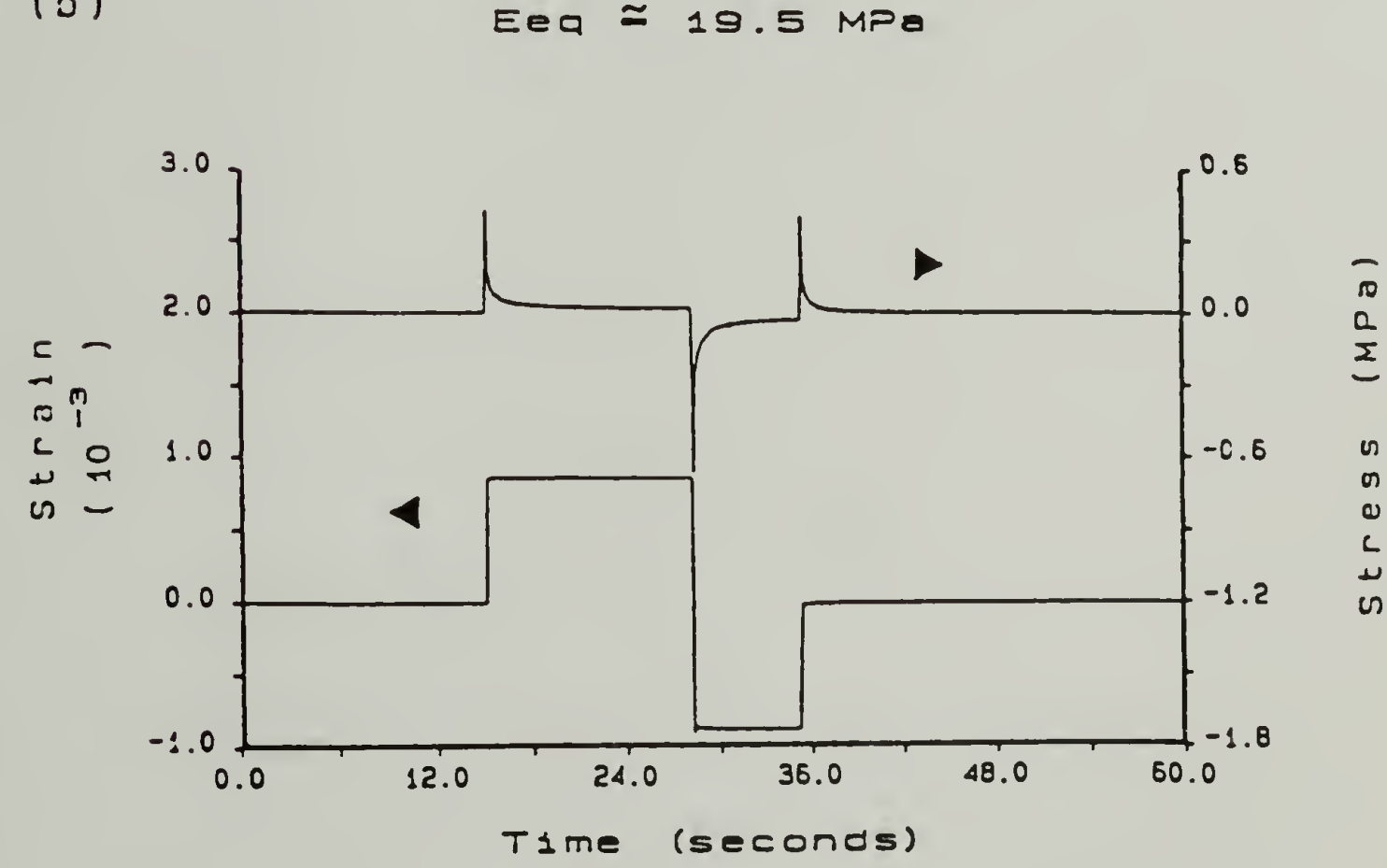

Figure 5.4. Stress response to deformation for a cured Jeffamine® T-403/Epon 828 epoxy (A/E = 1.3) at a temperature of 75° C for a a) triangular, b) double step (+) waveform

(continued on next page)

(c)

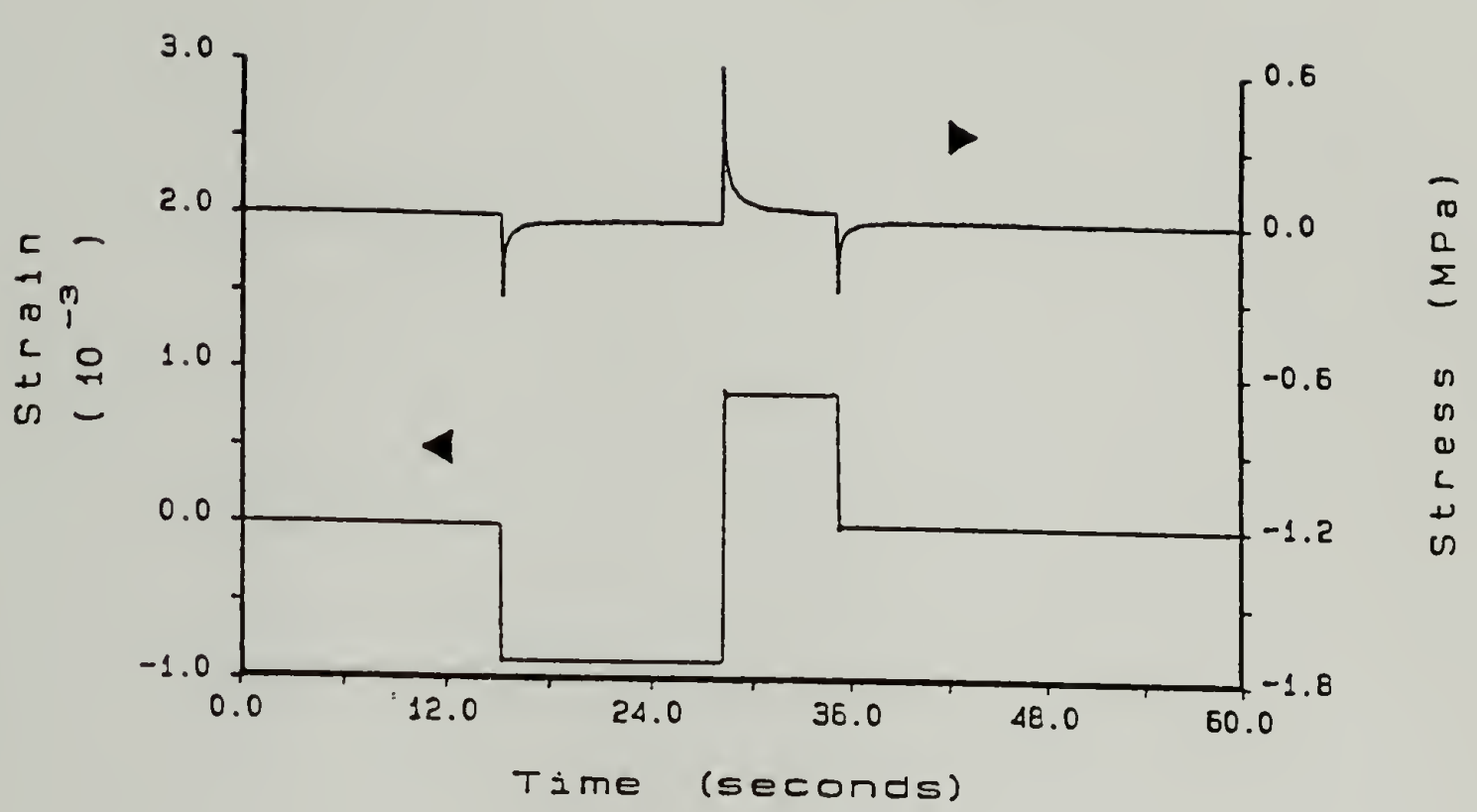

(d)

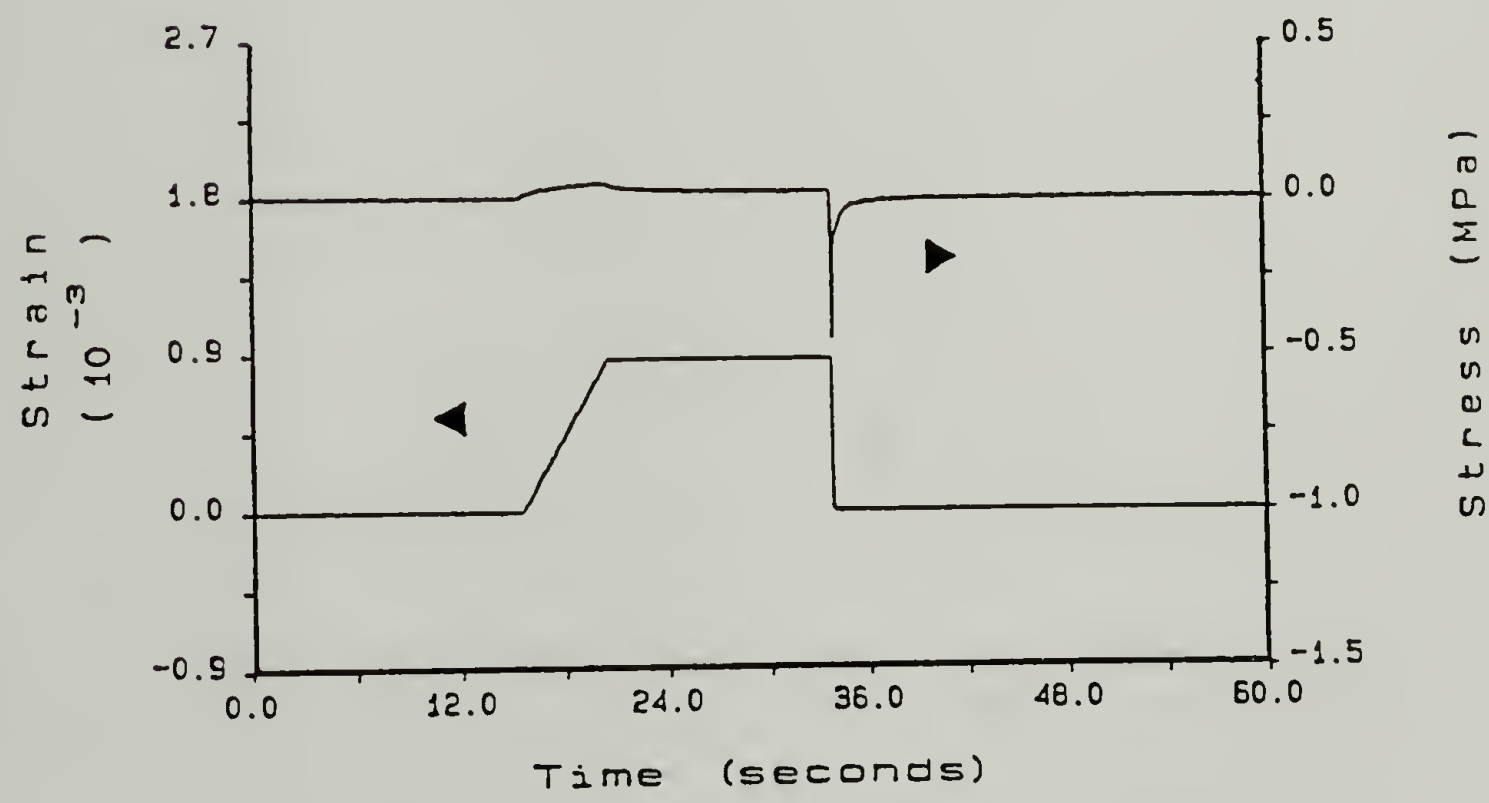

Figure 5.4 (cont). Stress response to deformation for a cured Jeffamine® T-403/Epon 828 epoxy (A/E = 1.3) at a temperature of 75° C for a c) double step (-) and d) ramp waveform.

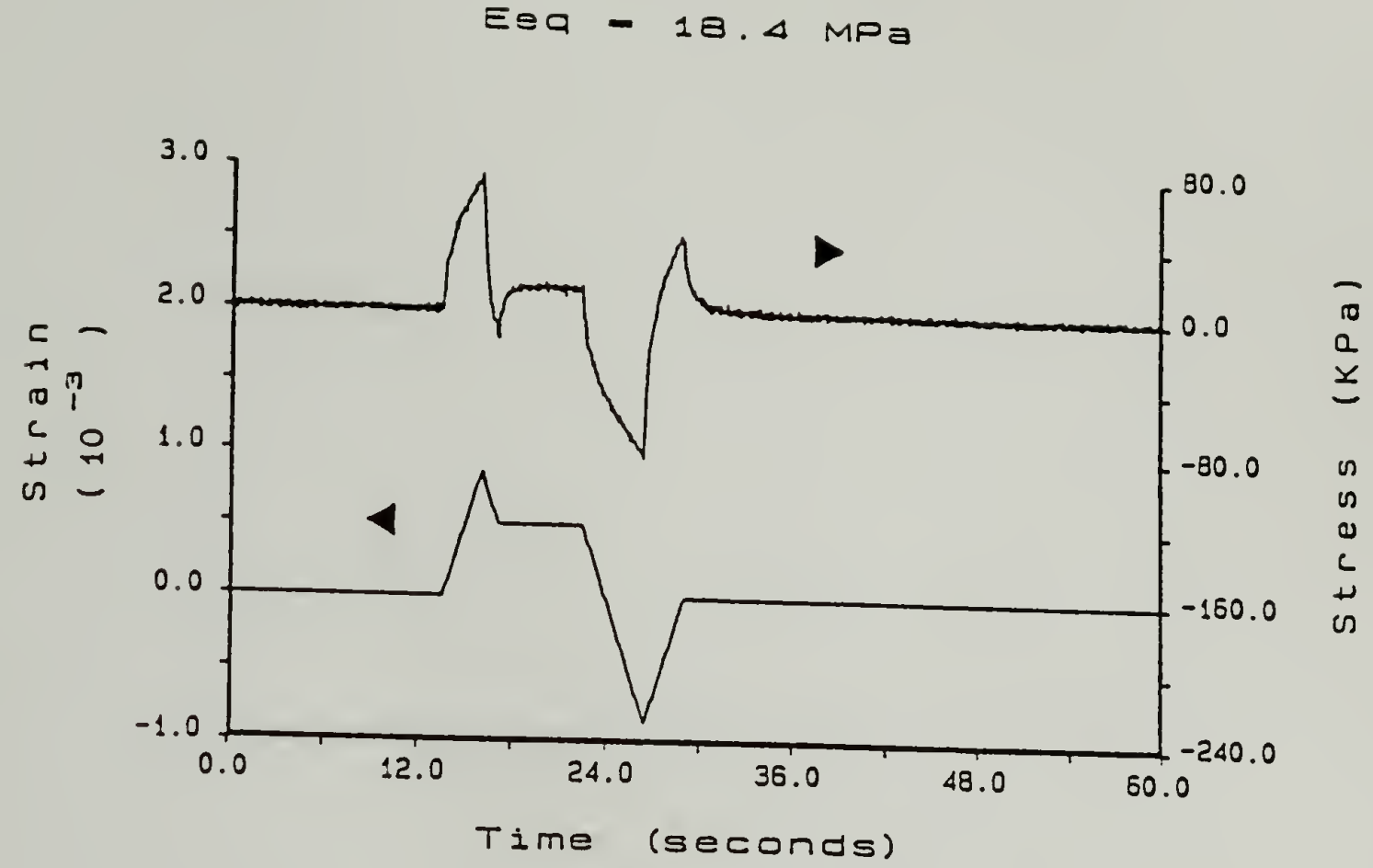

Figure 5.5. Stress response to two randomly shaped deformation waveforms for a cured Jeffamine^{R} T-403/Epon 828 (A/E = 1.3) epoxy at a temperature of 75° C.

Table 5.6

Eeq/E' as a Function of Pulse Shape for a Cured Jeffamine[R] T-403/Epon 828 Epoxy

Waveform	Sign	Eeq/E' @ .003 Hz	Eeq/E' @ .035 Hz	Eeq/E' @ .135 Hz	Eeq/E' @ .535 Hz	Eeq/E' @ .935 Hz
Triangular	(+)	.99	.59	.27	.11	.07
Double Step	(+)	.99	.57	.28	.08	.07
Double Step	(-)	.97	.56	.29	.10	.08
Ramp	(+)	.99	.61	.30	.11	.07

given deformation. For the uniaxial double step strain deformations, this corresponds to the large stress relaxations which occur immediately following the imposition or removal of the strain. In order to appreciate the difference of a waveform to calculate higher order information such as the SSEV and MRT, the stress relaxation behavior of a double step deformation should be contrasted with deformations of a smoother profile. This is graphically evidenced on Figure 5.4d by comparing the magnitude of the stress relaxation during the ramp portion of the deformation with that observed upon the removal of the deformation.

From the results presented in this section it can be stated that the Eeq determined by the Impulse Viscoelastic technique does not depend upon the shape of the deformation. The relaxation data, such as the SSEV and MRT are somewhat sensitive to the shape of the deformation. Though these measurements were performed at 75° C, it is suggested that the observed trends in Eeq, SSEV and MRT would be similar at other temperatures.

5.3 Modeling Results

In this section, the mathematics of the Impulse Viscoelastic technique were applied to the response of a simple viscoelastic model to a uniaxial pulse-strain deformation. From the results of such a simulation it would

be expected that one could develop an appreciation of the limitations of the calculated mechanical properties associated with the Impulse Viscoelastic technique. The model chosen was a standard linear solid (SLS) [119]. This three element model is composed of an elastic spring in parallel with a Maxwell element and is shown in Figure 5.6. It is one of the simplest representations of a viscoelastic solid. A similar type of simulation was performed by Cohen who used triangular pulse deformations to characterize a hypothetical linear viscoelastic material [120].

The primary experimental limitation of the Impulse Viscoelastic method lies in defining the end of the pulse experiment, i.e., the time at which the stress returns to its initial value. This limitation only becomes significant when the relaxation times of the sample become long. For these cases, it is difficult to define when the stress has returned to its initial value. For example, it was shown in Chapter II, section 2.2, that if one tries to calculate the (n+1)th moment of the relaxation spectrum, it requires integrating the product of time raised to the nth power by the stress which is a small value at long period of time. These types of calculations can be dependent upon the time taken as the end of the pulse experiment. As such, the parameter of interest in this study is the time defined as the end of the pulse experiment. For displacement-

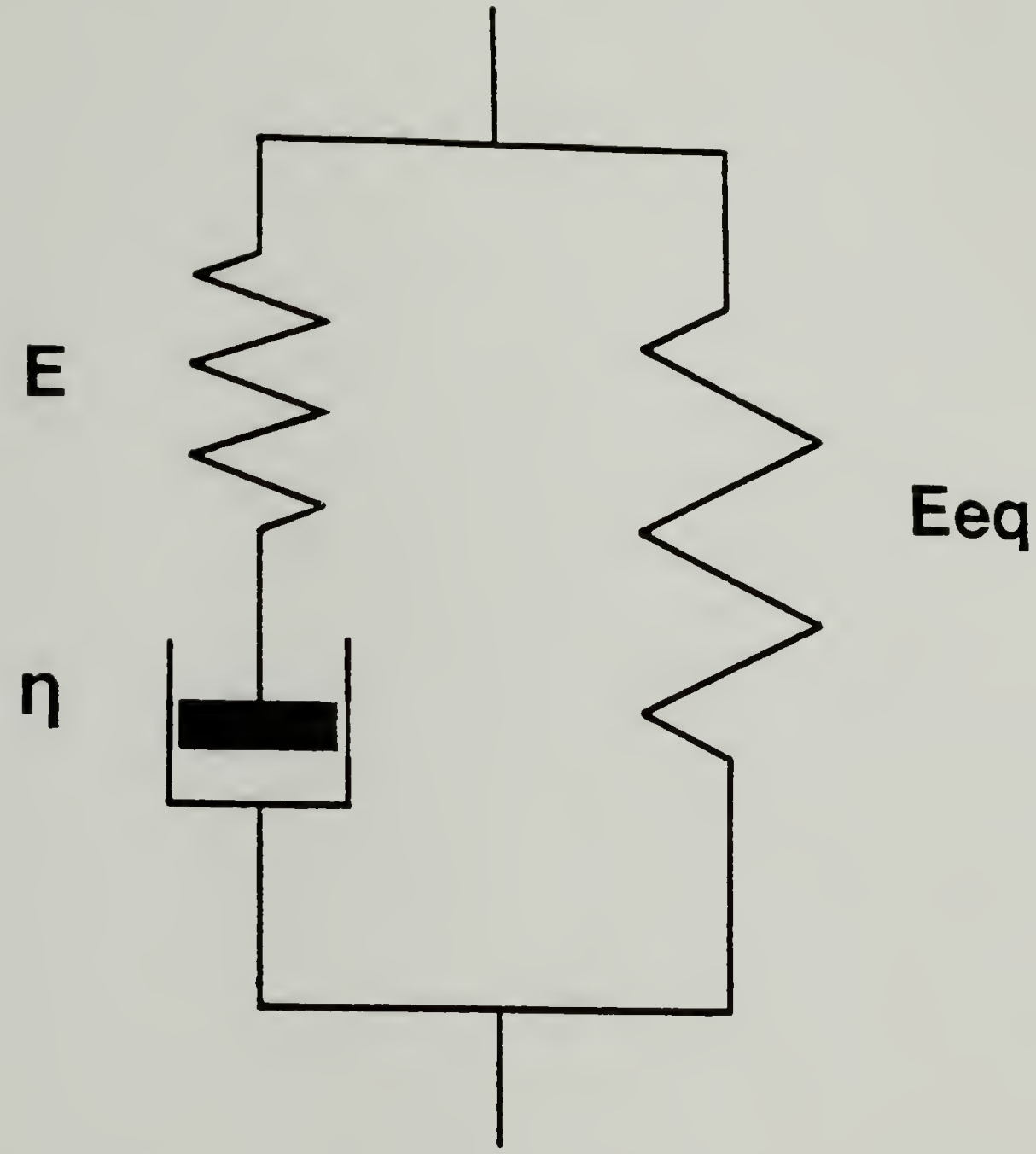

Figure 5.6. Schematic of a standard linear solid.

controlled experiments, it is the time at which the stress returns to its pre-deformation level.

5.3.1 Equilibrium Tensile Modulus

The constitutive equation for the SLS is given by Equation (5.1). In order to mimic the experimental deformations used in these Impulse Viscoelastic studies a uniaxial pulse-strain deformation of duration δ was chosen. This deformation can be regarded as two step-strains of equal magnitude and opposite in sign, separated by time δ. Given this deformation, as shown in Figure 5.7, the stress response of this model is given by Equation (5.1):

$$\sigma_1(t) = \varepsilon_o \{E \exp[-t/\tau] + Eeq\}$$

$$\sigma_2(t) = -\varepsilon_o \{E \exp[(\delta-t)/\tau] + Eeq\}, \qquad (5.1)$$

where τ is the relaxation time given by η/E. For times $0 \leq t \leq \delta$, the overall stress response $\sigma(t)$ of the standard linear solid is simply $\sigma_1(t)$. For times greater than δ, $\sigma(t)$ is given by $\sigma_1(t) + \sigma_2(t)$, as stated by the Boltzmann superposition principle. The true equilibrium tensile modulus for the standard linear solid is Eeq. This can be shown mathematically be letting $t = \infty$ in Equation (5.1). If, however, the $\sigma(t)$ integration is terminated prematurely at time $t = \phi$, the value for Eeq that one obtains is higher than the Eeq calculated at $t = \infty$. In order to simplify the calculation of the apparent Eeq of the SLS for conditions where the $\sigma(t)$ integrations are terminated early, an

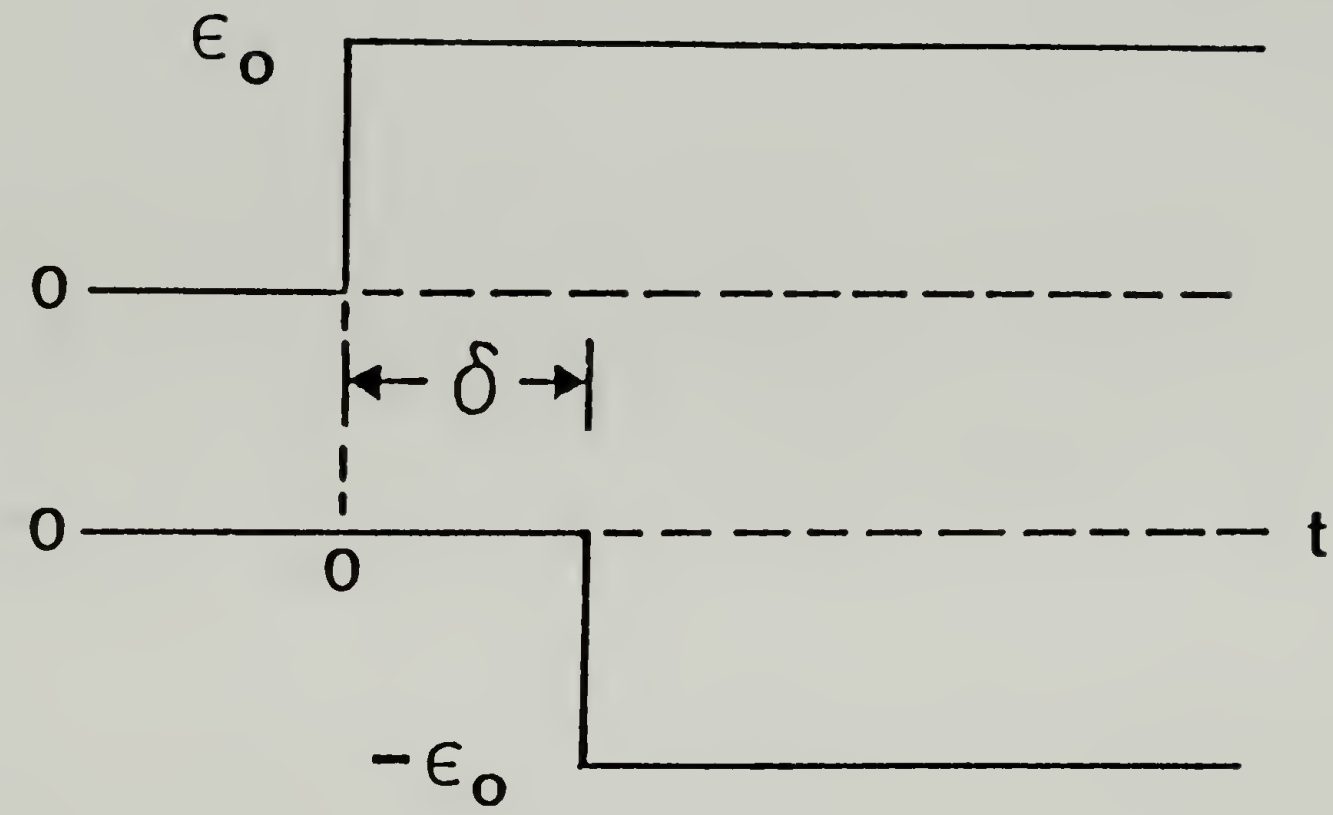

Figure 5.7. Deformations used as input to the standard linear solid.

analysis involving dimensionless variables will be performed. Introducing $\Delta = \delta/\tau$ as the dimensionless pulse duration and $\Phi = \phi/\tau$ as the dimensionless integration time, then Equation (5.2) can be used to calculate the apparent equilibrium tensile modulus (Eeq_{APP}):

$$Eeq_{APP} = Eeq + \frac{E \exp(-\Phi)[\exp(\Delta) - 1]}{\Delta} . \qquad (5.2)$$

Clearly the lower limit of Eeq_{APP} is Eeq. Note that since both Φ and Δ begin at the onset of deformation ($t = 0$), Φ can never be less than Δ. Rearrangement of Equation (5.2) to Equation (5.3) yields the relative or fractional modulus (Eeq_{APP}/Eeq) that one ould measure experimentally:

$$Eeq_{APP}/Eeq = 1 + \frac{E \exp(-\Phi)[\exp(\Delta) - 1]}{Eeq\ \Delta} . \qquad (5.3)$$

The lower limit of the relative modulus Eeq_{APP}/Eeq is unity. In Figure 5.8 the log of Eeq_{APP}/Eeq is plotted against $\log(\Phi)$ for values of E/Eeq equal to 0.1, 1, 10, 100 and 1000 for a given Δ value of 0.001. This range in E/Eeq describes nearly elastic to glassy materials. A Δ value of 0.001 is indicative of the experimental conditions used when characterizing a glassy material, since the pulse duration is usually small in comparison to the relaxation time. Similarly, for a glassy material a value of E/Eeq of 100-1000 would be expected. From Figure 5.8 in order to obtain a relative modulus Eeq_{APP}/Eeq of unity requires a Φ value of at least 5-10 times longer than the relaxation time. This

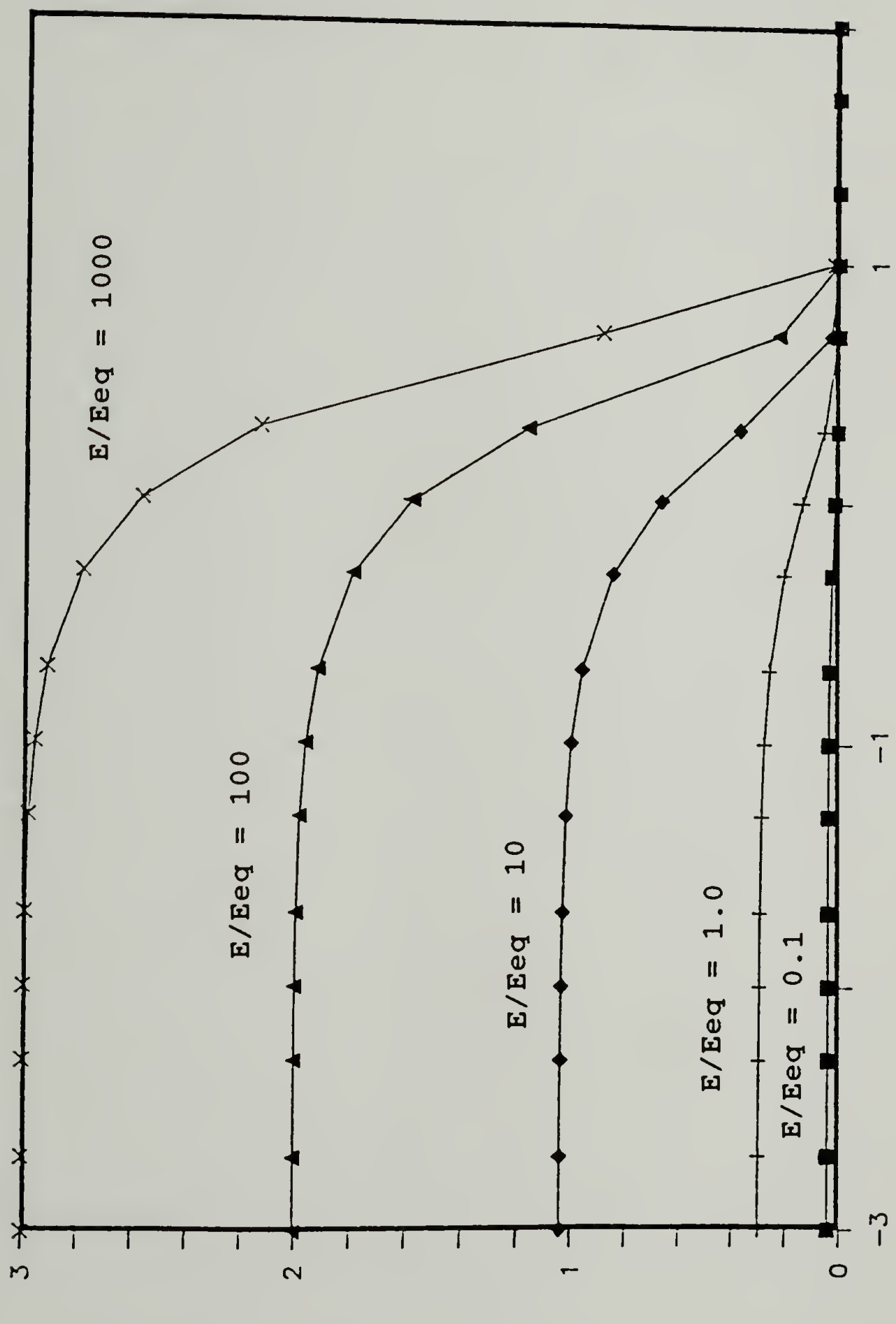

Figure 5.8. Log(Eeq_{APP}/Eeq) versus log(Φ) for Δ = 0.001 at E/Eeq values of 0.1, 1, 10, 100 and 1000.

is an exceedingly long time and makes the measurement of the true Eeq of a glass impractical experimentally. Clearly, for elastomers and other materials where the relaxation times are shorter and when E and Eeq are comparable, it is relatively easy to obtain true estimates of Eeq. Interestingly the data in Figure 5.8 indicates that the reduced modulus Eeq_{APP}/Eeq is relatively insensitive to Φ (for relatively small values of Φ) for a wide range of E/Eeq values. It is unlikely that such behavior would be observed experimentally except for very glassy materials. It is believed that this insensitivity of Eeq_{APP}/Eeq is the result of the simple model that was used to calculate the data, which assumes a single exponential relaxation time. From the preceding analysis it is possible to estimate the errors associated with the calculation of mechanical properties.

In order to view the effect of the dimensionless integration time upon the fractional modulus, Figure 5.9 plots the log of Eeq_{APP}/Eeq against $\log(\Delta)$ for Φ values of 0.1, 0.2, 0.5, 1, 2 and 5 using an E/Eeq ratio equal to unity. The E/Eeq value of unity used in Figure 5.9 represents a non-glassy viscoelastic solid. As expected for this type of material, the times required in order to obtain an Eeq close to the true Eeq are smaller. The data in Figure 5.9 indicate that in the range where the pulse durations are relatively short in comparison to the relaxation time, Eeq_{APP}/Eeq remains unchanged for this range

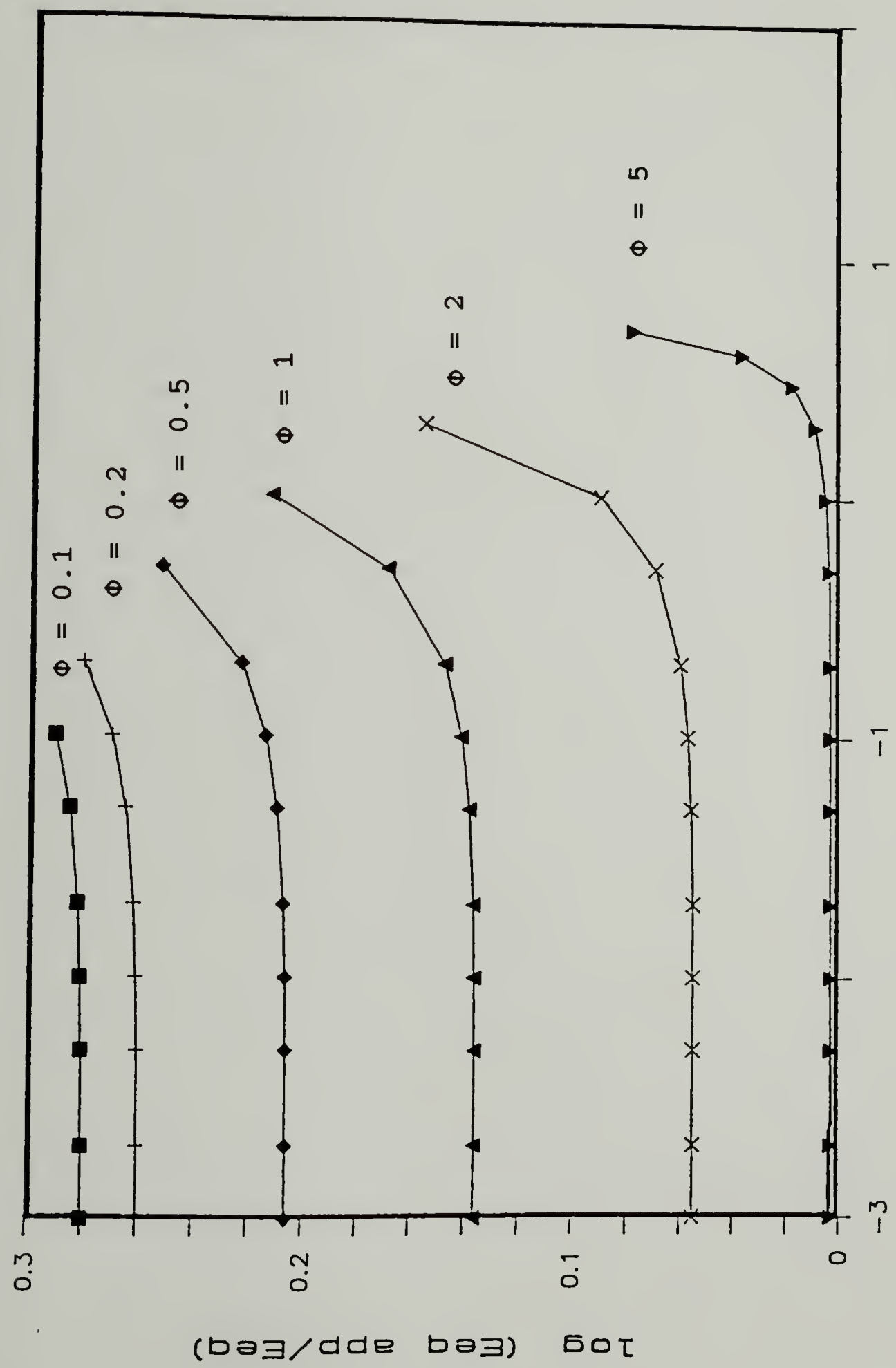

Figure 5.9. Log(Eeq_{APP}/Eeq) versus log(Δ) for E/Eeq = 1 at Φ values of 0.1, 0.2, 0.5, 1, 2 and 5.

of Φ values. This again demonstrates the experimental need for pulse durations which are a significant fraction of the relaxation time, coupled with long data collection periods.

The behavior of a Maxwell model can be recovered from that of the standard linear solid by letting Eeq = 0. Recall that the Maxwell model represents a viscoelastic liquid. As in the case of the SLS, by prematurely terminating the σ(t) integration one can measure an Eeq_{APP} for the Maxwell model. Using Eeq = 0 simplifies Equation (5.3) to Equation (5.4):

$$Eeq_{APP}/E = \frac{\exp(-\Phi)[\exp(\Delta) - 1]}{\Delta} . \qquad (5.4)$$

The lower limit of Eeq_{APP} for the Maxwell model is clearly 0. In order to demonstrate the effect of the dimensionless integration time Φ, Figure 5.10 displays the dimensionless modulus Eeq_{APP}/E versus log(Φ) for Δ values of 0.01, 0.1, 0.5, 1, 2.5 and 5 using an E value of 1.0. From Figure 5.10, it is necessary to use dimensionless integration times on the order of 1-10 in order to obtain an Eeq_{APP}/E close to zero. Conversely, the effect of the dimensionless pulse time is displayed on Figure 5.11 where Eeq_{APP}/E is plotted against the log(Δ) for Φ values of 0.1, 0.25, 0.5, 1 and 2.5 using an E value of 1.0. As expected for a given pulse duration, Eeq_{APP}/E increases with decreasing integration times. The trends on Figure 5.11 indicate that for a given

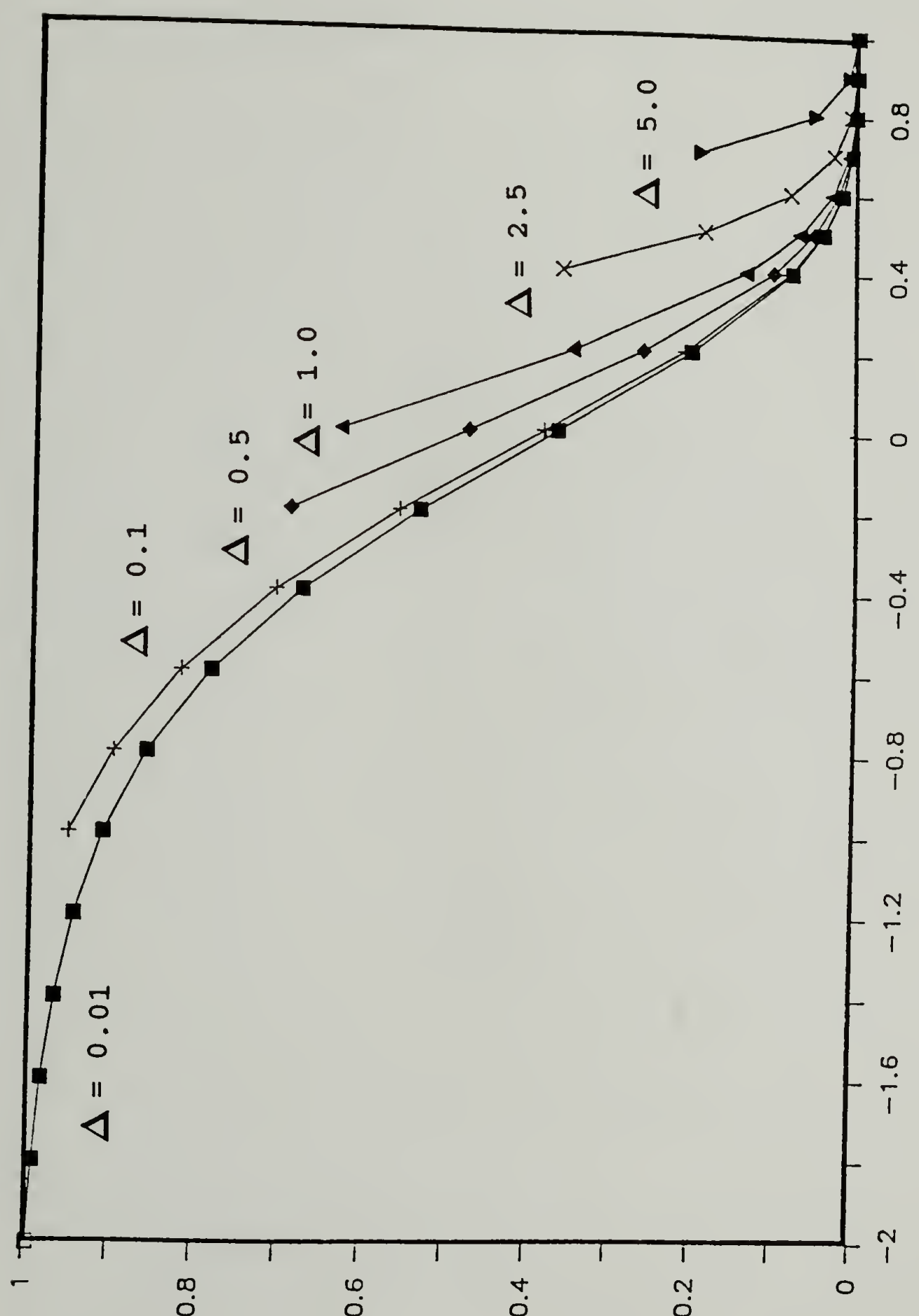

Figure 5.10. $E_{eq_{APP}}/E$ versus log(Φ) for E = 1.0 at Δ values of 0.01, 0.1, 0.5, 1, 2.5 and 5.

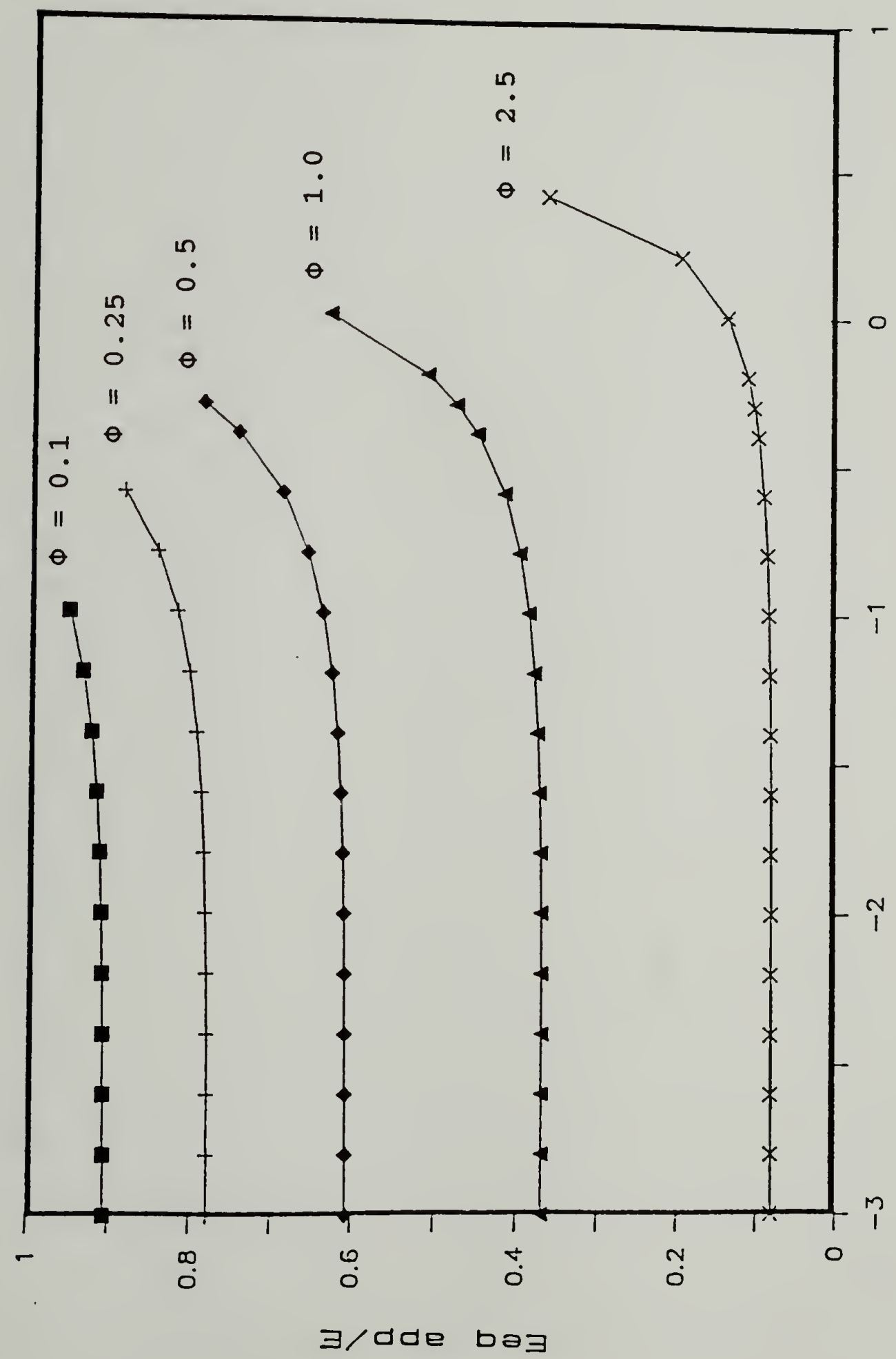

Figure 5.11. Eq_{APP}/E versus log(Δ) for E = 1.0 at Φ values of 0.1, 0.25, 0.5, 1 and 2.5.

value of Φ, Eeq_{APP}/E decreases with decreasing Δ values. In order to obtain Eeq_{APP} values close to 0, Φ values near 2.5 should be used.

5.3.2 Steady State Elongational Viscosity

Using the equations outlined in Chapter II, a similar analysis to that shown for Eeq_{APP} can be performed for the calculation of η_{APP}, the apparent steady state elongational viscosity for the standard linear solid. This relationship is given in Equation (5.5):

$$\eta_{APP} = E_T\{1 + \exp(-\Phi)[\exp(\Delta) - 1][\tfrac{1}{2} - \Phi/\Delta - 1/\Delta]\} \quad (5.5)$$

At $t = \infty$ this equation yields the expected result of $\eta_{APP} = \eta = \tau E$. Equation (5.5) can be rearranged to Equation (5.6) to yield the fractional or reduced viscosity (η_{APP}/η) that would be obtained experimentally.

$$\eta_{APP}/\eta = 1 + \exp(-\Phi)[\exp(\Delta) - 1][\tfrac{1}{2} - \Phi/\Delta - 1/\Delta] \quad (5.6)$$

The upper limit of the reduced viscosity η_{APP}/η is unity. In order to illustrate the effect of the dimensionless integration time Φ, Figure 5.12 plots the reduced η as a function of $\log(\Phi)$ for Δ values equal to 0.1, 1, 2, 5 and 10. The trends displayed in Figure 5.12 demonstrate short duration pulses (relative to the relaxation time) or equivalently, short duration collection times (relative to the relaxation time) result in measured viscosities which

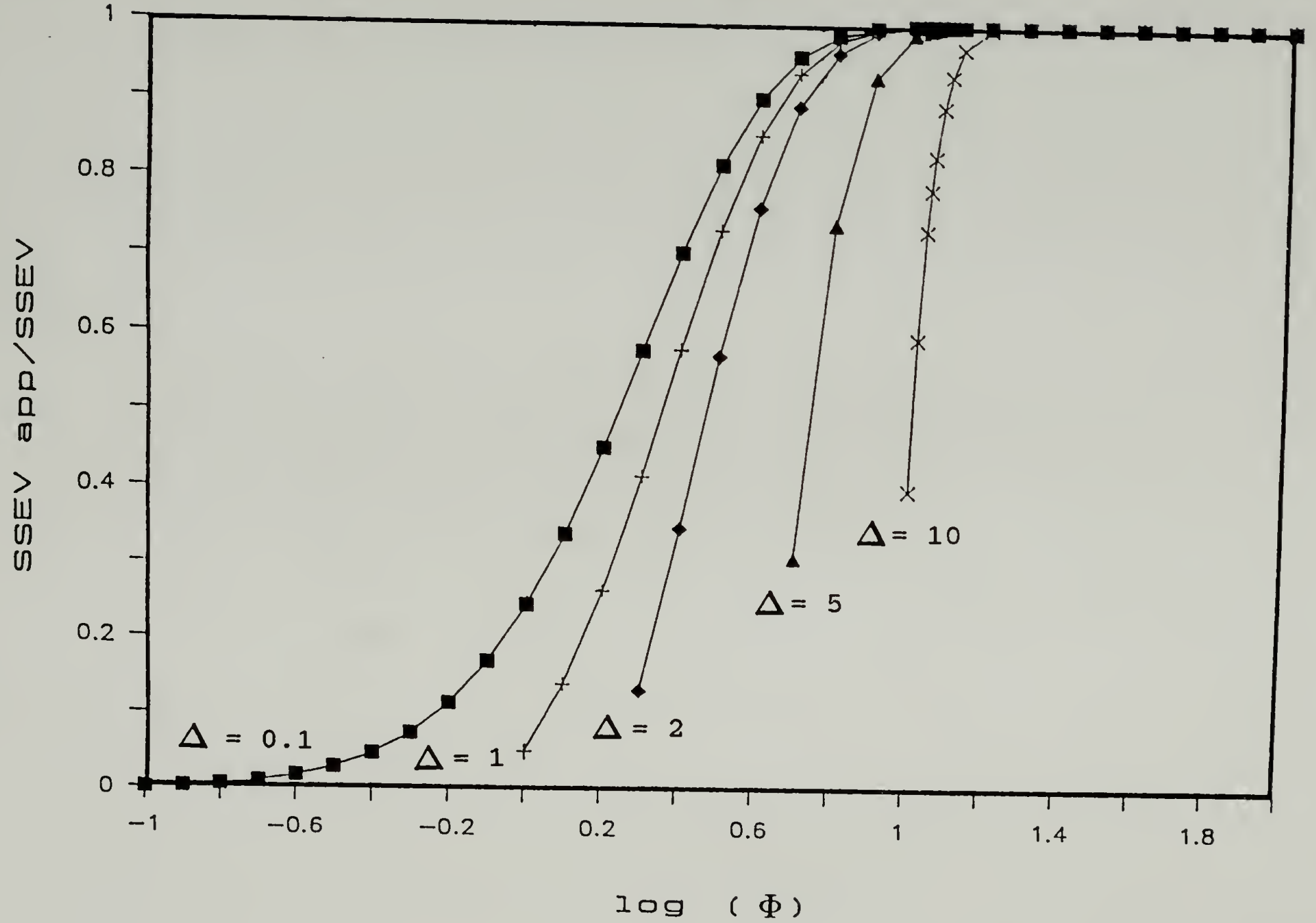

Figure 5.12. η_{APP}/η versus log(Φ) for Δ values of 0.1, 1, 2, 5 and 10.

are too small. The η_{APP}/η behavior for the SLS can equivalently be observed on Figure 5.13 where η_{APP}/η is plotted against $\log(\Delta)$ for Φ values of 0.5, 1, 2, 5 and 10. The data in Figure 5.13 indicate that the calculated η_{APP}/η is insensitive to relatively short pulse durations over this range of Φ values. The results obtained for η_{APP}/η for the Maxwell model are identical to those obtained for the SLS, since Eeq does not appear in Equation (5.5). In order to view the response of the standard linear solid over a large range in experimental conditions, Table 5.7 summarizes the behavior of the Eeq_{APP}/Eeq and η_{APP}/η for seven decades of Φ and Δ using a value of Eeq/E = 1.0.

5.4 Discussion

It is interesting to compare the experimental pulse deformation results presented in section 5.2.1 with those obtained using the standard linear solid calculations. Clearly the trends in Eeq and η for the Jeffamine^R T-403/Epon 828 epoxy sample with increasing pulse duration (summarized in Table 5.1) are in good qualitative agreement with the predictions of Eeq_{APP}/Eeq and η_{APP}/η.

For this Jeffamine^R/Epon 828 sample it is possible to calculate an equivalent value of E based upon the deformation results presented in Table 5.1 and Figure 5.8. At a deformation temperature of 70° C, the 10 second pulse

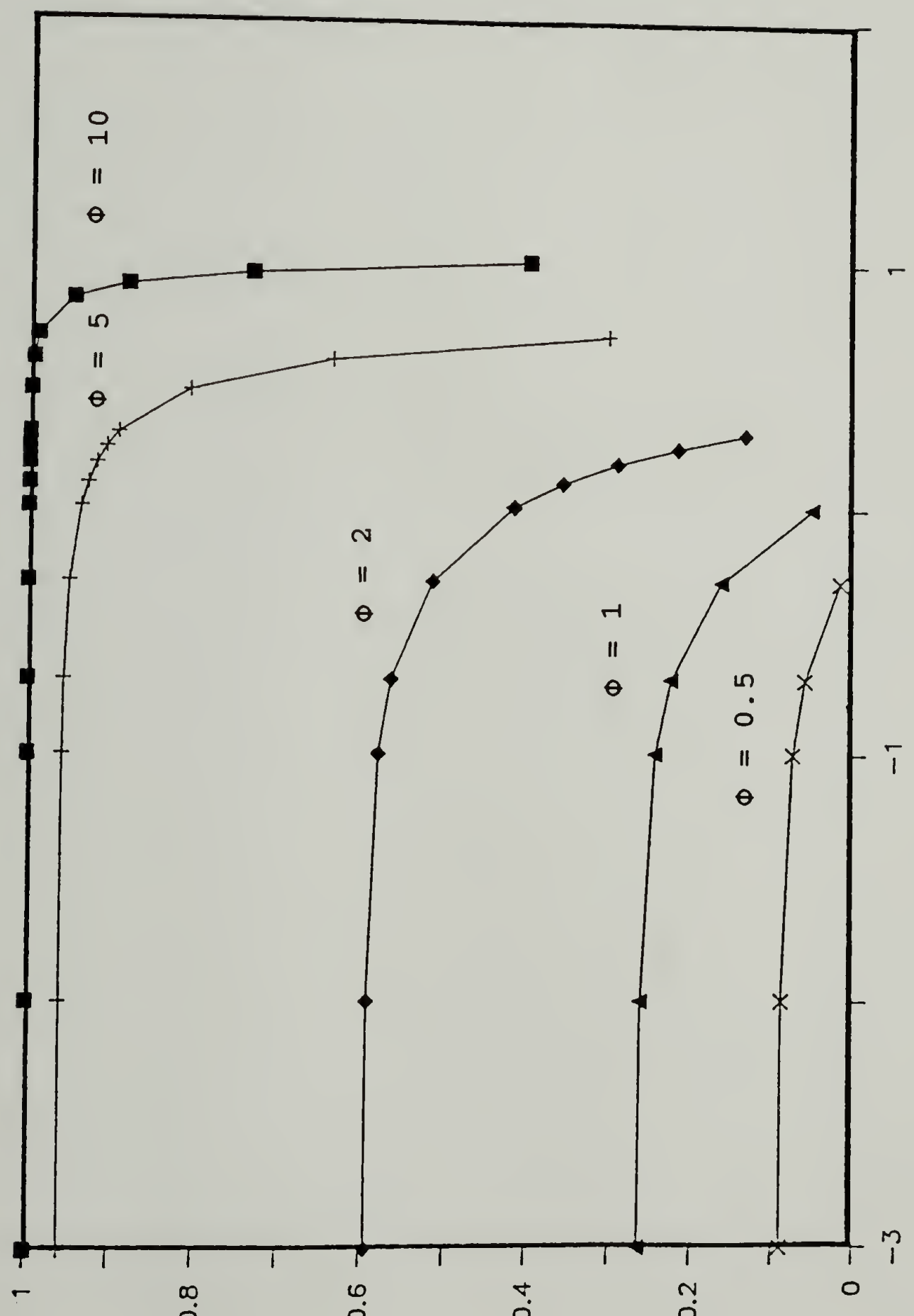

Figure 5.13. η_{APP}/η versus $\log(\Delta)$ for Φ values of 0.5, 1, 2, 5 and 10.

Table 5.7

Mechanical Response of the Standard Linear Solid Using the Dimensionless Quantities Φ and Δ for Eeq/E = 1.0

$\Phi = \phi/\tau$	$\Delta = \delta/\tau$	Eeq_{APP}/Eeq	η_{APP}/η
0.001	0.001	2.000	8.33×10^{-6}
0.01	0.001	1.991	4.48×10^{-5}
0.1	0.001	1.905	4.63×10^{-3}
1.0	0.001	1.368	2.64×10^{-1}
10	0.001	1.000	1.000
100	0.001	1.000	1.000
1000	0.001	1.000	1.000
0.01	0.01	1.995	8.29×10^{-6}
0.1	0.01	1.909	4.23×10^{-3}
1.0	0.01	1.370	2.62×10^{-1}
10	0.01	1.000	1.000
100	0.01	1.000	1.000
1000	0.01	1.000	1.000
0.1	0.1	1.952	7.93×10^{-4}
1.0	0.1	1.387	2.46×10^{-1}
10	0.1	1.000	1.000
100	0.1	1.000	1.000
1000	0.1	1.000	1.000
1.0	1.0	1.632	5.18×10^{-2}
10	1.0	1.000	9.99×10^{-1}
100	1.0	1.000	1.000
1000	1.0	1.000	1.000
10	10	1.100	4.00×10^{-1}
100	10	1.000	1.000
1000	10	1.000	1.000
100	100	1.010	4.90×10^{-1}
1000	100	1.000	1.000

duration can be used to approximate a Δ value of 0.001. From the linear regression results presented in Table 3.4 (section 3.4.2 of Chapter III) it is suggested that the true equilibrium tensile modulus of this material at 70° C is 17.6 MPa. This results in an Eeq_{APP}/Eeq value of about 5.0. For this deformation condition data were collected for about 90 seconds or correspondingly a Φ value of 0.009. From Equation (5.3) these parameters result in an E of 70 MPa. From Figure 5.8 it can be seen that these deformation conditions are in the region where Eeq_{APP}/Eeq is dominated by the contribution of E to the mechanical response. As a result, the calculated E value is very similar to the Eeq measured experimentally. A similar analysis can be performed at the 65° C deformation temperature where it is assumed that the 100 second pulse duration approximates a value of 0.001. The true Eeq at this temperature is approximately 17.1 MPa and results in an Eeq_{APP}/Eeq value of about 35. Since a collection time of 600 seconds was used for this deformation, a Φ value of 0.006 may be obtained. From Equation (5.3) an E value of 600 is determined. Once again, these deformation conditions are in the range of Eeq_{APP}/Eeq where it is insensitive to small changes in Φ. In order to obtain Eeq values which approach the true Eeq for both deformation temperatures would require collection periods two orders of magnitude longer than those used in these studies. At the temperatures of 65 and 70° C this

corresponds to a collection period of 17 and 3 hours, respectively.

The modeling results presented in section 5.3 should serve as a guide to the dependence of the mechanical properties on two of the more important experimental variables: the pulse duration and integration time. With regard to the choice of the proper pulse duration and data collection period, it is necessary to use values that are comparable to the longer relaxation times of the material. Since polymeric materials have a wide distribution in relaxation times, usually including some very long ones, it is probably necessary to exclude the extremely long relaxations when performing Impulse Viscoelastic experiments. In this regard it would be convenient if one had the relaxation spectrum for each material of interest so that one could judge the severity of such an assumption. This is not often the case.

The trends in Figures 5.8-13 and Table 5.7 indicate that for a material with a single relaxation time that more accurate values for E_{eq} and η are obtained if one uses a relatively short duration deformation with a long data collection period rather than using a long pulse duration and short data collection period. In order to appreciate this concept numerically, consider several deformation experiments using a material with a relaxation time of 1 sec. The use of a 1 second pulse duration and 1 sec

integration time yield values of 1.632 and 5.18 x 10^{-2} for Eeq_{APP}/Eeq and η_{APP}/η, respectively. The combination of a 0.1 sec pulse duration with an integration time of 1 second yields values of 1.387 and 2.46 x 10^{-1} for Eeq_{APP}/Eeq and η_{APP}/η, respectively. Clearly for these two deformation conditions, the latter set of values are closer to the true value of unity for Eeq_{APP}/Eeq and η_{APP}/η. In contrast to the previous two non-ideal experimental conditions, a 1 second pulse duration with an integration time of 10 seconds yields an Eeq_{APP}/Eeq of 1.000 and an η_{APP}/η of 0.999.

As an experimenter it is important to understand the limitations of equipment and the numerical significance of one's data. In any experiment it is important to segregate first order from second order effects. This requires intuition on the part of the operator to understand the nature of a material and judiciously choose the important variables. For example, in Chapter IV the curing results of epoxy copolymerized with ring opening monomer were presented. For some of those samples vitrification was a significant contribution to the mechanical response. As a result, measurements were complicated by the presence of long term molecular relaxations. Despite this, however, data were obtained under non-isothermal conditions during the cooling portion of those experiments using relatively short duration deformations and data collection times. It is the author's opinion that it is unrealistic to perform

isothermal experiments that may last hours for deformation data at each individual temperature. In cases where phenomena such as vitrification are significant, the approach that has been used by the author is the determination of an estimate of the mechanical behavior and the concurrent realizations of the limitations of the data.

Extending these thoughts further, consider if one were to apply the Impulse Viscoelastic technique to characterize the mechanical properties of an amorphous, uncrosslinked thermoplastic polymer, such as atactic polystyrene. Assuming that one had an injection molded bar made from polystyrene above its entanglement molecular weight, most people would view this bar as a solid. This is because the bar would behave like a solid at the time scales of deformation normally encountered in everyday experiences. The question that one can ask is the following: neglecting the presence of permanent loops, is it reasonable that the equilibrium tensile modulus of such a material would be zero at extremely long time scales? The answer in all likelihood is no. It has been suggested by Plazek that thermoplastics even above T_g have extremely long relaxation times [71]. The fact that the polystyrene bar is below Tg at room temperature suggests that the relaxation times are still longer. Even if the answer were yes, one could not perform the experiment to verify it. The discussion here is not intended as an exercise in triviality, but it is of a

philosophical nature meant to bring out the complexities associated with the study of polymer materials. Basically, the question of the elasticity of a material, whether a material is a solid or a liquid, must be referenced to some time scale. For the case of the amorphous polystyrene bar the time scale on which it behaves like a liquid is well out of the realm of our everyday experiences. Finally, it should be remembered that the limitations presented in this chapter are not limited to the Impulse Viscoelastic technique but are present in other mechanical test methods such as creep, stress relaxation and dynamic mechanical measurements as well.

C H A P T E R 6

CONCLUSIONS

6.1 Overview

In this dissertation, the technique of Impulse Viscoelasticity was presented from a theoretical and experimental perspective. The technique involves the analysis of the stress response of a material to an arbitrary deformation. Emphasis was placed on understanding the solidification process in polymers. In this regard, it was demonstrated that Impulse Viscoelasticity is a viable and useful technique for measuring the mechanical properties of thermosetting materials during cure. Among the properties which were determined are: gelation time and temperature, equilibrium tensile modulus, one-dimensional cure stress, volumetric shrinkage due to cure, thermal expansion coefficient, glass transition temperature, steady state elongational viscosity, relaxation spectrum and dynamic mechanical properties.

The results of two curing systems were presented. The first system examined was the amine curing of an epoxy resin. The results were presented in Chapter III. It was found that these epoxies cured elastically during polymerization and the network properties could be correlated with results derived from rubber elasticity

theory. In Chapter IV the network formation process was ascertained for the complicated system of an epoxy resin copolymerized with ring opening monomer. It was found that while the addition of ring opening monomer reduces the volumetric shrinkage, the reduction in the one-dimensional cure stress is negligible relative to the cure stresses of the neat epoxy. As a result of the particular copolymerization chemistry, it is believed that two distinct, and possible interpenetrating, networks form.

As a general result for the thermosetting systems examined in this dissertation and for a variety of other materials (polyamide-cured epoxies, polyesters, unsaturated polycarbonates and polyurethanes), it was found that the one-dimensional stresses generated during isothermal cure are generally small ($\approx$ 0.1 MPa) despite relatively large volumetric changes ($\approx$ 10%). Such a stress is small in comparison to a load bearing stress or the thermal stress associated with a few degree temperature change for a glassy material.

Chapter V presented results on the limitations of the Impulse Viscoelastic method. Both an experimental and theoretical approach were taken. A series of isothermal deformation experiments were conducted on a fully cured epoxy sample. The effects of pulse duration, amplitude, shape and deformation temperature were investigated. Using this experimental approach it was found that longer pulse

durations help recover the true mechanical properties of a material. In addition, abrupt deformations, such as uniaxial step pulses, yield results more indicative of the true mechanical behavior. Non-step deformations yielded accurate equilibrium tensile modulus data but calculated viscosity and relaxation properties that were low in comparison to the data obtained from step deformations. Theoretical results using a standard linear solid as a model were found to be in qualitative agreement with those obtained experimentally.

Considering that until now dynamic mechanical measurements have been the predominant method used to characterize the properties of solidified materials, it seems clear that the Impulse Viscoelastic technique is superior. It requires no special equipment or deformation mode. More importantly, the technique of Impulse Viscoelasticity offers a wealth of information regarding the mechanical properties of a material which are unavailable by any other single technique, especially dynamic mechanical measurements. Furthermore, if one is particularly interested in the dynamic properties of a material it was demonstrated in Chapter II, section 2.5.2, that the Fourier transform approach to dynamic mechanical data yields results which are in excellent agreement with those obtained using traditional dynamic methods.

An Impulse Dielectric method for monitoring cure was proposed. This method is the electrical equivalent of Impulse Viscoelasticity. It employs mathematics similar to those presented for the Impulse Viscoelastic technique and embodies the same philosophy. Drawing on the similarities of the two techniques, the Impulse Dielectric method avoids the limitations encountered by dynamic dielectric methods. In contrast to the Impulse Viscoelastic technique, the Impulse Dielectric technique should yield information regarding cure on a molecular level. The two techniques should complement each other to yield an even better understanding of the solidification process.

6.2 Future Studies

Based on the results presented in this dissertation it is the opinion of the author that future studies employing the technique of Impulse Viscoelasticity should be directed in two areas. First, the solidification of high performance thermoset resins and thermoplastics should be examined in order to help address questions of composite toughness. Second is the development of the Impulse Dielectric method for *in situ* curing measurements. A brief research outline for both of these areas is discussed below.

The first area of future research should include work on the *in situ* mechanical characterization of the solidification of high performance thermosets and

thermoplastics as neat materials and in unidirectional fiber-matrix composites. This suggestion is motivated on the basis that high performance composites are finding increasingly widespread use and are of technological importance. The mechanical properties of these composites are, in general, outstanding when compared to metals on an equivalent weight basis. There are, however, composite properties which are relatively poor in comparison to metals. One such property is toughness, or the ability to withstand damage without a loss in mechanical properties.

In past years, the emphasis on improving composite toughness was directed at using different fibers and altering the fiber-matrix adhesion. While these approaches have their benefits, these efforts have not yielded the needed improvements in toughness. Recently, it seems that the matrix has played a more important role in fiber-matrix composite toughness. In this regard many microstructural studies have been conducted on matrix materials in an effort to understand the deformation process and the toughness question. The approach suggested here is on a macroscopic level and focuses on the development of residual stresses during composite formation. It is believed that in this regard the Impulse Viscoelastic method can lend insight.

As discussed in Chapters II and IV, regions of volumetrically constrained material, such as in the tricot of material between tightly packed unidirectional fibers,

results in large stresses. It is suggested that these stresses may be high enough to cause matrix cracking, fiber fracture, interfacial failure or other deleterious phenomena. In order to investigate this, Impulse Viscoelastic experiments should first be conducted on the curing of the neat high performance resins, such as CIBA GEIGY's MY 720. Uniaxial deformations with superimposed pressure are suggested. In this way, a measure of Poisson's ratio will be obtained. Subsequent curing experiments should be performed on unidirectional fiber composites which are based upon the same resins, in directions parallel and perpendicular to the fiber axis.

The second half of this research effort should be directed towards the use of the Impulse Viscoelastic technique to study the solidification of thermoplastics as neat materials and in high performance composites. As a motivation for this study, it is known that amorphous and semi-crystalline thermoplastics, such as polysulfone and poly(ether ether ketone), have begun to challenge thermosets as the matrix of choice in high performance composites. When compared to thermosets, thermoplastic resins offer toughness and solvent resistance but suffer from relatively low service temperatures. In particular, the emphasis has shifted towards amorphous rather than crystalline thermoplastics where the volumetric changes during solidification are smaller. In addition, the fact that

thermoplastics, especially crystalline ones, undergo large volumetric changes during solidification make them an ideal material for studying the relationship between residual stress and volumetric change.

These Impulse Viscoelastic measurements should be coupled to measures of the volumetric changes which occur prior to solidification. These can be determined using *in situ* dilatometry or commercial instruments which measure the pressure-volume-temperature relationship for a material. The theoretical analyses used to determine the mechanical properties from these Impulse Viscoelastic measurements may require the use of more complicated constitutive relations which incorporate mechanical anisotropy. The composite solidification results should be compared to those of the neat materials. It should be noted that in order to compare these data it may be required to assume that the solidification process of the matrix in the composite is unaffected by the presence of the fibers, i.e., the matrix solidifies as if it were in the bulk neat state. Whether this is a reasonable assumption is not well known.

Impulse Viscoelastic measurements on solidification should be supplemented with mechanical data from tests used to determine such properties as modulus, strength, toughness and the long term properties for both the neat and composite materials. Together with the Impulse Viscoelastic data on the neat and composite materials it should be possible to

properly address the question of composite toughness. Finally, the fact that thermoset and thermoplastic solidification occur by two completely different mechanisms might further elucidate the effect of the matrix on composite properties in general.

Impulse Dielectric measurements during cure should also be pursued. As mentioned, this technique can provide dielectric information on a molecular level. First, the viability of such a method should be demonstrated. This can be done by using the Impulse Dielectric method to characterize an unknown electrical circuit and evaluate its ability to determine an "equivalent" circuit. Assuming that the method yields satisfactory results, it can then be used to characterize the dielectric properties of a material during cure. It is suggested that some of the thermosetting materials that have been studied in this dissertation be examined. In this way, the mechanical properties during cure have already been determined and will serve as a basis for the evaluation of the Impulse Dielectric results.

REFERENCES

1. R.J. Morgan, C.M. Walkup and T.H. Heisel, *J. Appl. Polym. Sci.*, 30, 289 (1985).

2. P. Peyser and W.D. Bascom, *J. Appl. Polym. Sci.*, 21, 2359 (1977).

3. L.T. Pappalardo, *J. Appl. Polym. Sci.*, 21, 809 (1977).

4. C.C. Riccardi, H.E. Adabbo and R.J.J. Williams, *J. Appl. Polym. Sci.*, 29, 2481 (1984).

5. R.B. Prime and E. Sacher, *Polymer*, 13, 455 (1972).

6. J. Delmonte, *J. Appl. Polym. Sci.*, 2, 108 (1959).

7. S.D. Senturia and N.F. Sheppard, Jr., *Adv. Polym. Sci.*, 80, 1 (1986).

8. S.D. Senturia, N.F. Shepard, Jr., H.L. Lee and D.R. Ray, *J. Adhes.*, 15, 69 (1982).

9. D. Kranbuehl, S. Delos, E. Yi, J. Mayer, T. Jarvie, W. Winfree and T. Hou, *Polym. Eng. Sci.*, 26, 338 (1986).

10. J.W. Lane, J.C. Seferis and M.A. Bachmann, *Polym. Eng. Sci.*, 26, 346 (1986).

11. N.F. Sheppard, Jr. and S.D. Senturia, *Polym. Eng. Sci.*, 26, 354 (1986).

12. W.W. Bidstrup, N.F. Sheppard, Jr. and S.D. Senturia, *Polym. Eng. Sci.*, 26, 358 (1986).

13. D.R. Day, *Polym. Eng. Sci.*, 26, 362 (1986).

14. Z.N. Sanjana, *Polym. Eng. Sci.*, 26, 373 (1986).

15. G.A. Sofer and E.A. Hauser, *J. Polym. Sci.*, 8, 6 (1952).

16. R.T. Harrold and Z.N. Sanjana, *Polym. Eng. Sci.*, 26, 367 (1986).

17. J.A. Happe, R.J. Morgan and C.M. Walkup, *Polymer*, 26, 827 (1985).

18. C. Di Giulio, M. Gautier and B. Jasse, *J. Appl. Polym. Sci.*, 29, 1771 (1984).

19. A. Gupta, M. Cizmecioglu, D. Coulter, R.H. Liang, A. Yavrouian, F.D. Tsay and J. Moacanin, *J. Appl. Polym. Sci.*, 28, 1011 (1983).

20. P.J. Dynes and D.H. Kaelble, *J. Appl. Polym. Sci.*, 22, 837 (1978).

21. D.E. Kline, *J. Appl. Polym. Sci.*, 4, 123 (1960).

22. S. Newman, *J. Appl. Polym. Sci.*, 2, 333 (1959).

23. G.C. Papanicolaou, S.A. Paipetis and P.S. Theocaris, *J. Appl. Polym. Sci.*, 20, 903 (1976).

24. R.G.C. Arridge and J.H. Speake, *Polymer*, 13, 443 (1972).

25. D. Harran and A. Laudouard, *Rheol. Acta*, 24, 596 (1985).

26. C.Y. Tung and P.J. Dynes, *J. Appl. Polym. Sci.*, 27, 569 (1982).

27. H.H. Winter and F. Chambon, *J. Rheol.*, 30(2), 367 (1986).

28. W.X. Zukas, Ph.D. Dissertation, University of Massachusetts, Amherst, 1983.

29. G.A. Senich, W.J. MacKnight and N.S. Schneider, *Polym. Eng. Sci.*, 19, 313 (1979).

30. M.T. Aronhime and J.K. Gillham, *Adv. Polym. Sci.*, 78, 83 (1986).

31. J.K. Gillham, *AIChE J.*, 20, 1066 (1974).

32. P.G. Babayevsky and J.K. Gillham, *J. Appl. Polym. Sci.*, 17, 2067 (1973).

33. B. Hartmann and G.F. Lee, *J. Appl. Polym. Sci.*, 21, 1341 (1977).

34. C.Y-C. Lee and I.J. Goldfarb, *Polym. Eng. Sci.*, 21, 390 (1981).

35. R.J. Farris, *J. Rheol.*, 28(4), 347 (1984).

36. H. Lee and K. Neville, Epoxy Resins, Their Application and Technology, McGraw-Hill, New York, 1957.

37. J.D. LeMay and F.N. Kelley, *Adv. Polym. Sci.*, 78, 115 (1986).

38. M. Shimbo, M. Ochi and Y. Shigeta, *J. Appl. Polym. Sci.*, 26, 2265 (1981).

39. I.K. Varma and P.V.S. Bhama, *J. Compos. Mater.*, 20, 410 (1986).

40. M. Shimbo, N. Nishitani and T. Takahama, *J. Appl. Polym. Sci.*, 29, 1709 (1984).

41. J.P. Bell, *J. Polym. Sci., A-2*, 6, 417 (1970).

42. T. Murayama and J.P. Bell, *J. Polym. Sci., A-2*, 8, 437 (1970).

43. D.A. Whiting and D.E. Kline, *J. Appl. Polym. Sci.*, 18, 1043 (1974).

44. J.D. Keenan, J.C. Seferis and J.T. Quinlivan, *J. Appl. Polym. Sci.*, 24, 2375 (1979).

45. J. Bastide, C. Picot and S. Candau, *J. Macromol. Sci., Phys.*, B19, 13 (1981).

46. B. Stenberg and J.F. Jansson, *J. Macromol. Sci., Phys.*, B19, 143 (1981).

47. R.J. Morgan, F-M. Kong and C.M. Walkup, *Polymer*, 25, 375 (1984).

48. K. Dusek, *Adv. Polym. Sci.*, 78, 1 (1986).

49. T. Kamon and H. Furukawa, *Adv. Polym. Sci.*, 80, 173 (1986).

50. R.J. Farris and C. Lee, *Polym. Eng. Sci.*, 23, 586 (1983).

51. A.M. Zihlif, O. Federico and R.J. Farris, *Appl. Phys. Comm.*, 3, 211 (1983).

52. W.J. Bailey, R.L. Sun, H. Katsuki, T. Endo, H. Iwama, R. Tsushima, K. Saigou, M.M. Bitritto, Ring Opening Polymerization, T. Saegusa and E. Goethals, Eds., ACS Symposium Series 59, American Chemical Society, Washington, D.C., p 38, 1977.

53. T. Endo and W.J. Bailey, *J. Polym. Sci., Polym. Lett. Ed.*, 13, 193 (1975).

54. T. Endo and W.J. Bailey, *J. Polym. Sci., Polym. Chem. Ed.*, 13, 2525 (1975).

55. I.S. Klaus and W.S. Knowles, *J. Appl. Polym. Sci.*, 10, 887 (1966).

56. Technical literature, Epolin Inc., Morristown, NJ.

57. Y.C. Fung, A First Course in Continuum Mechanics, 2nd ed., Prentice-Hall, Englewood Cliffs, NJ, 1977.

58. A.V. Tobolsky, Properties and Structure of Polymers, Wiley, New York, 1960.

59. J.D. Ferry, Viscoelastic Properties of Polymers, 3rd ed., Wiley, New York, 1980.

60. C.R. Wylie, Advanced Engineering Mathematics, 3rd ed., McGraw Hill, New York, 1960.

61. J.J. Aklonis and W.J. MacKnight, Introduction to Polymer Viscoelasticity, 2nd ed., Wiley, New York, 1983.

62. M.S. Vratsanos and R.J. Farris, *J. Appl. Polym. Sci.*, 33, 915 (1987).

63. W.G. Miller, L. Kou, K. Tohyama and V. Voltaggio, *J. Polym. Sci., Polym. Symp. Ser.*, 65, 91 (1978).

64. A.K. Murthy and M. Muthukumar, *Macromolecules*, 20, 564 (1987).

65. D.E. Floyd, D.E. Peerman and H. Wittcoff, *J. Appl. Chem.*, 7, 250 (1957).

66. D.E. Peerman, W. Tolberg and H. Wittcoff, *J. Am. Chem. Soc.*, 76, 6085 (1954).

67. D.E. Floyd, Polyamide Resins, 2nd ed., Reinhold, New York, 1966.

68. M.S. Vratsanos and R.J. Farris, in Composite Interfaces, H. Ishida and J.L. Koenig, Eds., Elsevier, New York, p 71, 1986.

69. W.W. Graessley, *Adv. Polym. Sci.*, 47, 67 (1982).

70. R.C. Ball, M. Doi, S.F. Edwards and M. Warner, *Polymer*, 22, 1011 (1981).

71. D.J. Plazek, *J. Polym. Sci., Polym. Phys. Ed.*, 20, 1533 (1982).

72. D.C. Prevorsek and B.T. De Bona, *J. Macromol. Sci., Phys.*, B19(4), 605 (1981).

73. A. Ziabicki, *Colloid Polym. Sci.*, 254, 1 (1976).

74. P. Zoller and P. Bolli, *J. Macromol. Sci., Phys.*, B18, 555 (1980).

75. P. Zoller, *J. Polym. Sci., Polym. Phys. Ed.*, 20, 1453 (1982).

76. J.A. Nairn and P. Zoller, *J. Mater. Sci.*, 20, 355 (1985).

77. B. Harris, *J. Mater. Sci.*, 13, 173 (1978).

78. E. Alfthan and A. de Ruvo, *Int. J. Polym. Mater.*, 7, 163 (1979).

79. H.T. Hahn, *J. Compos. Mater.*, 10, 266 (1976).

80. C.L. Brett, *J. Appl. Polym. Sci.*, 20, 1431 (1976).

81. B.W. Cherry and K.W. Thomson, *Int. J. Polym. Mater.*, 7, 191 (1979).

82. M.S. Vratsanos, E.L. Thomas and R.J. Farris, *J. Mater. Sci.*, 22, 419 (1987).

83. M.S. Vratsanos, E.L. Thomas and R.J. Farris, in Composite Interfaces, H. Ishida and J.L. Koenig, Eds., Elsevier, New York, p 151, 1986.

84. J.E. Bailey and A. Parvizi, *J. Mater. Sci.*, 16, 649 (1981).

85. N.K. Asamoah and W.G. Wood, *J. Strain Anal.*, 5, 88 (1970).

86. Y.M. Ito, M. Rosenblatt, L.Y. Cheng, F.F. Lange and A.G. Evans, *Int. J. Fract.*, 17, 483 (1981).

87. I.M. Daniel and A.J. Durelli, *Exp. Mech.*, 2, 240 (1962).

88. A.J. Durelli and J.V. Parks, *Exp. Mech.*, 3, 263 (1963).

89. T. Koufopoulos and P.S. Theocaris, *J. Compos. Mater.*, 3, 308 (1969).

90. P.S. Theocaris and E. Marketos, *Fibre Sci. Technol.*, 3, 21 (1970).

91. F. Hospers and L.B. Vogelesang, *Exp. Mech.*, 15, 107, (1975).

92. E.G. Koroneos, *Colloid Polym. Sci.*, 256, 741 (1978).

93. B. Cunningham, J.P. Sargent, K.H.G. Ashbee, *J. Mater. Sci.*, 16, 620 (1981).

94. A.T. Andonian and S. Danyluk, *J. Mater. Sci.*, 20, 4459 (1985).

95. H. Dannenberg, *SPE J.*, 21, 669 (1965).

96. S.G. Croll, *J. Coat. Technol.*, 50, 33 (1978).

97. S.G. Croll, *J. Coat. Technol.*, 51, 49 (1979).

98. T. Suzuki, *Colloid Polym. Sci.*, 254, 775 (1976).

99. I.M. Cuckson, B. Haworth, G.J. Sandilands and J.R. White, *Int. J. Polym. Mater.*, 9, 21 (1981).

100. A.K. Srivastava and J.R. White, *J. Appl. Polym. Sci.*, 29, 2155 (1984).

101. S. Bruller, *Int. J. Polym. Mater.*, 5, 125 (1976).

102. G. Odian, Principles of Polymerization, 2nd ed., Wiley, New York, 1981.

103. Technical literature, Texaco Chemical Co., Bellaire, TX.

104. L.R.G. Treolar, The Physics of Rubber Elasticity, Clarendon Press, Oxford, 1958.

105. P.J. Flory, Principles of Polymer Chemistry, Cornell University Press, Ithaca, NY, 1953.

106. A.V. Tobolsky, D.W. Carlson and N. Indictor, *J. Polym. Sci.*, 54, 175 (1961).

107. A. Ciferri, *J. Polym. Sci.*, 54, 149 (1961).

108. D. Katz and A.V. Tobolsky, *Polymer*, 4, 417 (1963).

109. R.E. Lyon and R.J. Farris, *Polymer*, 28, 1127 (1987).

110. R.D. Andrews, A.V. Tobolsky and E.E. Hanson, *J. Appl. Phys.*, 17, 352 (1946).

111. P.J. Flory, *Trans. Faraday Soc.*, 56, 722 (1960).

112. A.S. Lodge, *Kolloid Z.*, 171, 46 (1960).

113. A.L. Andrady, M.A. Llorente and J.E. Mark, *J. Chem. Phys.*, 72, 2282 (1980).

114. J.T. Lim, M.R. Piggott and W.J. Bailey, *SAMPE Q.*, 15, 25 (1984).

115. M.R. Piggott and M.S. Woo, *Polym. Compos.*, 7, 182 (1986).

116. M. Shimbo, M. Ochi, T. Inamura and M. Inoue, *J. Mater. Sci.*, 20, 2965 (1985).

117. M.S. Vratsanos, University of Massachusetts, Amherst, unpublished results.

118. C.P. Buckley, *J. Rheol.*, 29(6), 1035 (1985).

119. I.M. Ward, Mechanical Properties of Solid Polymers, 2nd ed., Wiley, New York, 1983.

120. R.E. Cohen, *Int. J. Polym. Mater.*, 5, 1 (1976).

APPENDIX A

Summary of Computer Software

Summary of Computer Software

The following programs have been written for use with the Impulse Viscoelastic method. They are grouped into those used for data collection, analysis and display.

Data Collection

COLTIME: The COLTIME program collects up to three analog signals (usually displacement, load and temperature) and stores the digitized data on the hard disk of the DEC PRO 380. As input, the program requires a sample length, diameter, displacement transducer sensitivity and voltage tolerance for convergence. During an Impulse Viscoelastic experiment the program displays the start and end times as well as Eeq for each pulse. The operator controls the frequency of collection, collection time and the time between collections. The maximum amount of data that can be collected per deformation pulse per channel is given by the following formula:

$$(\text{Collection Frequency})(\text{Collection time}) \leq 5460$$

Should the data collection needs change during an experiment, it is possible to change any or all of the collection parameters. Two files are generated at the end of collection; a .DAT file which contains the raw data and a .PR1 file which contains a summary of the pulse start and end times along with Eeq.

Data Analysis

BASLIN: BASLIN recomputes the baseline (start and end times for a pulse) of the collected data using a new, operator-chosen voltage tolerance and creates a new .DAT file. This program is useful if it is necessary to reanalyze the data using a different voltage tolerance, or equivalently, to check the sensitivity of the calculated parameters upon the time defined as the end of the pulse.

DEDIT: DEDIT allows the operator to create a new data file (.SDT file) from the originally collected data file. The purpose of this program is to allow the operator to create a shorter data file composed of typical pulses or to remove any non-convergent pulses from the original data file. It is also possible to change the end integration time from that calculated by BASLIN.

DSTAT: DSTAT was developed especially for experiments which involve no deformation. It is particularly useful for monitoring the cure or thermal stresses of a sample held at constant strain. The program can generate an .STC file which contains the sample dimensions, stress and temperature.

INTEG: This program accepts the exact sample dimensions, displacement transducer sensitivity and performs the moment and Fourier transform analyses listed in Chapter II.

Quadrature techniques such as Simpson's rule are used to perform the integrations. It stores the reduced parameters in a .PLT file.

Data Display

DUMP: Dump displays the collected data in digital form. These are the actual collected voltages. Every ten points the mean and standard deviation of the displacement, load and temperature signals are displayed. At the top of each pulse display is general information regarding the sample, i.e., pulse start and end times, collection frequency, etc.

PULSE: This program displays the collected data in graphical form using approximate or exact values for the sample length, area and transducer sensitivity. Plots of individual pulses can be made and full adjustment of the stress, strain and time axes is possible. The program is useful for examining the viscoelastic character of a material and checking the convergence of the stress at the end of data collection.

PRINTP: PRINTP is a program that displays the calculated parameters stored in the .PLT file in a hardcopy format. It summarizes the reduced data for each pulse.

TREND: This program is useful for observing trends in the data. It compiles the information obtained from each pulse

in a sequential fashion so as to form a composite plot of a particular property. TREND allows the operator to plot any of the following parameters against any other:

1. Integration time
2. Temperature
3. Shrinkage stress
4. End baseline
5. Oth moment of strain
6. 1st moment of strain
7. 2nd moment of strain
8. 0th moment of stress
9. 1st moment of stress
10. 2nd moment of stress
11. Equilibrium tensile modulus
12. Steady state elongational viscosity
13. Mean relaxation time
14. E'
15. E"
16. E*
17. Tan δ
18. Equilibrium tensile modulus/E'
19. Time

The option to eliminate individual or groups of data points is available. Plots can be generated and the axes limits can be chosen by the operator.

APPENDIX B

List of Publications

List of Publications

Parts of this dissertation appear in the open literature in the following publications:

1. M.S. Vratsanos and R.J. Farris, "A Novel Method for Measuring the Uniaxial Mechanical Properties of an Epoxy Resin During Polymerization," J. Appl. Polym. Sci., 33, 915 (1987).

2. C.L. Bauer, R.J. Farris and M.S. Vratsanos, "Determination of the Stresses and Properties of Polymer Coatings," Proceedings of the ACS, PMSE Div., Denver, CO, 56, p 560, 1987.

3. M.S. Vratsanos and R.J. Farris, "A New Method for Determining Shrinkage Stresses and Properties of Curing Thermosets," in Composite Interfaces, H. Ishida and J.L. Koenig, Eds., Elsevier, New York, p 71, 1986.

4. M.S. Vratsanos and R.J. Farris, "Impulse Viscoelasticity: A New Method for Characterizing Cure," Proceedings of the ACS, PMSE Div., Anaheim, CA, 55, p 902, 1986.

5. M.S. Vratsanos, R.J. Farris and E.L. Thomas, "The Adhesive Behavior of Poly(p-phenylene benzobisthiazole) (PBT)/Epoxy Composites," J. Mater. Sci., 22, 419 (1987).

6. M.S. Vratsanos and R.J. Farris, "Effect of Cure Temperature on the Adhesive Behavior of Poly(p-phenylene benzobisthiazole) (PBT)/Epoxy Composites," in Composite Interfaces, H. Ishida and J.L. Koenig, Eds., Elsevier, New York, p 151, 1986.

BIBLIOGRAPHY

Aklonis, J.J. and MacKnight, W.J., Introduction to Polymer Viscoelasticity, 2nd ed., Wiley, New York, 1983.

Alfthan, E. and de Ruvo, A., *Int. J. Polym. Mater.*, 7, 163 (1979).

Andonian, A.T. and Danyluk, S., *J. Mater. Sci.*, 20, 4459 (1985).

Andrady, A.L., Llorente, M.A. and J.E. Mark, *J. Chem. Phys.*, 72, 2282 (1980).

Andrews R.D., Tobolsky, A.V. and Hanson, E.E., *J. Appl. Phys.*, 17, 352 (1946).

Aronhime, M.T. and Gillham, J.K., *Adv. Polym. Sci.*, 78, 83 (1986).

Arridge, R.G.C. and Speake, J.H., *Polymer*, 13, 443 (1972).

Asamoah, N.K. and Wood, W.G., *J. Strain Anal.*, 5, 88 (1970).

Babayevsky, P.G. and Gillham, J.K., *J. Appl. Polym. Sci.*, 17, 2067 (1973).

Bailey, W.J. and Parvizi, A., *J. Mater. Sci.*, 16, 649 (1981).

Bailey, W.J., Sun, R.L., Katsuki, H., Endo, T., Iwama, H., Tsushima, R., Saigou, K. and Bitritto, M.M., Ring Opening Polymerization, T. Saegusa and E. Goethals, Eds., ACS Symposium Series 59, American Chemical Society, Washington, D.C., p 38, 1977.

Ball, R.C., Doi, M., Edwards, S.F. and Warner, M., *Polymer*, 22, 1011 (1981).

Bastide, J., Picot, C. and Candau, S., *J. Macromol. Sci., Phys.*, B19, 13 (1981).

Bell, J.P., *J. Polym. Sci., A-2*, 6, 417 (1970).

Bidstrup, W.W., Sheppard, N.F., Jr. and Senturia, S.D., *Polym. Eng. Sci.*, 26, 358 (1986).

Brett, C.L., *J. Appl. Polym. Sci.*, 20, 1431 (1976).

Bruller, S., *Int. J. Polym. Mater.*, 5, 125 (1976).

Buckley, C.P., *J. Rheol.*, 29(6), 1035 (1985).

Cherry, B.W. and Thomson, K.W., *Int. J. Polym. Mater.*, 7, 191 (1979).

Ciferri, A., *J. Polym. Sci.*, 54, 149 (1961).

Cohen, R.E., *Int. J. Polym. Mater.*, 5, 1 (1976).

Croll, S.G., *J. Coat. Technol.*, 50, 33 (1978).

Croll, S.G., *J. Coat. Technol.*, 51, 49 (1979).

Cuckson, I.M., Haworth, B., Sandilands, G.J. and White, J.R., *Int. J. Polym. Mater.*, 9, 21 (1981).

Cunningham, B., Sargent, J.P. and Ashbee, K.H.G., *J. Mater. Sci.*, 16, 620 (1981).

Daniel, I.M. and Durelli, A.J., *Exp. Mech.*, 2, 240 (1962).

Dannenberg, H., *SPE J.*, 21, 669 (1965).

Day, D.R., *Polym. Eng. Sci.*, 26, 362 (1986).

Delmonte, J., *J. Appl. Polym. Sci.*, 2, 108 (1959).

Di Giulio, C., Gautier, M. and Jasse, B., *J. Appl. Polym. Sci.*, 29, 1771 (1984).

Durelli, A.J. and Parks, J.V., *Exp. Mech.*, 3, 263 (1963).

Dusek, K., *Adv. Polym. Sci.*, 78, 1 (1986).

Dynes, P.J. and Kaelble, D.H., *J. Appl. Polym. Sci.*, 22, 837 (1978).

Endo, T. and Bailey, W.J., *J. Polym. Sci., Polym. Chem. Ed.*, 13, 2525 (1975).

Endo, T. and Bailey, W.J., *J. Polym. Sci., Polym. Lett. Ed.*, 13, 193 (1975).

Epolin Inc., Morristown, NJ, Technical literature.

Farris, R.J., *J. Rheol.*, 28(4), 347 (1984).

Farris, R.J. and Lee, C., *Polym. Eng. Sci.*, 23, 586 (1983).

Ferry, J.D., Viscoelastic Properties of Polymers, 3rd ed., Wiley, New York, 1980.

Flory, P.J., Principles of Polymer Chemistry, Cornell University Press, Ithaca, NY, 1953.

Flory, P.J., *Trans. Faraday Soc.*, 56, 722 (1960).

Floyd, D.E., Polyamide Resins, 2nd ed., Reinhold, New York, 1966.

Floyd, D.E., Peerman, D.E. and Wittcoff, H., *J. Appl. Chem.*, 7, 250 (1957).

Fung, Y.C., A First Course in Continuum Mechanics, 2nd ed., Prentice-Hall, Englewood Cliffs, NJ, 1977.

Gillham, J.K., *AIChE J.*, 20, 1066 (1974).

Graessley, W.W., *Adv. Polym. Sci.*, 47, 67 (1982).

Gupta, A., Cizmecioglu, M., Coulter, D., Liang, R.H., Yavrouian, A., Tsay, F.D. and Moacanin, J., *J. Appl. Polym. Sci.*, 28, 1011 (1983).

Hahn, H.T., *J. Compos. Mater.*, 10, 266 (1976).

Happe, J.A., Morgan, R.J. and Walkup, C.M., *Polymer*, 26, 827 (1985).

Harran D. and Laudouard, A., *Rheol. Acta*, 24, 596 (1985).

Harris, B., *J. Mater. Sci.*, 13, 173 (1978).

Harrold, R.T. and Sanjana, Z.N., *Polym. Eng. Sci.*, 26, 367 (1986).

Hartmann, B. and Lee, G.F., *J. Appl. Polym. Sci.*, 21, 1341 (1977).

Hospers, F. and Vogelesang, L.B., *Exp. Mech.*, 15, 107, (1975).

Ito, Y.M., Rosenblatt, M., Cheng, L.Y., Lange, F.F. and Evans, A.G., *Int. J. Fract.*, 17, 483 (1981).

Kamon, T. and Furukawa, H., *Adv. Polym. Sci.*, 80, 173 (1986).

Katz, D. and Tobolsky, A.V., *Polymer*, 4, 417 (1963).

Keenan, J.D., Seferis, J.C. and Quinlivan, J.T., *J. Appl. Polym. Sci.*, 24, 2375 (1979).

Klaus, I.S. and Knowles, W.S., *J. Appl. Polym. Sci.*, 10, 887 (1966).

Kline, *J. Appl. Polym. Sci.*, 4, 123 (1960).

Koroneos, E.G., *Colloid Polym. Sci.*, 256, 741 (1978).

Koufopoulos, T. and Theocaris, P.S., *J. Compos. Mater.*, 3, 308 (1969).

Kranbuehl, D., Delos, S., Yi, E., Mayer, J., Jarvie, T., Winfree, W. and Hou, T., *Polym. Eng. Sci.*, 26, 338 (1986).

Lane, J.W., Seferis, J.C. and Bachmann, M.A., *Polym. Eng. Sci.*, 26, 346 (1986).

Lee, C.Y-C. and Goldfarb, I.J., *Polym. Eng. Sci.*, 21, 390 (1981).

Lee, H. and Neville, K., Epoxy Resins, Their Application and Technology, McGraw-Hill, New York, 1957.

LeMay, J.D. and Kelley, F.N., *Adv. Polym. Sci.*, 78, 115 (1986).

Lim, J.T., Piggott, M.R. and Bailey, W.J., *SAMPE Q.*, 15, 25 (1984).

Lodge, A.S., *Kolloid Z.*, 171, 46 (1960).

Lyon, R.E. and Farris, R.J., *Polymer*, 28, 1127 (1987).

Miller, W.J., Kou, L., Tohyama, K. and Voltaggio, V., *J. Polym. Sci., Polym. Symp. Ser.*, 65, 91 (1978).

Morgan, R.J., Kong, F-M. and Walkup, C.M., *Polymer*, 25, 375 (1984).

Morgan, R.J., Walkup, C.M. and Heisel, T.H., *J. Appl. Polym. Sci.*, 30, 289 (1985).

Murayama, T. and Bell, J.P., *J. Polym. Sci., A-2*, 8, 437 (1970).

Murthy, A.K. and Muthukumar, M., *Macromolecules*, 20, 564 (1987).

Nairn, J.A. and Zoller, P., *J. Mater. Sci.*, 20, 355 (1985).

Newman, S., *J. Appl. Polym. Sci.*, 2, 333 (1959).

Odian, G., Principles of Polymerization, 2nd ed., Wiley, New York, 1981.

Papanicolaou, G.C., Paipetis, S.A. and Theocaris, P.S., *J. Appl. Polym. Sci.*, 20, 903 (1976).

Pappalardo, L.T., *J. Appl. Polym. Sci.*, 21, 809 (1977).

Peerman, D.E., Tolberg, W. and Wittcoff, H., *J. Am. Chem. Soc.*, 76, 6085 (1954).

Peyser, P. and Bascom, W.D., *J. Appl. Polym. Sci.*, 21, 2359 (1977).

Piggott, M.R. and Woo, M.S., *Polym. Compos.*, 7, 182 (1986).

Plazek, D.J., *J. Polym. Sci., Polym. Phys. Ed.*, 20, 1533 (1982).

Prevorsek, D.C. and De Bona, B.T., *J. Macromol. Sci., Phys.*, B19(4), 605 (1981).

Prime, R.B. and Sacher, E., *Polymer*, 13, 455 (1972).

Riccardi, C.C., Adabbo, H.E. and Williams, R.J.J., *J. Appl. Polym. Sci.*, 29, 2481 (1984).

Sanjana, Z.N., *Polym. Eng. Sci.*, 26, 373 (1986).

Senich, G.A., MacKnight, W.J. and Schneider, N.S., *Polym. Eng. Sci.*, 19, 313 (1979).

Senturia, S.D. and Sheppard, N.F., Jr., *Adv. Polym. Sci.*, 80, 1 (1986).

Senturia, S.D., Sheppard, N.F., Jr., Lee, H.L. and Ray, D.R., *J. Adhes.*, 15, 69 (1982).

Sheppard, N.F., Jr. and Senturia, S.D., *Polym. Eng. Sci.*, 26, 354 (1986).

Shimbo, M., Nishitani, N. and Takahama, T., *J. Appl. Polym. Sci.*, 29, 1709 (1984).

Shimbo, M., Ochi, M., Inamura, T. and Inoue, M., *J. Mater. Sci.*, 20, 2965 (1985).

Shimbo, M., Ochi, M. and Shigeta, Y., *J. Appl. Polym. Sci.*, 26, 2265 (1981).

Sofer, G.A. and Hauser, E.A., *J. Polym. Sci.*, 8, 6 (1952).

Srivastava, A.K. and White, J.R., *J. Appl. Polym. Sci.*, 29, 2155 (1984).

Stenberg, B. and Jansson, J.F., *J. Macromol. Sci., Phys.*, B19, 143 (1981).

Suzuki, T., *Colloid Polym. Sci.*, 254, 775 (1976).

Texaco Chemical Co., Bellaire, TX, Technical literature.

Theocaris, P.S. and Marketos, E., *Fibre Sci. Technol.*, 3, 21 (1970).

Tobolsky, A.V., Properties and Structure of Polymers, Wiley, New York, 1960.

Tobolsky, A.V., Carlson, D.W. and Indictor, N., *J. Polym. Sci.*, 54, 175 (1961).

Treolar, L.R.G., The Physics of Rubber Elasticity, Clarendon Press, Oxford, 1958.

Tung, C.Y. and Dynes, P.J., *J. Appl. Polym. Sci.*, 27, 569 (1982).

Varma, I.K. and Bhama, P.V.S., *J. Compos. Mater.*, 20, 410 (1986).

Vratsanos, M.S. and Farris, R.J., in Composite Interfaces, H. Ishida and J.L. Koenig, Eds., Elsevier, New York, p 71, 1986.

Vratsanos, M.S. and Farris, R.J., *J. Appl. Polym. Sci.*, 33, 915 (1987).

Vratsanos, M.S., Thomas, E.L. and Farris, R.J., in Composite Interfaces, H. Ishida and J.L. Koenig, Eds., Elsevier, New York, p 151, 1986.

Vratsanos, M.S., Thomas, E.L. and Farris, R.J., *J. Mater. Sci.*, 22, 419 (1987).

Vratsanos, M.S., University of Massachusetts, Amherst, unpublished results.

Ward, I.M., Mechanical Properties of Solid Polymers, 2nd ed., Wiley, New York, 1983.

Whiting, D.A. and Kline, D.E., *J. Appl. Polym. Sci.*, 18, 1043 (1974).

Winter, H.H. and Chambon, F., *J. Rheol.*, 30(2), 367 (1986).

Wylie, C.R. Advanced Engineering Mathematics, 3rd ed., McGraw Hill, New York, 1960.

Ziabicki, A., *Colloid Polym. Sci.*, 254, 1 (1976).

Zihlif, A.M., Federico, O. and Farris, R.J., *Appl. Phys. Comm.*, 3, 211 (1983).

Zoller, P., *J. Polym. Sci., Polym. Phys. Ed.*, 20, 1453 (1982).

Zoller, P. and Bolli, P., *J. Macromol. Sci., Phys.*, B18, 555 (1980).

Zukas, W.X., Ph.D. Dissertatation, University of Massachusetts, Amherst, 1983.